NASA CR-145043

PROGRAM FOR ESTABLISHING LONG-TIME FLIGHT SERVICE PERFORMANCE OF COMPOSITE MATERIALS IN THE CENTER WING STRUCTURE OF C-130 AIRCRAFT

PHASE IV - GROUND/FLIGHT ACCEPTANCE TESTS

September 1976

by W. E. Harvill and J. A. Kizer

Prepared under Contract No. NAS 1-11100 by
LOCKHEED-GEORGIA COMPANY
Marietta, Georgia

for

Langley Research Center
NATIONAL AERONAUTICS AND SPACE ADMINISTRATION

FOREWORD

This Phase IV - Final Technical Report is submitted in fulfillment of the requirements of Contract NAS1-11100 and reports contract effort from July 1974 through June 1976. Phase IV consisted of structural qualification tests, including ground and flight acceptance tests, in support of the in-service evaluation of the two C-130H center wing boxes that were selectively reinforced with boron-epoxy composites. The ground tests consisted of a static and fatigue test of the first of the composite reinforced C-130H center wing boxes fabricated, and a ground vibration test of a C-130H aircraft having a composite reinforced center wing box. Prior to conducting Phase IV, Phases I, II, and III were accomplished and were previously reported in NASA CR-112126, NASA CR-112272, and NASA CR-132495, respectively. Extensive advanced composite reinforcement development work was performed in Phase I. In Phase II a detailed design of the C-130H wing box, including the necessary analytical and component test substantiation of the selected design, was accomplished. Three composite reinforced C-130H composite center wing boxes, one for ground tests and two for in-service evaluation, were fabricated. One remaining program phase, Phase V, is in progress and is scheduled to be completed in early 1978. In Phase V two of the composite reinforced center wing boxes are being in-service evaluated on C-130H aircraft for a period of three years to demonstrate the long-time capabilities of composite utilization.

This contract is conducted under the sponsorship of the Materials Application Branch of the Materials Division of the NASA Langley Research Center. Mr. H. Benson Dexter, Composites Section, is the NASA Project Monitor. Mr. W. E. Harvill is the Lockheed-Georgia Company Program Manager.

Major contributions to the effort described herein were provided by the following Lockheed-Georgia personnel:

Structural Tests:	W. M. McGee
Instrumentation for Structural Tests:	C. R. Waguespack
Structural Analysis:	D. C. Gibson (Static) H. R. Horsburgh (Fatigue)
Quality Assurance:	C. E. Smith
Experimental Shops:	M. J. Brown
Reliability:	J. J. Duhig

This report is also identified as LG76ER0095 for Lockheed-Georgia Company internal control purposes.

ABSTRACT

One of the most advantageous structural uses of advanced filamentary composites has been shown, in previous studies, to be in areas where selective reinforcement of conventional metallic structure can improve static strength/fatigue endurance at lower weight than that possible if metal reinforcement were used. These advantages are now being demonstrated by design, fabrication, and test of three boron-epoxy reinforced C-130 center wing boxes. This structural component was previously redesigned using an aluminum build-up to meet the increased severity of fatigue loadings.

The first four phases of a five-phase NASA program to demonstrate the long-time flight service performance of a selectively reinforced center wing box have been completed. During the first phase of program activity, the advanced development work necessary to support detailed design of a composite reinforced C-130 center wing box was conducted. Activities included the development of a basis for structural design, selection and verification of materials and processes, manufacturing and tooling development, and fabrication and test of full-scale portions of the center wing box. Phase I activities are documented in NASA CR-112126.

Phase II activities consisted of preparing detailed design drawings, and conducting necessary analytical structural substantiation including static strength, fatigue endurance, flutter, and weight analyses. Some additional component testing was conducted to verify the design for panel buckling, and to evaluate specific local design areas. Development of the "cool tool" restraint concept was completed, and bonding capabilities were evaluated using full-length skin panel and stringer specimens. Phase II activities are reported in NASA CR-112272.

Phase III activities consisted of the fabrication of three C-130 center wing boxes, selectively reinforced with boron-epoxy composites. The first of the center wing boxes was delivered to the Structural Test Laboratory for fatigue testing. The remaining two center wing boxes were installed on Air Force C-130 aircraft Serial Numbers AF73-01592 and AF73-01594 to demonstrate the long-time flight worthiness of advanced composite reinforced aluminum alloy structures. Phase III activities are reported in NASA CR-132495.

Phase IV activities principally consisted of ground and acceptance tests of the three C-130 center wing boxes. Fatigue testing of the center wing test article was completed through four simulated lifetimes with no failures in boron-epoxy laminates or their bondlines. After completion of the fatigue test, an additional proof load test was successfully conducted on the center wing test article applying the limit load upbending condtion. Artificial damage was inflicted in the center wing test article at twelve locations after completion of the proof load test and a crack growth test was conducted using the same cyclic loads spectrum applied in the four lifetimes of fatigue testing. Upon completion of the crack growth test, a residual strength test was performed on the center wing test article. The first of the C-130 aircraft, Serial Number AF73-01592, on which the composite-reinforced center wing was installed was ground vibrated to establish that existing flutter speeds had not been affected by the wing modification. Also, flight acceptance tests were conducted on both C-130 aircraft on which the composite-reinforced center wings are installed. Detailed inspections of those two composite-reinforced center wings are being performed under Phase V program activities.

TABLE OF CONTENTS

TABLE OF CONTENTS (Continued)

LIST OF FIGURES

LIST OF FIGURES (Continued)

LIST OF FIGURES (Continued)

LIST OF FIGURES (Continued)

LIST OF TABLES

ABBREVIATIONS

Abbreviation	Description
AFPRO	Air Force Plant Representative's Office
AFQA	Air Force Quality Assurance
Avg	Average
$\mathbb{C}_L$	Centerline
C_p	Center of Pressure
CWB	Center Wing Box
DR	Discrepancy Report
FACI	First Article Configuration Inspection
ft	Foot or Feet
g	Gram
in	Inch
kip	One thousand pounds force
ksi	One thousand pound force per square inch
lb	Pound (*mass or force*)
m	Meter
MRB	Materials Review Board
μ	Micro
N	Newton (force)
N/m^2	Newton per Square Meter
psi	Pounds Force per Square Inch
SI	*International System of Units*
W.S. or WS	Wing Station

ABBREVIATIONS (Cont'd)

Abbreviation	Description
LHS	Left-hand side
RHS	Right-hand side
F.E.M.	Finite Element Model

PROGRAM FOR ESTABLISHING LONG-TIME FLIGHT SERVICE PERFORMANCE OF COMPOSITE MATERIALS IN THE CENTER WING STRUCTURE OF C-130 AIRCRAFT

PHASE IV - GROUND/FLIGHT ACCEPTANCE TESTS

By W. E. Harvill and J. A. Kizer

1.0 SUMMARY

One of the most advantageous structural uses of advanced filamentary composites is in areas where selective reinforcement of conventional metallic structure can improve static strength/fatigue endurance at lower weight than would be possible if metal reinforcement were used. The first four phases of a five-phase NASA program to demonstrate the long-time flight service performance of a selectively reinforced center wing box have been completed. During the first phase of program activity, the advanced development work necessary to support detailed design of a composite-reinforced C-130 center wing box was conducted. Activities included the development of a basis for structural design, selection and verification of materials and processes, manufacturing and tooling development, and fabrication and test of full-scale portions of the center wing box. Phase I activities have been previously documented in NASA CR-112126, Reference 1.

During Phase II, the basic C-130E aluminum center wing box design was changed by removing aluminum and adding unidirectional boron-epoxy reinforcing laminates bonded to the crown of the hat stiffeners and to the skin under the stiffeners. The laminates were added in a nominal 80/20 area ratio of aluminum to boron/epoxy. Sufficient material was provided to meet ultimate load requirements of the C-130E wing box and the fatigue life of the C-130 B/E wing box.* Laminates are tapered out at the rainbow end fittings and access door openings by progressively stopping individual plies of the tape. Fasteners are used at the ends of the laminates to prevent peeling. Adequate bearing surface was provided in fastener penetration areas by titanium doublers integrally bonded into the laminates. Careful design and manufacturing techniques were used to reduce the number of fasteners (particularly blind fasteners) which penetrate the laminates, thus minimizing potential installation and inspection problems. A total of 129 detailed design drawings were prepared for initiation of the production program. Detailed substantiating structural, fatigue, and flutter analyses were conducted to assure structural integrity of the reinforced center wing box. Phase II activities are fully reported in NASA CR-112272, Reference 2.

---

*NOTE: The terminology "C-130 B/E" or "B/E" refers to the existing metallic center wing box which is installed in Model C-130B, C-130E, and C-130H aircraft. The C-130H is the designation of the aircraft model currently in production. This aircraft has the metal-reinforced center wing which has been retrofitted to a sizeable part of the total C-130 fleet. The two composite reinforced center wing boxes (flight articles) were installed in C-130H aircraft. In this report, the "B/E" designation always refers to an aircraft model and never means boron-epoxy. Where boron-epoxy is discussed, the words are not abbreviated.

In Phase III, three composite-reinforced center wing boxes were fabricated, one for ground tests, and two for installation on C-130H aircraft for flight evaluation. During fabrication of the wing boxes, boron-epoxy laminates were laid up, cured, and bonded to the metal adherends to form subassemblies. These subassemblies along with fabricated metal parts were assembled into complete wing boxes in the normal C-130 production flow. Throughout the fabrication and assembly activity, thorough inspections were conducted by both Lockheed and Air Force inspectors to assure a high-quality final product. First Article Configuration Inspections (FACI) were conducted on both flight articles to verify that all requirements had been satisfied. The first flight article shown in Figure 1 was installed in C-130H Serial No. AF73-01592 (Lockheed Serial No. 4557) in June 1974, and the second flight article was installed in C-130H Serial No. AF73-01594 (Lockheed Serial No. 4563) in July 1974.

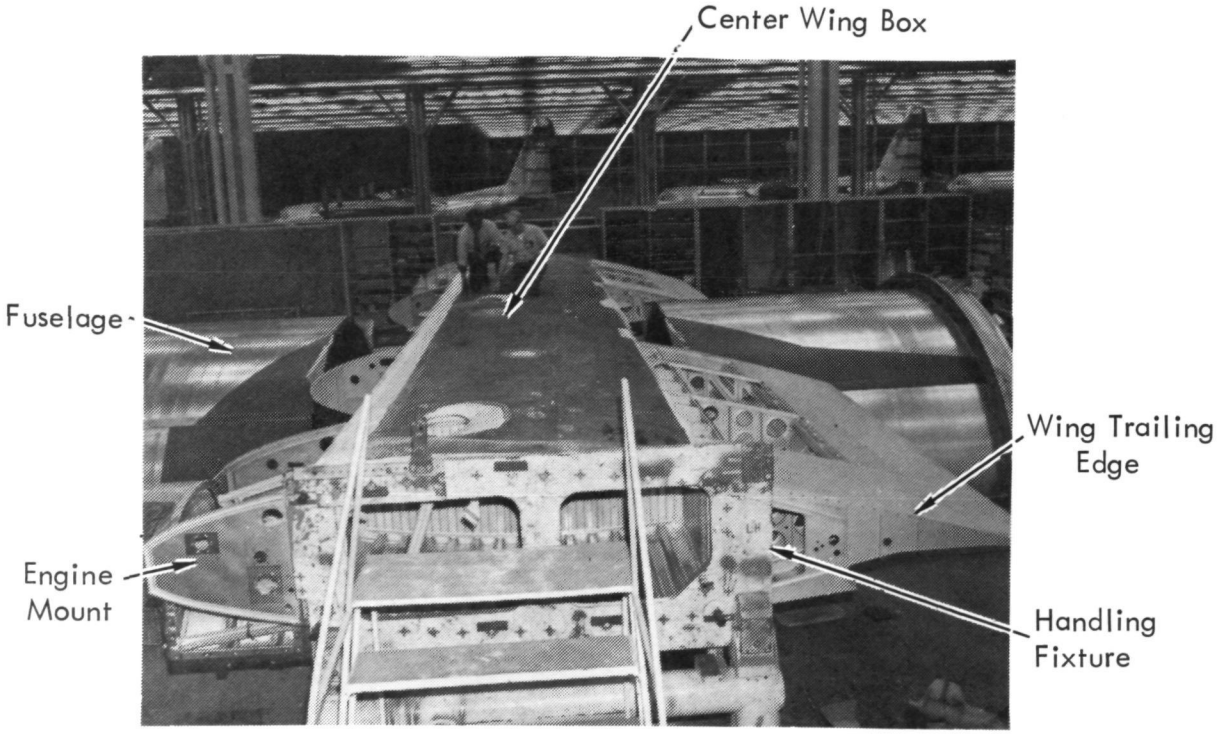

FIGURE 1 - INSTALLATION OF CENTER WING BOX IN C-130H SERIAL NO. AF73-01592

Although weight saving was not a major program goal, and was actually subordinated to accomplishment of flight service program goals, it is, nevertheless, an important factor, and a weight saving of 229 kg (506 lb). was predicted. This prediction, based on calculations from the final production drawings, indicated a saving in total box weight of slightly more than 10 percent. Minor design changes to facilitate production reduced this indicated value to 225 kg (494 lb). Actual weighings of the completed wing boxes showed savings of 222 kg (448 lb) for the test article and 205 kg (450 lb) for the flight articles. These values fall within anticipated manufacturing tolerances. The 318 kg (700 lb) total of boron-epoxy being used in two wing boxes for the 3-year flight evaluation represents a sizeable exposure of boron-epoxy materials to the representative service environment encountered during the life of an aircraft.

It is interesting to note that, in the wing surfaces where composite reinforcements were added, an average metal removed/composite added ratio of approximately 2.5 was achieved. Thus, a high potential for weight saving exists for future similar applications particularly where a less conservative criteria is used.

Cost projections for production quantities of C-130 composite-reinforced center wing boxes were made based on accumulated cost data using an eighty percent cumulative average cost curve. The total cost increase to add boron-epoxy reinforcement is projected for the 200th production wing box to be $40,120 for labor and materials in 1974 dollars. The computed cost per pound of weight saved is approximately $79.29. Phase III activities have been previously documented in NASA CR-132495, Reference 3.

In the fourth program phase, reported in detail in this document, the ground and flight acceptance tests were completed. The ground tests consisted of proof load tests, a four-lifetime fatigue test, a crack growth test, and a residual strength test on the wing box test article. After installing the test article in the test fixture and installing the instrumentation, it was proof loaded to design limit load for both critical upbending and downbending conditions. The center wing test article is shown in Figure 2 sustaining limit downbending design load.

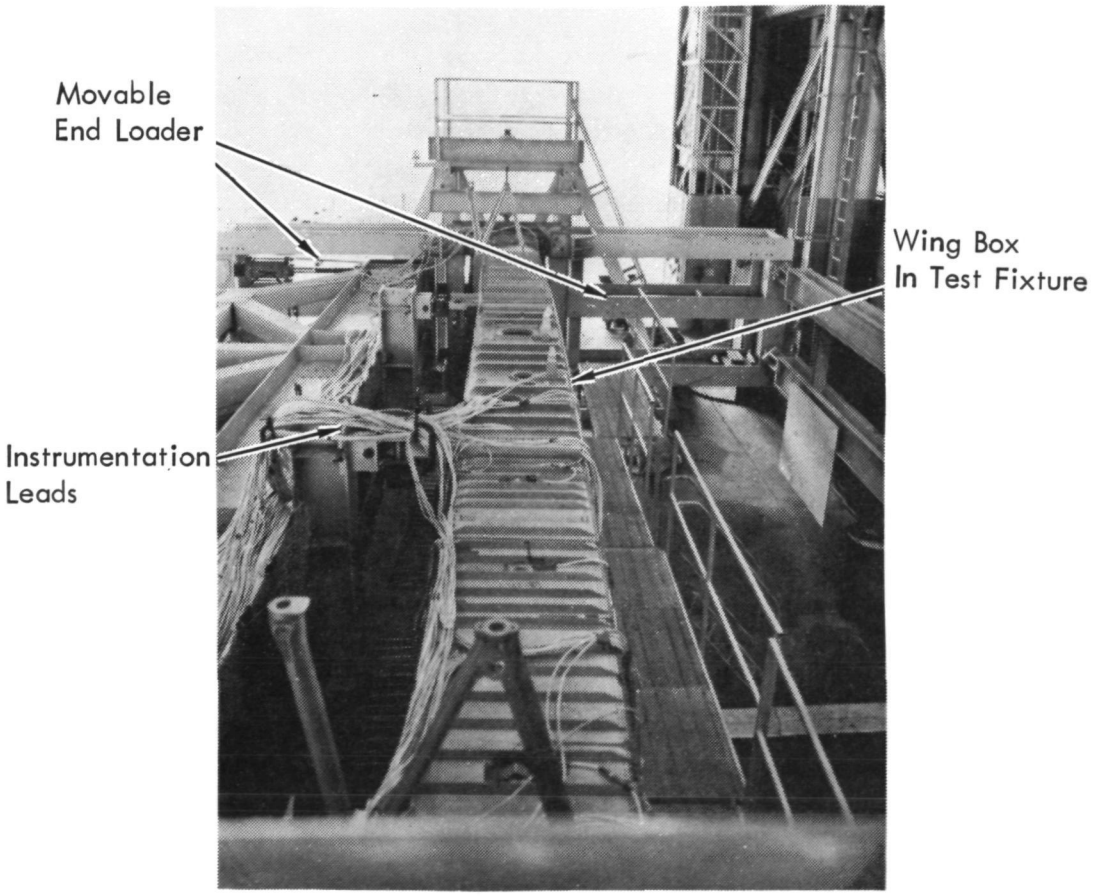

FIGURE 2 - LIMIT LOAD DOWNBENDING TEST

Upon ultrasonically and visually inspecting the wing test article, it was successfully fatigue tested for four lifetimes. Four lifetimes consist of forty load passes. After each load pass in the test spectrum, the wing test article was visually inspected and the bondline areas containing suspected disbonds were ultrasonically inspected. Also, the wing test article was thoroughly ultrasonically and visually inspected after each lifetime. During the course of cycling the test article, several fasteners failed in the wing station 220 region near the ends of the test article but remote from the boron-epoxy laminates. The fastener failures were attributed to a local condition produced by stiff shear loading members in the test fixture. The failures were considered to be minor, and failed fasteners were replaced with repair fasteners after which cycling was continued. In the last cyclic load pass of the fourth lifetime of the fatigue test (i.e., 99.7 percent complete), two cracks were detected in the front beam web of the test article. Both cracks were located in the vicinity of the wing-fuselage frame intersection at the edge of the beam web attached to the lower front beam cap. The fourth lifetime of fatigue cycling was completed without repair of the cracks after they were judged as not being detrimental to completion of the test. After thoroughly inspecting the wing test article and repairing the cracked area in the front beam web, the test article was proof loaded for the limit load upbending condition for the second time. Then the wing test article was artificially damaged at twelve locations. The artificial damage consisted of sharpened saw cuts in the wing surface planks and disbonding of the ends of boron-epoxy laminates from the wing surface planks. A crack growth test was conducted on the damaged test article using the same load spectrum used in the fatigue test. During the crack growth test, the crack propagation in the wing surface plank and the attached hat-section stringer at W.S. 120, left and right, reached such proportions that crack initiation in the adjacent wing surface plank was likely. Repairs were made to the hat-section stringer only and a third upbending proof load was successfully applied to the wing test article. The hat-section stringer repairs were removed and the wing test article was static tested to 133 percent design limit load at which the test was suspended because the stroke on a major hydraulic loading jack was exhausted.

Ground vibration tests were conducted on C-130H (Serial No. AF73-01592) aircraft on which the first composite-reinforced center wing was installed. The purpose of these tests was to verify that existing C-130 aircraft flutter speeds had not been affected by the wing modification. One set of measurements was taken with shakers mounted at each wing tip and another set taken with the shakers mounted at the aft end of each external fuel tank. Plots of output acceleration versus frequency were made to identify the resonant frequencies. The resonant frequencies obtained from these vibration tests were compared with similar results from an aircraft with an all-metal center wing. It was concluded from the comparative results that the vibration characteristics of the aircraft with the composite-reinforced center wing are essentially the same as those for the aircraft with the all-metal center wing.

Flight acceptance tests were conducted on both C-130H aircraft on which the composite-reinforced center wings were installed. After pre-flight functional tests, flight tests were conducted which consisted of the normal flight activities associated with delivery of C-130H aircraft to the United States Air Force. No specific problems associated with the composite-reinforced center wings occurred in either of the C-130H aircraft during the flight acceptance tests. Upon delivery of the first C-130H having a composite-reinforced center wing, one and a half lifetimes of fatigue loads had been applied to the ground test article.

A reliability and quality assurance program was continued in accordance with the approved program plan. The reliability assessment at the end of Phase III showed that a high degree of hardware conformance to detail design had been achieved. No disbond propagation was detected in four lifetimes of fatigue testing and approximately one and a half years of flight evaluation of two composite-reinforced center wing boxes.

2.0 INTRODUCTION

Application studies and Advanced Development tests (References 4 and 1, respectively), conducted for NASA by Lockheed, have shown that boron-epoxy composite laminates bonded to the skin and stiffeners of the C-130 aircraft center wing box can significantly improve the overall fatigue endurance of the structure, at a lower weight than that possible if metal reinforcements were used to achieve the same endurance levels. These advantages are being demonstrated by designing, fabricating, and testing three boron-epoxy reinforced C-130E center wing boxes, in a five-phase program extending over 5 1/2 years. The program phases and associated schedules are illustrated in Figure 3. Phases I, II, III, and IV have been completed. Documentation of activities is included in this report and in References 1 through 3.

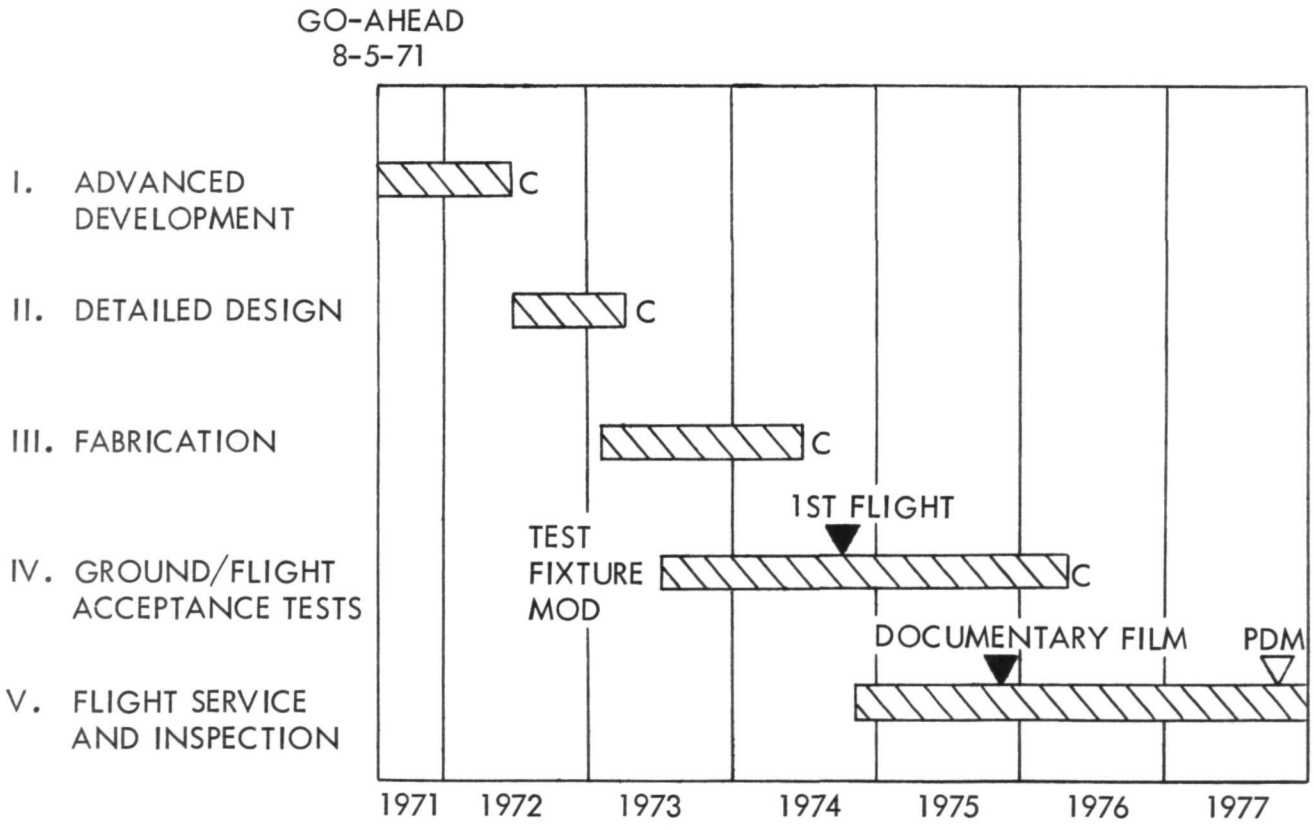

FIGURE 3 - PROGRAM SCHEDULE

The center wing box size and location in the C-130 aircraft are illustrated in Figure 4. It is 11.2 m (440 in.) in length, 2.03 m (80 in.) in chord and, in the all-metal configurations, weighs approximately 2243 kg (4944 lb.). The center wing box consists of upper and lower surfaces that are reinforced with hat-shaped stringers, the forward and aft wing beams, and truss-type ribs. The all-metal wing box configuration is illustrated in Figure 5.

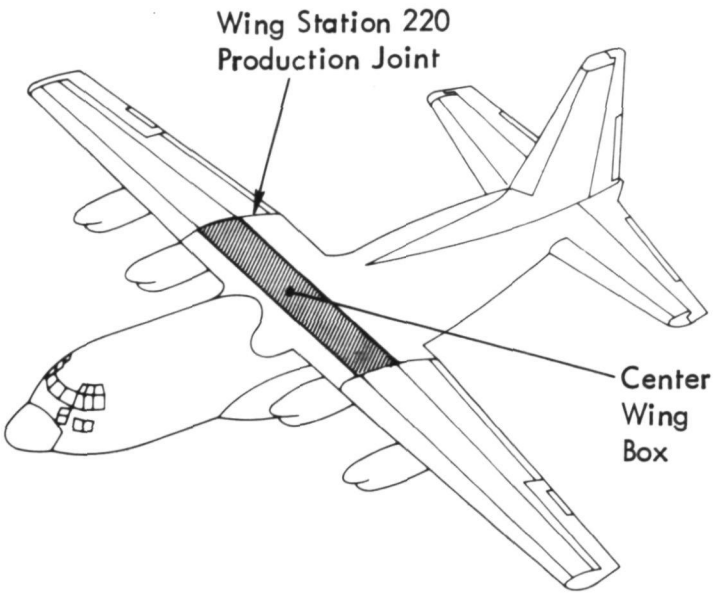

FIGURE 4 - C-130 CENTER WING BOX LOCATION

1. UPPER SURFACE PANELS
2. UPPER SURFACE STRINGERS
3. UPPER SURFACE RAINBOW FITTING
4. LOWER SURFACE PANELS
5. LOWER SURFACE STRINGERS
6. LOWER SURFACE RAINBOW FITTING
7. FRONT BEAM
8. REAR BEAM

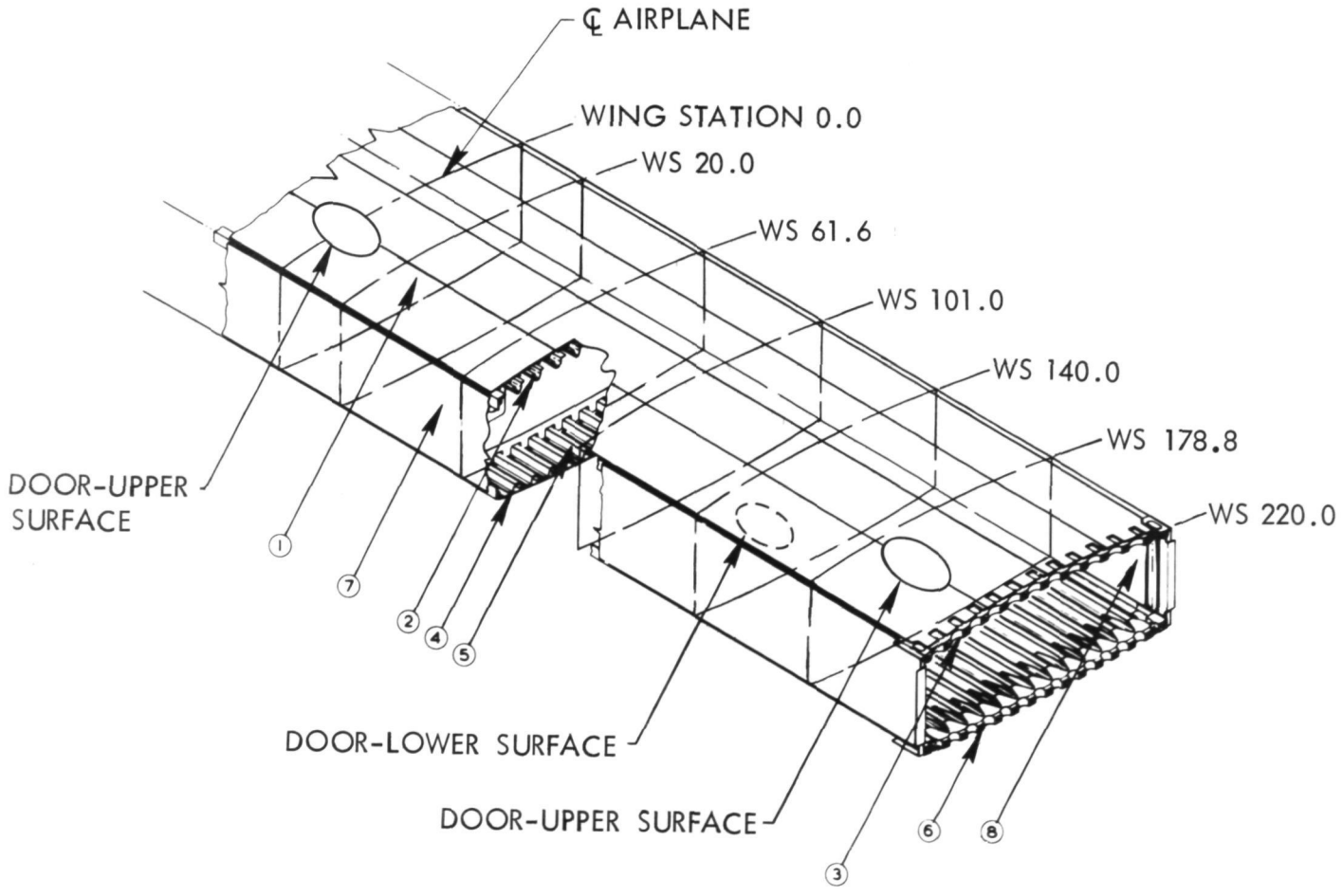

FIGURE 5 - MODEL C-130B/E CENTER WING BOX

During Phase I, the advanced development work necessary to support detailed design of a composite-reinforced C-130 center wing box was conducted. Activities included the development of a basis for structural design, selection of materials and processes, manufacturing and tooling development, and fabrication and test of full-scale portions of the center wing box. The Phase I results further confirmed that, with boron-epoxy reinforcements as shown in Figure 6, equivalent static strength and fatigue endurance could be provided with a significant weight savings. The aluminum skins and stringers have thicknesses less than those of the existing metallic center wing box in Model C-130B/E aircraft. Equivalent strength is provided by the unidirectional boron-epoxy composite.

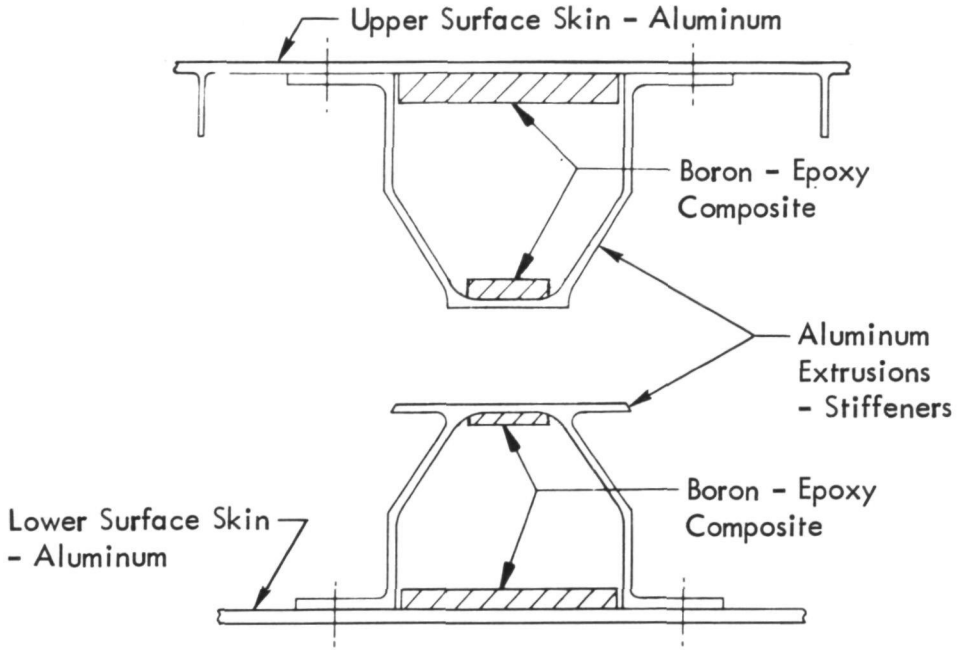

FIGURE 6 - COMPOSITE REINFORCEMENT CONCEPT

Phase II activities consisted of preparing detailed design drawings and conducting the substantiating static strength, fatigue endurance, flutter, and weight analyses required for proceeding into Phase III wing box fabrication. Some additional component testing was conducted to complete the panel buckling evaluation and to evaluate specific local design concepts. Tooling development activities were continued to further refine the "cool tool" concept and to evaluate residual stresses with full-length skin panels and stringers. The final design configuration is structurally and functionally interchangeable with the production C-130B/E wing box.

In Phase III, fabrication and assembly of three composite-reinforced center wing boxes were completed. The first of the wing boxes was fabricated for ground testing. After a joint USAF-NASA-Lockheed configuration review, the remaining two center wing boxes were released for installation in two Air Force C-130H aircraft to be flight

evaluated in regular operational service by the Military Airlift Command. During fabrication and assembly of the composite-reinforced center wing boxes, thorough visual and ultrasonic inspections were conducted by Lockheed and Air Force inspectors to assure that the final product was of high quality. In addition, the reliability and quality assurance program continued in Phase III concluded that a high degree of hardware conformance to detail design was achieved.

During Phase IV, reported herein, the ground and flight acceptance tests were completed. The ground tests consisted of proof load tests, a fatigue test, a crack growth test, and a residual strength test on the composite-reinforced wing box test article. Also, the first wing box to be flight evaluated was ground vibrated for comparison of resonant frequencies with those of the all-metal production wing boxes. The purpose of the ground vibration tests was to establish that existing C-130 aircraft flutter speeds had not been affected by the wing modification. Also, flight acceptance tests were conducted on both C-130 aircraft on which the composite-reinforced center wings were installed. Detailed inspections of these two composite-reinforced wing boxes, including the use of sophisticated nondestructive test techniques, are scheduled to coincide with regular USAF isochronal aircraft inspections, and will be conducted in Phase V.

3.0 ACCEPTANCE/VERIFICATION TESTS

Both acceptance and verification tests were accomplished during Phase IV of this program to establish structural adequacy of the C-130H composite-reinforced center wing boxes. Both static and fatigue tests were conducted on the first of the three C-130H composite-reinforced center wing boxes. The static tests consisted of proof loading the center wing box for both design limit upbending and downbending load conditions. Upon completion of the proof load tests and ultrasonically inspecting the wing box, it was fatigue tested for four lifetimes. The fatigue test spectra applied was that used for the C-130 B/E wing fatigue tests. Upon completing each pass in the fatigue test spectrum, the areas of the composite-reinforced bondlines having disbonds and/or voids were ultrasonically inspected to establish if any growth occurred during that pass. Also, upon completion of each lifetime, the wing box internal and external surfaces were visually inspected, and all of the composite-reinforced bondlines were ultrasonically inspected.

A ground vibration test was conducted on the C-130H aircraft, Serial No. AF73-01592, on which the first composite-reinforced center wing box was installed. The objective of this test was to establish any significant differences in wing vibration mode shapes and frequencies compared to those of the production all-metal wings.

Flight acceptance tests were conducted on the two C-130H aircraft on which the composite-reinforced center wing boxes were installed. These flight tests were accomplished by both Lockheed and Air Force flight crews and they were conducted using the same procedures performed in flight acceptance tests on all C-130 airplanes delivered to the United States Air Force.

3.1 COMPOSITE-REINFORCED CENTER WING BOX STATIC AND FATIGUE TESTS

Prior to initiation of the static and fatigue tests, a test plan for conducting these tests was prepared and submitted to NASA Langley Research Center and Warner Robins Air Logistics Command for review and approval. Approvals were granted prior to proceeding with the static and fatigue tests of the composite-reinforced center wing box. The following is a list of the more significant areas included in the test plan.

- Test article preparation and instrumentation
- Test article fixture description and modification
- Load control system
- Upbending and downbending proof tests
- Fatigue test
- Residual strength test
- Test article inspections
- Documentation and reporting

The first composite-reinforced center wing box that was manufactured was proof loaded, fatigue tested, and residual strength tested. Overall span of the center wing boxes that were ground tested and flight service evaluated was 11.18m (440 in.). The center wing box relative size and location in the aircraft are illustrated in Figure 7.

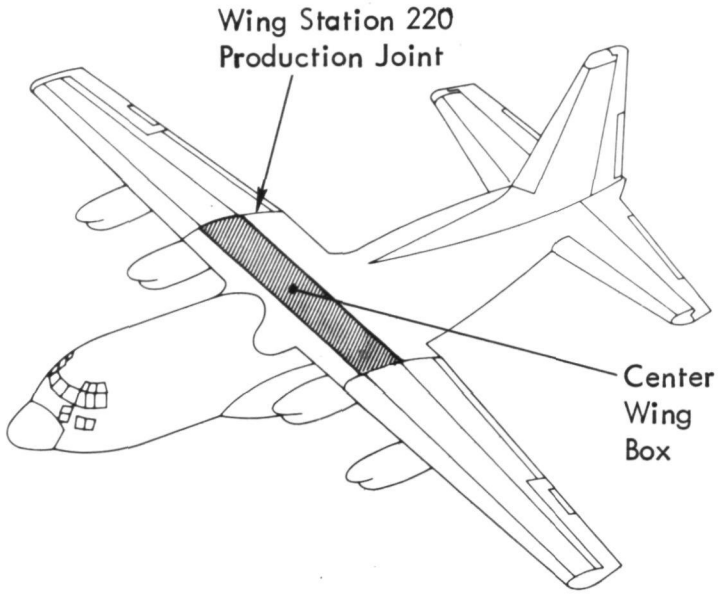

FIGURE 7. - C-130 CENTER WING BOX LOCATION

The wing box extended spanwise from the left wing station 220 (W.S. 220L) to the right wing station 220 (W.S. 220R). The chord of the wing box section was approximately 2.03 m (80 in.). The wing box that was static, fatigue, and residual strength tested was structurally complete but did not include the leading and trailing edge sections. Also, non-structural brackets and hangers that are used to support the electrical, hydraulic, and pneumatic systems were not installed. Structurally, the wing box test article was identical to the two composite reinforced wing boxes installed on the C-130H operational aircraft.

The wing box test article was installed in the test fixture in which the following tests were conducted.

1. Upbending Proof Load Test
2. Downbending Proof Load Test
3. Fatigue Test
4. Residual Strength Test

Detail descriptions and results from the above tests are presented in subsequent sections of this report.

3.2 TEST FIXTURE AND EQUIPMENT

A special fixture for static and fatigue testing C-130 center wings was designed, fabricated, and used by Lockheed under a previous NASA contract (Reference 6). This special fixture was modified in this program for conducting the static and fatigue tests. The basic design of this special fixture facilitated the application of wing bending moments and shear loads at each end of the test article, W.S. 220R and W.S. 220L, which was reacted by balancing forces at W.S. 61R and W.S. 61L. Wing torsional loads was accomplished by applying variable loads by the wing shear loading actuators. Figure 8 is a simplified illustration of the test fixture arrangement.

Modification including several repairs were accomplished on the special fixture for improvement of the test operations and satisfaction of requirements of this program. The repairs involved replacement of several wing test article attachment blocks at W.S. 220 joints, left and right, as shown in Figure 9.

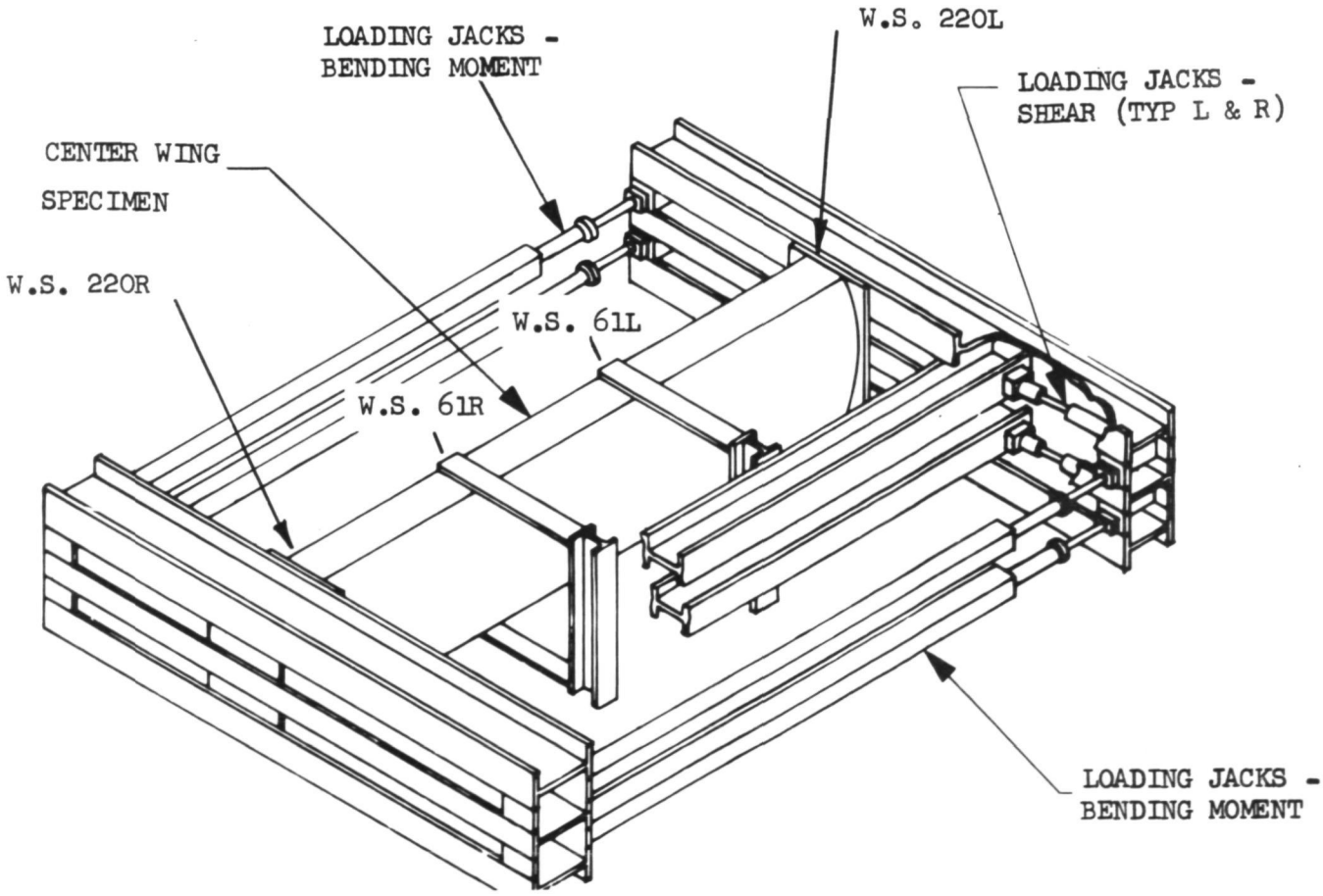

FIGURE 8. - FIXTURE FOR STATIC AND FATIGUE TESTS OF COMPOSITE-REINFORCED WING BOX

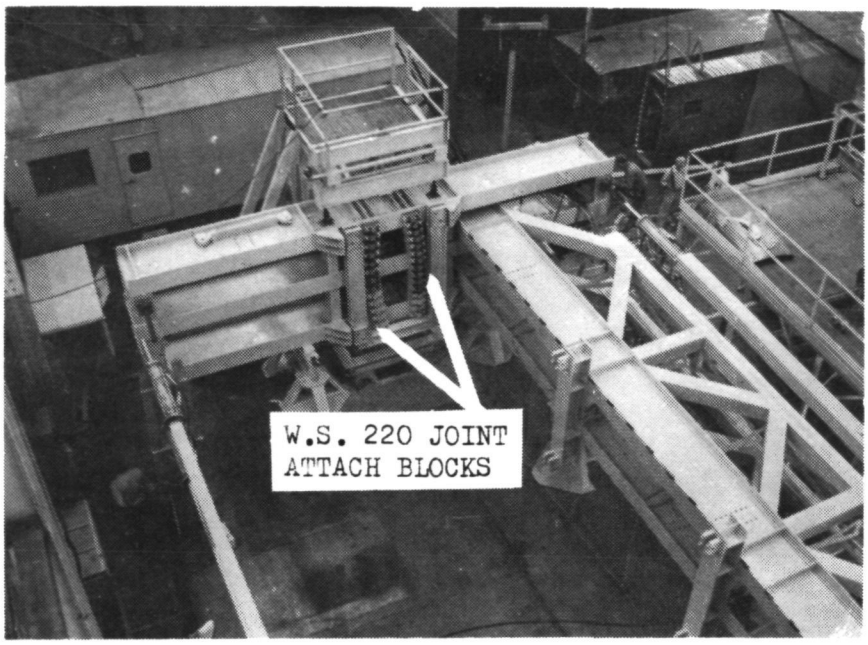

FIGURE 9. - PHOTOGRAPH OF TEST FIXTURE SHOWING SIMULATED OUTER WING FITTING ATTACHED TO ONE END-LOADER

The end loaders of the test fixture were attached to each end of the wing test article for all tests, and are connected by bending moment load frames as depicted in Figure 10. Application of a tension load in the bending moment load frame and a compression load in the other frame resulted in a constant bending moment applied to the wing test article.

Figure 11 illustrates the test fixture with the shear load frame installed. In this illustration one of the bending moment load frames has been omitted for clarity. Shear loads were applied to the wing test article by shear load actuators which were attached to the end-loader at one end and to the ends of the shear load frame at the other. The shear load frame was attached to the wing test article by two dummy wing sticks on each wing spar. In this arrangement, the shear load actuators applied shear loads at the W.S. 220 joint, and it was reacted through the dummy wing sticks. Application of torsional loadings to the wing test article was accomplished by loads of different magnitudes by the forward and aft shear load actuators. The shear load frame was movable for prevention of development of secondary loads in the test article due to test article deflection.

Figure 12 shows a top view of the completed test fixture prior to installing the wing test article, and Figure 13 is a similar view with the wing test box installed in the test fixture.

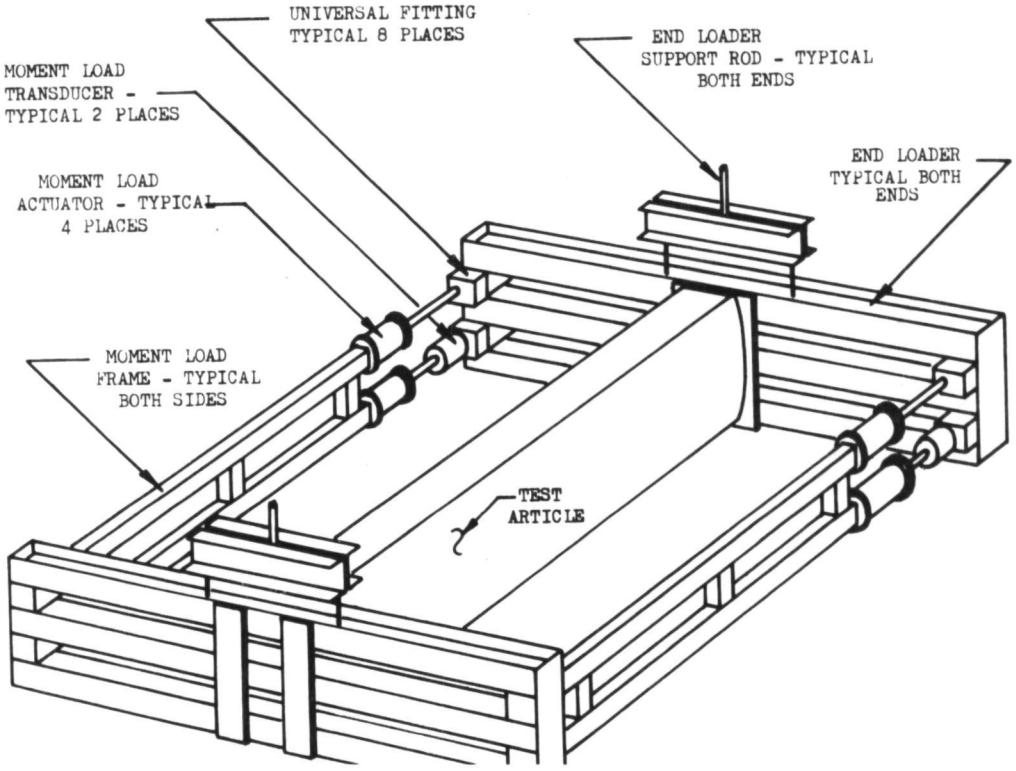

FIGURE 10 - ILLUSTRATION OF TEST FIXTURE ASSEMBLY FOR APPLYING BENDING MOMENT TO THE TEST ARTICLE

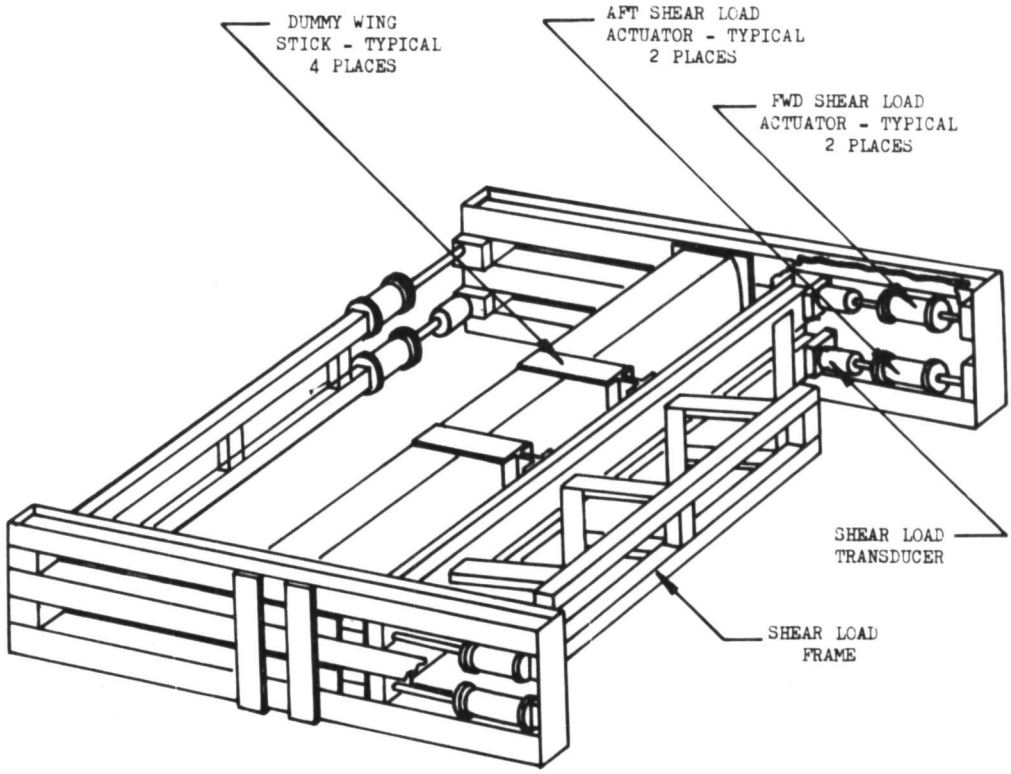

FIGURE 11 - ILLUSTRATION OF TEST FIXTURE WITH SHEAR LOAD FRAME IN PLACE - ONE MOMENT LOAD FRAME HAS BEEN OMITTED FOR CLARITY

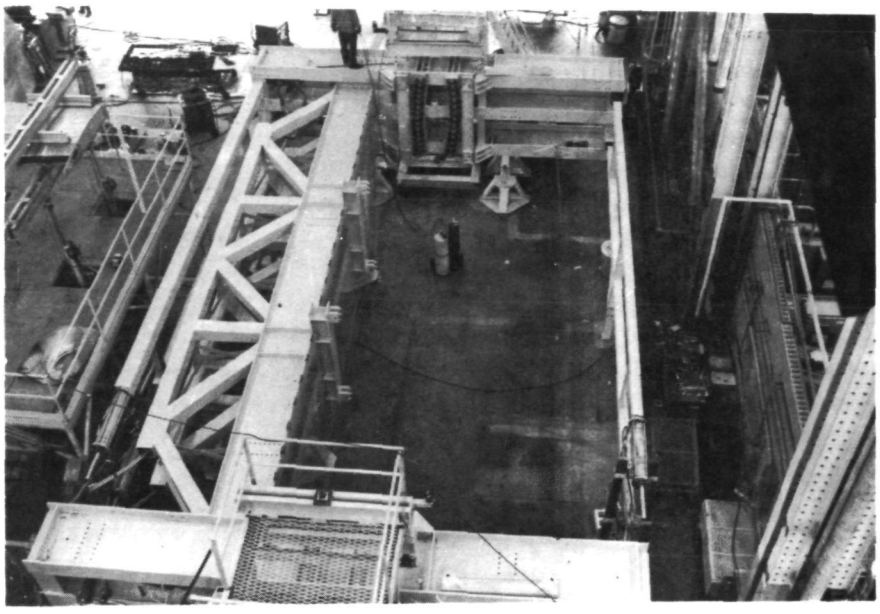

FIGURE 12 - TEST FIXTURE PRIOR TO WING BOX INSTALLATION

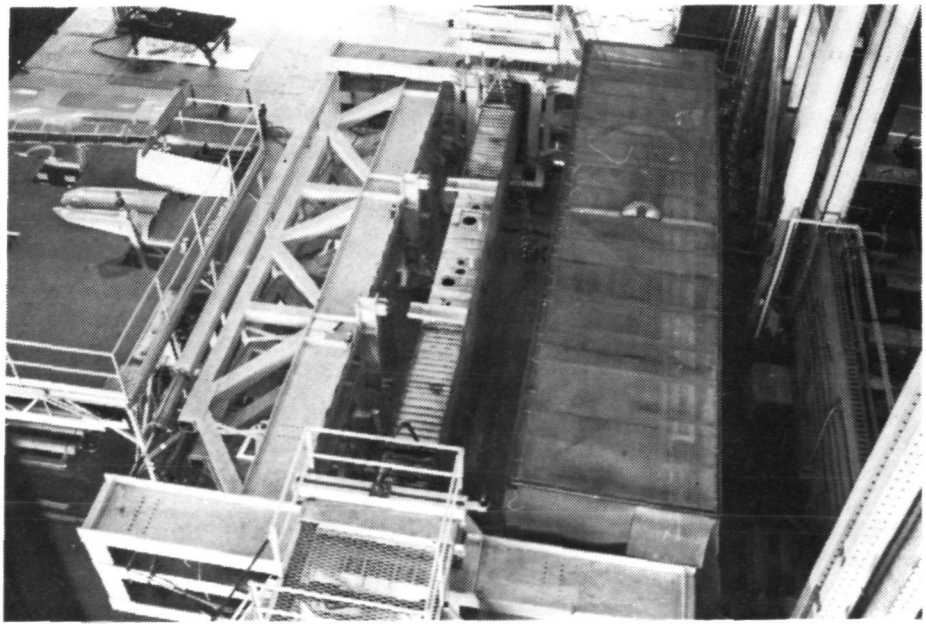

FIGURE 13 - WING BOX INSTALLED IN TEST FIXTURE

3.3 PREPARATION OF THE COMPOSITE-REINFORCED CENTER WING BOX FOR TESTING

Preparations for the composite-reinforced center wing test article were mainly comprised of applying strain gage instrumentation and assembling simulated fuselage attachment structure to the ends of the front and rear beams. Simulated fuselage attachment structure was installed on the front and rear beams at W.S. 61R and W.S. 61L. A typical installation is shown in Figure 14. During the test, shear loads were reacted through the simulated structure similarly to that in the actual airplane installation.

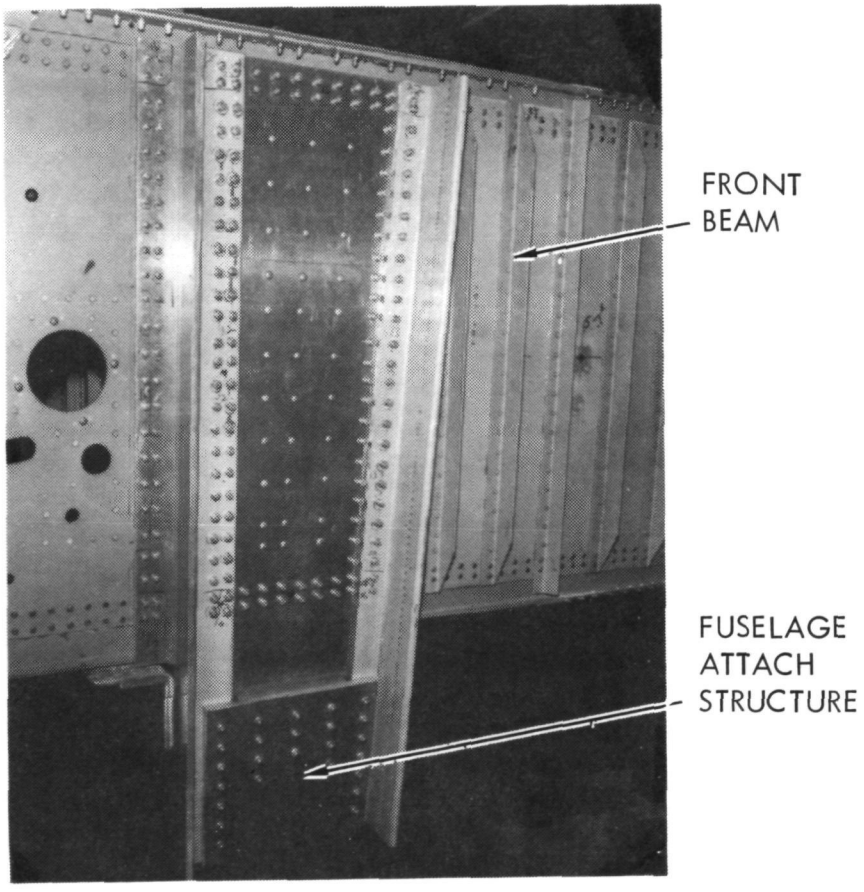

FIGURE 14 - TYPICAL INSTALLATION OF SIMULATED FUSELAGE ATTACHMENT STRUCTURE ON FRONT BEAM OF TEST ARTICLE

The test article was instrumented with a mixture of axial, shear and rosette electrical resistance strain gages. Strain gage locations are shown on Figures 15 through 19, and a photograph of the major portion of the instrumented upper wing surface is shown in Figure 20. Initially, 199 channels were installed but, since many of the channels required "back-up" strain gages to cancel bending strains, 337 gage elements were required to provide the 199 channels. The primary data acquisition system was a 200-channel B&F Model SY156 shown in Figure 21.

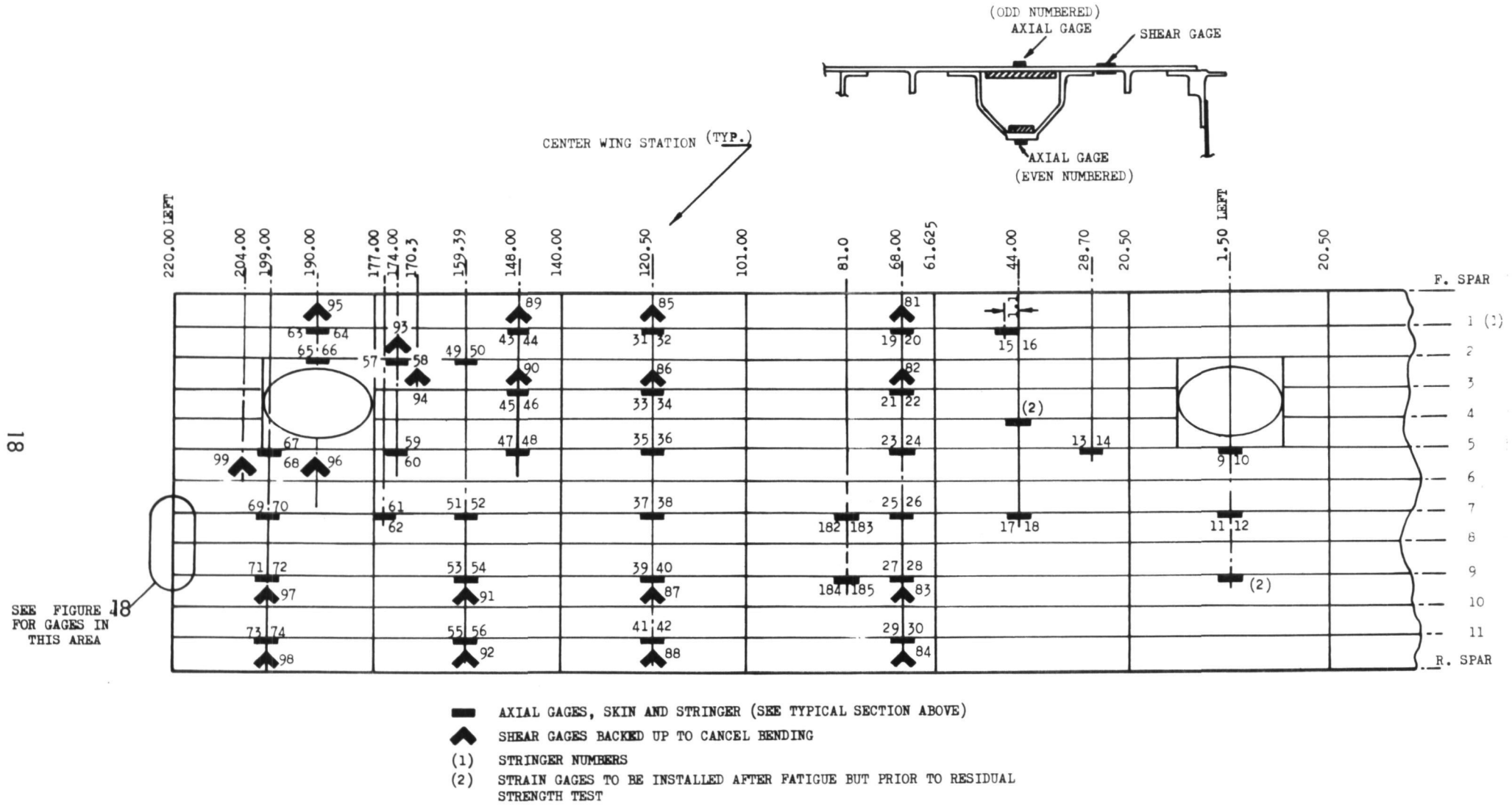

FIGURE 15 - STRAIN GAGE LOCATIONS FOR UPPER SURFACE

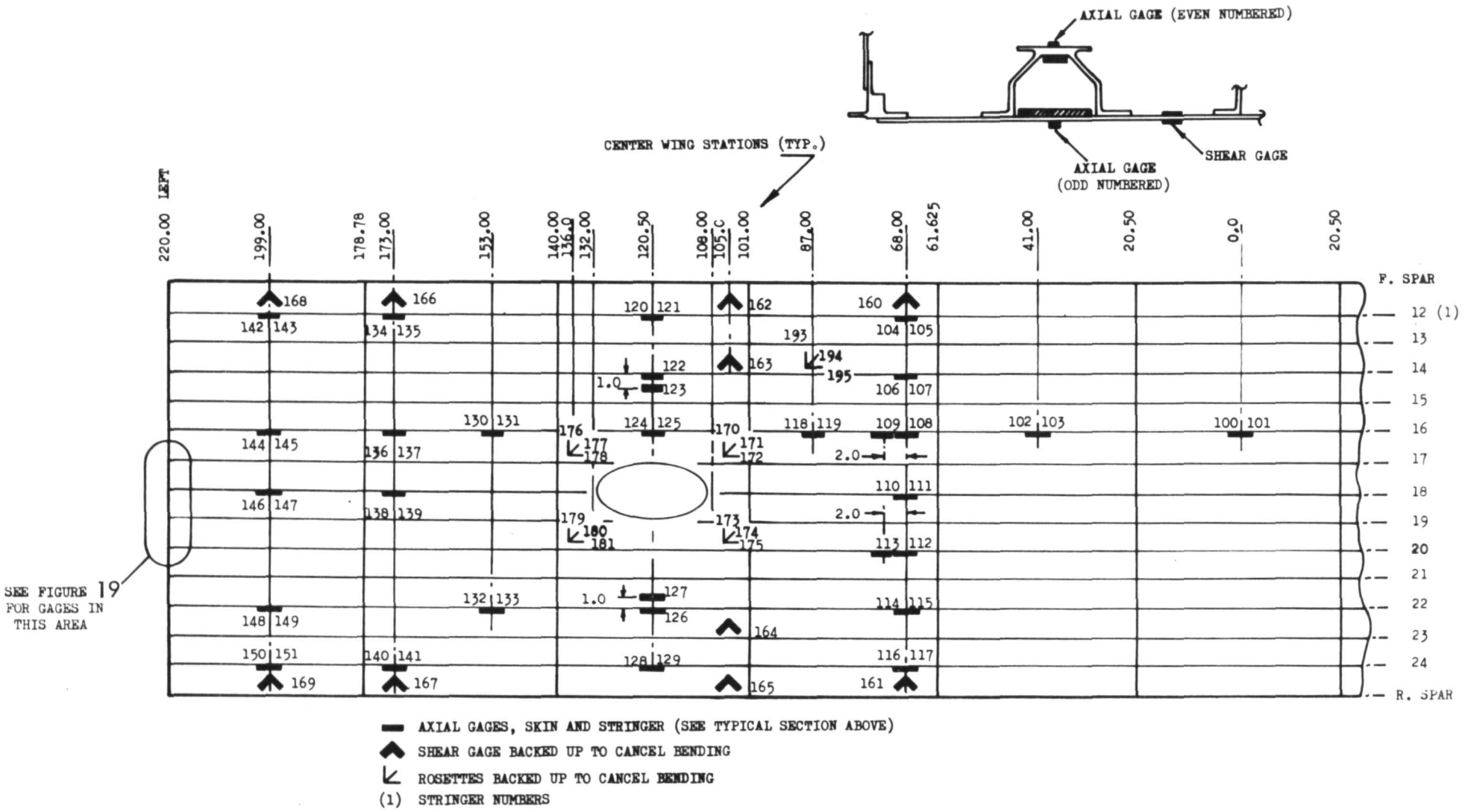

FIGURE 16. - STRAIN GAGE LOCATIONS FOR LOWER SURFACE

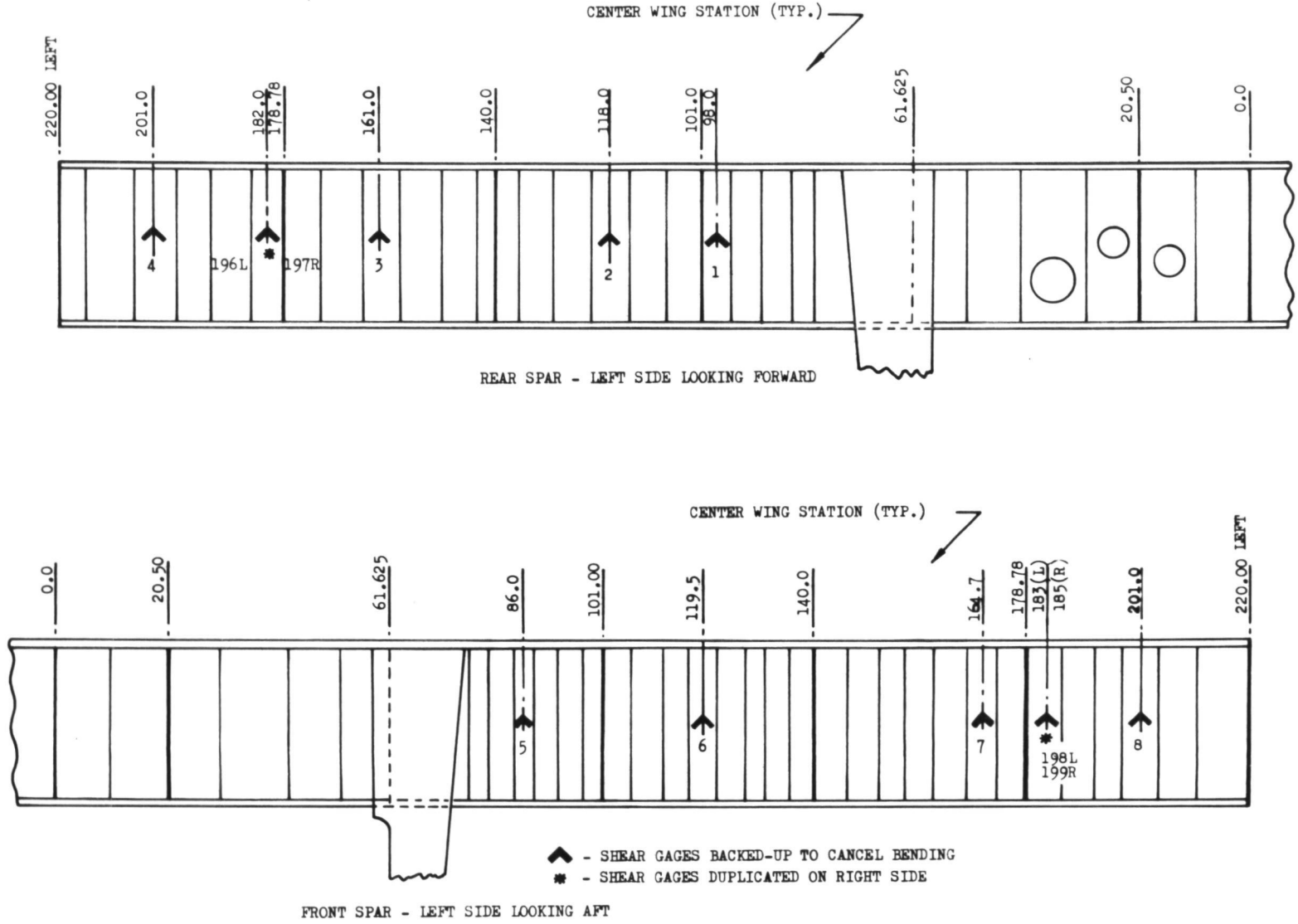

FIGURE 17. - STRAIN GAGE LOCATIONS FOR FRONT AND REAR BEAMS

CHANNEL NUMBERS

LOCATION	STRINGER NO.		
	7L	9L	7R
B	75	78	186
C	76	79	187
D	77	80	188
E	200	201	202

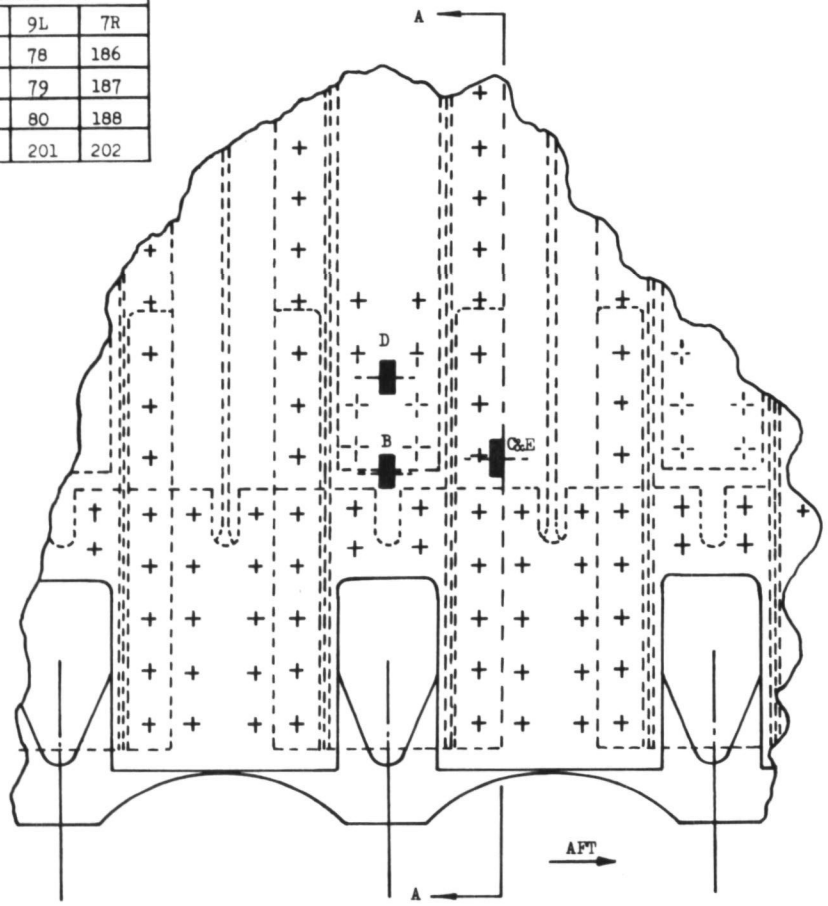

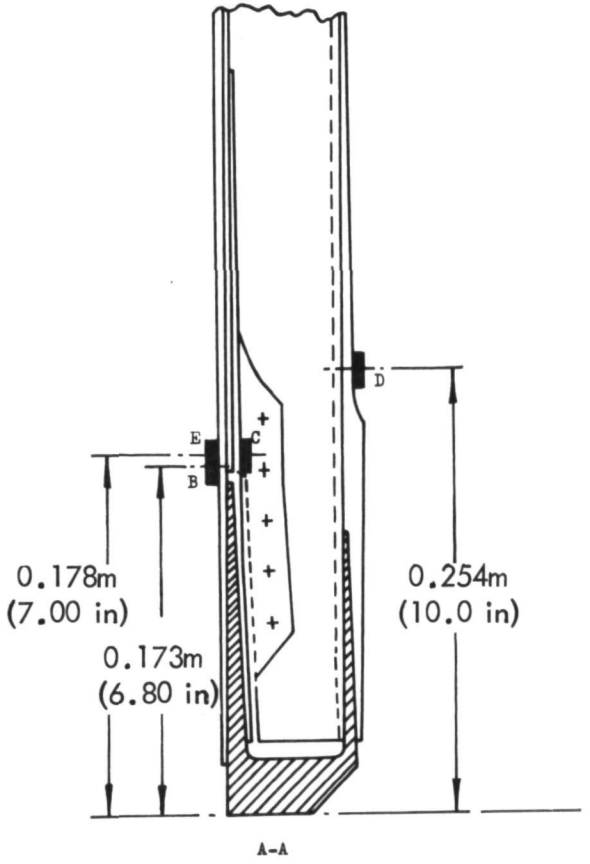

AXIAL GAGE LOCATIONS - TYPICAL FOR STRINGERS 7L, 7R AND 9L - SEE FIGURE 15

FIGURE 18. - STRAIN GAGE LOCATIONS FOR UPPER SURFACE IN VICINITY OF W.S. 220 JOINT

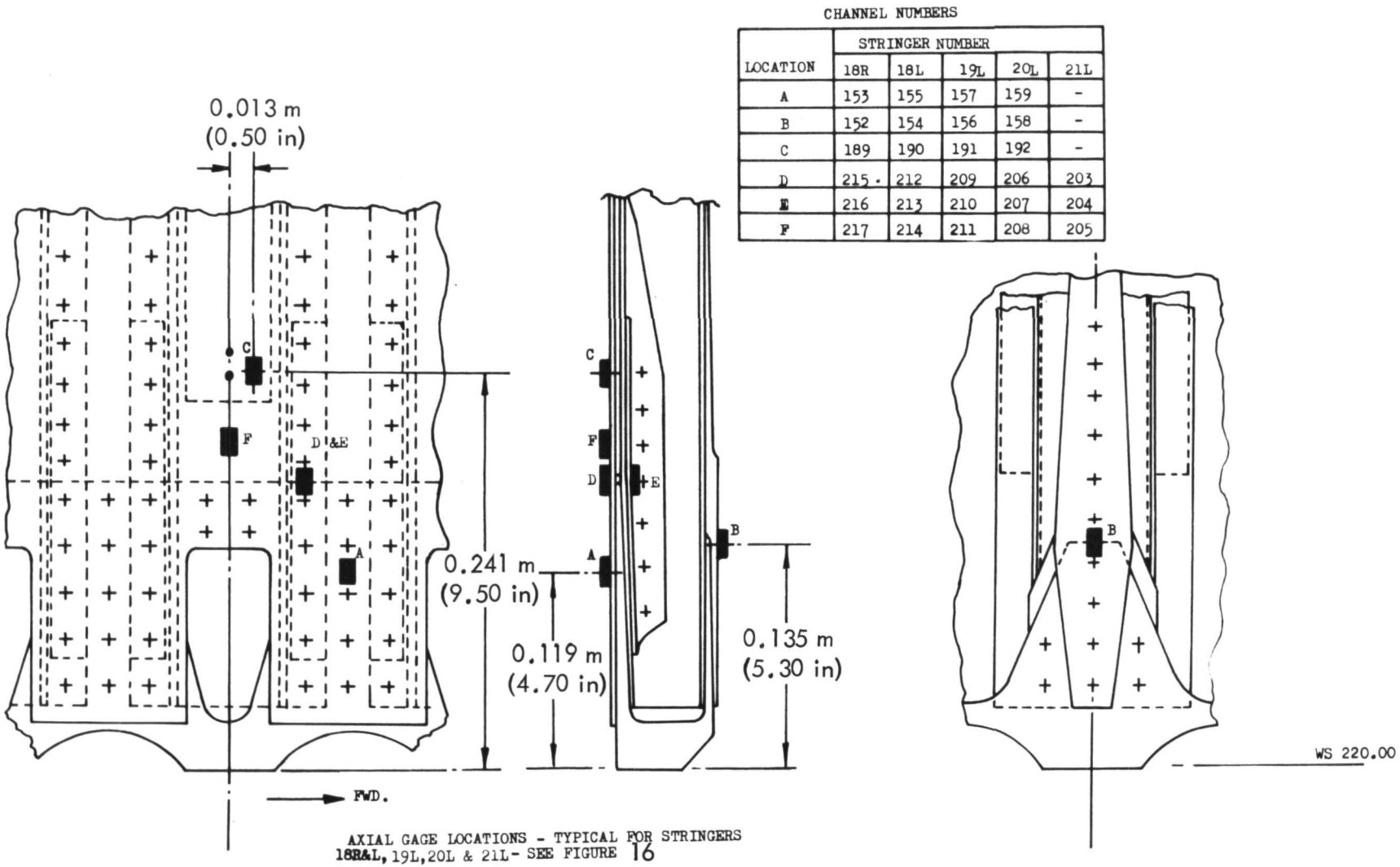

FIGURE 19. - STRAIN GAGE LOCATIONS FOR LOWER SURFACE IN VICINITY OF W.S. 220 JOINT

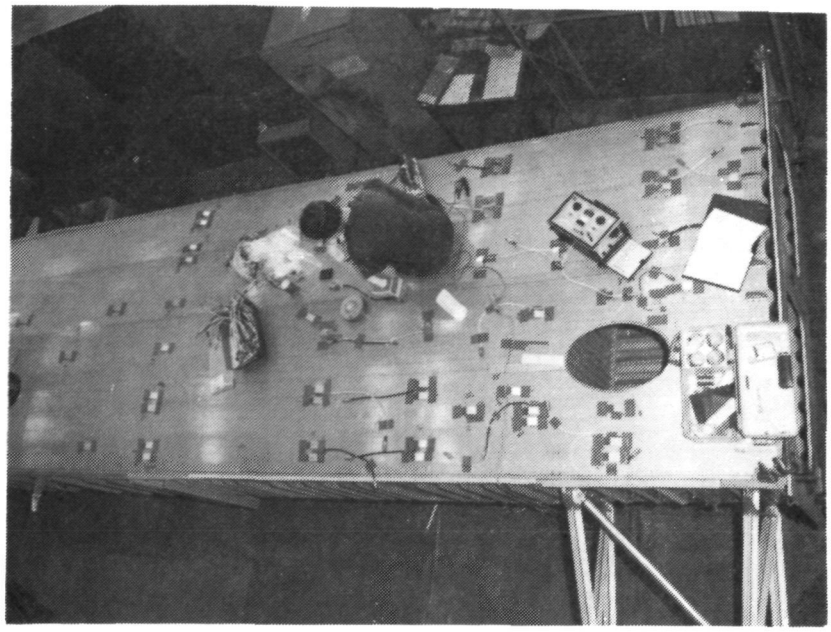

FIGURE 20. - STRAIN GAGE INSTALLATION ON TEST UNIT UPPER SURFACE

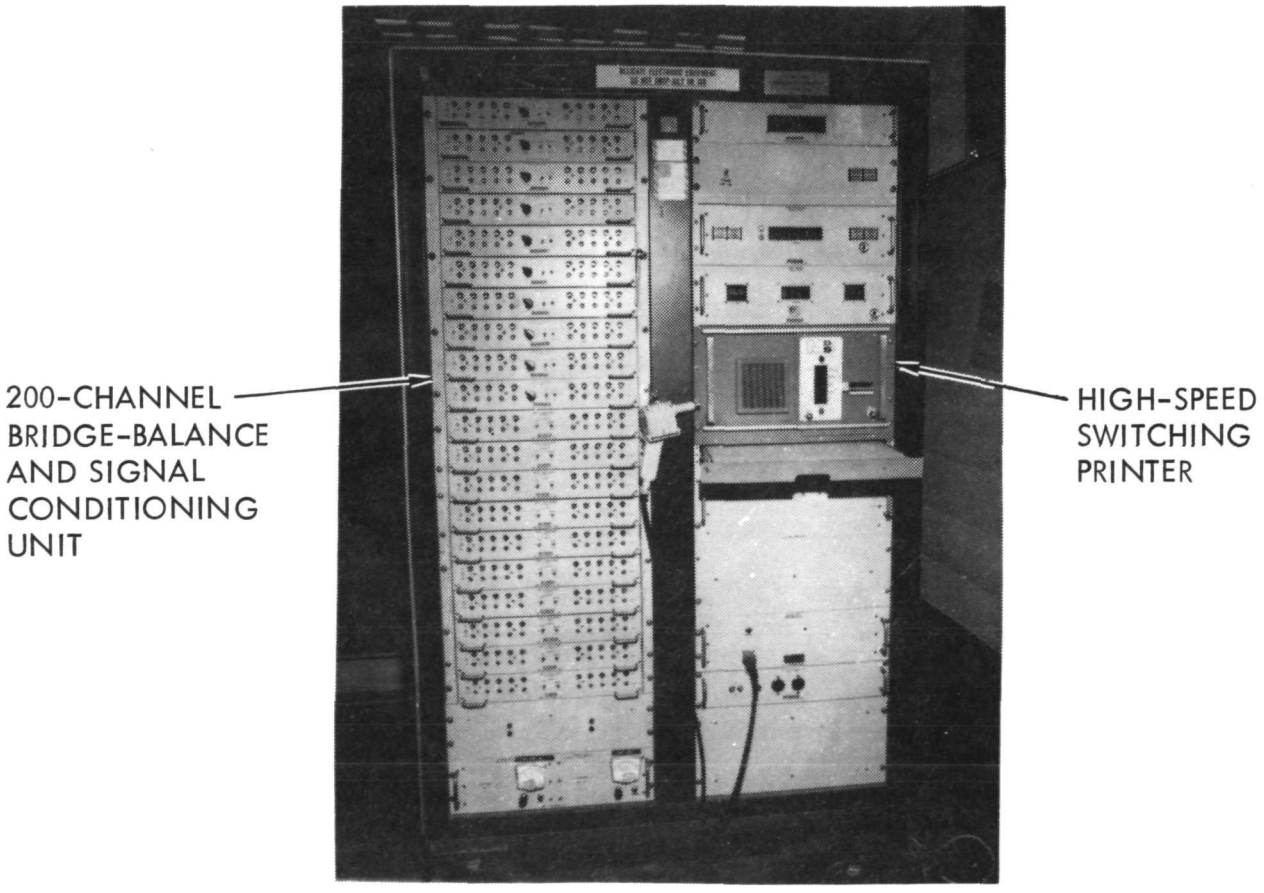

FIGURE 21. - STRAIN DATA ACQUISITION SYSTEM

3.4 TEST LOAD CONTROL AND MONITORING SYSTEM

The hydraulic actuators in the test fixture were electro-hydraulic servo controlled and hydraulic servo controlled with hydraulic power. Also, a calibrated dual bridge load transducer was located in series with each actuator in each load control channel. A photograph of the electronic equipment is shown in Figure 22, and a schematic of the load control and monitoring system is shown in Figure 23.

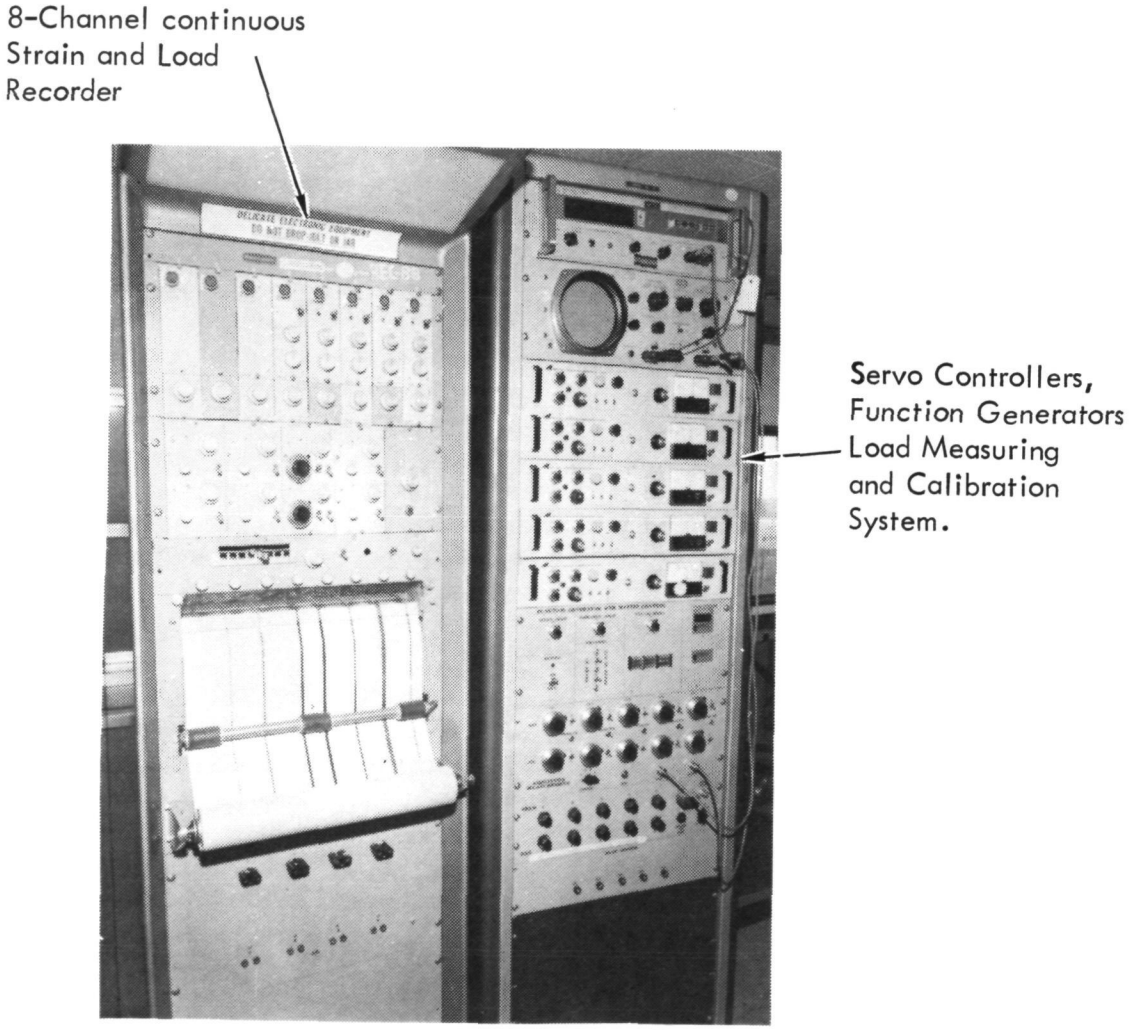

FIGURE 22. - PHOTOGRAPH OF LOAD CONTROL AND MONITOR SYSTEM

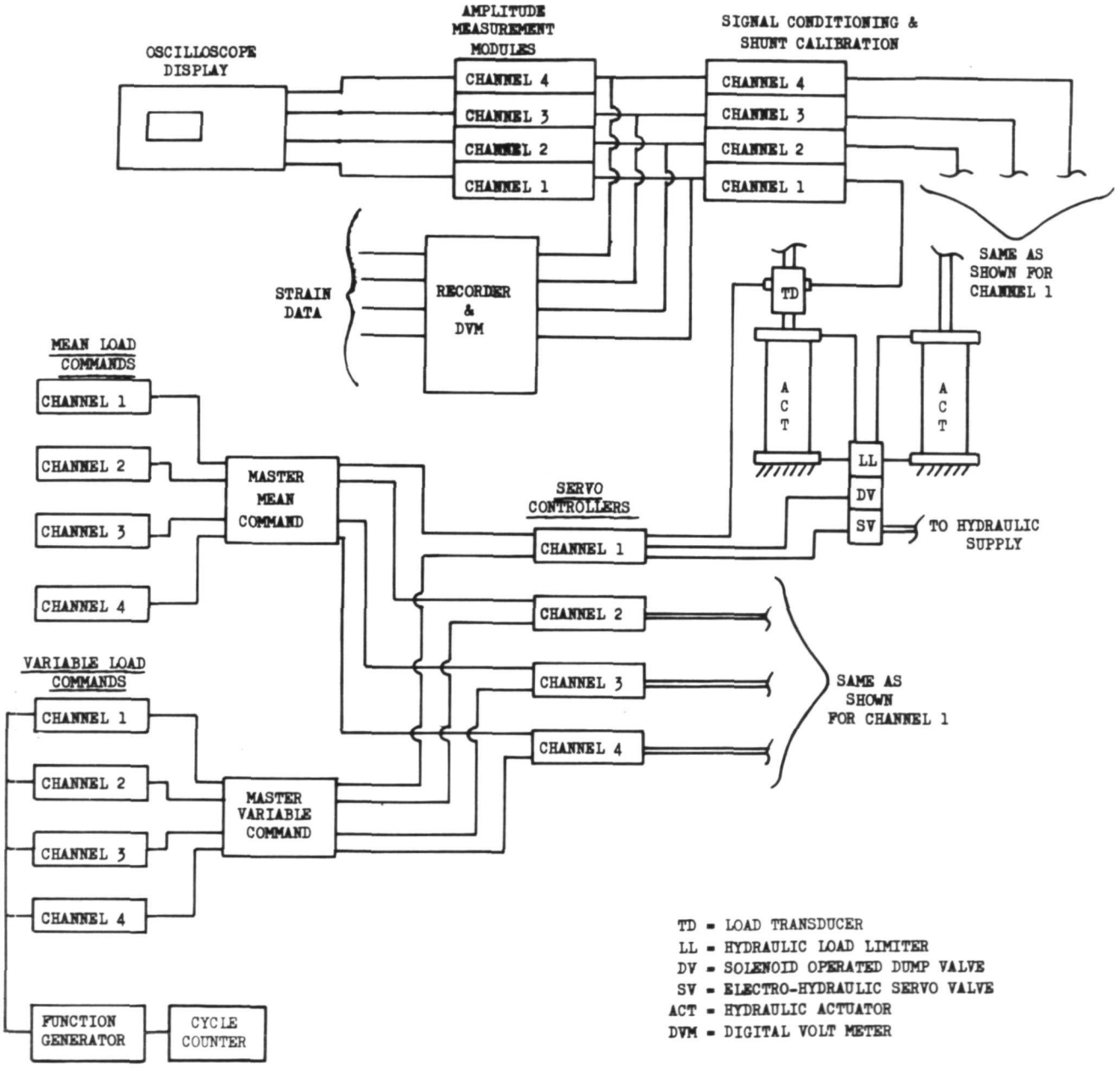

FIGURE 23. - SCHEMATIC OF THE LOAD CONTROL AND MONITOR SYSTEM

3.5 PROOF LOAD TESTS -- LOADS, TESTS, INSPECTIONS, AND EVALUATION

Proof test loads were selected for the most critical of the upbending and downbending conditions identified in the center wing structural analysis. Critical upbending and downbending load conditions were selected as the analytical conditions that produced the lowest margins of safety in the center wing structure. The selected loading cases were:

Upbending - Analysis Case 1102

This case presents the loads encountered during a symmetrical flight maneuver to a positive load factor of 2.5. The analysis represents the aircraft at maximum gross weight of 70308 kg (155,000 lbs.) with 11340 kg (25,000 lbs.) of fuel. The design condition occurs at 167 m/s (325 knots) equivalent airspeed and a 4176-meter (13,700-foot) altitude.

Downbending - Analysis Case 1134

Maximum downbending loads on the center wing are incurred during taxi conditions. The critical loads are encountered while taxiing the aircraft with capacity wing fuel and at maximum gross weight. The dynamic response of the aircraft structure to a specified lump height and shape was analyzed in detail to derive the loads.

These two loading conditions were simulated during proof loading to design limit load. As shown in Figures 24 and 25, the vertical bending moments were closely matched at the W.S. 220 structural joint and at the W.S. 68 fuselage attachment points. Between these load introduction and restraint points, the test bending moments were slightly higher than those required.

The simplified nature of the test fixture allowed application of vertical shear and torsion loads through the end-loaders only. A constant shear load was applied -- approximating the average shear across the span. Since this exceeded the required analytical shear on the outboard end of the wing box, the test torsion was adjusted to preclude local overloading of the front and rear beams. The torsional load for the test conditions was small, and this adjustment did not significantly affect the test results.

Both upbending and downbending proof load tests were satisfactorily completed. For both tests, prior to applying design limit load, preliminary strain surveys were conducted. Load was applied in ten percent increments to sixty percent of limit load, and strain data were recorded at each increment. Evaluation of these data led to the installation of several additional strain gages to provide a better definition of strain distributions in selected areas.

Following installation of additional strain gages, the upbending load test was conducted. Limit load was applied in ten percent increments, and strain data were collected at each increment. After the limit load application, the loading was relaxed to 20 percent, and strain readings were taken. A similar procedure was followed for the downbending test.

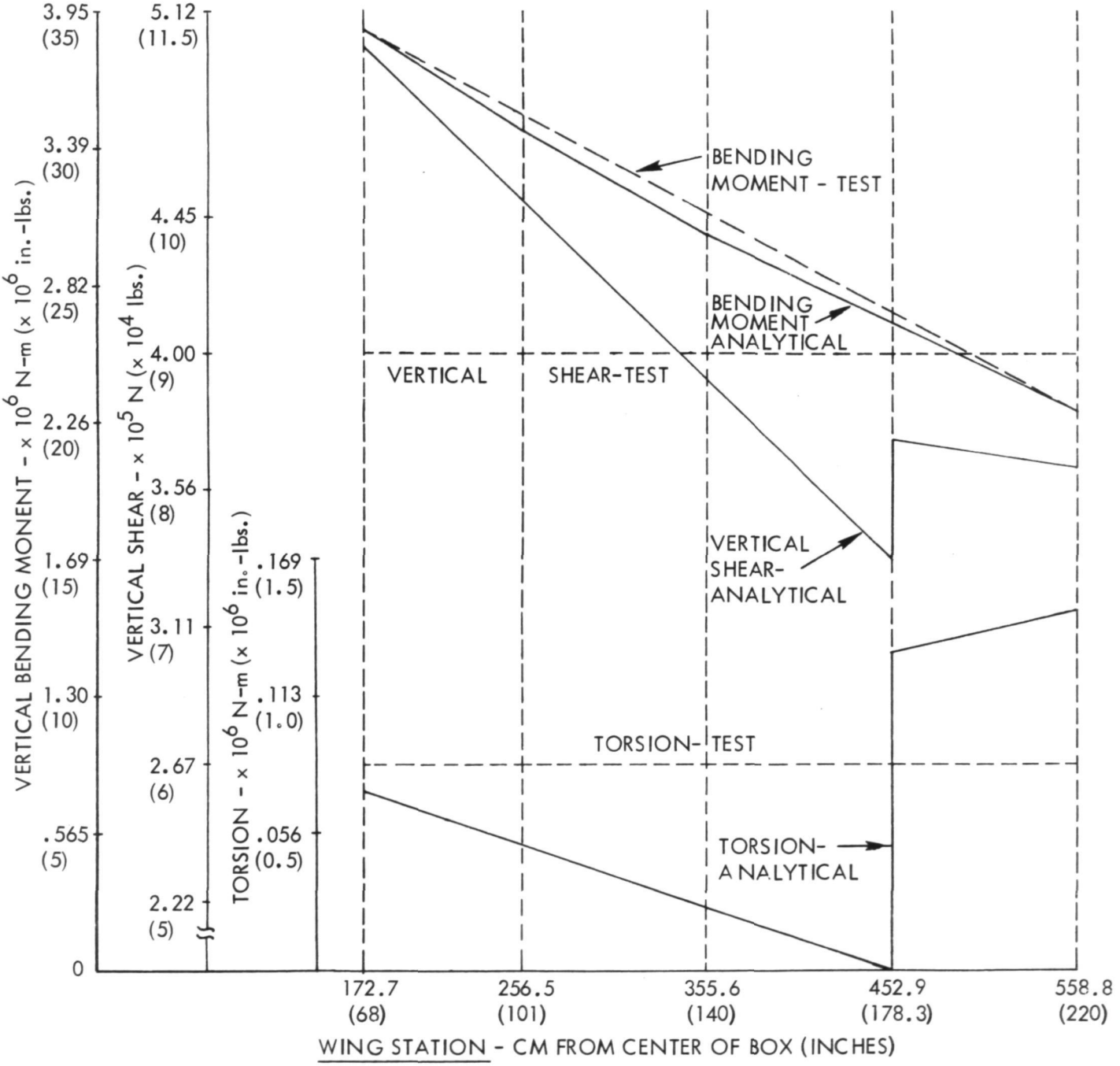

FIGURE 24. LIMIT LOAD DISTRIBUTIONS FOR UPBENDING TEST

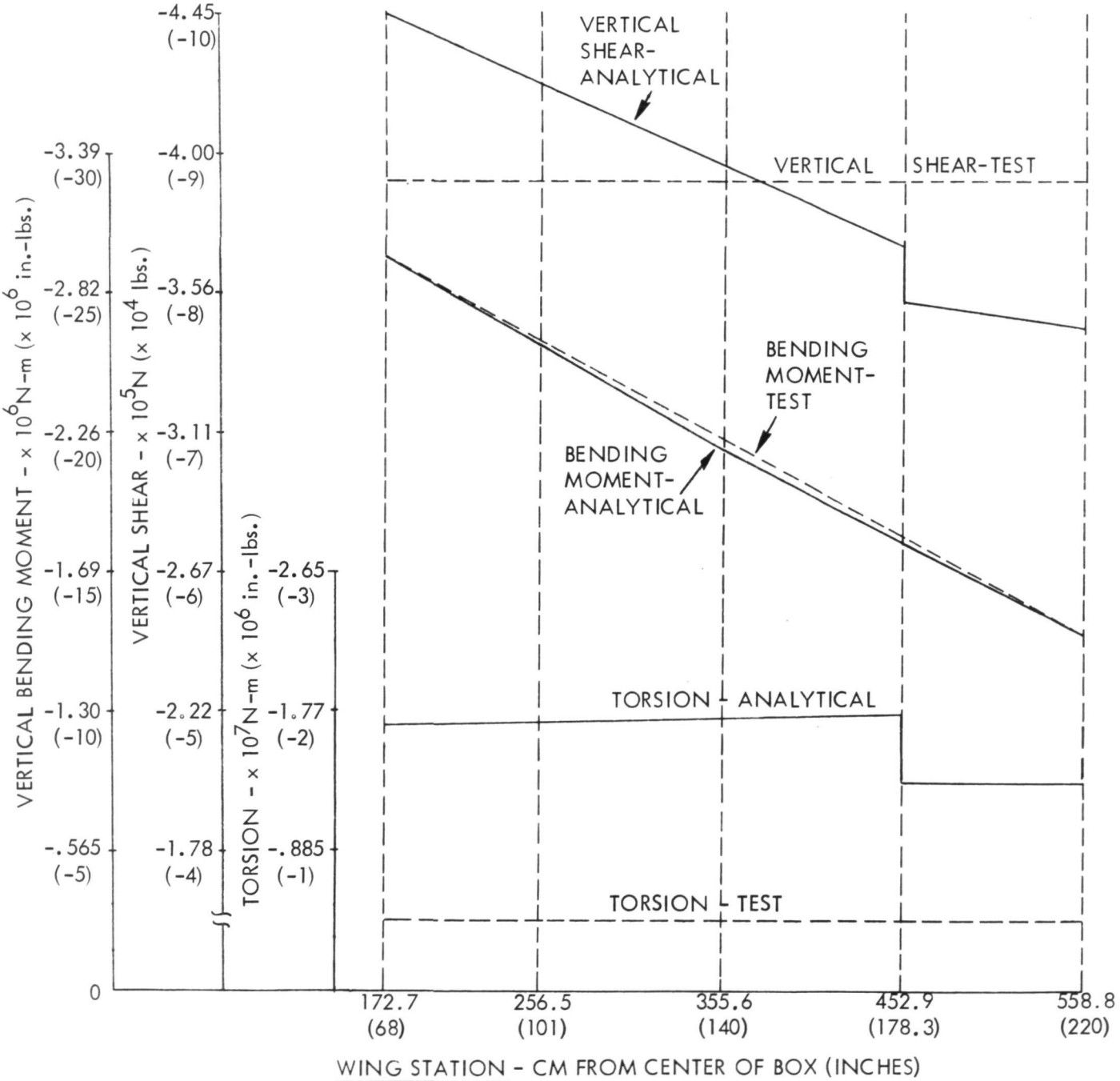

FIGURE 25. LIMIT LOAD DISTRIBUTIONS FOR DOWNBENDING TEST

While the proof loadings were successful, examination of strain data for the upbending condition indicated the desirability of a design change on the upper surface in vicinity of the W.S. 220 joints. This area of the test article was not of concern during proof loading, but rather was of concern from a local instability standpoint at design ultimate load. In general, examination of measured strains for both upbending and downbending proof load tests showed good agreement with predicted strains except in the area of the upper surface skin/stringer/rainbow fitting splice at W.S. 220. Measured strains in this area were higher than predicted and also higher than measured strains on the previously tested JE-2 component (Reference 1) which represented the same structural area. Comparisons of measured and predicted strains are shown on Figure 26. The higher strain survey and proof load test strains were attributed to the inherent differences between the centroidal locations of applied loads in the full-scale center wing box test when compared to the component test and/or analytical assumptions. Extrapolation of the measured strain data showed a need for a minor reinforcement to preclude the possibility of a local instability failure at design ultimate load. The reinforcement consisted of adding 20.3-cm(8-inch) long aluminum alloy angles on each side of the five aftmost stringers on the upper wing surface at W.S. 220, left and right, as shown on Figure 27. This minor change was incorporated on the test article and the two composite-reinforced center wings that are being flight evaluated. The existing fastener pattern in stringer-to-wing plank joint was used in attaching the reinforcement angles, and the change did not interfere with the boron-epoxy laminates. Figures 27 and 28 depict the configuration of the reinforcement angles, and Figure 29 shows a typical installation.

Ultrasonic inspection of the test article before the downbending proof test indicated several small (suspect) disbond areas, primarily in the regions of repaired edge voids detected during manufacture. These suspected disbonds were confined to wing skin areas -- no disbonds were indicated in any of the stringer crowns -- and were primarily on the upper surface. Two of these, both in areas repaired with splice plates, were considered significant. One of these two suspected disbonds propagated approximately 43.2 cm(17 in.) during the upbending proof test while the other propagated slightly wider without any increase in length. Figure 30 identifies the larger disbond in the upper surface of the test article. The suspected disbonded areas were not repaired, but were monitored after each static test and fatigue test pass to evaluate any tendency to propagate. Upon completion of the inspection after the upbending proof load test, the downbending proof load test was conducted. Ultrasonic inspection of the bondlines in the test article after the downbending proof test resulted in no propagation of the suspected disbonds.

A second upbending limit load test was conducted on the fatigue test article after completing four simulated lifetimes of fatigue loading. The same load increments and sequence of application were used in this second upbending limit load test as those applied in the first test. Strain data were recorded with existing strain gages as on the previous upbending limit load test. Differentials in strain readings taken in this test and those taken in the previous upbending limit load test were within the normal scatter for the strain gage measurements.

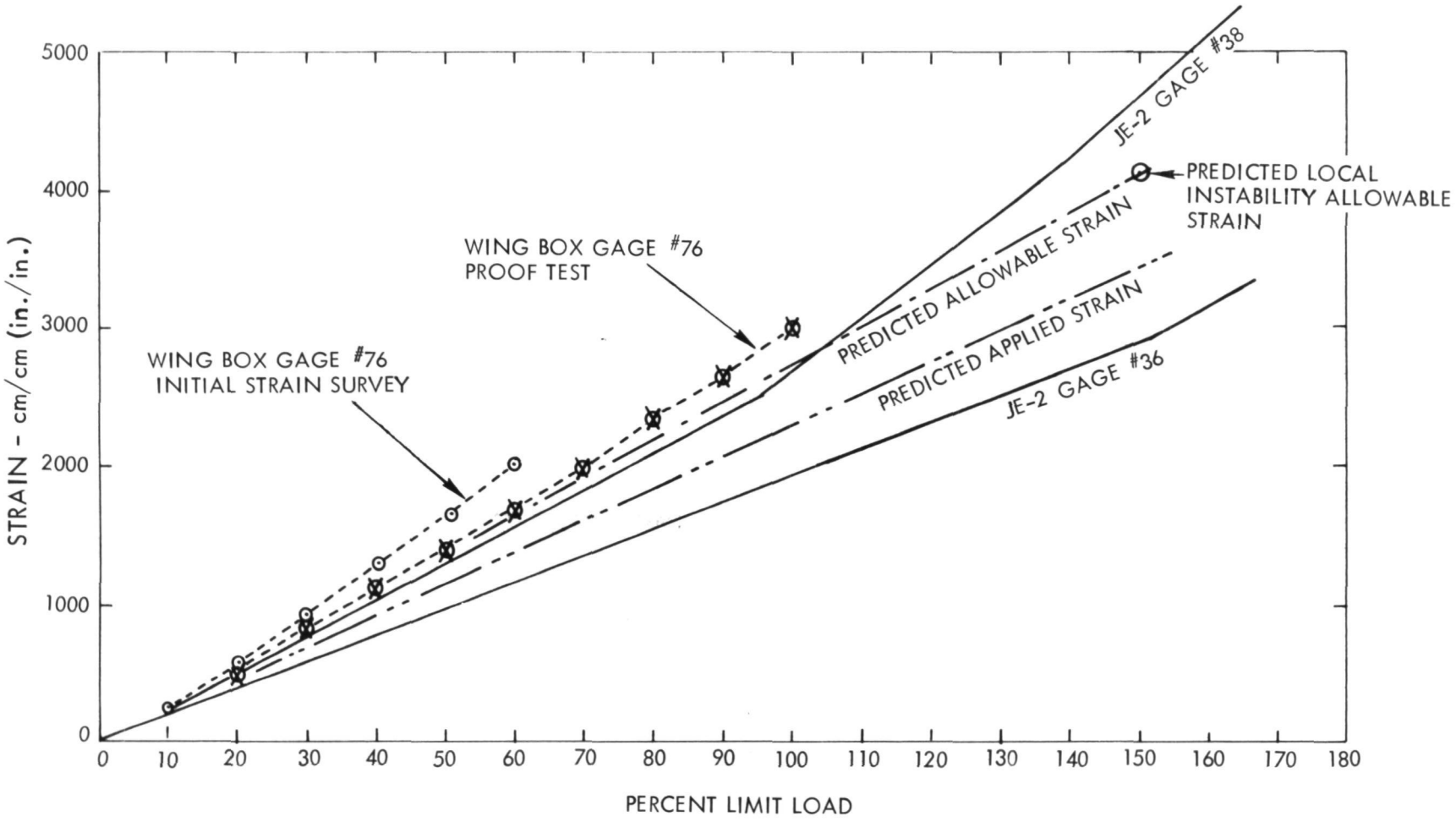

FIGURE 26. - COMPARATIVE STRAINS IN AREAS OF W.S. 220 UPPER SURFACE SKIN/STRINGER/RAINBOW FITTING SPLICE

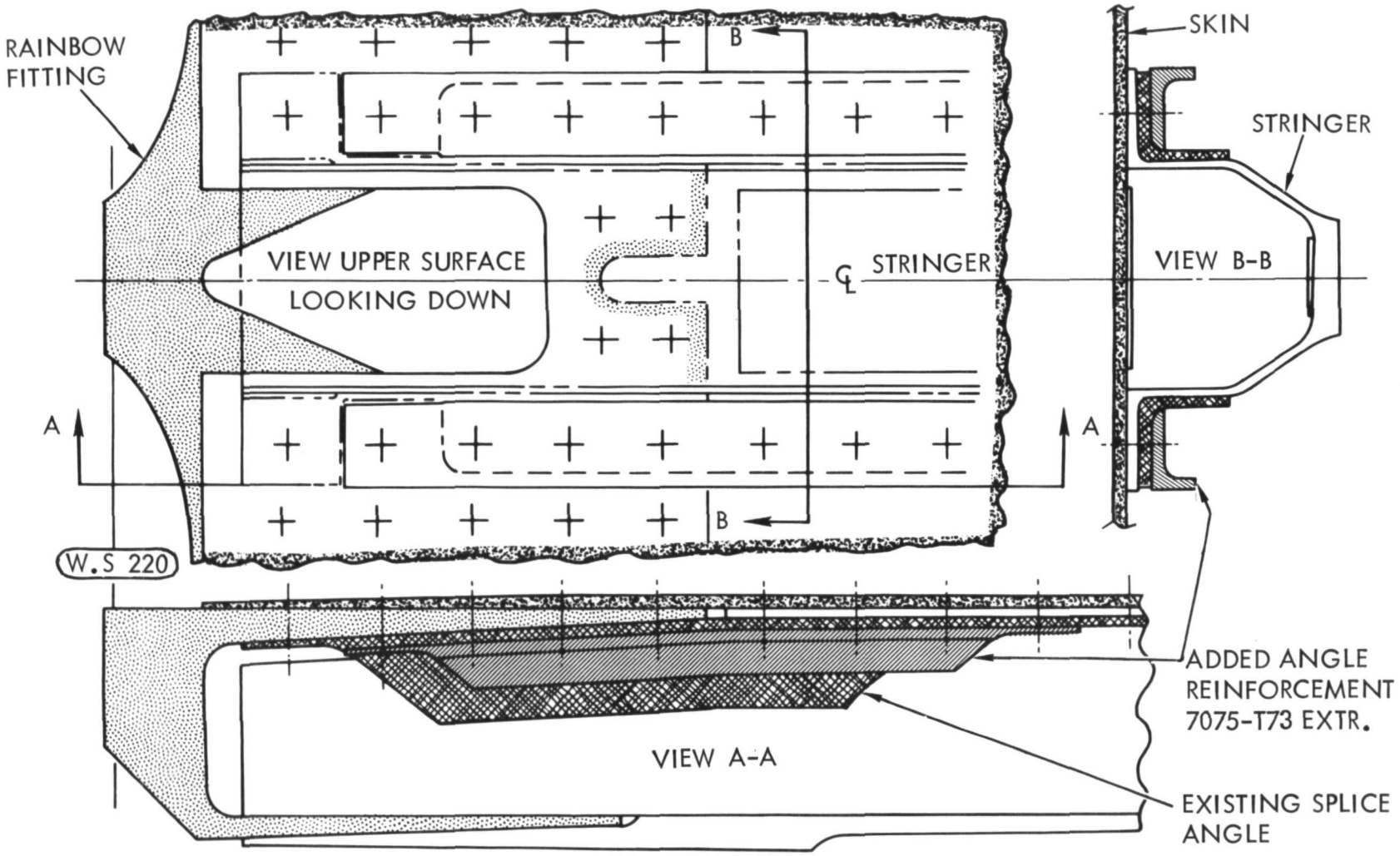

FIGURE 27. - ANGLE REINFORCEMENT - STRINGERS 7 THROUGH 11
UPPER SURFACE - CENTER WING

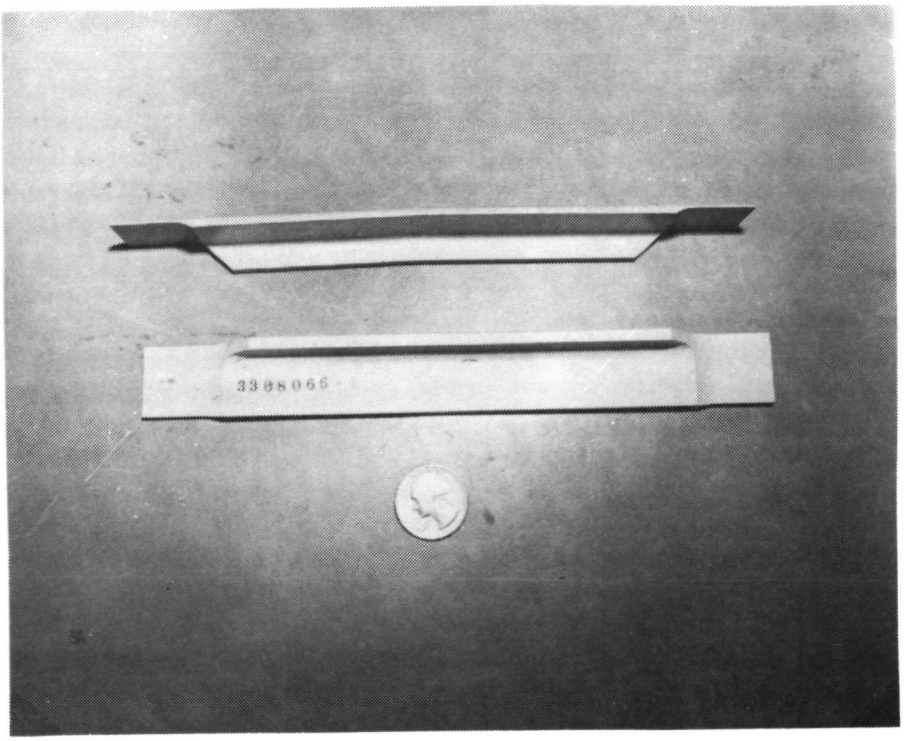

FIGURE 28. - CONFIGURATION OF ANGLES INSTALLED IN VICINITY OF W.S. 220 JOINT

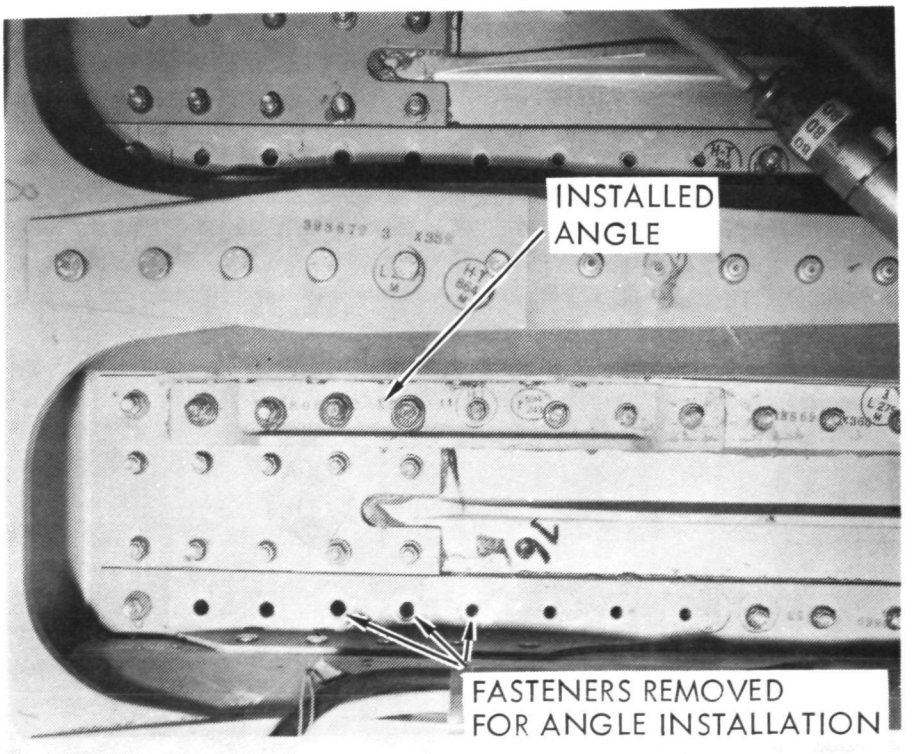

FIGURE 29. - TYPICAL INSTALLATION OF ANGLE

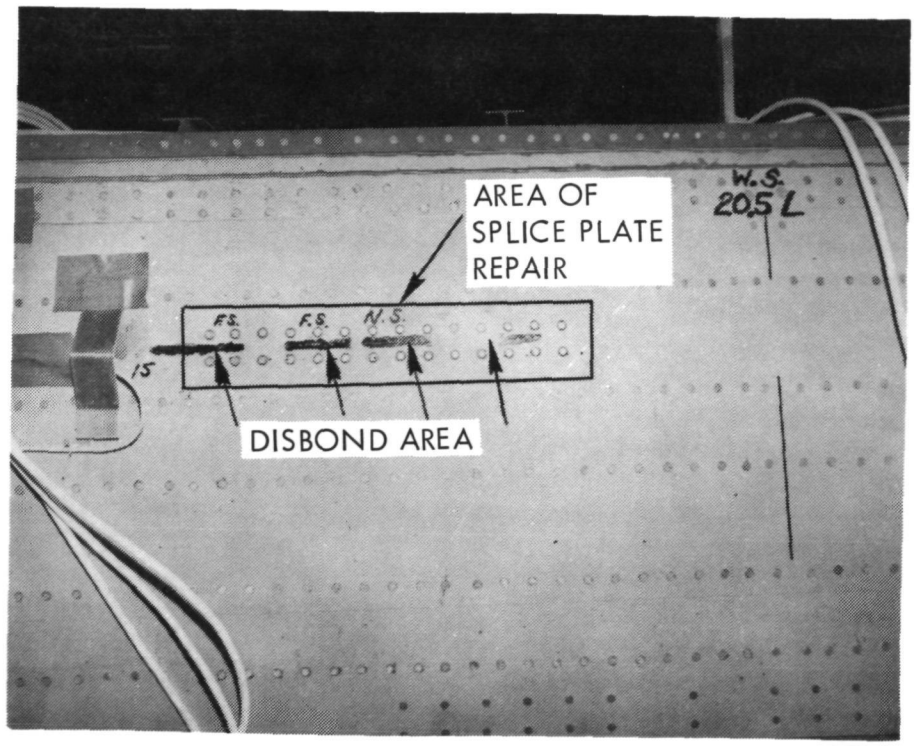

(a) BEFORE PROOF TEST

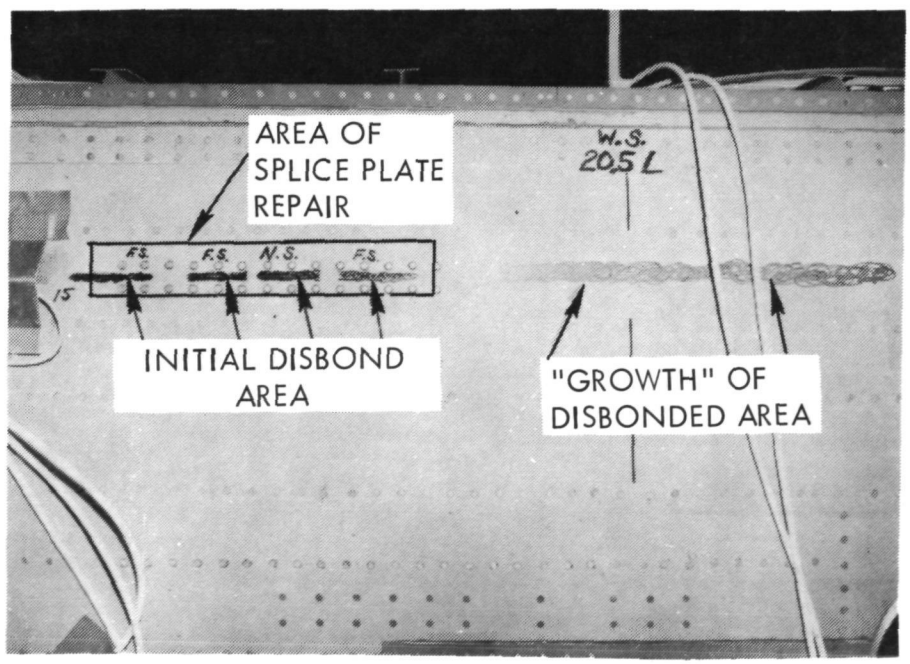

(b) AFTER UPBENDING PROOF TEST

FIGURE 30. - INDICATED DISBOND ON UPPER SURFACE OF TEST WING BOX

Upon completion of the second upbending limit load test, the fatigue test article was visually and ultrasonically inspected. During the visual inspection, a two-inch long crack was detected in the aft beam web of the test article at W.S. 145.5 (left side of test article). The crack traversed the double row of fasteners attaching the rear beam web to the lower beam cap and was remote from the boron-epoxy laminate reinforcements. Repair of the crack was accomplished before starting the crack growth tests described in Section 3.10. Also, an ultrasonic inspection of all accessible bondlines in the fatigue test article did not reveal any new bondline defects nor propagation of any of the previously detected disbonds.

3.6 GROUND VIBRATION TESTS

Vibration tests were conducted on the first aircraft with the composite-reinforced center wing to verify that the existing C-130 flutter speeds had not been adversely affected by the modification. Accelerometers were attached to selected locations on the aircraft structure to measure amplitude vectors at each important resonant frequency. The overall vibration test setup is shown in Figure 31. The aircraft was excited by vertical electromagnetic vibrators. For one set of measurements, the shakers were attached to the wing rear beam at each wing tip as shown in Figure 32. A second set of measurements was made with the shakers located at the aft end of each external fuel tank as noted in Figure 32. Each vibration test was conducted by making constant force frequency sweeps from 0.5 Hz to 50 Hz, symmetrically and antisymmetrically, with the shakers located vertically at the wing tip rear beams. Selected accelerometer outputs were recorded on a 14-channel magnetic tape recorder and on a direct record strip chart. Plots (X-Y plane) of output acceleration versus frequency were made to identify the resonant frequencies. A modal survey was made at each important resonant frequency using a roving accelerometer to take readings at pre-selected locations on the structure. The shakers were then moved to the aft end of the external fuel tank where additional frequency sweeps and modal surveys were made. Figure 33 shows a close-up view of the shaker attached to the wing tip, and Figure 34 shows the control and recording equipment used in the vibration tests.

The aircraft configuration on which the ground vibration tests were conducted was similar to that of the standard FY73 C-130H airplane on which previous ground vibration tests had been conducted. The following is a list of significant parameters that defined the configuration.

- Zero wing fuel; zero external wing tank fuel
- Gust locks installed on ailerons and elevator
- No hydraulic boost on the control surfaces
- Essentially an empty cargo compartment

The resonant frequencies obtained from the vibration test conducted on the aircraft with the composite-reinforced center wing are compared with results from a similar test on an aircraft with an all-metal center wing. These comparative results are shown in Table I. It is concluded from this comparison that the vibration characteristics of the two aircraft are essentially identical.

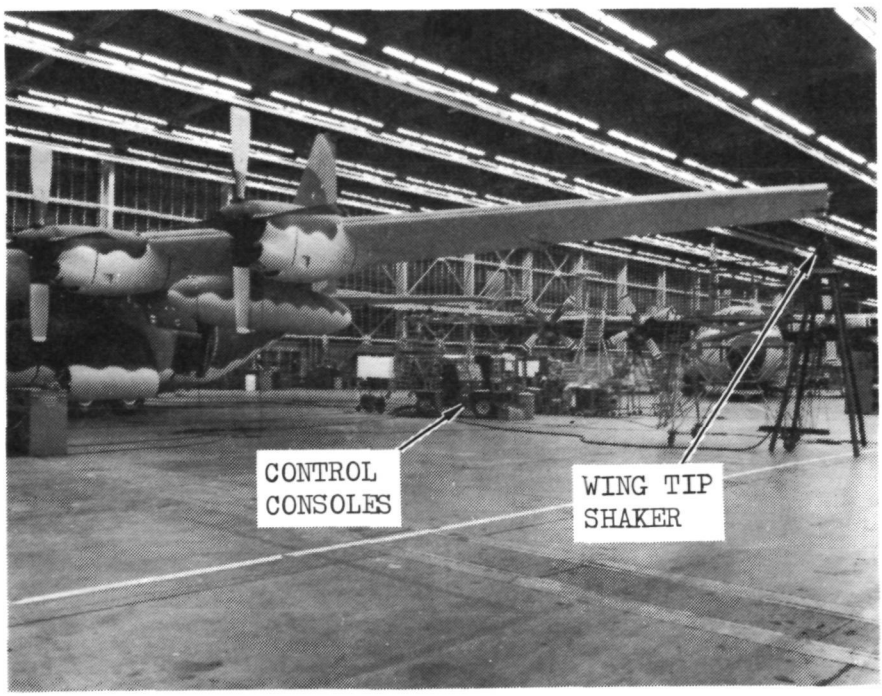

FIGURE 31. - AIRCRAFT 73-01592 (LAC 4557)
DURING GROUND VIBRATION TESTS

FIGURE 32. - GROUND VIBRATION TEST SETUP
(OVERALL VIEW)

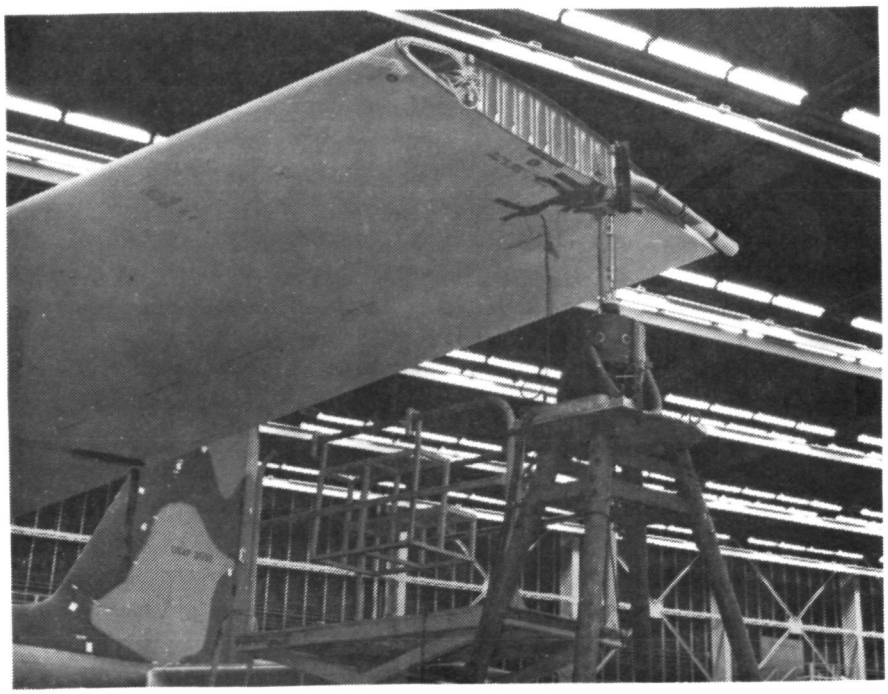

FIGURE 33. - GROUND VIBRATION TEST - DETAIL OF WING SHAKER

FIGURE 34. - GROUND VIBRATION TEST - DETAIL OF CONTROL AND RECORDING EQUIPMENT

TABLE I

ZERO FUEL RESONANT FREQUENCY COMPARISON
FY73 C-130H (TAC) AIRCRAFT

	RESONANT FREQUENCY - HERTZ	
	FIRST FY73 AIRCRAFT AF 73-01581	FIRST AIRCRAFT WITH COMPOSITE-REINFORCED C.W.B. AF 73-01592
SYMMETRIC MODES	1.80	1.85
	3.12	3.26
	4.21	4.18
	4.87	4.92
	5.54	5.68
	6.27	6.25
	7.45	7.53
	9.10	9.26
	11.75	11.80
	12.60	12.30
	15.21	15.44
		16.22
	19.07	19.08
	19.85	19.67
	24.50	23.66
ANTISYMMETRIC MODES	4.15	4.18
	5.16	5.25
	6.36	6.36
	8.22	8.14
	9.34	9.56
		11.34
	12.30	12.60
	13.71	13.84
	13.97	
	15.38	15.70
	16.10	16.08
	18.30	18.73
	20.44	20.30
	24.66	25.65
		26.90

3.7 FLIGHT ACCEPTANCE TESTS

After pre-flight functional tests, flight acceptance tests were conducted which consisted of the normal flight activities associated with checkout and delivery of C-130H aircraft. Such flights are routinely conducted by Lockheed and Air Force personnel to assure that the aircraft systems are functioning satisfactorily. No specific structural flight demonstration was required for the two C-130 aircraft with the composite-reinforced center wing boxes.

The first of the two aircraft with the composite-reinforced center wing box, Serial No. AF73-01592 was first flown on 8 October 1974, in a 3-hour, 39 minute flight. The flight pattern covered areas from Marietta, Georgia, to Centre, Alabama, to Chattanooga, Tennessee, and return to Marietta. A maximum altitude of 9144 meters (30,000 ft.) was attained. During the flight, the aircraft hydraulic systems, gyro compass, and engines were checked out. Figure 35 shows the aircraft taxiing prior to the first flight.

FIGURE 35. - AIRCRAFT 73-01592 (LAC 4557) ON TAXIWAY

Nothing unusual occurred and the aircraft performed in a similar manner to other C-130H aircraft. After Air Force acceptance flights, the aircraft was formally delivered to the Air Force on 23 October 1974.

Flight acceptance tests were conducted on the second C-130H aircraft with the composite-reinforced center wing box, Serial No. AF73-01594, similarly to the first aircraft. Nothing unusual occurred during the tests, and the aircraft performed in a similar manner to other C-130H aircraft. After Air Force acceptance flights, the aircraft was formally delivered to the Air Force on 27 November 1974.

3.8 FATIGUE TEST -- LOADS, TEST, INSPECTIONS AND EVALUATION

Upon completion of the proof tests, fatigue testing was initiated. Spectrum loads were applied that were identical to those used for full-scale testing of the C-130 B/E wing structure. The spectrum consisted of ten passes per lifetime and the wing box was tested for four lifetimes. Strain surveys were accomplished at the beginning of the fatigue test and after completing each lifetime. Ultrasonic inspections were performed before beginning the fatigue test and after each lifetime. In addition, spot ultrasonic inspections were accomplished in areas of suspected disbonds after each load pass to determine disbond propagation, if any. Detailed descriptions of the more significant parts of the fatigue test are given in the following paragraphs.

3.8.1 Test Loads

Spectrum loads applied in the fatigue test are given in Table II. These loads comprise "Spectrum B" which were used in the fatigue analysis of the composite-reinforced center wing and also the full-scale test of the C-130 B/E wing. This spectrum was applied four times for simulation of 40,000 flight hours and 28,868 aircraft landings. Application of the loads spectrum given in Table II was performed in ten passes, and forty passes were completed in the fatigue test which accounted for 1,028,900 load cycles.

Fatigue test loads applied by shear and bending moment actuators including the number of cycles for one pass with the wing center-of-pressure at 30 percent chord are presented in Table III. Similar data for the wing center-of-pressure at 42 percent chord are given in Table IV. During the fatigue test, the loads and numbers of cycles given in Table III were applied first followed by those presented in Table IV. This order of application of the fatigue loads resulted in a reversed sequence of test conditions after each pass. It is noted in the majority of load increments the number of cycles required per pass is not even; consequently, adjustments had to be made during application of each group of ten passes to produce the required total number of cycles for each condition. For example, the GUST 1.1 condition required 871 cycles per simulated lifetime (ten passes) or 87.1 cycles per pass. During each ten passes, 87 cycles were applied for nine passes and 88 cycles for one pass.

3.8.2 Conducting the Fatigue Test

Upon completion of the inspections of the test article after the downbending proof load test, strain surveys were conducted. Each strain survey consisted of application of maximum upbending condition and maximum downbending condition from the fatigue test spectrum. The GUST 1.1 condition was defined as the maximum upbending condition and the TAXI 1.1 condition was the maximum downbending condition. Loads were applied in incremental percentages of 0, 20, 40, 60, 80, 100, and 20. Strains were recorded at each load increment for comparison with initial strain measurements. The strain survey data are presented in Reference 7. In addition, strain data were recorded for monitoring purposes at the maximum load of GUST 2.4 condition during each pass. Four channels were used for continuous strain monitoring on a strip recorder.

TABLE II - GENERAL FATIGUE SPECTRUM REPRESENTING 10,000 FLIGHT HOURS AND 7217 LANDINGS

CONDITION		CYCLES	(M_{WS61}) Ref. Mean $\pm$ Var. $\times 10^6$ N-m ($\times 10^6$ in-lb)	M_{WS220} Mean $\pm$ Var. $\times 10^6$ N-m ($\times 10^6$ in-lb)	P_{WS220} Mean $\pm$ Var. $\times 10^3$ N ($\times 10^3$ lb)
Gust	1.1	871	0.974 ± 0.758 (8.62 ± 6.71)	0.606 ± 0.472 (5.36 ± 4.18)	91.19 ± 70.77 (20.50 ± 15.91)
	1.2	2327	0.974 ± 0.554 (8.62 ± 4.90)	0.606 ± 0.343 (5.36 ± 3.04)	91.19 ± 52.04 (20.50 ± 11.70)
	1.3	4595	0.974 ± 0.452 (8.62 ± 4.00)	0.606 ± 0.281 (5.36 ± 2.49)	91.19 ± 42.26 (20.50 ± 9.50)
	1.4	7676	0.974 ± 0.400 (8.62 ± 3.54)	0.606 ± 0.249 (5.36 ± 2.20)	91.19 ± 37.50 (20.50 ± 8.43)
	1.5	18254	0.974 ± 0.323 (8.62 ± 2.86)	0.606 ± 0.208 (5.36 ± 1.84)	91.19 ± 28.56 (20.50 ± 6.42)
	1.6	94518	0.974 ± 0.251 (8.62 ± 2.22)	0.606 ± 0.156 (5.36 ± 1.38)	91.19 ± 23.49 (20.50 ± 5.28)
Gust	2.1	1760	0.798 ± 0.649 (7.06 ± 5.74)	0.496 ± 0.403 (4.39 ± 3.57)	74.68 ± 60.72 (16.79 ± 13.65)
	2.2	4995	0.798 ± 0.481 (7.06 ± 4.26)	0.496 ± 0.301 (4.39 ± 2.66)	74.68 ± 44.75 (16.79 ± 10.06)
	2.3	21212	0.798 ± 0.359 (7.06 ± 3.18)	0.496 ± 0.224 (4.39 ± 1.98)	74.68 ± 33.58 (16.79 ± 7.55)
	2.4	81367	0.798 ± 0.295 (7.06 ± 2.61)	0.496 ± 0.184 (4.39 ± 1.63)	74.68 ± 27.40 (16.79 ± 6.16)
Gust	3.1	6805	0.435 ± 0.572 (3.85 ± 5.06)	0.271 ± 0.357 (2.40 ± 3.16)	40.57 ± 53.15 (9.12 ± 11.95)
Taxi	1.1	5328	-0.828 ± 0.402 (-7.33 ± 3.56)	-0.506 ± 0.246 (-4.48 ± 2.18)	-79.71 ± 38.61 (-17.92 ± 8.68)
GAG	1	467	0.138 ± 1.300 (1.22 ± 11.51)	0.073 ± 0.695 (0.65 ± 6.15)	15.92 ± 149.94 (3.58 ± 33.71)
	2	508	0.050 ± 1.220 (0.44 ± 10.80)	0.027 ± 0.651 (0.24 ± 5.76)	5.56 ± 141.00 (1.25 ± 31.70)
	3	900	0.192 ± 1.071 (1.70 ± 9.48)	0.103 ± 0.572 (0.91 ± 5.06)	22.11 ± 123.65 (4.97 ± 27.80)
	4	1200	0.119 ± 1.045 (1.05 ± 9.25)	0.063 ± 0.559 (0.56 ± 4.95)	13.70 ± 120.27 (3.08 ± 27.04)
	5	1567	0.072 ± 0.975 (0.64 ± 8.63)	0.040 ± 0.521 (0.35 ± 4.61)	8.096 ± 112.45 (1.82 ± 25.28)
	6	2875	-0.056 ± 0.829 (-0.50 ± 7.34)	-0.029 ± 0.443 (-0.26 ± 3.92)	-6.72 ± 95.68 (-1.51 ± 21.51)

TABLE III - PART 1 - FATIGUE TEST LOADS FOR C_p AT 30% CHORD

TEST CONDITION		NUMBER OF CYCLES PER PASS	ACTUATOR LOADS (NEWTONS PER ACTUATOR)							
			SHEAR ACTUATORS				MOMENT ACTUATORS			
			FORWARD		AFT		FORWARD		AFT	
			MEAN	VARIABLE	MEAN	VARIABLE	MEAN	VARIABLE	MEAN	VARIABLE
GUST	1.1	87.1	95,952	74,468	-4,768	- 3,701	34,743	27,106	-34,743	-27,106
	1.2	232.7	↕	54,764	↕	- 2,722	↕	19,691	↕	-19,691
	1.3	459.5	↕	44,467	↕	- 2,211	↕	16,146	↕	-16,146
	1.4	767.6	↕	39,458	↕	- 1,962	↕	14,256	↕	-14,256
	1.5	1825.4	↕	30,051	↕	- 1,495	↕	12,032	↕	-12,032
	1.6	9451.8	95,952	24,713	-4,768	- 1,228	34,743	8,945	-34,743	- 8,945
	2.1	176.0	78,587	63,891	-3,906	- 3,176	28,463	23,143	-28,463	-23,143
	2.2	499.5	↕	47,087	↕	- 2,340	↕	17,263	↕	-17,263
	2.3	2121.2	↕	35,339	↕	- 1,757	↕	12,837	↕	-12,837
	2.4	8136.7	78,587	28,832	-3,906	- 1,432	28,463	10,577	-28,463	-10,577
	3.1	680.5	42,687	55,934	-2,122	- 2,780	15,569	20,505	-15,569	-20,505
TAXI	1.1	532.8	-56,289	27,266	-23,419	11,342	-28,908	14,073	28,908	-14,073
GAG	1	46.7	10,346	97,416	5,578	52,526	4,030	38,142	- 4,030	-38,142
	2	50.8	3,612	91,607	1,948	49,395	1,499	35,704	- 1,499	-35,704
	3	90.0	14,363	80,340	7,744	43,315	5,649	31,372	- 5,649	-31,372
	4	120.0	8,900	78,142	4,799	42,131	3,470	30,718	- 3,470	-30,718
	5	156.7	5,258	73,054	2,838	39,391	2,189	28,592	- 2,189	-28,592
	6	287.5	- 4,364	62,161	- 2,353	33,516	- 1,597	24,308	1,597	-24,308

NOTE: Positive load is tension load in actuator.

TABLE III - PART 2 - FATIGUE TEST LOADS FOR C_p AT 30% CHORD

TEST CONDITION		NUMBER OF CYCLES PER PASS	ACTUATOR LOADS (POUNDS PER ACTUATOR)							
			SHEAR ACTUATORS				MOMENT ACTUATORS			
			FORWARD		AFT		UPPER SURFACE		LOWER SURFACE	
			MEAN	VARIABLE	MEAN	VARIABLE	MEAN	VARIABLE	MEAN	VARIABLE
GUST	1.1	87.1	21,572	16,742	-1,072	-832	7,811	6,094	-7,811	-6,094
	1.2	232.7	↕	12,312	↕	-612	↕	4,427	↕	-4,427
	1.3	459.5	↕	9,997	↕	-497	↕	3,630	↕	-3,630
	1.4	767.6	↕	8,871	↕	-441	↕	3,205	↕	-3,205
	1.5	1825.4	↕	6,756	↕	-336	↕	2,705	↕	-2,705
	1.6	9451.8	21,572	5,556	-1,072	-276	7,811	2,011	-7,811	-2,011
	2.1	176.0	17,668	14,364	-878	-714	6,399	5,203	-6,399	-5,203
	2.2	499.5	↕	10,586	↕	-526	↕	3,881	↕	-3,881
	2.3	2121.2	↕	7,945	↕	-395	↕	2,886	↕	-2,886
	2.4	8136.7	17,668	6,482	-878	-322	6,399	2,378	-6,399	-2,378
	3.1	680.5	9,597	12,575	-477	-625	3,500	4,610	-3,500	-4,610
TAXI	1.1	532.8	-12,655	6,130	-5265	2,550	-6,499	3,164	6,499	-3,164
GAG	1	46.7	2,326	21,901	1,254	11,809	906	8,575	-906	-8,575
	2	50.8	812	20,595	438	11,105	337	8,027	-337	-8,027
	3	90.0	3,229	18,062	1,741	9,738	1,270	7,053	-1,270	-7,053
	4	120.0	2,001	17,568	1,079	9,472	780	6,906	-780	-6,906
	5	156.7	1,182	16,424	638	8,856	492	6,428	-492	-6,428
	6	287.5	-981	13,975	-529	7,535	-359	5,465	359	-5,465

NOTE: Positive load is tension load in actuator.

TABLE IV - PART 1 - FATIGUE TEST LOADS FOR C_p AT 42% CHORD

TEST CONDITION		NUMBER OF CYCLES PER PASS	ACTUATOR LOADS (NEWTONS PER ACTUATOR)							
			SHEAR ACTUATORS				MOMENT ACTUATORS			
			FORWARD		AFT		FORWARD		AFT	
			MEAN	VARIABLE	MEAN	VARIABLE	MEAN	VARIABLE	MEAN	VARIABLE
GAG	6	287.5	- 4,363	62,161	- 2,353	33,516	- 1,597	24,308	1,597	-24,308
	5	156.7	5,258	73,054	2,838	39,391	2,189	28,592	- 2,189	-28,592
	4	120.0	8,900	78,142	4,800	42,131	3,470	30,718	- 3,470	-30,718
	3	90.0	14,363	80,340	7,744	43,315	5,649	31,372	- 5,649	-31,372
	2	50.8	3,612	91,607	1,948	49,395	1,499	35,704	- 1,499	-35,704
	1	46.7	10,346	97,416	5,578	52,526	4,030	38,142	- 4,030	-38,142
TAXI	1.1	532.8	-56,289	27,266	-23,419	11,342	-28,908	14,073	28,908	-14,073
GUST	3.1	680.5	23,757	31,127	16,809	22,026	15,569	20,505	-15,569	-20,505
	2.4	8136.7	43,733	16,044	30,949	11,356	28,463	10,577	-28,463	-10,577
	2.3	2121.2	↕	19,665	↕	13,918	↕	12,837	↕	-12,837
	2.2	499.5	↕	26,203	↕	18,544	↕	17,263	↕	-17,263
	2.1	176.0	43,733	35,553	30,949	25,162	28,463	23,143	-28,463	-23,143
	1.6	9451.8	53,398	13,753	37,786	9,732	34,743	8,945	-34,743	- 8,945
	1.5	1825.4	↕	16,724	↕	11,832	↕	12,032	↕	-12,032
	1.4	767.6	↕	21,960	↕	15,537	↕	14,256	↕	-14,256
	1.3	459.5	↕	24,744	↕	17,512	↕	16,146	↕	-16,146
	1.2	232.7	↕	30,478	↕	21,564	↕	19,691	↕	-19,691
	1.1	87.1	53,398	41,442	37,786	29,326	34,743	27,106	-34,743	-27,106

NOTE: Positive load is tension load in actuator.

TABLE IV - PART 2 - FATIGUE TEST LOADS FOR C_p AT 42% CHORD

TEST CONDITION		NUMBER OF CYCLES PER PASS	ACTUATOR LOADS (POUNDS PER ACTUATOR)							
			SHEAR ACTUATORS				MOMENT ACTUATORS			
			FORWARD		AFT		UPPER SURFACE		LOWER SURFACE	
			MEAN	VARIABLE	MEAN	VARIABLE	MEAN	VARIABLE	MEAN	VARIABLE
GAG	6	287.5	-981	13,975	-529	7,535	-359	5,465	359	-5,465
	5	156.7	1,182	16,424	638	8,856	492	6,428	-492	-6,428
	4	120.0	2,001	17,568	1,079	9,472	780	6,906	-780	-6,906
	3	90.0	3,229	18,062	1,741	9,738	1,270	7,053	-1,270	-7,053
	2	50.8	812	20,595	438	11,105	337	8,027	-337	-8,027
	1	46.7	2,326	21,901	1,254	11,809	906	8,575	-906	-8,575
TAXI	1.1	532.8	-12,655	6,130	-5,265	2,550	-6,499	3,164	6,499	-3,164
GUST	3.1	680.5	5,341	6,998	3,779	4,952	3,500	4,610	-3,500	-4,610
	2.4	8136.7	9,832	3,607	6,958	2,553	6,399	2,378	-6,399	-2,378
	2.3	2121.2	↕	4,421	↕	3,129	↕	2,886	↕	-2,886
	2.2	499.5	↕	5,891	↕	4,169	↕	3,881	↕	-3,881
	2.1	176.0	9,832	7,993	6,958	5,657	6,399	5,203	-6,399	-5,203
	1.6	9451.8	12,005	3,092	8,495	2,188	7,811	2,011	-7,811	-2,011
	1.5	1825.4	↕	3,760	↕	2,660	↕	2,705	↕	-2,705
	1.4	767.6	↕	4,937	↕	3,493	↕	3,205	↕	-3,205
	1.3	459.5	↕	5,563	↕	3,937	↕	3,630	↕	-3,630
	1.2	232.7	↕	6,852	↕	4,848	↕	4,427	↕	-4,427
	1.1	87.1	12,005	9,317	8,495	6,593	7,811	6,094	-7,811	-6,094

NOTE: Positive load is tension load in actuator.

Cyclic loading of the fatigue test article was accomplished for the first lifetime and only minor difficulties were encountered with the test system. Upon completion of the first lifetime of testing, both visual and ultrasonic inspections were performed on the fatigue test article. No visual damage was revealed and no changes were detected in the bondlines of the fatigue test article during the ultrasonic inspection including the disbonds discovered after the proof test. Although no fatigue cracks were detected during the visual inspections, it was discovered that two small reinforcement angles had not been installed during manufacture of the fatigue test article. These angles attach to a wing surface panel and the lower front beam cap at Wing Station 68, left and right. In the normal production sequence, these angles are installed when assembling the center wing into the fuselage. Since the fatigue test article was not installed in an operational aircraft, installation of the reinforcement angles was inadvertently omitted. The angles were not critical for the fatigue test, but they were installed prior to initiating cyclic testing into the second lifetime. A typical installation of a reinforcement angle is shown in Figure 36.

A strain survey was performed after the first lifetime of cyclic testing for the GUST 1.1 and TAXI 1.1 fatigue load conditions. These strain data are reported in Reference 7 and no unusual measurements were identified that indicated suspect conditions.

The second lifetime of cyclic testing was completed and only minor test system difficulties were encountered. After completing the second lifetime of testing, the fatigue test article was both visually and ultrasonically inspected. No fatigue cracks were detected in the aluminum structure; however, seven fasteners had sustained head failures. All of these failed fasteners were remote from the boron-epoxy reinforcements, and visual examination of the fracture surfaces revealed fatigue markings. The failed fasteners were not considered serious and were replaced with 0.397-mm (1/64-inch) oversize fasteners normally used for such repairs. Prior to installation, the

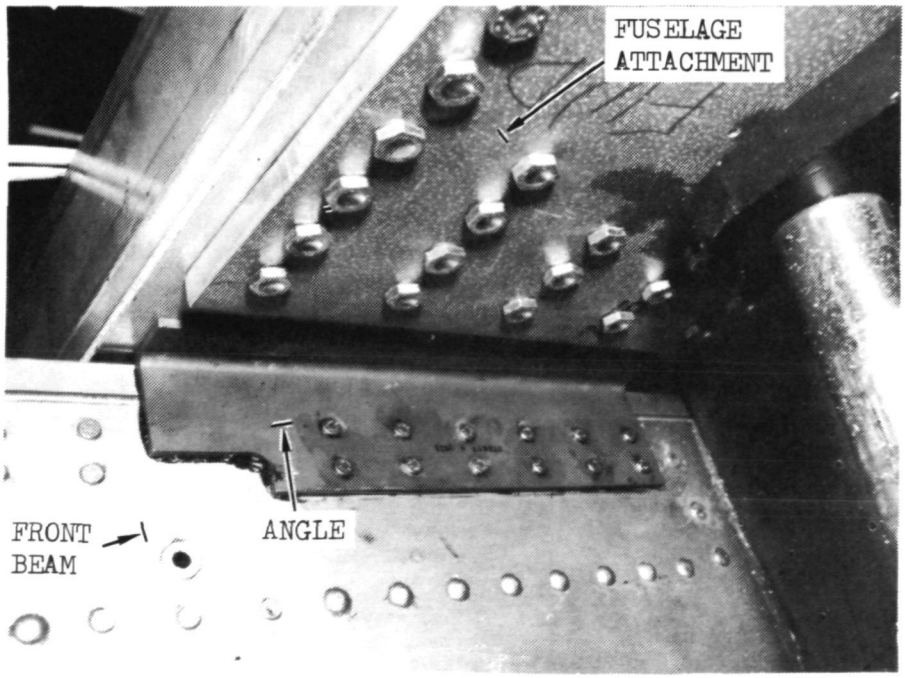

FIGURE 36.-TYPICAL INSTALLATION OF REINFORCEMENT ANGLE

fastener hole walls were inspected for cracks using the eddy-current inspection technique. Ultrasonic inspection of the boron-epoxy laminate-to-wing skin plank bondlines revealed no detectable changes. Upon completing the inspection, cyclic testing was continued.

The third lifetime of fatigue testing was initiated and upon completing five load passes in that lifetime, visual inspection revealed an additional six fastener failures. At this point in the fatigue test, a total of thirteen fastener failures had occurred of which nine failures were in the Wing Station 220 joint region where the test article interfaces with the test fixture. All of those failures occurred in the all-metallic C-130 structure and remote from the boron-epoxy laminates. Similar failures were not experienced during fatigue testing of the conventional center wing. On that test, shear loads in the Wing Station 220 joint region were induced through outer wings rather than through a special test fixture. It was concluded that the fastener failures were associated with a local condition produced by stiff shear loading members on the test fixture. These failures were considered minor, and failed fasteners were replaced with repair fasteners after which cycling was continued. Upon completion of the third simulated lifetime, the fatigue test article was visually and ultrasonically inspected. The ultrasonic inspection did not reveal any growth in previously detected disbonds or any new disbonds in the bondlines of the boron-epoxy laminates-to-aluminum structure. The visual inspection revealed a broken fastener at Wing Station 100 in the rear beam web. This failed fastener was replaced after the hole was inspected by an eddy current meter and the surfaces found free of cracks. Upon completing the inspection, cyclic testing was continued.

Cyclic testing continued into the fourth simulated lifetime with 2,811 load cycles remaining in the lifetime when two cracks were discovered in the front beam web of the fatigue test article at Wing Station 73 which is in the vicinity of the wing-fuselage frame intersection. Both cracks were in the area of the beam web where it is attached to the lower front beam cap. A photograph of the area in which the cracks are located is contained in the Fatigue Damage Reports, Damage Item Number 9, of Appendix C. The longer crack was estimated to be 12.7 cm (5.0 in.) in length and extended from the lower edge of the beam web through the double row of mechanical fasteners attaching the beam web to the beam cap, and it continued in the beam web on a curved path that ended beneath the load reaction fixture. The second crack was estimated to be 1.5 cm (0.6 in.) in length which extended through the adjacent pair of mechanical fasteners that the longer crack traversed and continued to the lower edge of the beam web. Fatigue cycling of the test article was continued after the discovery of the two cracks as this damage was judged as not being detrimental to completion of the fourth simulated lifetime of testing. The fourth lifetime was completed without propagation of either of the two cracks.

Upon completion of the fourth simulated lifetime, the fatigue test article was visually and ultrasonically inspected. The visual inspection revealed two failed mechanical fasteners at Wing Station 100. The first failed fastener was located in the double row of fasteners attaching the front beam web and reinforcement plate to the upper front beam cap. The second failed fastener occurred in the double row of fasteners attaching the rear beam web to the upper rear beam cap. Also, a crack was discovered

in the rear beam web at Wing Station 145.5. The estimated length of the crack was 5.1 cm (2.0 in.) and it traversed the double row of mechanical fasteners joining the rear beam web to the lower rear beam cap. Both cracks were repaired and the two failed fasteners were replaced prior to conducting an additional upbending limit load test. Ultrasonic inspection of the bondlines of the boron-epoxy laminate-to-aluminum structure showed no propagation in previously detected disbonds nor detection of any new disbonds.

3.8.3 Fatigue Damage Reports on Test Article

Fatigue damage reports were reported on each damage item discovered. All of these damage reports are included in Appendix C. Each report defines the damage item, its location, and when it occurred in the fatigue test spectrum. A photograph of each damage item is included in each damage report. Also, the damage report included a description of the repair accomplished on each damage item.

In summary, fatigue damage reports were prepared for 16 failed mechanical fasteners and two cracks in the front beam web during the fatigue test. In addition, fatigue damage reports for two failed mechanical fasteners, a crack in the rear beam web, and the buckled repair doubler on the front beam web were prepared prior to conducting the subsequent upbending limit load test. The aforementioned buckled doubler repair is described in Damage Item Number 13 in Appendix C.

3.8.4 Evaluation of Fatigue Test Results

Successful completion of four simulated lifetimes of fatigue testing on the fatigue article without any problems or failures in the boron-epoxy laminate reinforced areas provides a high level of confidence of accumulating a lifetime of in-service experience with minimal problems. Also, the few minor failures experienced in the areas that are remote from the boron-epoxy reinforcements provide additional confidence that no problems will develop during the course of the in-service flight evaluation program being conducted on the two composite-reinforced center wing boxes.

Review of strain measurements taken after each of the four simulated lifetimes of cyclic testing showed no unusual results indicating degradations of any types. In fact, differentials in strain measurements taken after each lifetime of cyclic testing was within the normal scatter for strain gage measurements. Since no disbonds developed in the bondlines of the boron-epoxy laminate-to-metal structure during the fatigue test, this attests to the soundness of the structural design.

3.9 ANALYTICAL DETERMINATION OF CRITICAL CRACK LENGTHS

Three structural locations were selected for critical crack length, residual strength, crack propagation, and disbonding analyses:

- o W.S. 180 Lower: an area of the lower surface panel remote from geometric complications other than the hat-section stringers and the boron-epoxy composite laminates.
- o W.S. 120 Lower: an area of the lower surface panel influenced by the access door cutout, the hat-section stringers, and the boron-epoxy composite laminates; termination of stringers and laminates inboard and outboard of door cutout.
- o W.S. 214 Lower: an area of the lower surface panel influenced by the wing joint fitting, the hat-section stringers, and the termination of the boron-epoxy composite laminates.

A fourth location, W.S. 214 Upper, was found to be comparable to W.S. 214 Lower except subject to less severe stresses.

The damage condition considered at the three locations was cracking of the skin element of the panel cross-section. As a result of the full-scale test (Sec. 3.10), the effect of associated cracking of the hat-section stringer flanges on the crack in the skin element was also investigated. Disbonding of the laminate bonded to the skin was investigated at the locations of laminate termination in the W.S. 120 access door area (Stringers 17 & 19 at W.S. 110 and W.S. 130) and in the W.S. 214 wing joint area.

Critical Crack Length - The strength of the singularity defining the stress at the tip of a crack (tip radius, $r \rightarrow 0$) is measured by the stress intensity factor (Ref. 8):

$$K_I = \sigma\sqrt{\pi a}\,\lambda \qquad \text{(Eq. 3.9.1)}$$

where: σ = applied tension stress away from the crack
a = measure of crack size; e.g., for a through-the-thickness symmetrical crack, a = half the crack length
λ = correction factor for proximity of boundaries, other geometric influences, and induced loads
Subscript I denotes crack opening under tension as opposed to II which defines shear and III which is tearing.

The critical value of the stress intensity factor, K_c, is a material property dependent upon grain orientation and crack tip strain restraint (which is principally determined by thickness).

For combinations of applied stress, correction factor, and crack length yielding $K_I \geq K_c$, the crack would propagate rapidly to the edge of the part or to some obstruction capable of arresting it; i.e., unstable crack propagation. For $K_I < K_c$, the crack

propagates slowly, such that if the applied stress were cyclic, incremental crack extension would occur; i.e., stable crack propagation. Unstable crack propagation may be arrested by an obstruction which removes the stress state singularity (e.g., a fastener hole, $r \neq 0$) or changed to stable propagation by a reduction in K_I caused by reduction in stress (e.g., a deflection limited part) and/or a reduction in the correction factor (e.g., crack opening displacement restraint from reinforcement). Hence, critical crack length, a_c, requires the specification of the applied stress, σ, plus the geometry defining the correction factor, $\lambda = \lambda(a)$, such that $K_I \geq K_c$ for $a \geq a_c$. In this analysis, the above criterion was assessed by solving Equation 3.9.1 for the applied stress yielding K_c as a function of the crack length (and its associated correction factor); i.e., the critical stress. Comparing the critical stress to applied stress cases then determines the critical crack length. Principally, the analysis involves evaluation of the correction factor, λ, as a function of the crack size parameter, a.

Residual Strength - Residual strength is the load sustaining capability of the remaining intact structure given that the part (skin element) has completely fractured, whether by stable or unstable crack propagation. That is, it is an assessment of the consequences of the cracked condition. If the critical stress is caused by a load greater than the residual strength, then application of that load (stress) would cause catastrophic failure; if not, then only the part under examination breaks. The likelihood of catastrophic failure therefore may be assessed by comparing the critical stress, the residual strength, and the applied load, especially limit load, and its associated probability of occurrence. A discussion of the analysis is in Section 3.9.4.

Crack Propagation - The stable crack propagation characteristic is germane to the question of the likelihood of encountering critical crack conditions. For this analysis initial crack sizes were selected based on inspection detectability criteria.

For this analysis the test load spectrum listed in Table II (Sec. 3.8.1), reduced to 1000 hours per pass, was used. In addition, crack retardation effects from stress level interactions were not considered.

The cyclic crack propagation rate may be described by Forman's equation (Ref. 8):

$$da/dN = C\,\Delta K^n / [(1-R)\,K_C - \Delta K] \qquad \text{(Eq. 3.9.2)}$$

where $\Delta K = K_{max} - K_{min}$ for an applied load (stress) cycle using Equation 3.9.1, σ_{max}, σ_{min}, specifying the crack size parameter, a, and using its associated correction factor, λ.

$R = \sigma_{min}/\sigma_{max}$

C, n = empirical material constants that are keyed to ranges of ΔK

Integration of Equation 3.9.2 was accomplished using a computer program which solves for the number of cycles required to propagate the crack by a selected increment Δa. The initial crack size for subsequent increments was $a_i = a_{i-1} + \Delta a$, and $a = a_i + \Delta a/2$ was used to evaluate λ_i resulting in ΔK_{ij} for each stress range $\Delta\sigma_j$ in the spectrum. The integration is greatly simplified by computing a cyclically weighted average ΔK for a pass of the spectrum, yielding the number of passes to propagate the crack by Δa.

This expedient generates significant errors if the crack growth rate is high enough to cause significant crack extension in a few passes. In that case, integration phase-by-phase or cycle-by-cycle must be resorted to.

Disbonding - Propagation of disbonding of the boron-epoxy composite laminate from the skin was investigated using methods reported in NASA TMX-71948 (Ref. 9). The cyclic disbond rate may be described by:

$$da/dN = C\,G^n \qquad \text{(Eq. 3.9.3)}$$

where G = strain energy release rate
C, n = empirical bond/adherend system constants

Conceptually, the stringer-laminate combination may be viewed as two members bonded together, member 1 being the composite laminate bonded to the skin, and member 2 the remainder (hat-section stringer plus laminate bonded to crown plus effective skin, as applicable). Then:

$$G = \sigma_2^2 \,(1 - A_2^*/A^* + A_1^*/A^*)\, A_2^*/2E_2 \qquad \text{(Eq. 3.9.4)}$$

where A_1^* = modulus weighted area of laminate (member 1)
A_2^* = modulus weighted area of remainder (member 2)
$A^* = A_1^* + A_2^*$
E_2 = reference modulus (in this analysis, it is aluminum)
σ_2 = stress in reference modulus material of A_2^* (in this analysis, aluminum)

Equation 3.9.3 could not be integrated directly due to the unavailability of material constants for the bond/adherend system employed here. However, qualitative results were obtained using data from Reference 9.

Reference Stresses - The limit upbending load case used in this analysis is shown in Figure 24. Figures 37 and 38 compare the stress distribution for this case:

- Using the stress-load ratio (Reference 2, Figure 17), $\sigma = (S/L)\, M_x$ and M_x from Figure 24.
- Results of the unit beam stress anslysis, adjusted for limit load, from the strength substantiation analysis (Reference 2, Sec. 4.1).
- Axial strain gage results from the limit load upbending test (Sec. 3.5) in which $\sigma = \epsilon E$.

The spanwise distribution, Figure 37, is shown along stringer 10; and the chordwise distribution, Figure 38, at W.S. 120. Comparisons are similar at other locations. It was concluded that $(S/L)\, M_x$ would be appropriate for crack propagation analyses; however, test results should be included for critical crack length and residual strength analyses.

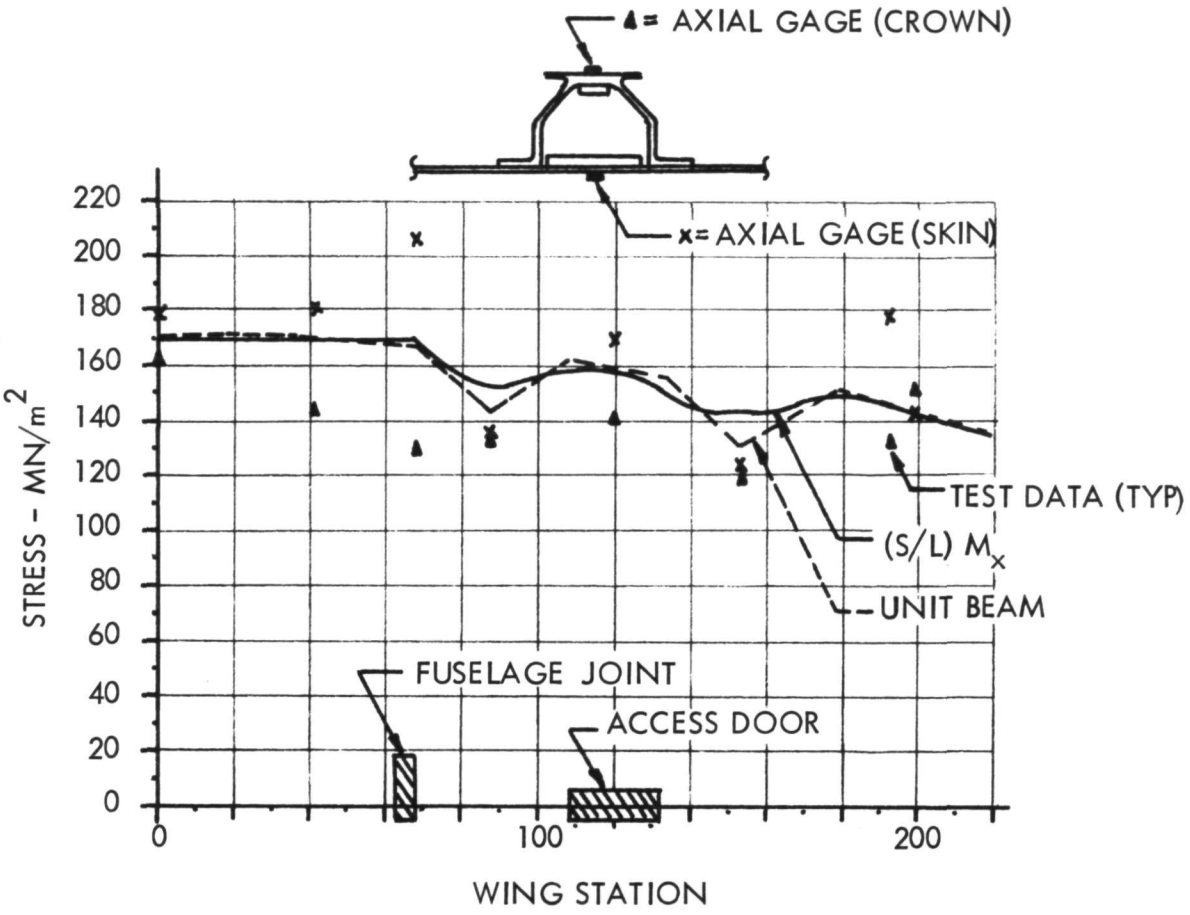

FIGURE 37. - SPANWISE LOWER SURFACE STRESS DISTRIBUTION (LIMIT LOAD)

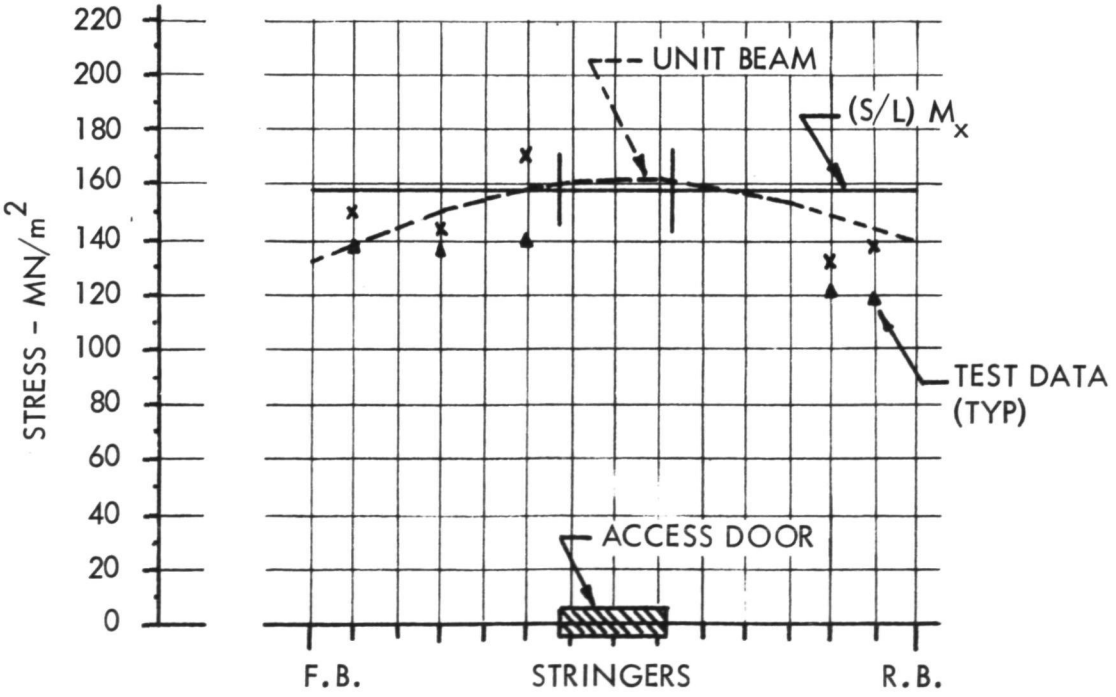

FIGURE 38. - CHORDWISE LOWER SURFACE STRESS DISTRIBUTION (LIMID LOAD) AT W.S. 120

3.9.1 W.S. 180 Lower Surface Panel Analysis

The sketch in Figure 39 depicts the lower surface panel in the region of W.S. 180 along with pertinent geometry. The crack location was chosen to be between Stringers 17 and 18 rather than emanating from a fastener hole in deference to the ability to inflict initial damage in the crack growth test without disassembling the structure. Furthermore, this choice isolates the crack so that only hat-section stringer and laminate effects need to be considered.

Correction Factor - The methods and data from NASA TR-R-358 (Ref. 10) were used to evaluate the correction factor, λ, as a function of the crack size parameter, a. The uniformly spaced stringers (stiffeners) specified in Reference 10 are attached with mechanical fasteners with spacings based on fastener spacing/stiffener spacing ratios, p/b. A p/b ratio of 1/12 closely approximates an integrally stiffened panel (Ref. 11). Observing the fastener lines in Figure 39, the hat-section stringers having the boron-epoxy laminates bonded to their crowns are attached to the skin surface planks by fasteners spaced at 2.34 cm (0.92 in.) acting as stiffeners spaced at b = 5.3 cm (2.1 in.) and 9.2 cm (3.6 in.) alternately. The laminates bonded to skin surface planks are superimposed on the stringer/crown laminate/surface plank system and are represented as integral stiffeners (i.e. p/b = 1/12) spaced at 14.5 cm (5.7 in.): $\lambda = (\lambda_{stringer})(\lambda_{laminate})$. The results are shown on Figure 40.

During the crack growth test (Sec. 3.10), the hat-section flange cracked at W.S. 120. The effect of this induced cracking was assumed to render the hat-section stringer and laminate bonded to the crown incapable of inhibiting crack opening displacement. The effect of this assumption (laminate bonded to the skin only) on the correction factor for the skin crack is also shown in Figure 40.

Critical Stress - Using $K_c = 101.2\ MN/m^2 \cdot \sqrt{m}$ ($92\ ksi\sqrt{in.}$) from Reference 8 and the correction factors from Figure 40, Equation 3.9.1 was solved for critical stress as a function of the crack size parameter, a. Results are shown in Figure 41. For comparison, results for an unstiffened sheet, i.e., $\lambda = 1$, are also shown. The critical stress was cut off at $F_{tu} = 469\ MN/m^2$ (68 ksi). Stress levels for residual strength, limit stress, and maximum test spectrum stress are superimposed.

In Figure 41 it is observed that the crack does not become critical for limit load as long as the boron-epoxy laminates remain effective. However, if both stringer and laminates were ineffective, the crack would become critical for limit load at a_c = 12.7 cm (5.0 in.); that is, when the crack is 25.4 cm (10.0 in.) long.

Thermal stresses, assuming the laminates intact, would raise the applied stress by $22\ MN/m^2$ (3.2 ksi) for normal operations or by $43.5\ MN/m^2$ (6.3 ksi) for the low temperature condition (218°K, -67°F). The conclusions remain the same except the critical crack length for the unstiffened sheet case does not apply.

Crack Propagation - The crack propagation characteristic from integrating Equation 3.9.2 for the test spectrum is shown in Figure 42, and is correlated with crack growth test observations in Figure 43. In Figure 42, results showing the effect of $22\ MN/m^2$ (3.2 ksi) thermally induced stress are also shown.

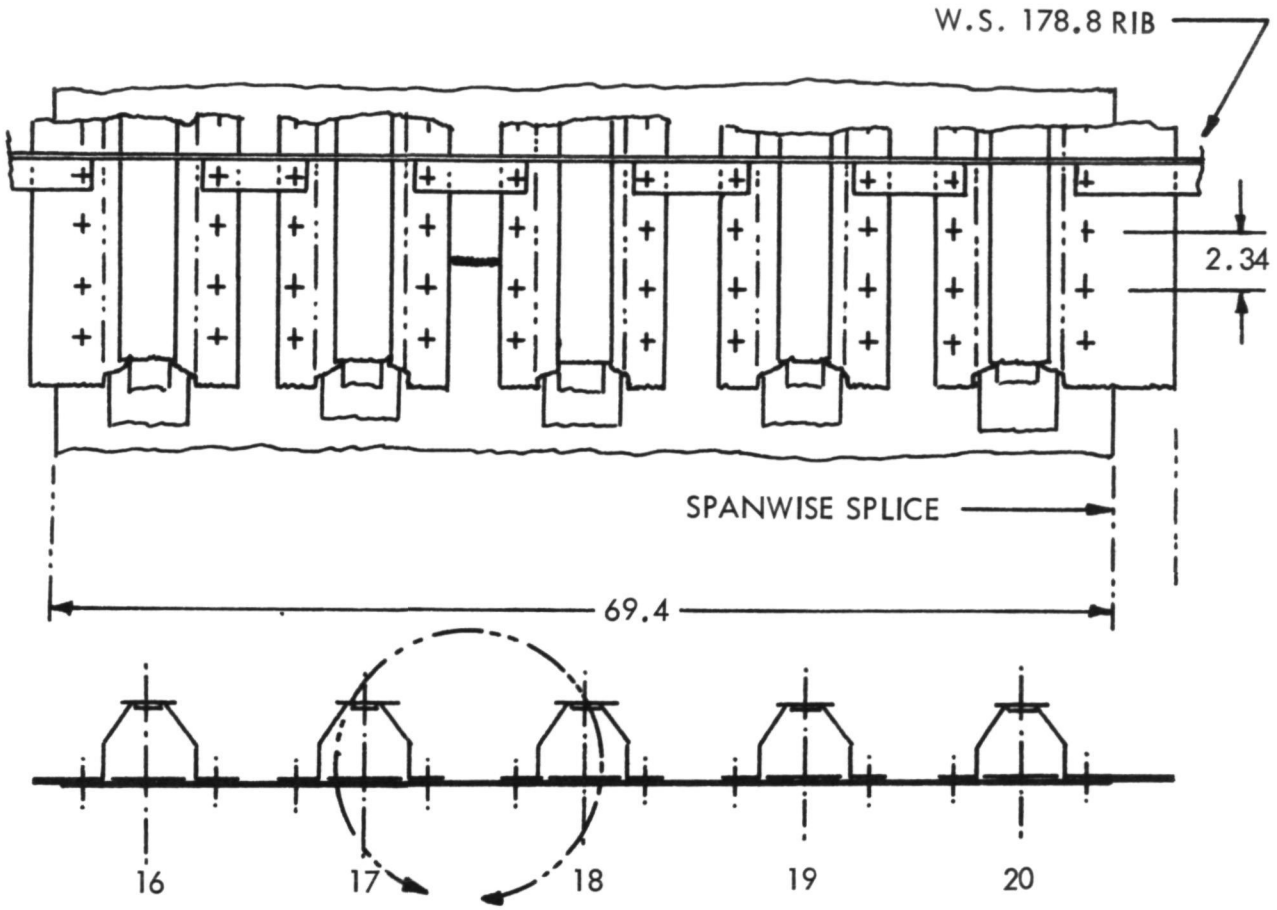

(Note: Dimensions in cm except as noted)

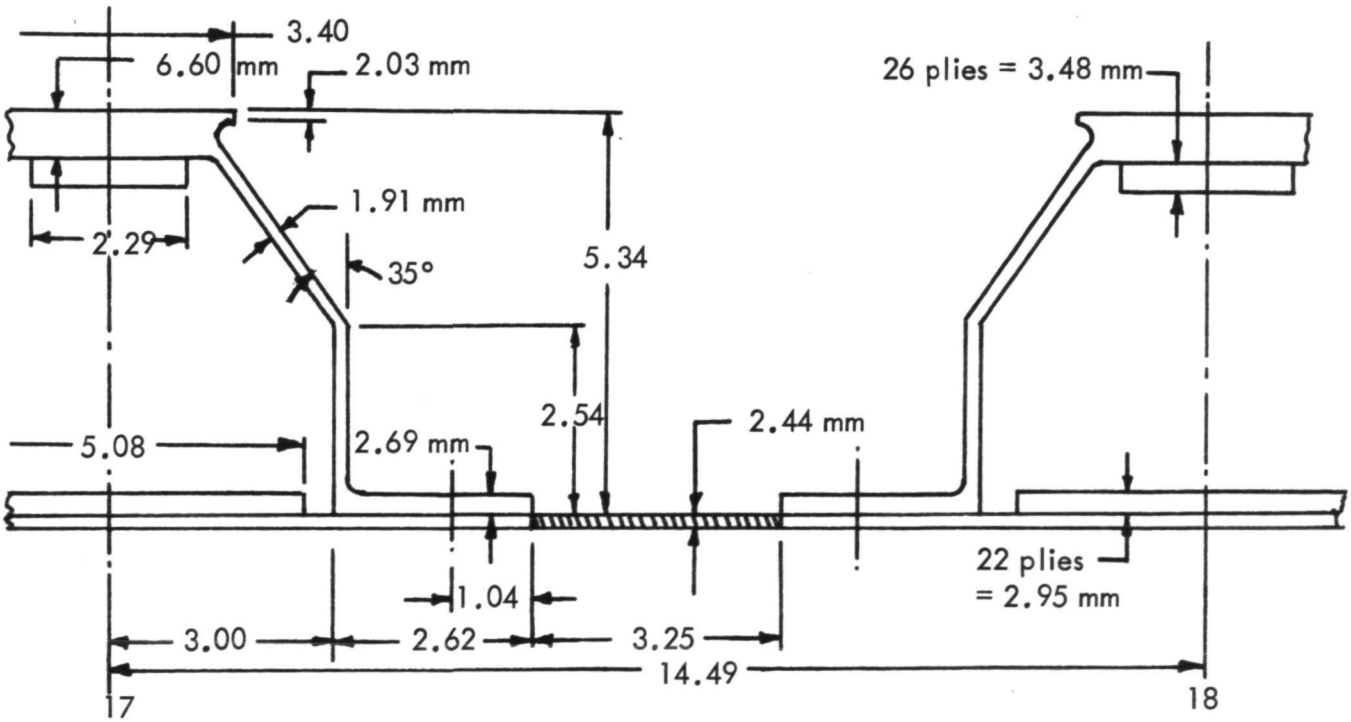

FIGURE 39. - W.S. 180 LOWER SURFACE CRACK

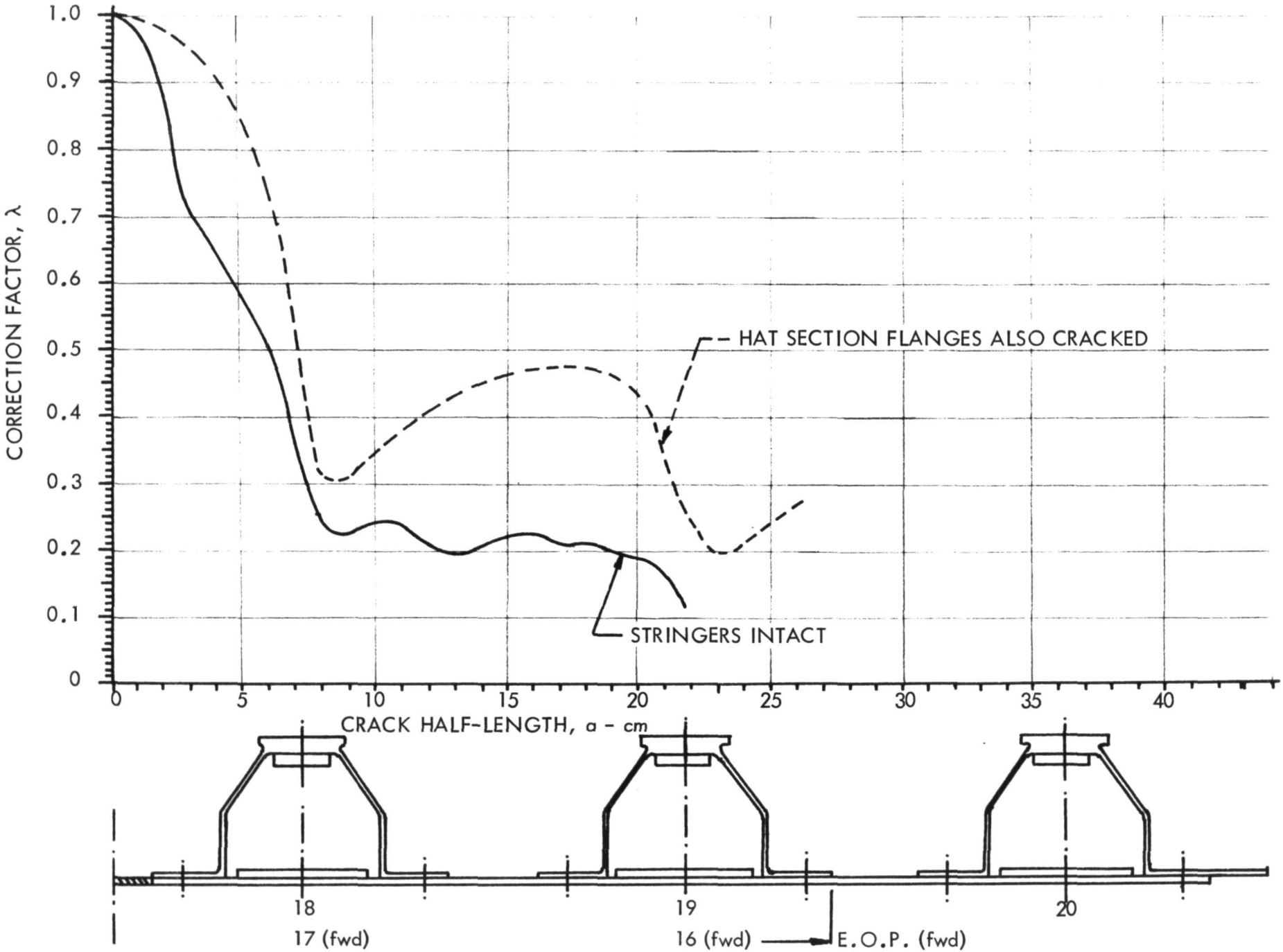

FIGURE 40. - STRESS INTENSITY CORRECTION FACTOR, W.S. 180 LOWER

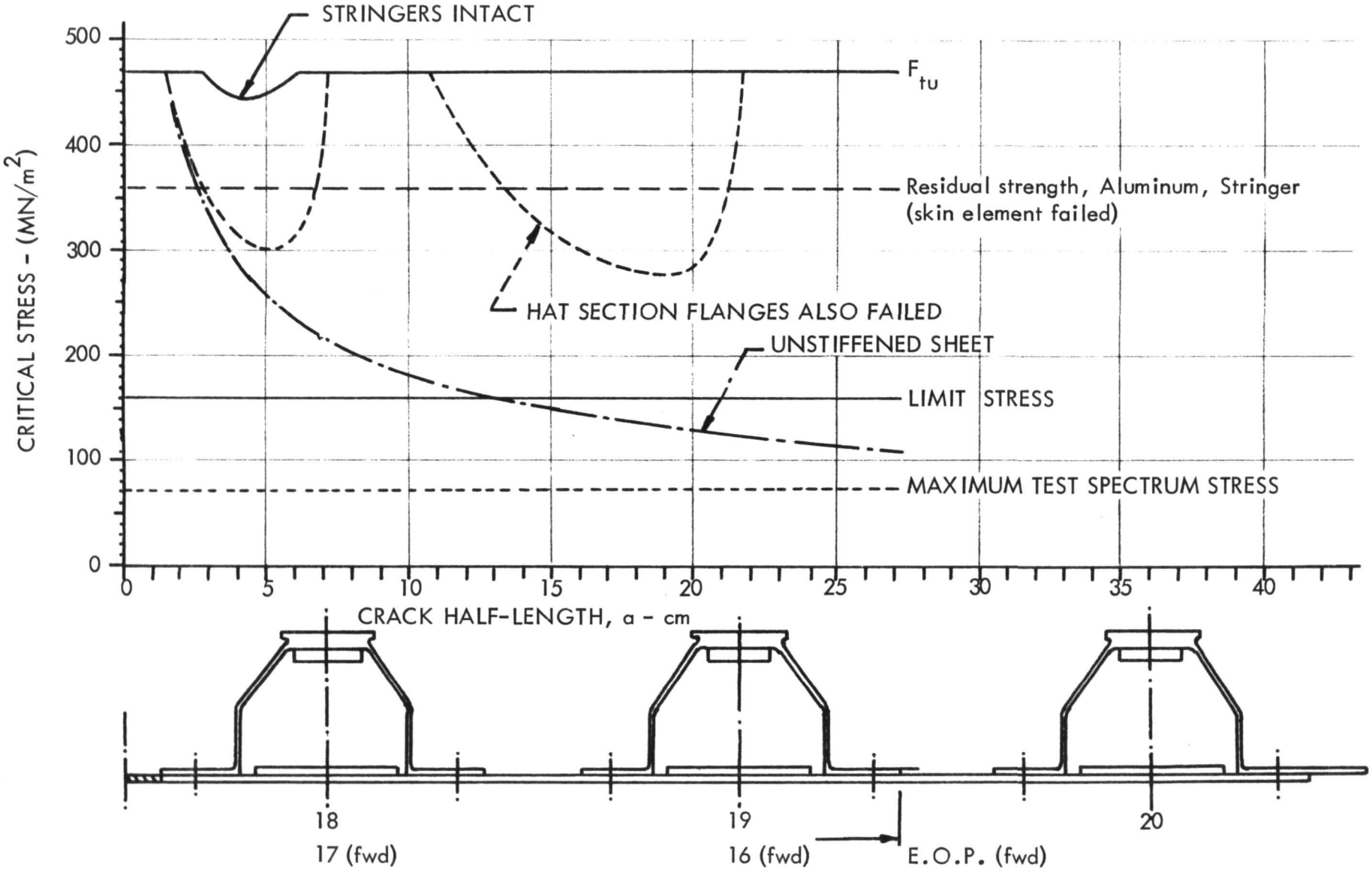

FIGURE 41. - CRITICAL STRESS, W.S. 180 LOWER

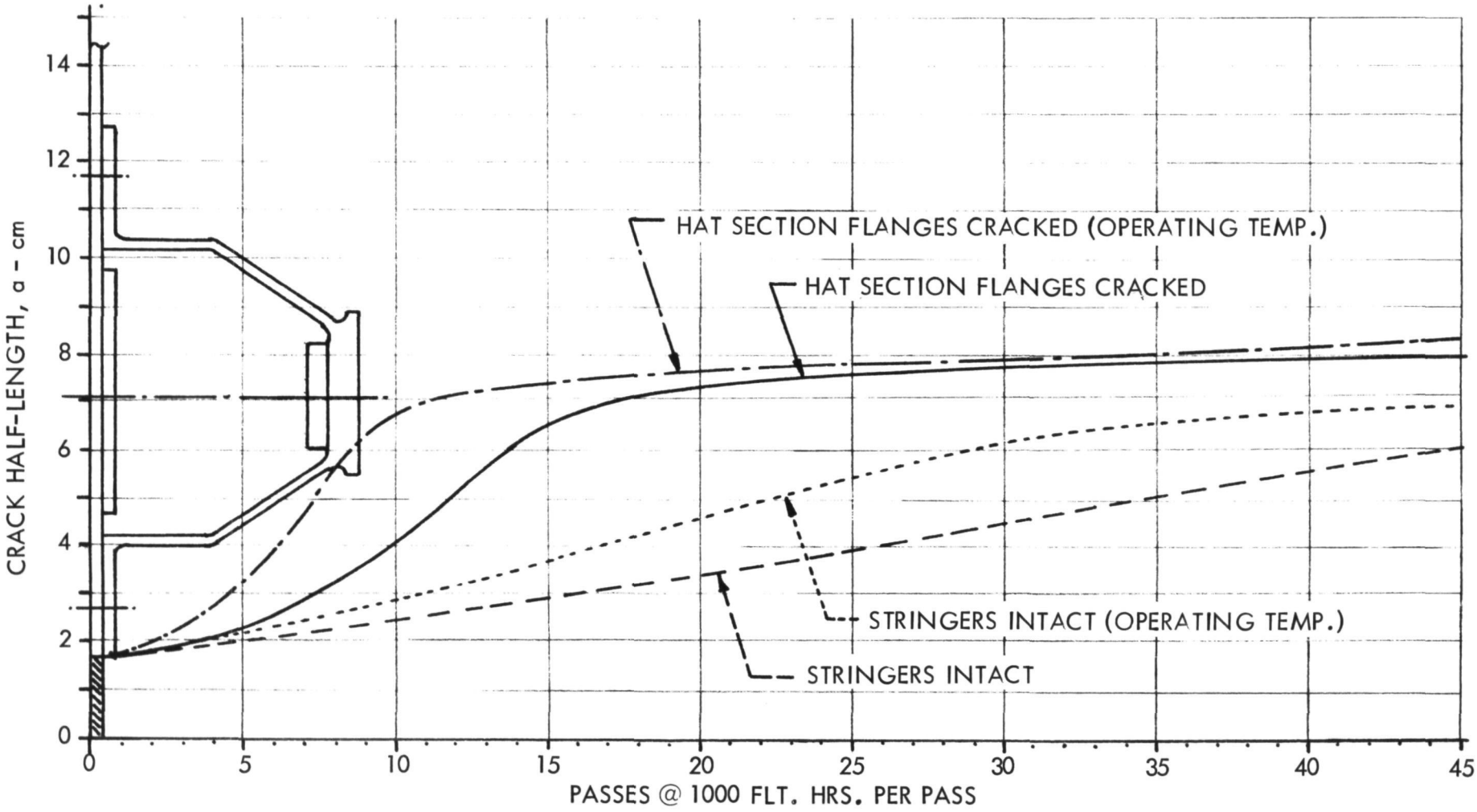

FIGURE 42. - CRACK PROPAGATION UNDER TEST SPECTRUM, W.S. 180 LOWER

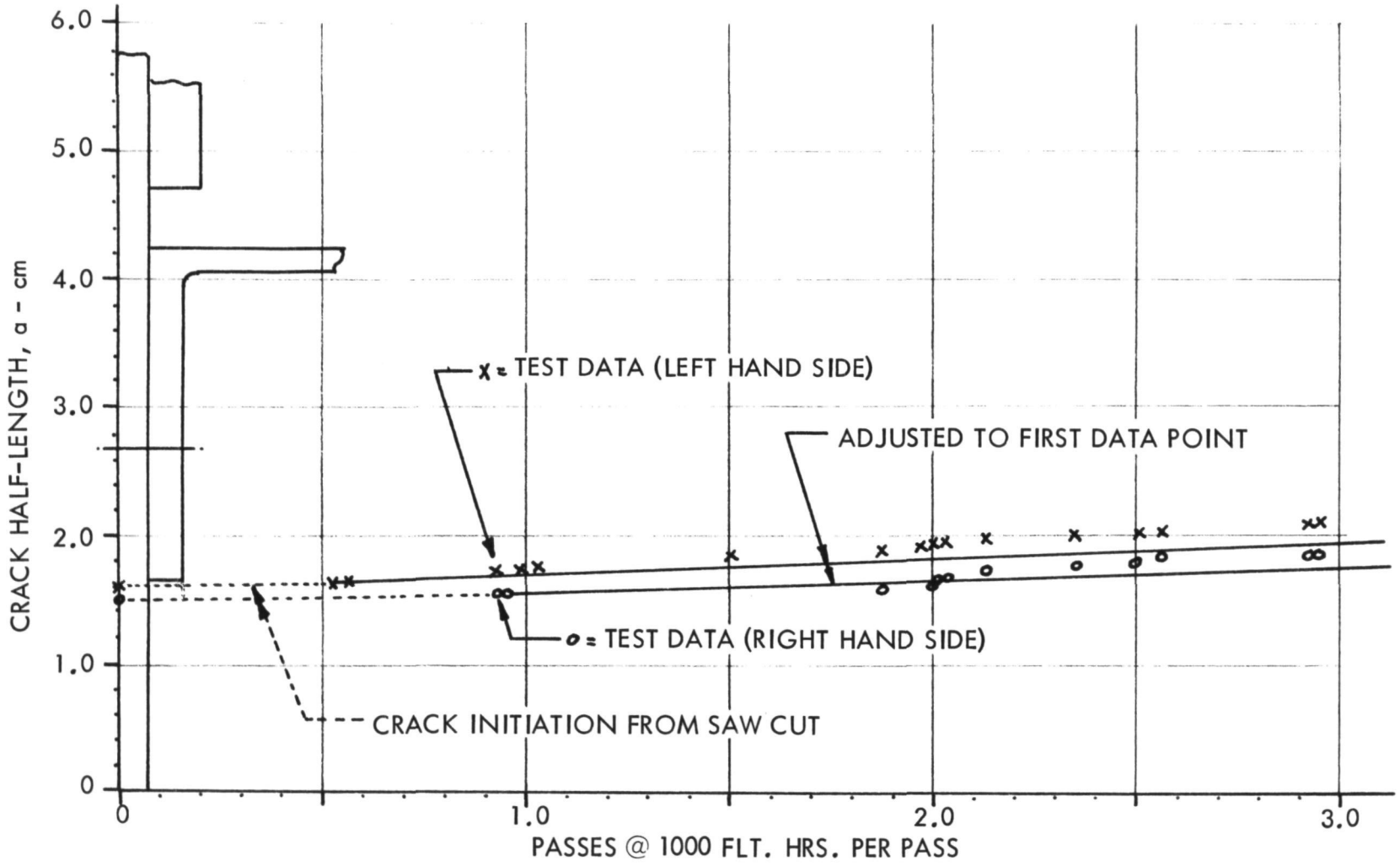

(Note: Fractional apportionment is based on cycles)

FIGURE 43. - CRACK PROPAGATION IN CRACK GROWTH TEST (SECTION 3.10), W.S. 180 LOWER

3.9.2 W.S. 120 Lower Access Door Area Analysis

The sketch shown in Figure 44 depicts the lower surface panel in the region of the W.S. 120 lower access door cutout. Cracking of the skin element from the aft side of the door cutout was investigated.

Correction Factor - The correction factor, λ, was evaluated by two methods, first, using the methods and data from Reference 12 and, secondly, using the NASTRAN computer program to solve a finite element model.

The concept of the finite element model is depicted in Figures 45 through 48. The model was configured to yield valid results while employing the simplest elements possible (e.g., Ref. 13) and to exploit the partitioning and looping capabilities of NASTRAN. Details of the model are shown in Figures 49 through 54. Mesh points were selected to coincide with fastener locations, and to provide a simulation of the bond. Model details away from the cracked area detail were phased out including no simulation of the spanwise splice nor the external splice strap. Essential influences on the correction factor were retained including the bending stiffness of the stringers normal to the plane of the skin element (Ref. 12). The cracked element (connected as shown in Figure 47) is essentially that reported in Reference 14 except a central node was added. Results of NASTRAN computer program analysis of the finite element model are shown in Figure 55.

Using the methods and data from Reference 12, the crack restraining effect of the hat-section stringer and laminates was superimposed on an effective length crack. Studies of an elliptical hole show that the effect of the hole has a limiting value of $\lambda = 2.3$ for $a \rightarrow 0$, and fairs to the "Bowie" factor for a circular hole (Ref. 8) as the crack becomes large. Using this factor, an effective through-thickness symmetrical crack may be defined using:

$$K_I = \sigma \sqrt{\pi a}\, \lambda_{Bowie} = \sigma \sqrt{\pi a_e}$$

$$\text{Thus, } a_e = a\, \lambda^2_{Bowie} \qquad \text{(Eq. 3.9.5)}$$

The condition as an asymmetrical crack approaches a stiffener, then uses a_e as a reference after scaling the true location by λ^2_{Bowie}. Since the data from Reference 12 did not go beyond the stringer, the hat-section stringer and laminates were lumped into an equivalent modulus weighted stringer bonded at the stringer center-line. The results are shown in Figure 55 for the combination of hat-section stringer plus laminates and for the case of the skin laminate alone (assuming the hat-section and crown laminate are ineffective if the stringer flange also cracks).

Test observations of crack length at times during the crack growth test (Sec. 3.10) were reduced to "test demonstrated" correction factors by assuming $\Delta a/\Delta N \triangleq da/dN$ within a phase, using Equation 3.9.2 to solve for ΔK, and using Equation 3.9.1 to solve for λ. These results are superimposed in Figure 55.

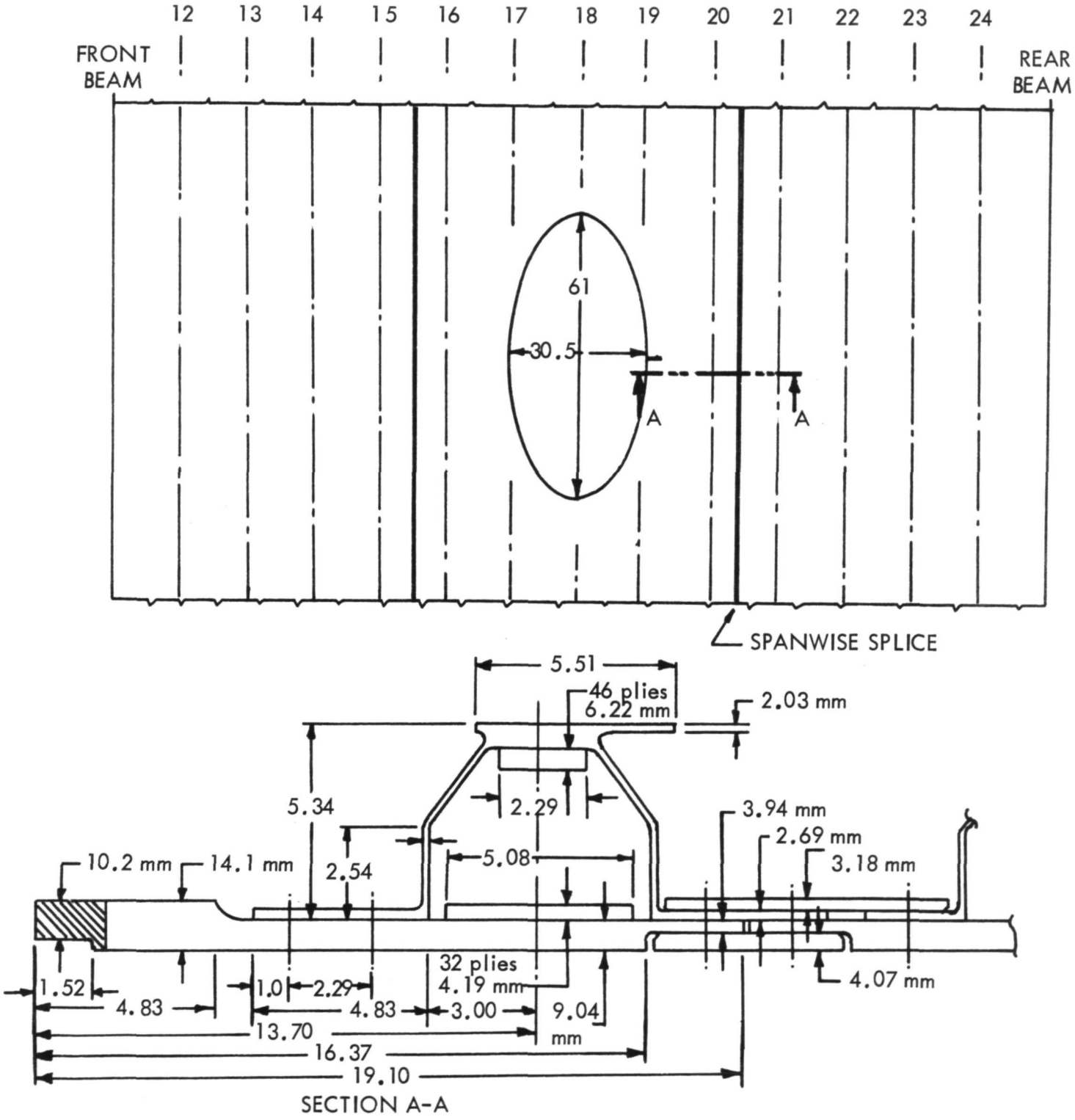

(Note: Dimensions in cm except as noted.)

FIGURE 44. - W.S. 120 LOWER ACCESS DOOR AREA CRACK

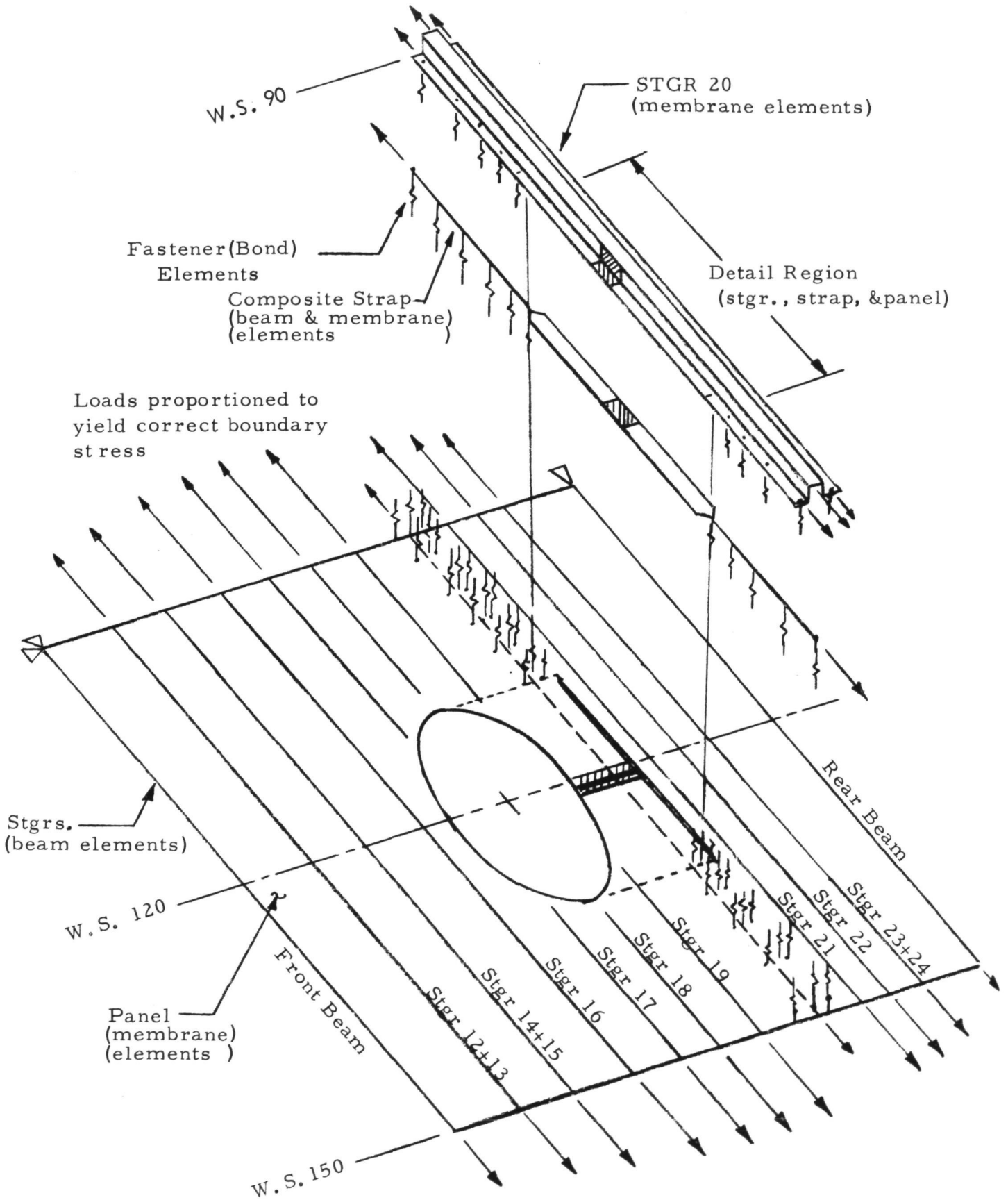

FIGURE 45. - MODEL CONCEPT OF W.S. 120 REGION

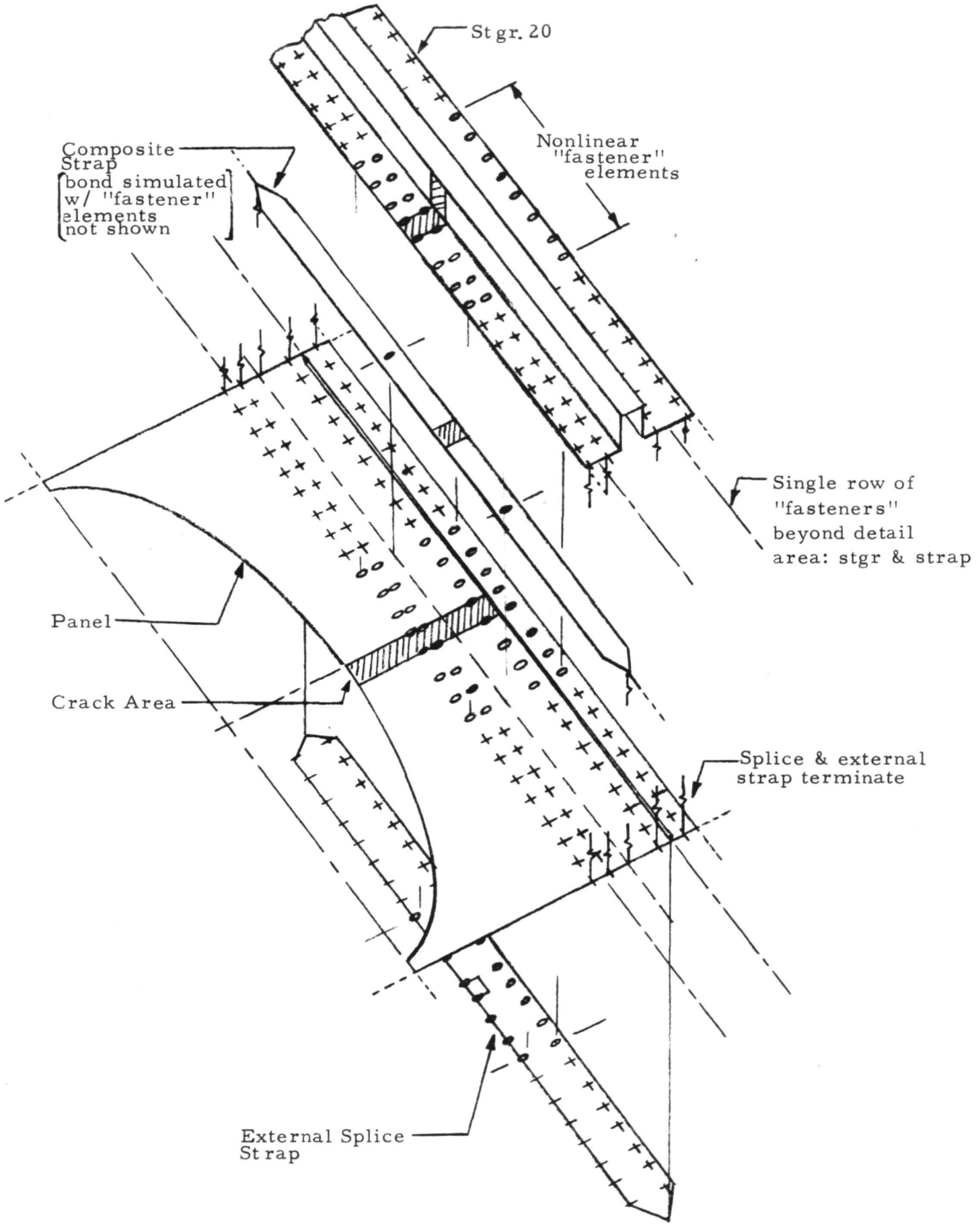

FIGURE 46. - DETAILED AREA OF W.S. 120 REGION

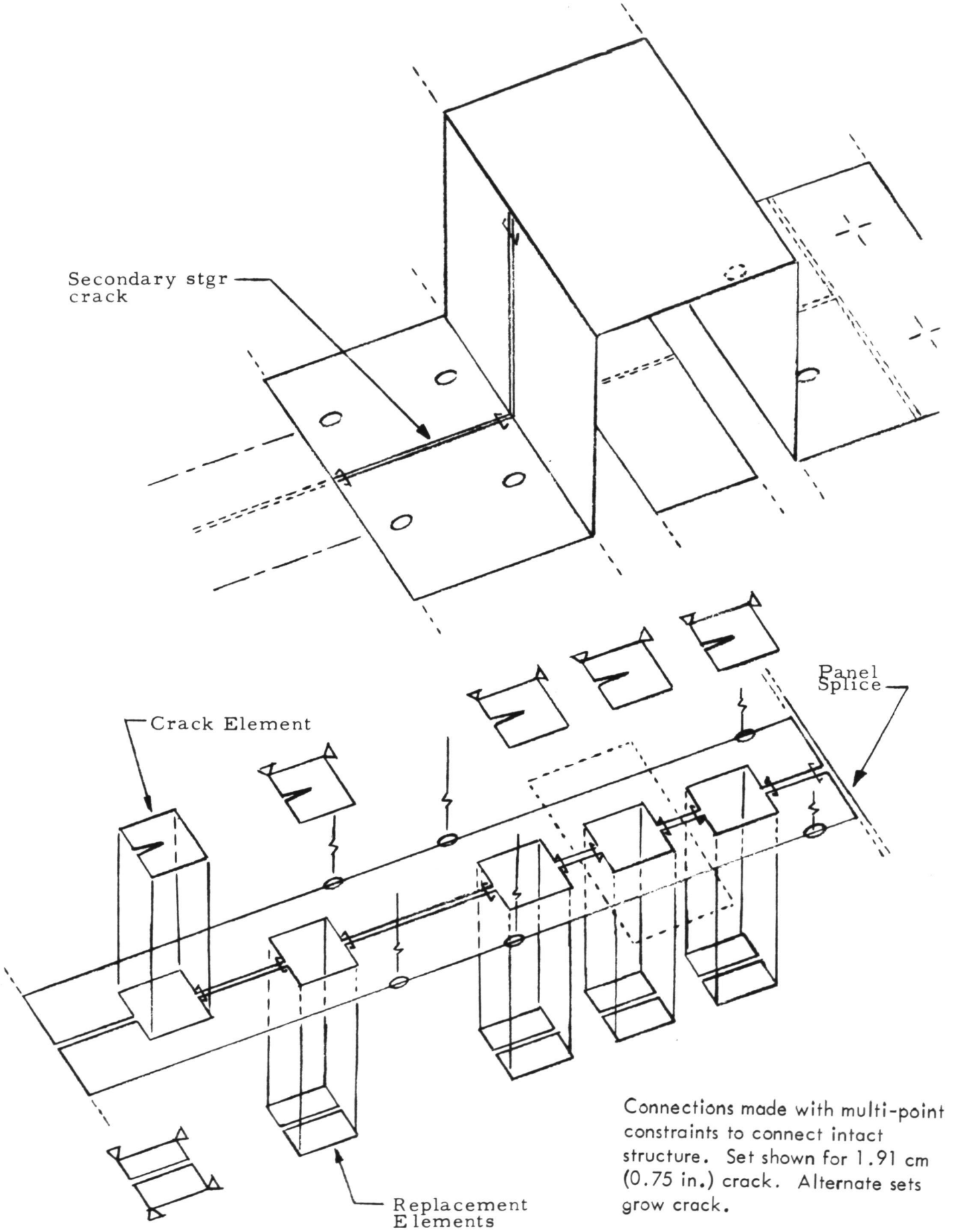

FIGURE 47. - DETAIL OF CRACKED AREA AT W.S. 120

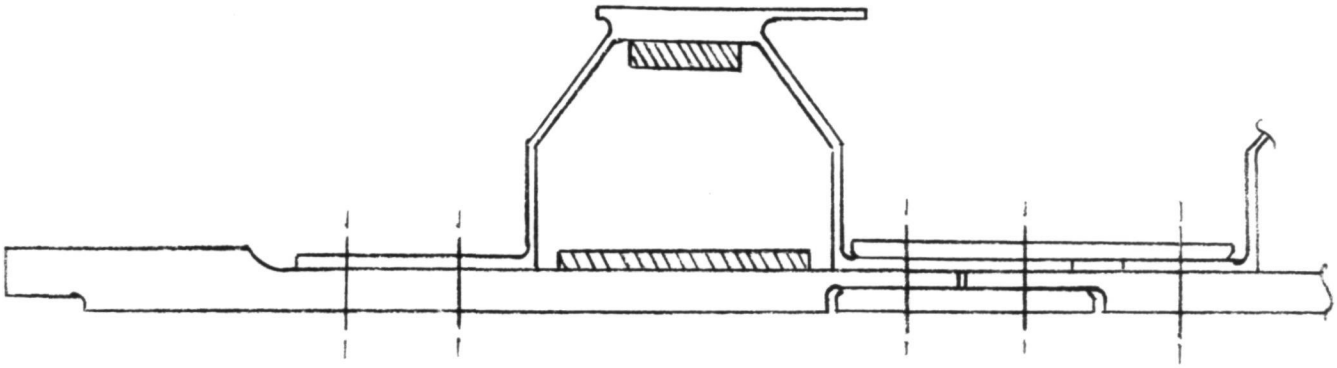

Model shown exploded for clarity.
All nodes not shown.

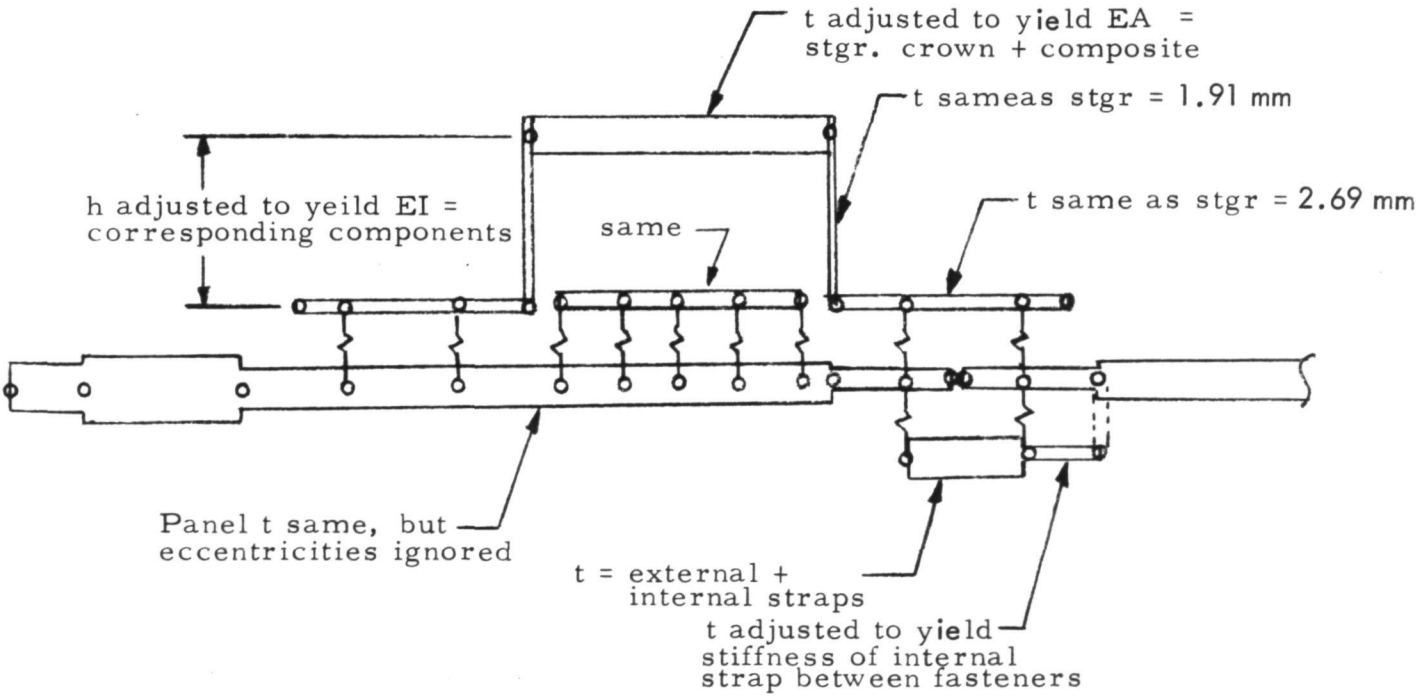

FIGURE 48. - STRINGER AND SPLICE IDEALIZATION

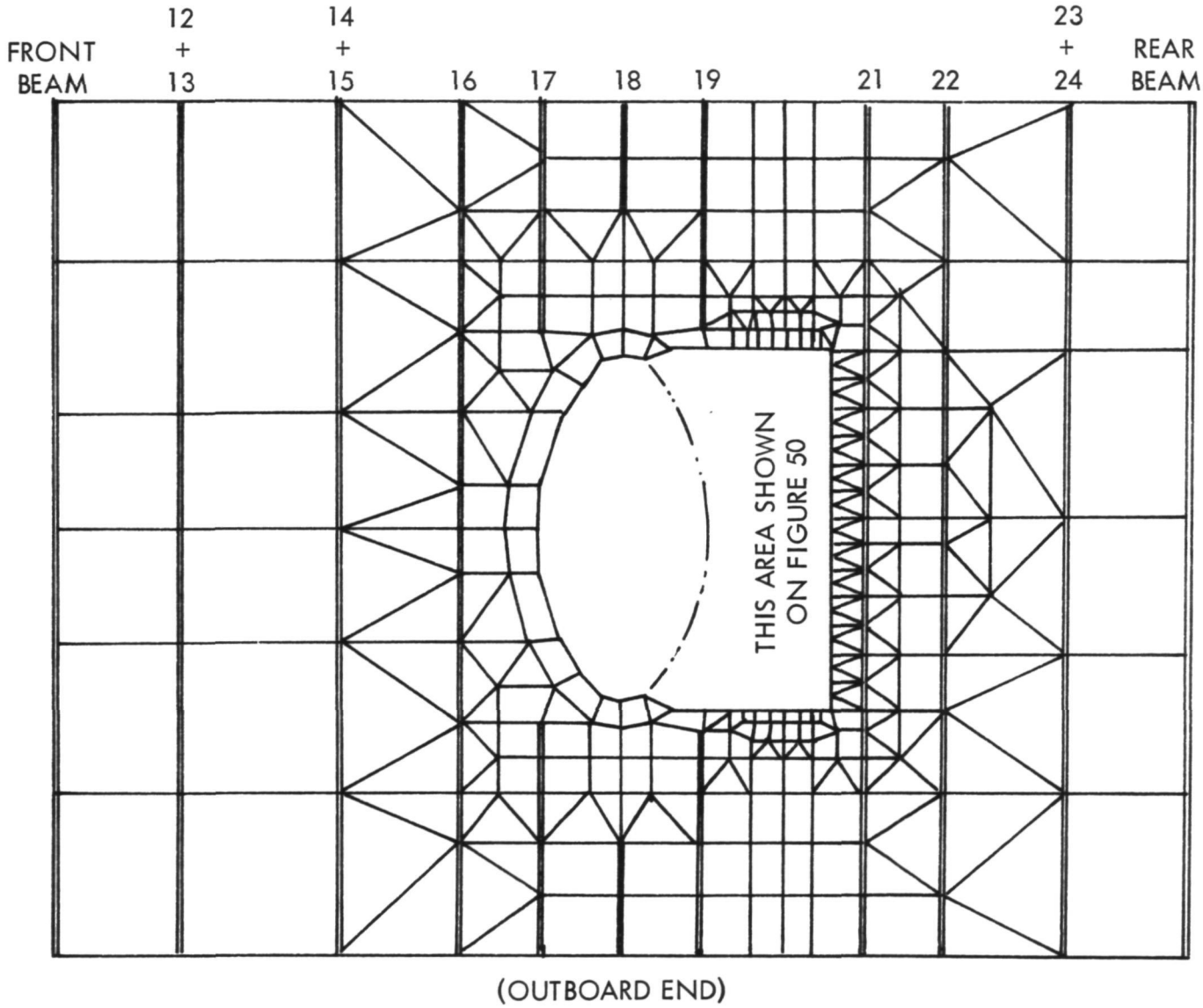

FIGURE 49. - FINITE ELEMENT MODEL PANEL & STRINGER ELEMENTS

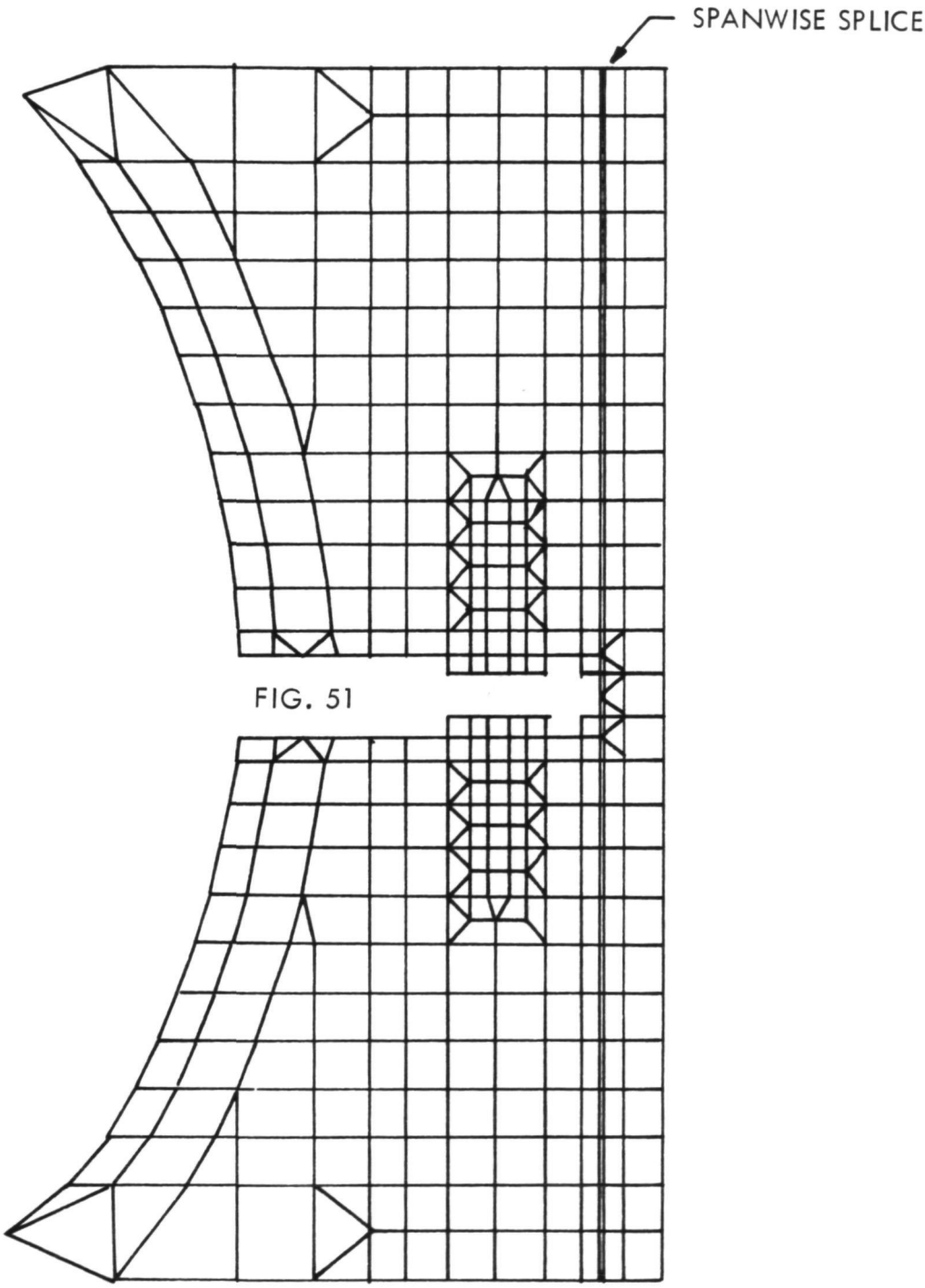

FIGURE 50. - FINITE ELEMENT MODEL PANEL ELEMENTS
AFT OF DOOR CUTOUT

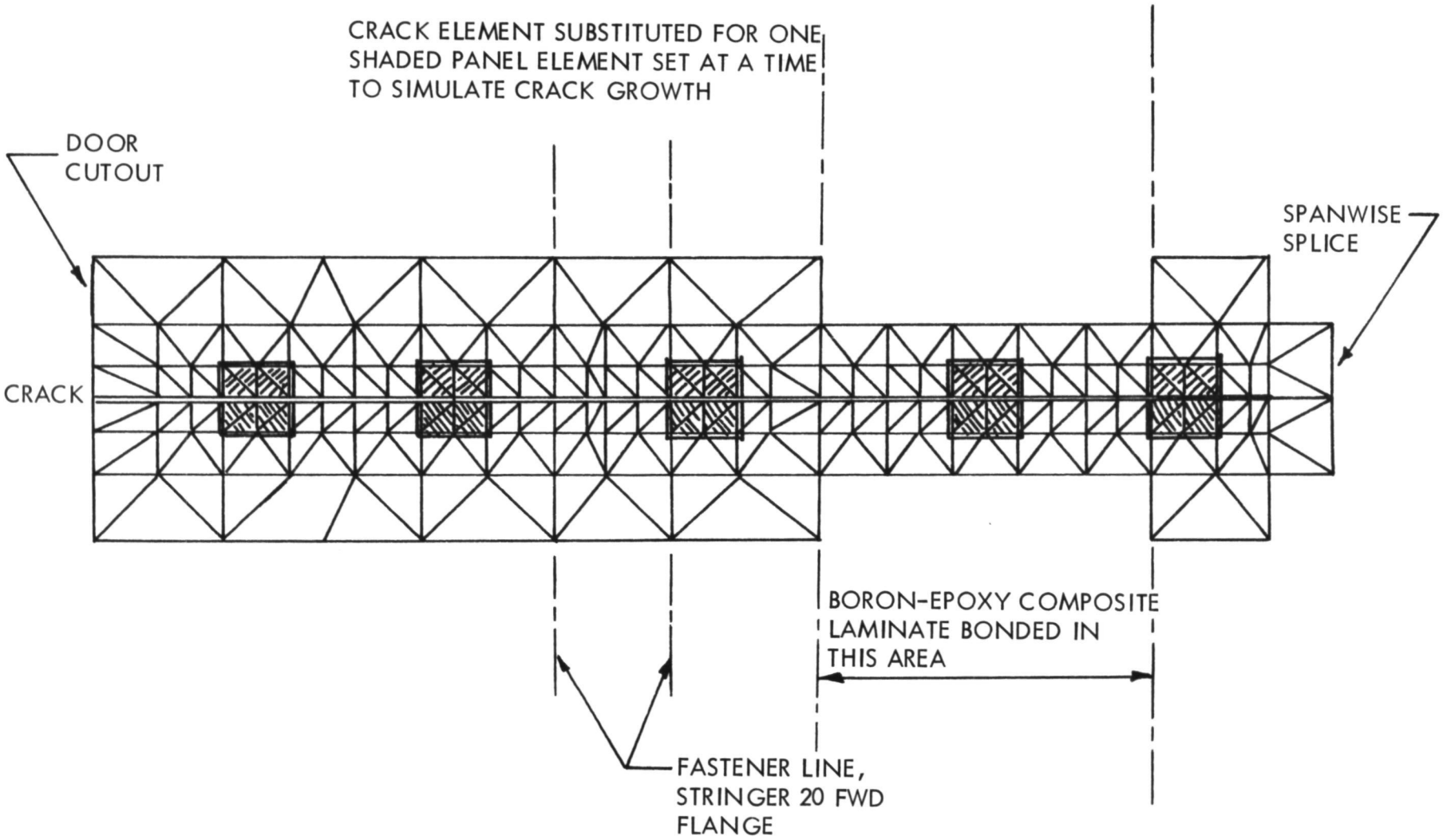

FIGURE 51. - FINITE ELEMENT MODEL PANEL ELEMENTS NEAR CRACK

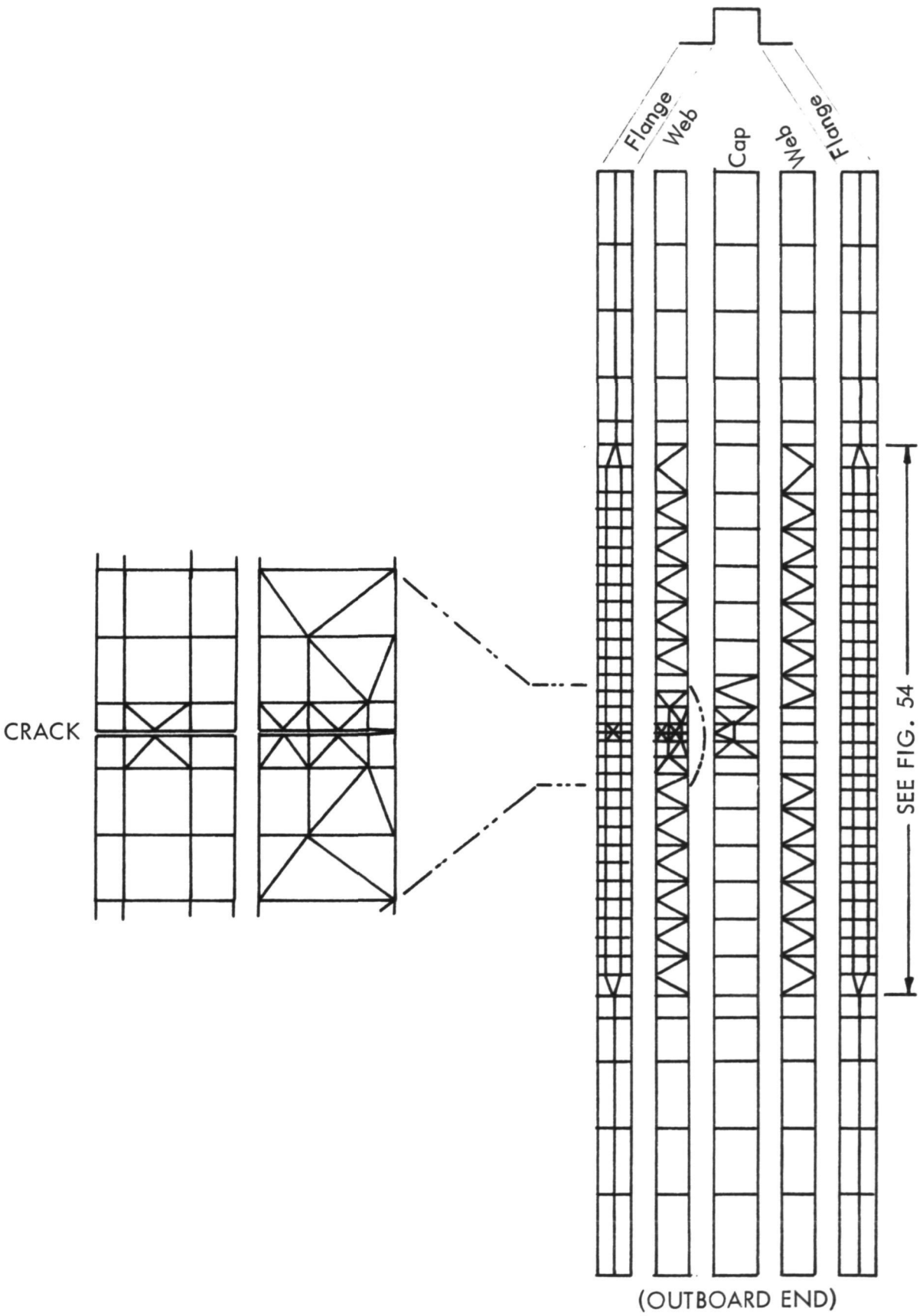

FIGURE 52. - FINITE ELEMENT MODEL STRINGER 20 ELEMENTS

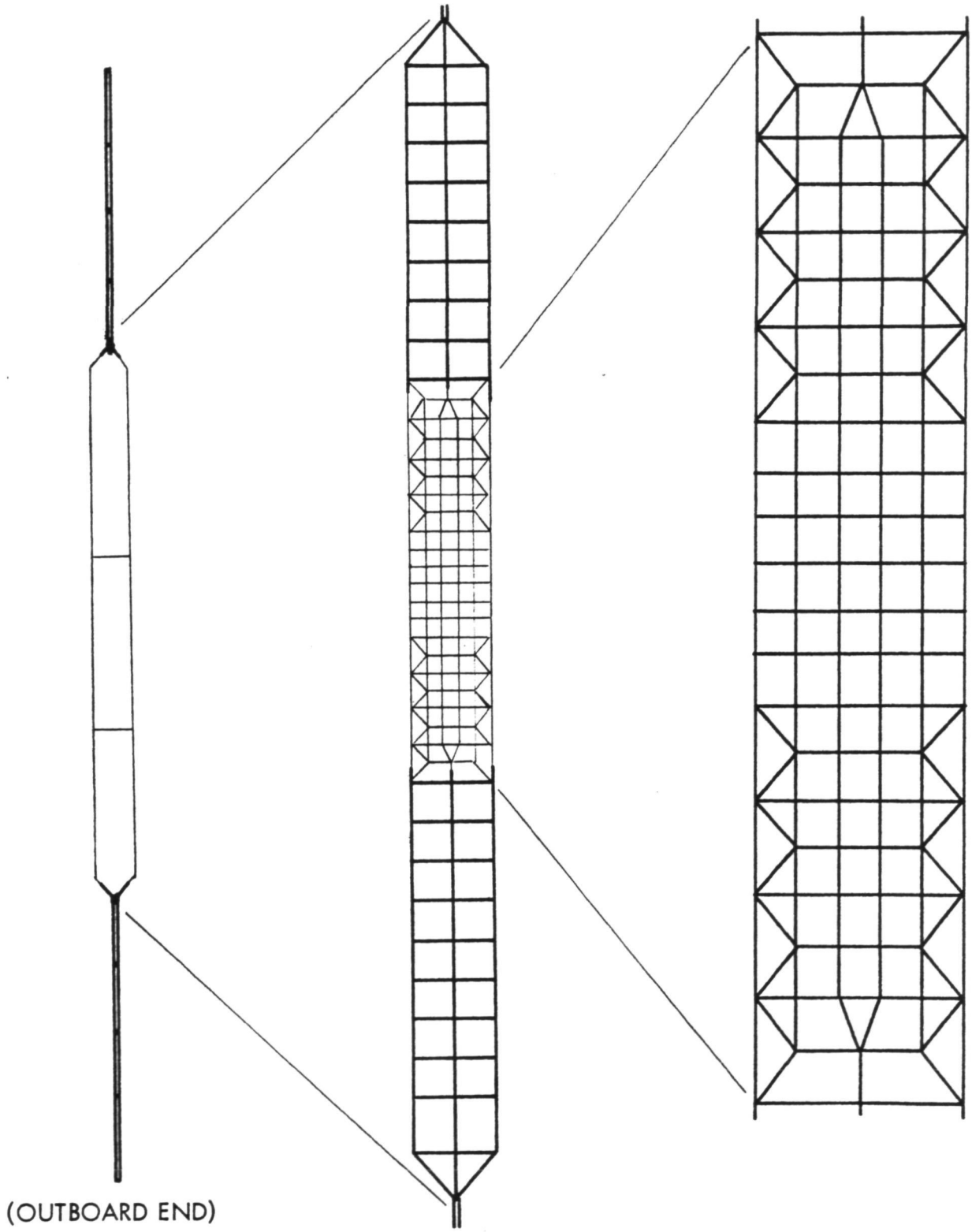

FIGURE 53. - FINITE ELEMENT MODEL BORON-EPOXY
COMPOSITE LAMINATE ELEMENTS

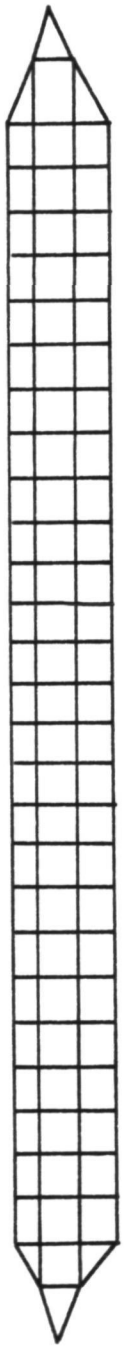

NOTE: This illustration corresponds to detail region on aft stringer flange as shown on FIG. 52.

FIGURE 54. - FINITE ELEMENT MODEL EXTERNAL SPLICE STRAP ELEMENTS

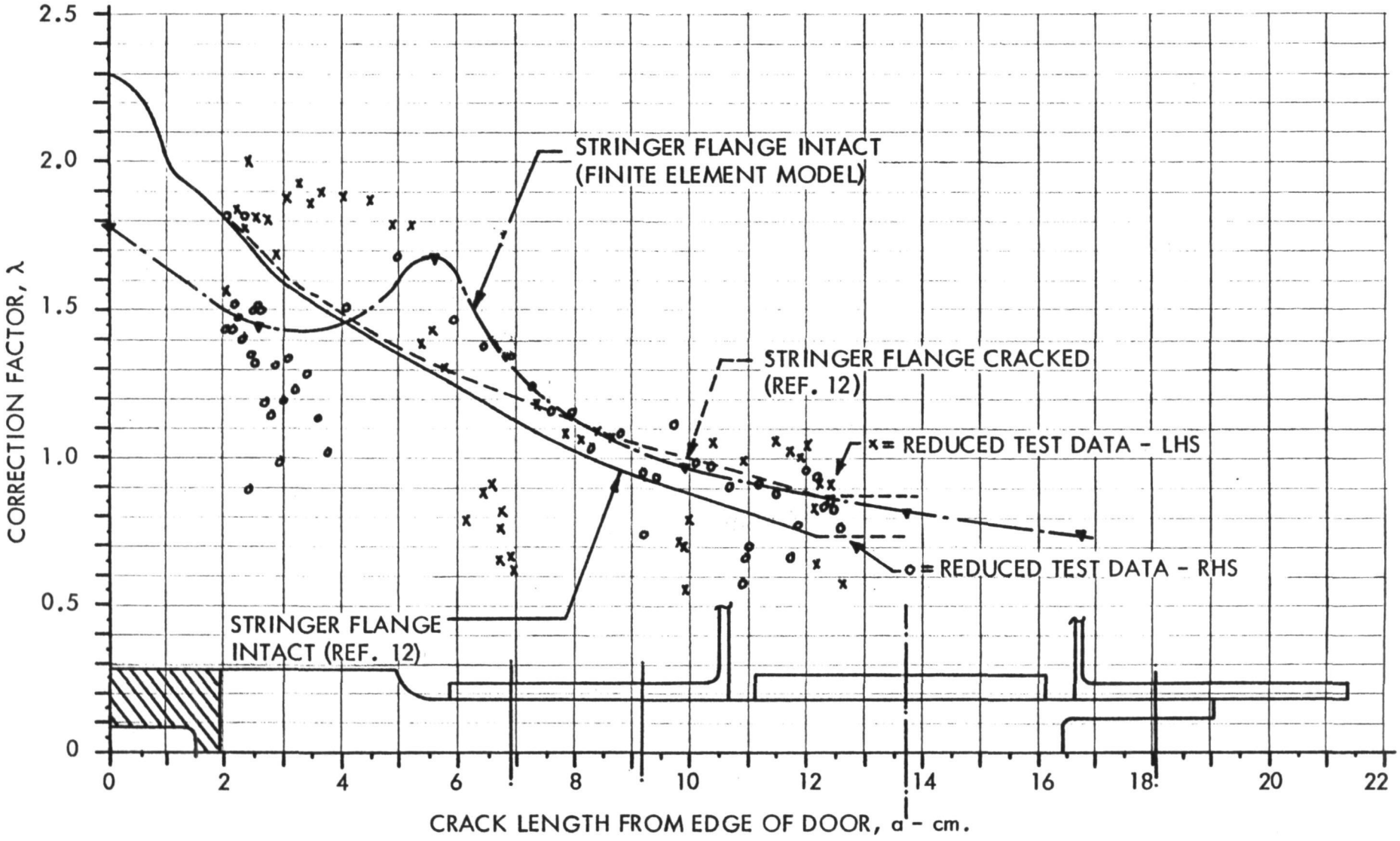

FIGURE 55 - STRESS INTENSITY CORRECTION FACTOR, W. S. 120 LOWER

The finite element model provided a means of analyzing the corresponding location on the C-130B/E all-metal configuration. Element thicknesses were adjusted and the composite laminate elements were removed. The correction factor results are compared with those of the boron-epoxy composite laminate reinforced configuration in Figure 56.

Critical Stress - Using $K_c = 78.6\ MN/m^2 \sqrt{m}$ (71.5 ksi$\sqrt{in.}$) and the correction factors from Figure 55, Equation 3.9.1 was solved for critical stress as a function of the crack size parameter, a. Results are shown in Figure 57 for the conditions of stringer and laminates intact and for the cracked stringer flange. The reduced test data from Figure 55 are also shown. The finite element model analysis results are also shown in Figure 57; indicating that for $a \geq 3.86$ cm (1.52 in.) the crack would be critical for limit stress. In the crack growth test, the cracks at this location (a = 11.61 cm (4.57 in.) LHS, and a = 12.12 cm (4.77 in.) RHS) propagated rapidly as the load was being incremented from 100 to 110 percent limit load. It arrested before reaching the edge of the panel in the splice, indicating that the finite element analysis is conservative. Critical stress results of the finite element model analysis for the C-130B/E configuration using correction factors from Figure 56 are compared with those of the boron-epoxy composite laminate reinforced configuration in Figure 58.

Crack Propagation - The crack propagation characteristic from integrating Equation 3.9.2 for the test spectrum is shown in Figure 59. Since significant crack growth occurred within a pass, phase-by-phase integration was resorted to. Results from both approaches using Reference 12 data and the finite element model analysis are shown for the stringer intact case. Test data from the crack growth test (Sec. 3.10) are superimposed including observations of the stringer flange crack. Apportionment of fractional parts of a pass was based on cycles. Demarcations of the Gust, Taxi, and GAG phases are shown.

Disbonding - Disbonding of the boron-epoxy laminates bonded to the wing skin at terminations inboard and outboard of the W.S. 120 access door (Stringers 17, 18, and 19) was investigated. At the termination, the thickness of the laminate, t, was reduced in steps to 1.02 mm (0.04 in.) while the hat-section stringer and the crown laminate were terminated leaving the wing skin as the only effective element of member 2 in Equation 3.9.4. Using $t_2 = 4.32$ mm (0.17 in.) and moduli from Reference 1 in Equation 3.9.4 yields the strain energy rate, $G = 0.000263\ \sigma_2^2$ Joules/meter where σ is measured in MN/m^2. In Reference 9, the fastest growing disbond condition (i.e., graphite-epoxy materials bonded with Epon 927 adhesive) yielded material constants, $C = 1.19 \times 10^{-9}$ and n = 3.3. Applying these conservative material constants and the test spectrum loads in Equation 3.9.3 results in negligible disbond growth at the locations investigated. The effects of mechanical fasteners and the trend established for the AF126 adhesive reported in Reference 9 tend to reduce the disbond propagation rate even more. Increasing the laminate thickness to 4.32 mm (0.17 in.) and considering the hat-section stringer and crown laminate effective increases the strain energy rate, G, to $0.00524\ \sigma_2^2$ Joules/meter where σ is in MN/m^2. Also, using the above conservative material constants, C and n, in Equation 3.9.3, the disbond propagation, Δa, is less than 0.001 mm per test spectrum load pass. Therefore, it is concluded that disbond propagation at these locations would not occur under normal operational stresses.

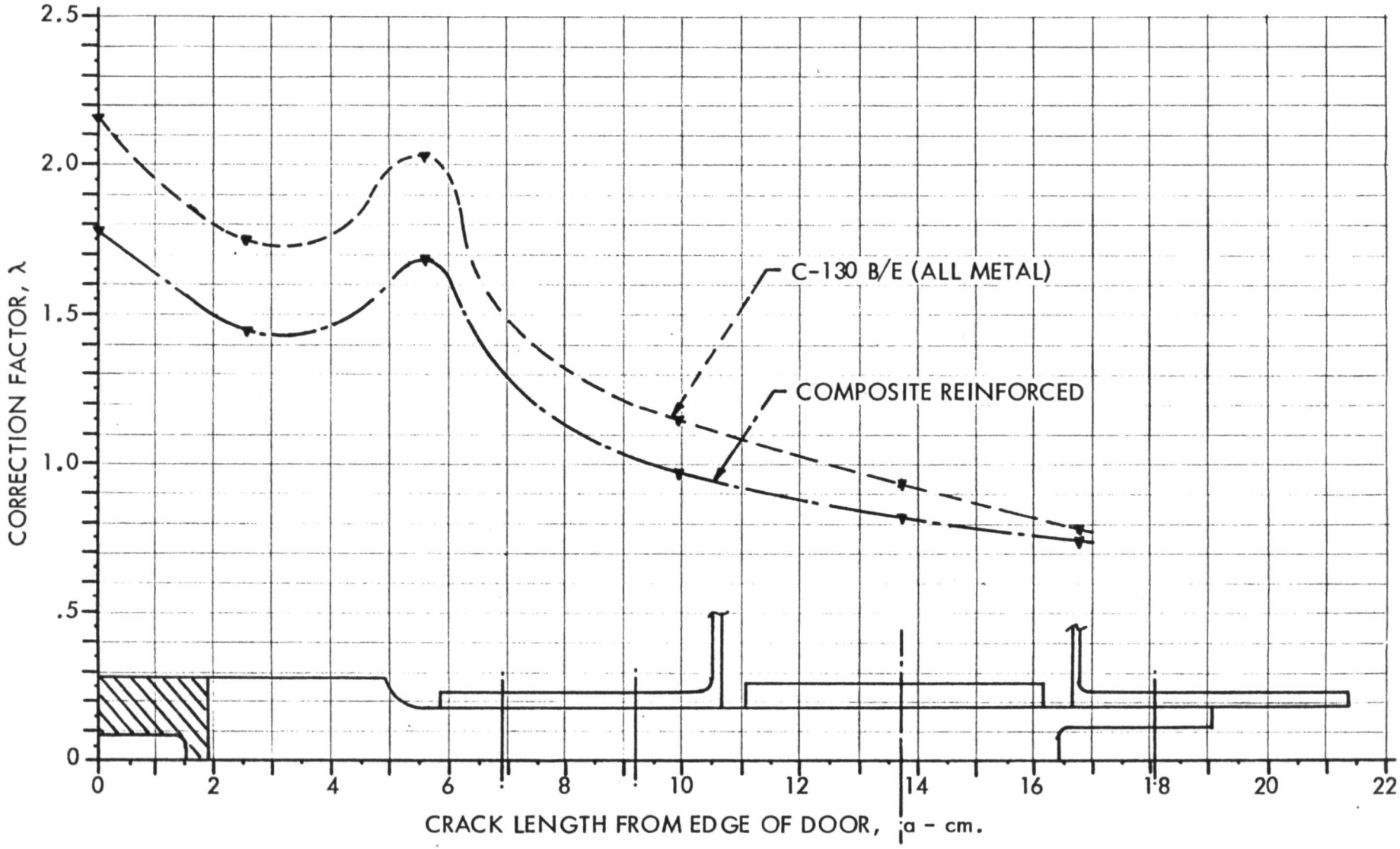

FIGURE 56 - STRESS INTENSITY CORRECTION FACTOR, W.S. 120 LOWER
COMPARISON OF COMPOSITE-REINFORCED WITH C-130 B/E

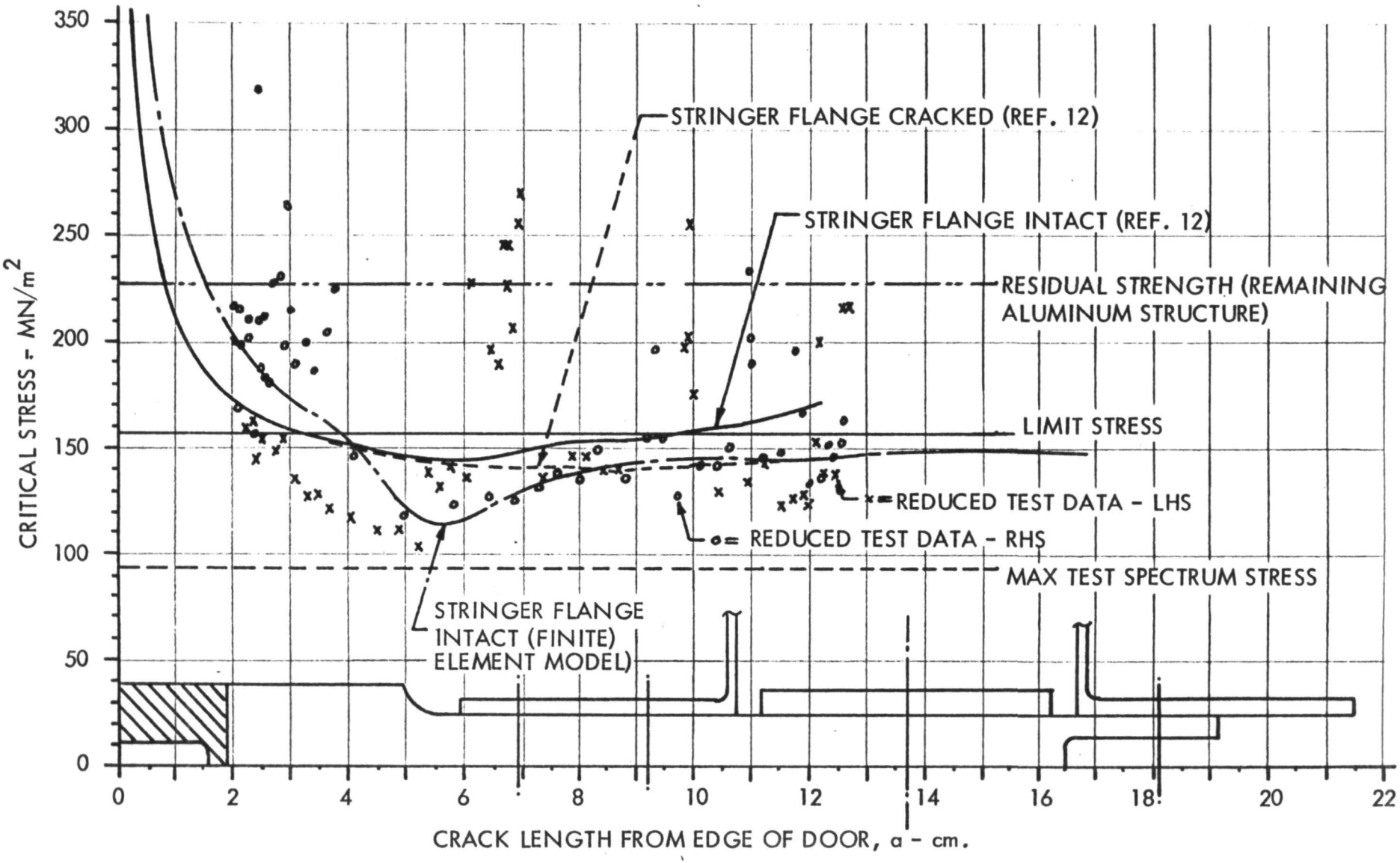

FIGURE 57- CRITICAL STRESS, W. S. 120 LOWER

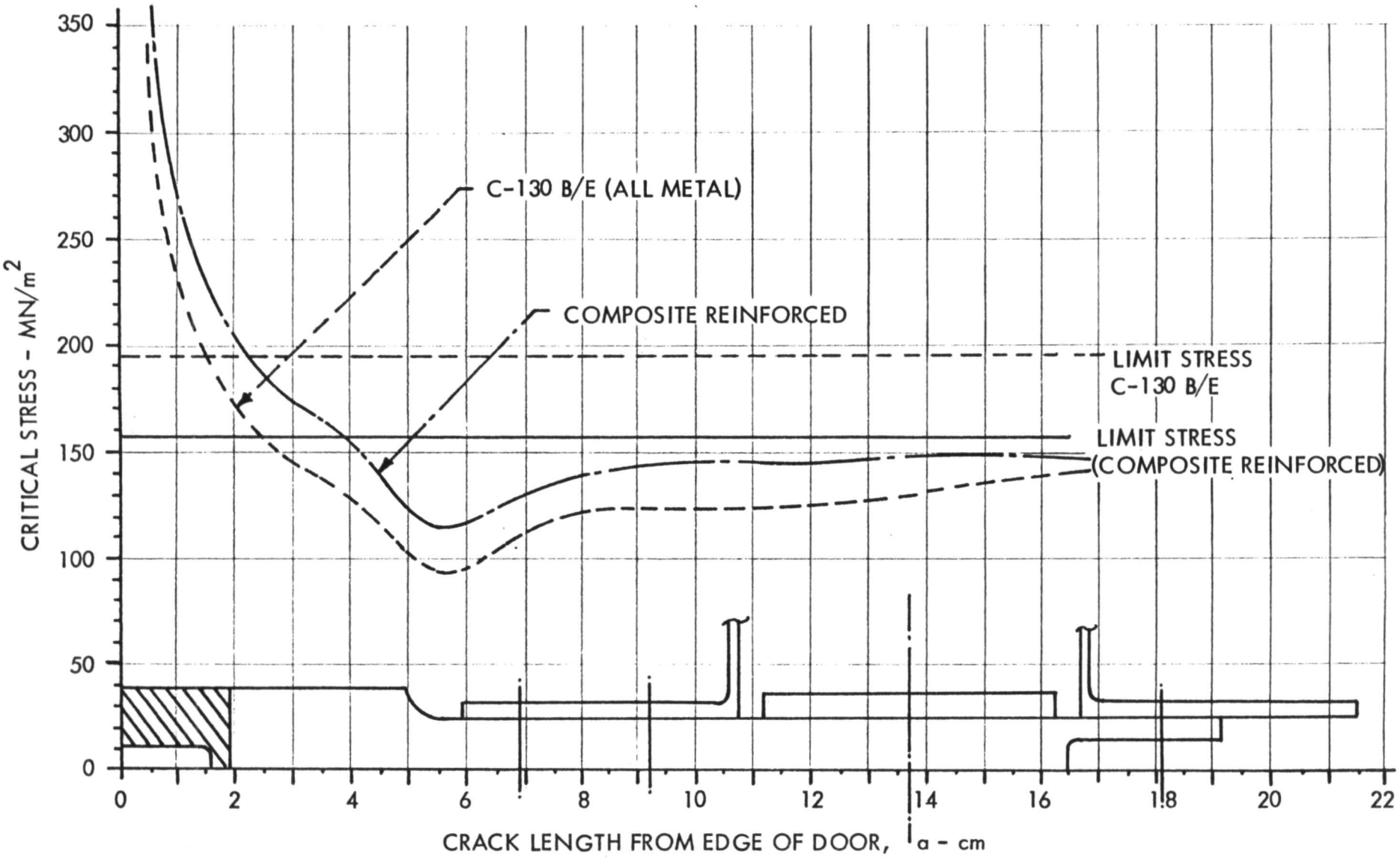

FIGURE 58 - CRITICAL CRACK LENGTH, W.S. 120 LOWER
COMPARISON OF COMPOSITE-REINFORCED WITH C-130 B/E

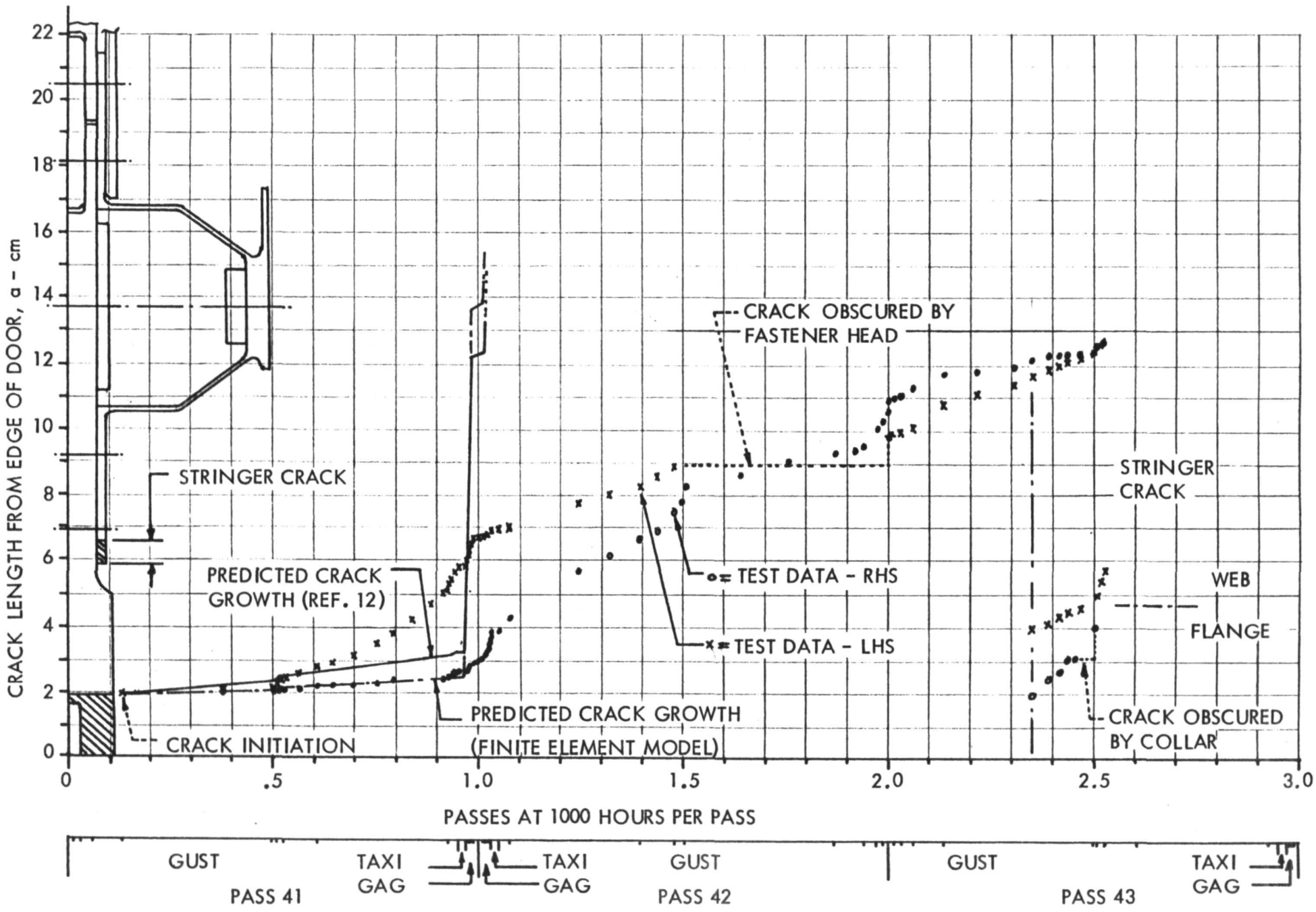

FIGURE 59 - CRACK PROPAGATION UNDER TEST SPECTRUM, W. S. 120 LOWER

3.9.3 W.S. 214 Lower Wing Joint Area Analysis

The sketch in Figure 60 depicts the lower surface panel in the wing joint area. Skin panel cracking extending from the fastener hole of the most outboard fastener in the termination region of the boron-epoxy laminate bonded to the skin panel was investigated. In the full-scale crack growth test (Sec. 3.10), a sawcut was induced as a "corner crack" as shown in Detail C of Figure 60. However, for analysis purposes, the crack was assumed to extend through the thickness as shown in Figure 61 which also depicts pertinent geometry. The reinforcement straps terminate immediately inboard of the crack location. Hence, they were considered ineffective in the analysis.

Correction Factor - The uncertainty of the effectiveness of the boron-epoxy laminate extending beyond the fastener hole led to the determination of a correction factor derived for two bounding conditions. The left-hand sketch in the lower portion of Figure 61 schematically shows the actual configuration. The lower bound for the correction factor assumes that the laminate extension is fully effective which is represented by a continuous bonded laminate. The upper bound for the correction factor assumes the laminate extension to be ineffective and the laminate causes a traction due to load transfer on the crack. Finally for comparison, the boron-epoxy laminate was considered to be disbonded which was representative of a condition imposed in the full-scale crack growth test (Sec. 3.10). The hat-section stringers including the reinforcing angles were considered to be continuous for the cases investigated as was the boron-epoxy laminate bonded to the crown of the hat-section stringer. The idealizations are sketched in Figure 61.

The methods of analysis and data from Reference 10 were used in determination of the correction factor, λ, for the lower bound case as a function of the crack size parameter, a. The crack opening displacement restraining effect of the laminate bonded to the wing skin was superimposed on that of the hat-section stringer including the reinforcing angles and crown laminate as described in Section 3.9.1 using an effective crack length defined in Equation 3.9.5 to account for the interaction of the fastener hole. The results of this analysis are presented in Figure 62.

In order to solve the upper bound case, the applied load was assumed to be distributed into the laminate bonded to the wing skin over a 5.08 cm (2.00 in.) transition length (Sec. 3.9.4). One-half of the effect of a traction load on the inboard side of the crack (Reference 15, Figure V-C-8) was added to one-half of the effect of the redistributed applied stress (outboard side of crack) using an image structure concept and an effective crack length as defined in Equation 3.9.5 to account for the interaction of the fastener hole. The shear stress in the transition length was considered to be uniformly distributed to simplify the integration of the traction force equation. Results of this analysis are presented in Figure 62.

The methods of analysis and data from Reference 10 were also used to determine the correction factor for the laminate disbonded case considering the hat-section stringer plus reinforcement angles and crown laminate (lower bound case without laminate bonded to wing skin) using an effective crack length as defined in Equation 3.9.5 to account for

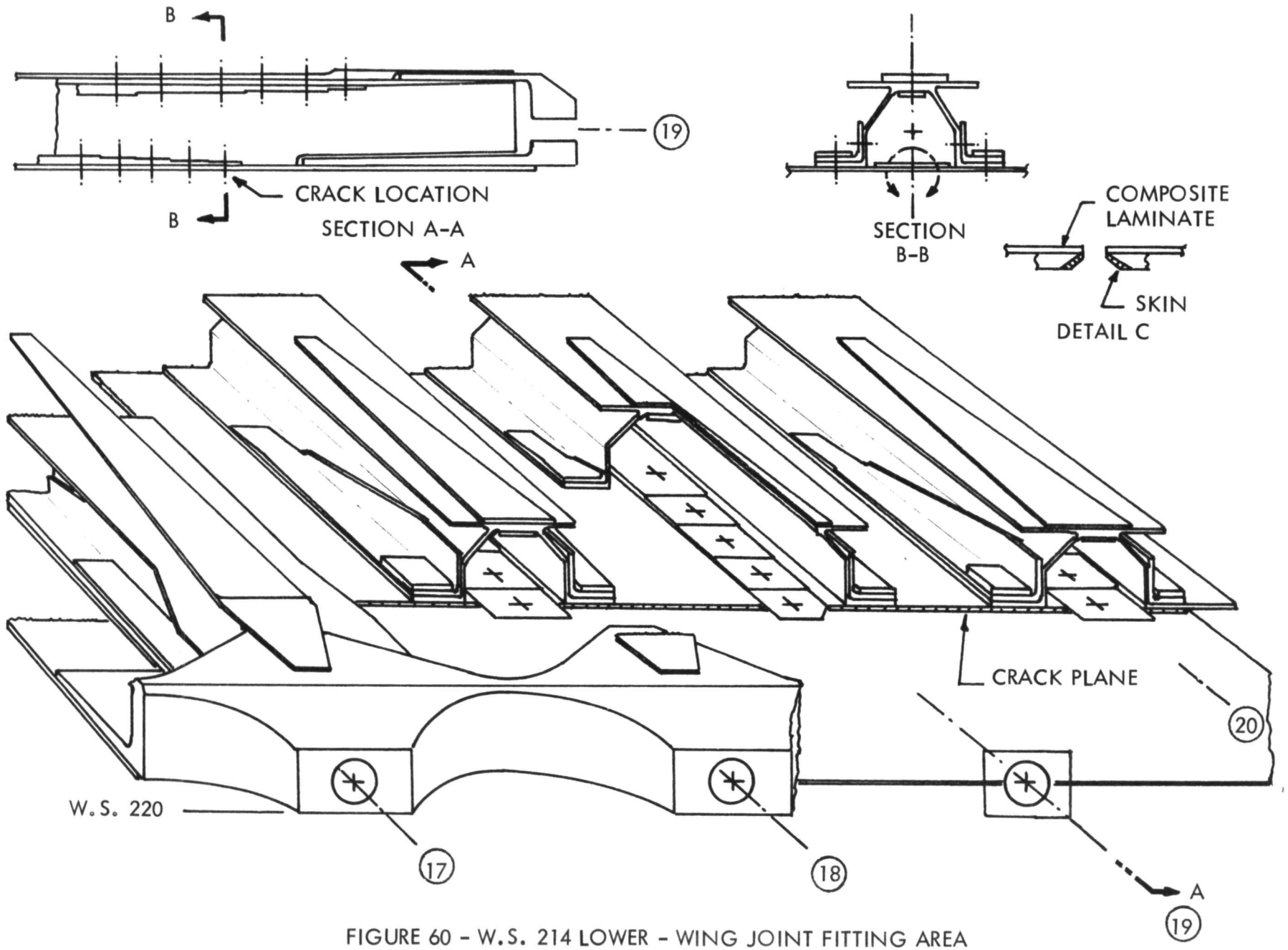

FIGURE 60 - W.S. 214 LOWER - WING JOINT FITTING AREA

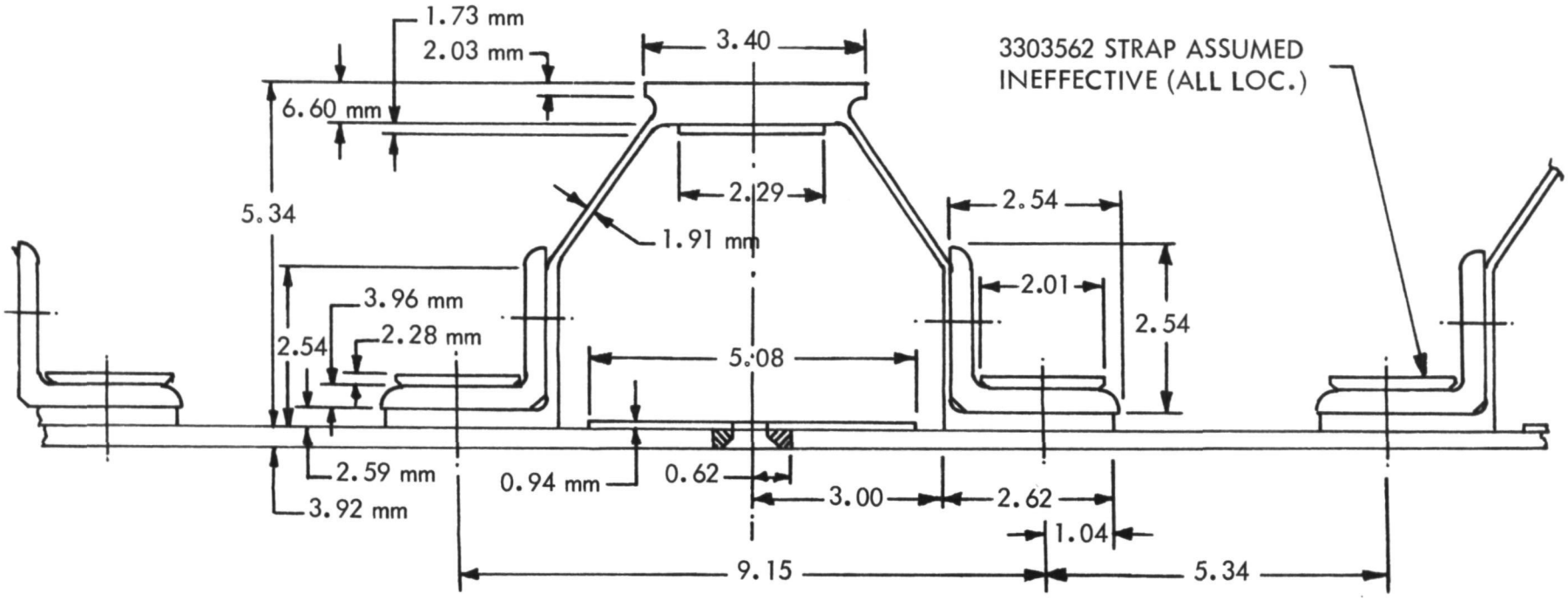

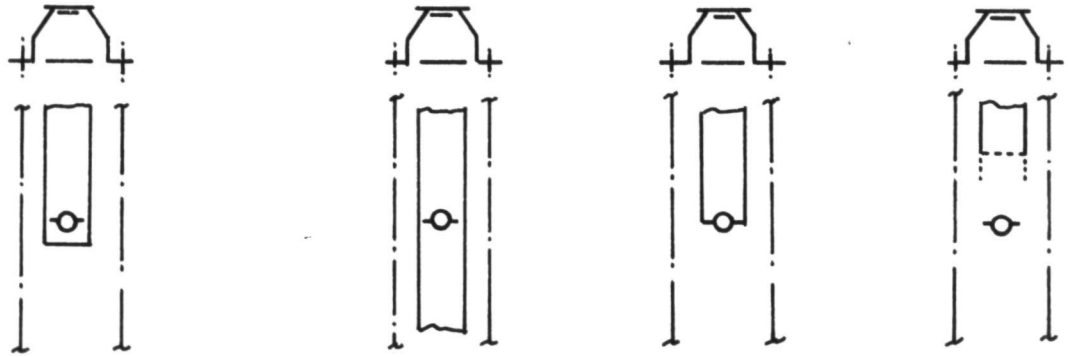

W.S. 214 SCHEMATIC-- LAMINATE TERMINATES 1.91 OUTB'D OF FASTENER

LOWER BOUND LAMINATE CONTINUOUS

UPPER BOUND LAMINATE CAUSES TRACTION ON CRACK

LAMINATE DISBONDED

NOTE: All dimensions are in centimeters unless otherwise specified.

FIGURE 61 - W.S. 214 GEOMETRY AND IDEALIZATION

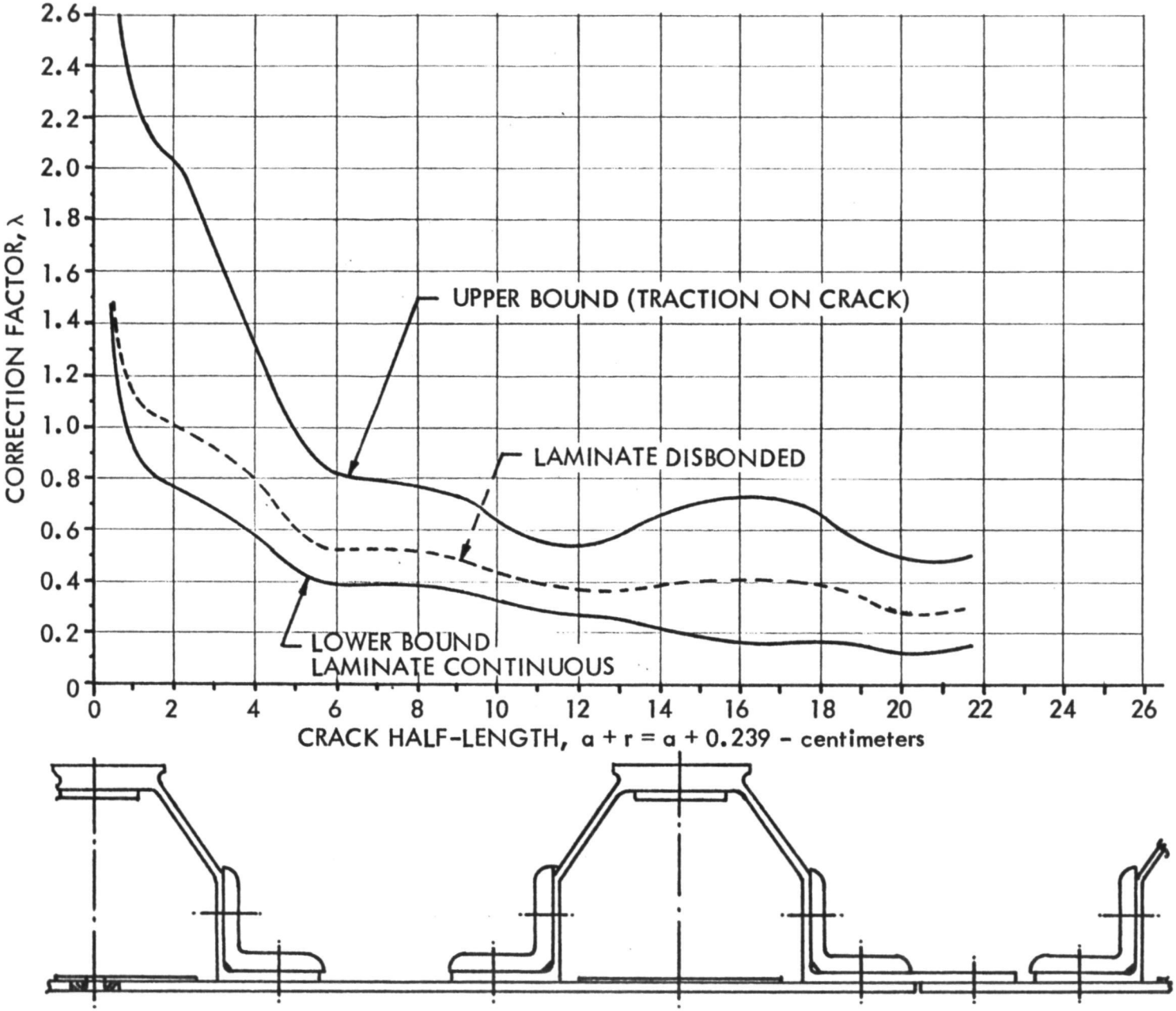

FIGURE 62 - STRESS INTENSITY CORRECTION FACTOR, W.S. 214 LOWER

the interaction of the fastener hole. The results of the analysis are also presented in Figure 62.

Critical Stress - Using $K_c = 101.1\ MN/m^2 \cdot \sqrt{m}$ (92 ksi $\sqrt{in.}$) from Reference 8 and the correction factors for the three cases from Figure 62, Equation 3.9.1 was solved for the corresponding critical stress as a function of the crack size parameter, a. The results are plotted in Figure 63. Limit stress and maximum test spectrum stress levels are shown for comparison in that figure.

If the upper bound case is taken to be the representative condition, crack lengths in the range of $15.4\ cm \leq a \leq 17.8\ cm$ ($6.1\ in. \leq a \leq 7.0\ in.$) with application of limit stress would cause immediate unstable crack propagation. Stable crack propagation may return when $a \geq 17.8$ cm (7.0 in.) due to the restraining influence of the hat-section stringer and reinforcement angles. Hence, the criterion that $K_I \geq K_c$ for $a \geq a_c$ is not satisfied and it is observed that critical crack length does not exist since the panel splice (limit of analysis applicability) is encountered at $a = 20.3$ cm (8.0 in.).

Crack Propagation - The crack propagation characteristics determined by integrating Equation 3.9.2 for the test spectrum using correction factors from Figure 62 are shown for the upper bound, lower bound, and disbonded laminate cases in Figure 64. Crack propagations for the lower bound case which considers continuous boron-epoxy laminates and the disbonded laminate case are very slow. Traction forces due to load transfer would tend to shift the true propagation characteristics toward the upper bound. However, in the full-scale test no crack extension resulted from the saw cuts as shown in Section 3.10.

Disbonding - Disbonding of the boron-epoxy laminate from the wing skin was investigated at the termination of the laminate and to the most inboard fastener in the laminate. Both of these disbonded conditions existed in the full-scale crack growth test. Figure 61 shows the geometry used in the analysis for disbonding at the laminate termination. Applying Equation 3.9.4, the strain energy release rate, $G = 0.00159\ \sigma_2^2$ Joules/meter where σ is measured in MN/m^2. Using the overly conservative material constants as described in Section 3.9.2, the resulting growth of the disbond, Δa, for each test spectrum load pass is 0.0005 mm.

The disbond condition for the laminate disbonded to the most inboard fastener is shown in Figure 61 considering the reinforcing angle no longer effective. Also, for analysis purposes, the boron-epoxy laminate bonded to the hat-section stringer crown is 4.06 mm (0.16 in.) thick and the laminate bonded to the wing skin is 2.79 mm (0.11 in.) thick. The strain energy release rate, $G = 0.000359\ \sigma_2^2$ Joules/meter where σ is measured in MN/m^2. Again, using the overly conservative material constants, the resulting growth of the disbond, Δa, for each test spectrum load pass is 0.00794 mm. Actual disbond growth increments are expected to be less due to the better adhesive used in assembly of the composite-reinforced wing box and the existence of mechanical fasteners.

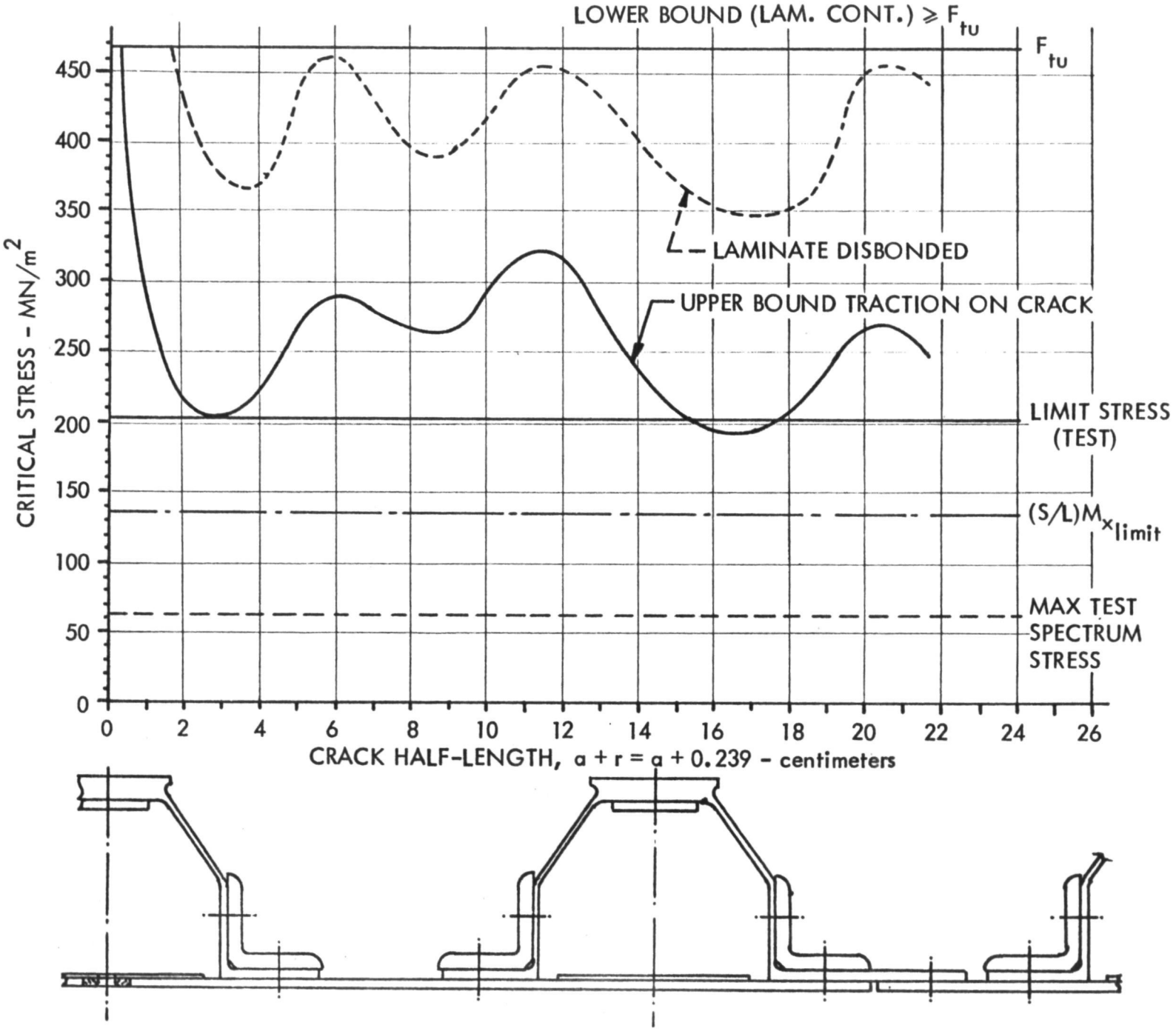

FIGURE 63 - CRITICAL STRESS, W.S. 214 LOWER

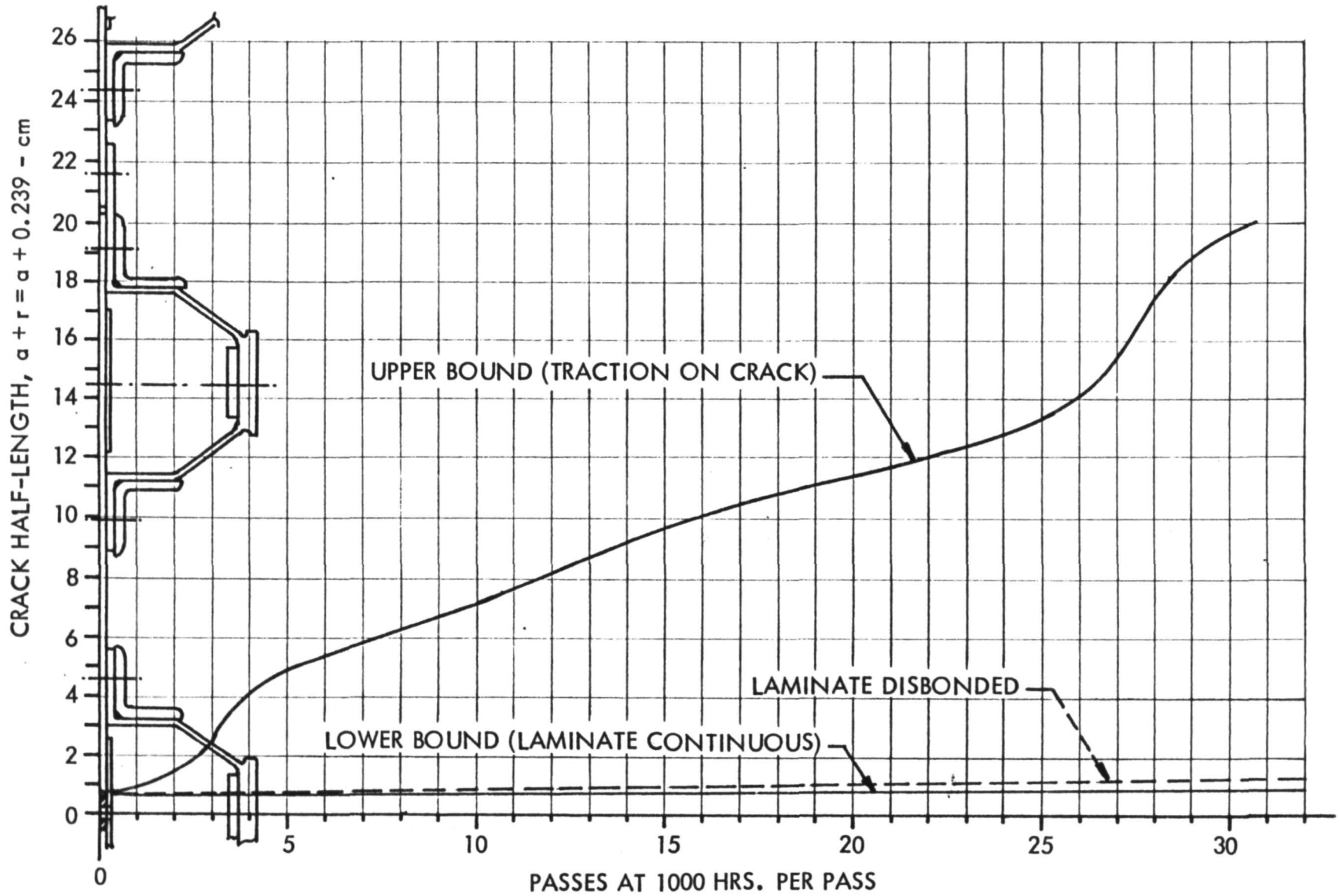

FIGURE 64 - CRACK PROPAGATION UNDER TEST SPECTRUM, W.S. 214 LOWER

3.9.4 Residual Strength Analysis

Residual strengths are determined at the W.S. 120, 180, and 214 locations with the assumption that the crack in the wing surface panel has progressed from spanwise splice to spanwise splice in the chordwise direction. The highest stress for this condition is in the hat-section stringers spanning the crack. Residual strengths are calculated for the hat-section stringers, boron-epoxy laminates, fastener bearing, and adhesive bond strength for the boron-epoxy laminate-to-wing skin panel joints.

The ratio of stringer load after the stringer has cracked to the stringer load prior to cracking (Ref. 10) is defined by:

$$L = F/(\sigma A^*_{ST}) \qquad \text{(Eq. 3.9.6a)}$$

$$\lim_{\sigma \to \infty} L = 1/\mu \qquad \text{(Eq. 3.9.6b)}$$

where L = load ratio (cracked to uncracked)

F = stringer load (cracked)

σ = applied stress

A^*_{ST} = modulus weighted stringer area

$\mu = A^*_{ST}/(A^*_{ST} + A^*_{skin})$

$A^*_{skin} = E_{skin}(bt)/E_{ref}$, in this case $A^*_{skin} = bt$

b = stringer spacing

t = skin thickness

Equations 3.9.6a and 3.9.6b were used to solve for the distribution of load into the hat-section stringer plus laminate bonded to the crown through the flange fasteners and into the laminate bonded to the skin through the bond using modulus weighted areas. At W.S. 120 an additional load distribution between the forward and aft flanges was taken into account.

That portion of the load carried by the wing skin panel before it was cracked which is transferred to the stringer through the flange attachment fasteners after the skin panel is cracked peaks at the fastener(s) nearest the crack. The peak load was calculated using methods and data from Reference 10. In Reference 16, it was determined that the peak load was reduced by a factor varying between two and five depending on fastener flexibility. A factor of two was conservatively applied for definition of the fastener bearing allowables for the tapered interference fastener system.

The load transferred to the laminate bonded to the skin is sheared into the laminate over an effective length depending on bondline thickness, adherend thickness, and bond and adherend elastic properties. This length was selected to be the laminate width of 5.08 cm (2.0 in.) based on data from AFFDL-TR-72-64 (Ref. 17). The bond shear

stress peaks at the crack at a magnitude of five times the average bond shear. Using a bond yield stress of 34.4 MN/m^2 (5.0 ksi) from Reference 18, the adhesive bond begins to form a plastic zone at 6.9 MN/m^2 (1.0 ksi) in the near vicinity of the skin panel crack. Ostensibly, the plastic zone could expand to accommodate the magnitude of load required; however, test results in Phases I and III (see Quarterly Reports #1, 2, 8 and 9) showed that this result precipitates failure. Accordingly, the bond yield is selected as the bond allowable.

The ultimate tensile strength, F_{tu}, for the aluminum and boron-epoxy laminates (Ref. 1), the fastener bearing allowable, and the adhesive bond yield constitute four failure criteria. The percentage of limit load (stress) at which these allowable strengths are reached are summarized in Table V for the three wing station locations. In addition to the basic skin panel failed condition presented as Condition 1 in Table V, results for two conditions involving associated (multiple) element failures are presented as Conditions 2 and 3 in Table V. Condition 4 in Table V is determined on the basis of the damage in the wing test article at the conclusion of the crack growth test (Table VI in Section 3.10).

The critical location of the three locations analyzed considering all four conditions in Table V is W.S. 120. At this location the forward flange of the hat-section stringer cracked during the crack growth test which exceeds the failsafe requirement of one failed primary structural element. Consequently, a repair for the stringer crack was devised and allowables for both unrepaired and repaired conditions are presented in Table V, Condition 4.

Finite Element Analysis - During the residual strength test both adhesive bond and fastener bearing allowables were exceeded without catastrophic results, although there was evidence of fastener bearing deformation at W.S. 120. A finite element analysis was accomplished using an adaptation of the NASTRAN computer program to mitigate the assumptions enumerated above for the adhesive bond and fastener allowables. The mathematical model used in the finite element analysis for the W.S. 120 region is described in sub-section 3.9.2. In particular, the finite element model employed simulations of fasteners and adhesive bonds capable of nonlinear response (Ref. 15). Using the piecewise linear analysis capability of the NASTRAN computer program, residual strength results for the boron-epoxy composite laminate reinforced configuration were obtained. Results for the residual strength of the aluminum hat-section stringer, the boron-epoxy composite laminate, bearing of the fasteners in the stringer flange, and bond yield are summarized in Table V and listed as "W.S. 120 F.E.M."

The finite element analysis showed that the bond starts to deform plastically at 27 percent limit for Conditions 1, 2 and 4. At 150 percent limit load the plastic zone had extended to 4.57 cm (1.80 in.) along the laminate, and the elements nearest the crack had exceeded the bond ultimate shear stress. Releasing these elements to simulate partial disbonding did not extend the plastic zone, but lowered all bond stresses below the ultimate shear stress. Extrapolation to complete bond failure was not possible, and failure is shown in Table V as >150 percent design limit load.

TABLE V - WING TEST ARTICLE RESIDUAL STRENGTH IN PERCENT DESIGN LIMIT LOAD

Location on Test Article (1)	Hat-Section Stringer (%)	Boron-Epoxy Laminate	Fastener Bearing	Adhesive Bond (2) (%)
Wing Skin Panel Failed (Condition 1)				
W.S. 180	226	227	342	88
W.S. 120	144	145	93	18
W.S. 120 F.E.M.	162(3)	180(3)	125	>150
W.S. 214, Outbd. Fastener	167	169	198	180
W.S. 214, Inbd. Fastener	169	170	275	65
Wing Skin Panel Plus One Hat-Section Stringer Failed (Condition 2)				
W.S. 180	217	219	113	74
W.S. 120	-	128	54	15
W.S. 120 F.E.M.	-	152(3)	113	>150
W.S, 214, Outbd. Fastener	160	162	165	151
W,S. 214, Inbd. Fastener	159	160	228	55
Wing Skin Panel Plus Boron-Epoxy Laminate Bondline Failed (Condition 3)				
W.S. 180	202	-	220	-
W.S. 120	141	-	61	-
W.S. 214, Outbd. Fastener	156	-	147	-
W.S. 214, Inbd. Fastener	130	-	140	-
Partially Failed Wing Skin Panel, Test Conditions (Condition 4)				
W.S. 180	258	-	750	-
W.S. 120 (Unrepaired)	-	128	54	15
F.E.M.(Unrepaired)	-	152(3)	113	>150
W.S. 120 (Repaired)	144	145	93	18
F.E.M. (Repaired)	162(3)	180(3)	125	>150
W.S. 214	171	173	186	91

NOTE: (1) All results presented for lower wing surface.

(2) Adhesive Bond allowable is based on a portion of bondline length being in the plastic zone and does not necessarily indicate complete bondline failure.

(3) Extrapolated by curve fit through data points $50 \leq F \leq 150$ percent limit load or stress.

As noted in the beginning paragraphs of this sub-section, the assumptions used for establishing the adhesive bond allowable included a transition length of 5.08 cm (2.00 in.) and a peak shear stress five times the average shear stress. Furthermore, the reason for including the allowable bond strength on the basis of bond yield is that in tests on components having run-out joints, partial failure appeared to precipitate other failures. The finite element model provided the necessary mechanism to perform the nonlinear analysis and was designed to simulate the adhesive bond as closely as practical. In the near vicinity of the wing skin panel crack, a fine rectangular network of elements having a 1.02 cm (0.40 in.) mesh size were connected with a set of rod elements capable of nonlinear response. These elements extended for a distance of 5.72 cm (2.25 in.) along the bondline and then transitioned to linear fastener elements whose network was phased into a coarser network of elements to facilitate practical machine run times but yet provide the necessary accuracy. Inasmuch as the assumptions and approximations necessary for constructing and analyzing the finite element model with reasonable economy were less restrictive than those described in earlier paragraphs of this sub-section, the finite element analysis results agree more closely with the test results as adhesive bond failure was not apparent upon the damaged wing test article reaching 133 percent design limit load. Furthermore, critical crack length results computed by finite element techniques are somewhat conservative as compared to test results. The conservatism may be partially due to the modeling of the adhesive bond. Although unsubstantiated by analysis, an increase in the adhesive bond stiffness would increase the skin-bonded boron-epoxy laminate effectivity, and thus lower the conservatism in the critical stress. However, such an increase would cause a more abrupt load transfer resulting in a shorter plastic zone in the bonded joint and, in turn, lowering the bondline allowable strength. As bondline failures did not occur in the tests, it is not justifiable to adjust the bond stiffness in the analysis.

As described in the third paragraph of this sub-section, the first fastener load reduction factor was selected to be two based on the joint having tapered interference fasteners. In the finite element model, rod elements having nonlinear response capability were used to model the fasteners spaced at 5.72 cm (2.25 in.) along the hat-section stringer, transitioning to linear fastener elements and finally to a single row of fasteners to maintain the number of elements to a minimum. The fastener load-deflection characteristics were extrapolated from test data on similar tapered interference fastener installations for use in the finite element analysis. As described above, the distribution of the load transferred between the forward and aft flanges of the stringers is important at this location because of the stringer-skin panel geometry and the wing spanwise splice. As for the adhesive bond, the finite element results for fastener bearing strengths agree more closely with the test results as shown on Table V for Conditions 1, 2 and 4. However, in the last static test on the wing test article, the 125 percent limit bearing allowable for the fasteners in the splice joints was exceeded upon application of 133 percent limit design load without catastrophic results.

3.10 CRACK GROWTH TEST

A crack growth test was conducted on the fatigue test article after completing the second upbending proof load test. The fatigue test article was intentionally damaged at twelve locations with ten locations in the lower surface and two locations in the upper surface. The damaged areas for both wing surfaces are depicted in Figure 65 and a detailed description of each area follows.

Wing Station 214 (Left, Upper and Lower Surfaces): At approximately W.S. 214 Left, fasteners through the wing surface panels and terminal ends of two boron-epoxy laminates were removed. Also, the adhesive bondlines attaching the laminates to wing surface panels were disbonded from the ends of the laminates to the most inboard fasteners. Corner notches, approximately 2.54 mm (0.10 in.), were machined in the wing surface panel fastener holes at the most outboard fastener locations. Diametrically opposite notches were machined in each surface panel hole and were oriented in the wing chordwise direction. None of the fasteners removed were reinstalled. One fastener hole in the lower surface panel at stringer 19 was notched, and two holes in the upper surface panel at stringer 5 were notched. Figure 66 shows the damaged area in the lower surface panel and Figure 67 shows the damaged area in the upper surface panel. The following procedure was employed in inducing damage described above.

- Removed all fasteners except the most inboard ones by drilling
- Counterbored the open holes to a 9.53-mm (3/8-in.) diameter through the aluminum wing surface panels to the adhesive bondline
- Bored additional holes 9.53-mm (3/8-in.) in diameter down to the adhesive bondline to use in disbonding the laminate from the surface panels. These additional holes are identified in Figures 66 and 67.
- Disbonded the boron-epoxy laminates from the wing surface panels by driving a 9.53-mm (3/8-in.) diameter pin against the laminates. Disbonding was initiated at the outboard holes with progression in an inboard direction.
- Verified disbonding by contact ultrasonic techniques
- Machined and sharpened notches in outboard fastener holes
- Removed most inboard fasteners by drilling

Prior to inducing the disbonds in the test article, the disbonding procedure described above was evaluated on scrapped boron-epoxy laminate reinforced assemblies.

Wing Station 214 (Right, Upper Surface): Artificial damage was accomplished at this location as described above for W.S. 214 Left. However, artificial damage on the right wing location was less severe as only the most outboard fastener holes were involved. The most outboard fasteners were removed by drilling, and 2.54-mm (0.10 in.) corner notches were machined in the holes in the aluminum wing surface panels as accomplished at W.S. 214 Left. No disbonding of the adhesive bondline was performed and the remaining fasteners were not disturbed. Figures 68 and 69 show the notched fastener holes having no natural crack growth and prior to installation of blind type fasteners.

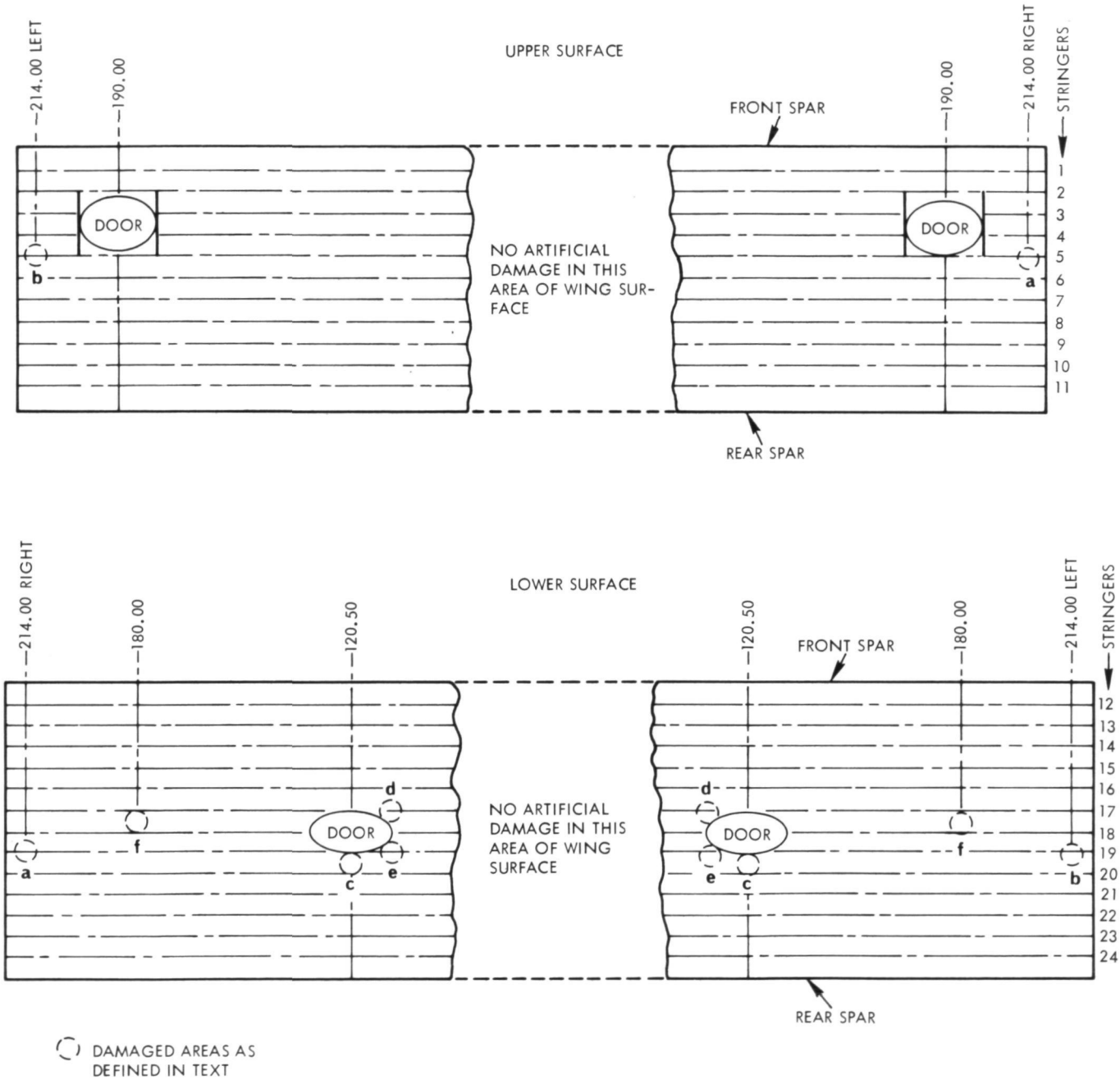

FIGURE 65 - DAMAGE AREA LOCATIONS ON UPPER AND LOWER SURFACES OF C-130 CENTER WING TEST ARTICLE

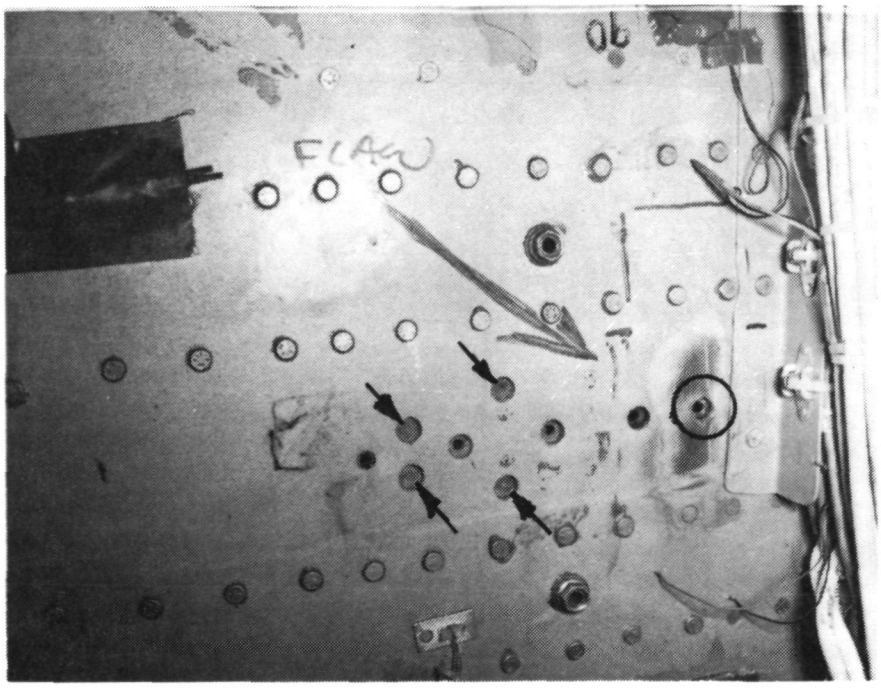

FIGURE 66 - DAMAGE IN LOWER SURFACE AT APPROXIMATE W.S. 214L. CIRCLED HOLE HAS NOTCHES. ARROWS POINT TO HOLES BORED IN SKIN TO FACILITATE DISBONDING.

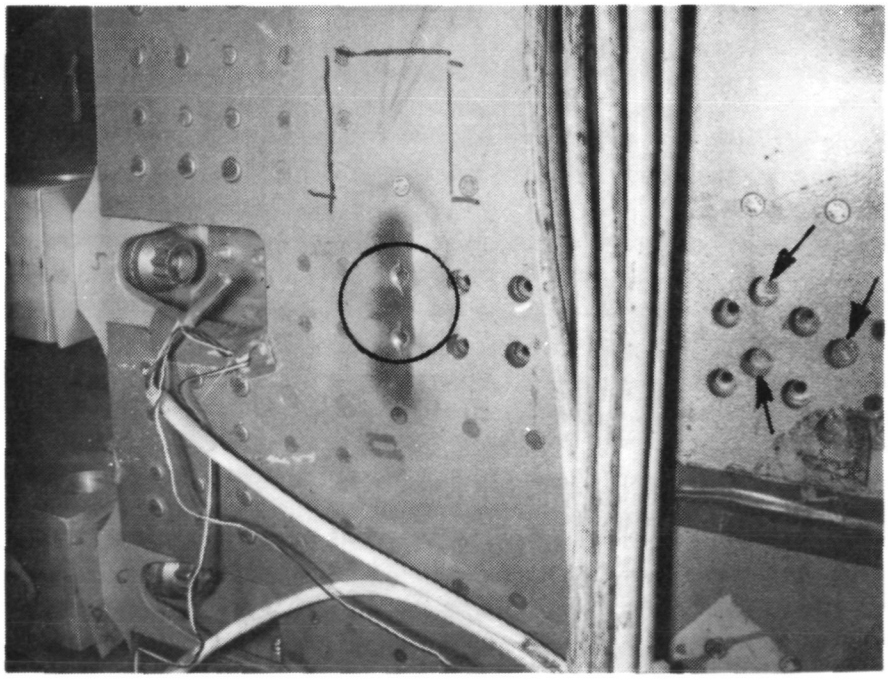

FIGURE 67 - DAMAGE IN UPPER SURFACE AT APPROXIMATE W.S. 214L. CIRCLED HOLES HAVE NOTCHES. ARROWS POINT TO HOLES BORED IN SKIN TO FACILITATE DISBONDING.

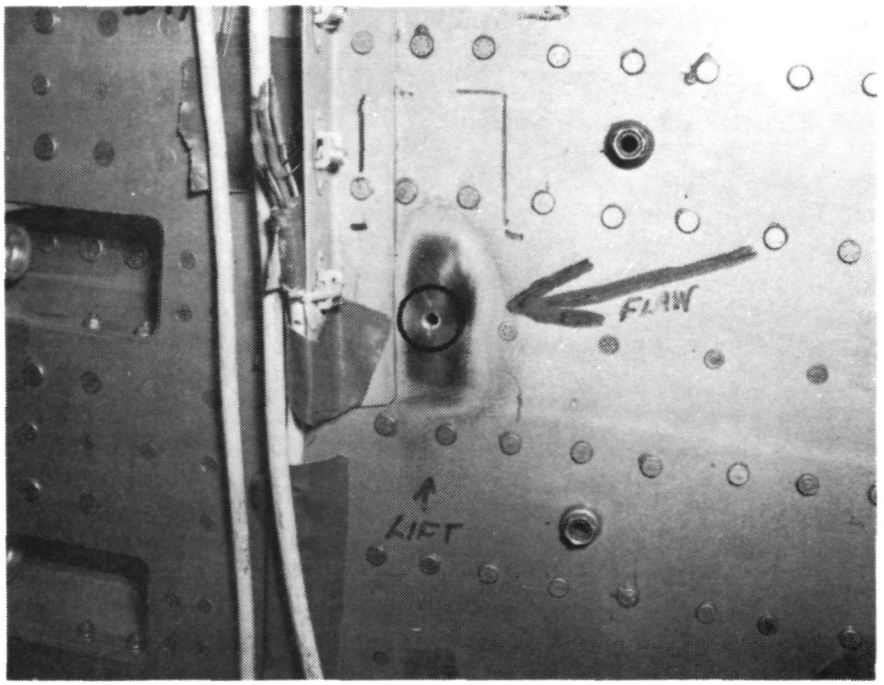

FIGURE 68 - DAMAGE IN LOWER SURFACE AT APPROXIMATE W.S. 214R. CIRCLED HOLE HAS NOTCHES.

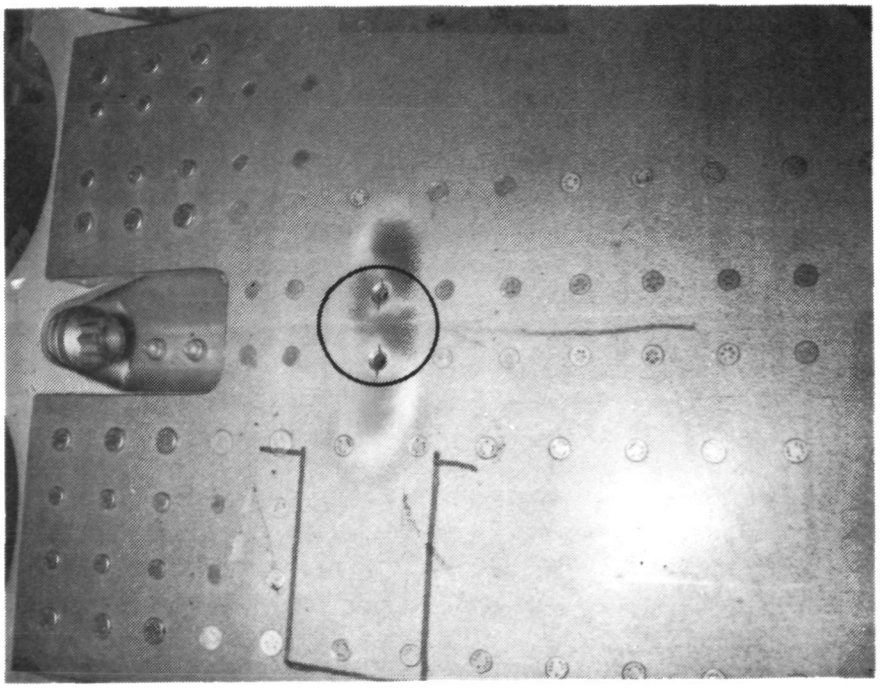

FIGURE 69 - DAMAGE IN UPPER SURFACE AT APPROXIMATE W.S. 214R. CIRCLED HOLES HAVE NOTCHES.

Wing Station 120 (Right and Left, Lower Surface): Sharpened saw cuts were made in the wing lower surface through the access door flanges at W.S. 120 Right and Left locations. The saw cuts were made in the aft edge of the access door flange in a wing chordwise direction. The sharpened saw cut extended approximately 2.54 mm (0.10-in.) beyond the access door flange. Figure 70 typifies the saw cuts made in both right and left access door locations.

Wing Station 180 (Left and Right, Lower Surface): Chordwise oriented sharpened saw cuts were made in the aluminum lower surface panel at W.S. 180 left and right locations. The saw cuts were approximately 2.54-cm (one-inch) in length and extended across the uninterrupted distance between stringers 17 and 18. Figure 71 shows the artificial damaged area typifying both locations. The small hole shown at the center of the saw cut was necessary for introduction of the saw blade.

Wing Station 110 (Lower Surface): Several boron-epoxy laminates and associated stringers terminate at approximately W.S. 110, left and right, because of the access doors centered at W.S. 120, left and right. The following artificial damages were accomplished at W.S. 110 on left and right sides of wing test article.

1. The adhesive bondline of boron-epoxy laminate-to-wing surface panel at Stringer 19 was disbonded from the termination of the boron-epoxy laminate to the first fastener. The disbond was approximately 1.27 cm (0.50 in.) in length and was accomplished at both W.S. 110 left and right. Since the boron-epoxy laminate terminations were accessible from the interior of the wing test article, disbonding was accomplished by prying the terminal end of the boron-epoxy laminate. Ultrasonic inspection of the disbonded area was performed to confirm the disbonded area.

2. Similarly, the boron-epoxy laminate beneath stringer 17 at W.S. 110 was disbonded as was the laminate at Stringer 19. The terminal end of this laminate was disbonded to the first fastener followed by removal of all fasteners in the termination area of the laminate. Artificial damage was accomplished at W.S. 110 left and right sides of the wing test article.

After producing the artificial damage, local polishing was performed at the notched areas to enhance optical detection of fatigue crack initiation. Fatigue cycling of the test article was then resumed using the same loads spectrum applied during the previous four simulated lifetimes. During cycling, the notched areas were periodically inspected to detect initiation of a natural fatigue crack. Once crack initiation was detected, the corresponding point in cycling history was recorded along with crack length. Similar recordings were then made periodically as cycling was continued.

The 41st fatigue load pass was initiated with the application of the Gust 1.1 load condition and concluded with the ground-air-ground (G-A-G) 6 load condition. During this pass, natural cracks were initiated at artificially damaged areas in the lower wing surface at W.S. 120, left and right, and W.S. 180, left and right. Upon completion of the 41st load pass, the fatigue test article was visually and ultrasonically inspected. No defects were visually detected other than the natural crack extensions at W.S. 120 and W.S. 180. The disbonds in the artificially damaged areas were ultrasonically

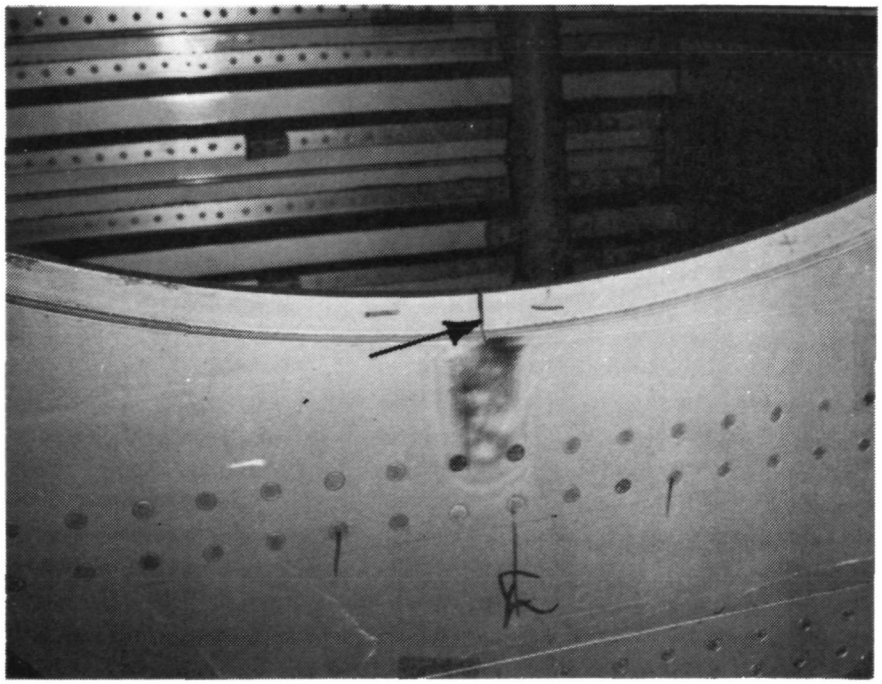

FIGURE 70 - CUT BESIDE LOWER SURFACE ACCESS DOOR - TYPICAL FOR W.S. 120 R AND L.

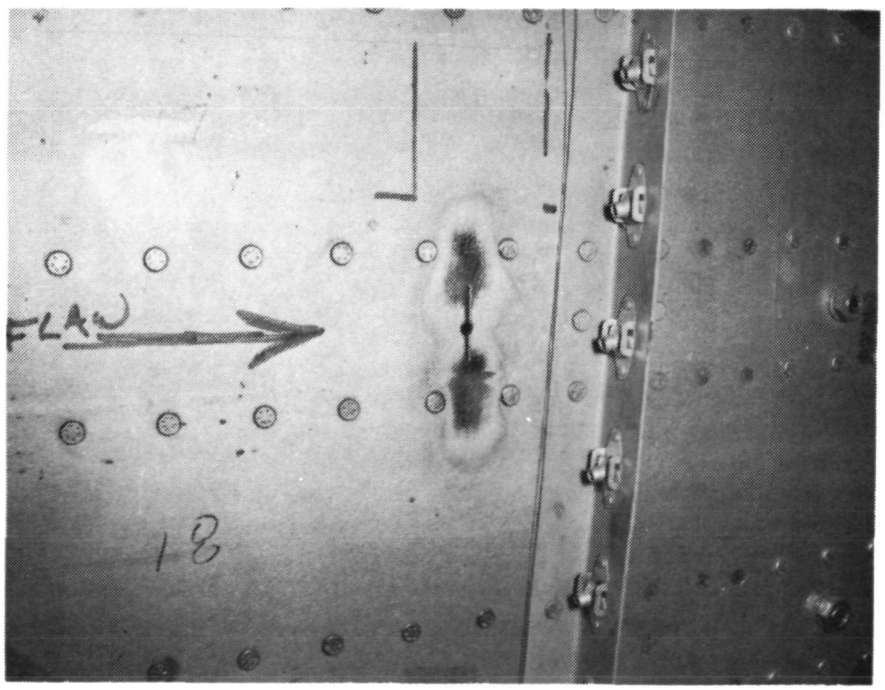

FIGURE 71 - CUT IN LOWER SURFACE WING PLANK - TYPICAL FOR W.S. 180 R AND L

inspected for propagation and none was detected. The crack growth test was continued with conducting the 42nd load pass. The 42nd load pass was initiated with the G-A-G 6 load condition and concluded with the Gust 1.1 load condition. After completing the 42nd load pass, the fatigue test article was visually and ultrasonically inspected. The boron-epoxy laminate-to-wing surface plank bondlines were ultrasonically inspected for disbonds. No growths in intentionally disbonded areas or new disbonds were detected. The major crack growths occurred at the W.S. 120 access doors and W.S. 180, left and right, in the lower wing surface plank. No crack growths occurred at the other artificially damaged areas and no new cracks were detected. Cyclic loading of the fatigue test article was continued into the 43rd load pass for approximately 30 percent completion of the pass at which time cracks were detected in the hat-section Stringer 20 flanges attached to the wing surface plank at W.S. 120, left and right. Both cracks were oriented in a fore and aft (chordwise) direction as were the cracks in the wing surface plank. Also, both cracks were located in the stringer flange mechanically fastened to the wing surface plank that is nearer to the access door. The length of the crack in the stringer flange at W.S. 120 left was 3.94 cm (1.55 in.) and the crack in the stringer flange at W.S. 120 right was 1.91 cm (0.75 in.) in length.

The crack growth test was continued until approximately 90 percent of the 43rd load pass was completed. All of the test load conditions in the pass were completed except the G-A-G load cycles. The test was suspended because the cracks in the hat-section stringer and wing surface plank at W.S. 120, left and right, had propagated to the point at which crack initiation in the adjacent wing surface plank was probable. Upon suspension of cyclic loading, the crack in Stringer 20 at W.S. 120 left had propagated across the total length of the flange attached to the wing surface plank and along the vertical leg for a distance of 2.74 cm (1.08 in.). Also, the crack in Stringer 20 at W.S. 120 right had completely traversed the stringer flange attached to the wing surface plank and extended into the vertical leg for a length of 2.16 cm (0.85 in.) The cracks in the wing surface plank at W.S. 120, left and right, had propagated across approximately two-thirds of the width of the boron-epoxy laminate-to-wing surface plank bondline.

A summary of crack length measurements for both upper and lower wing surface planks is presented in Table VI. The crack lengths in this table are the sum of the artificial damage lengths plus the fatigue crack lengths. As shown in the table, natural crack growths occurred only in the lower surface wing plank at W.S. 120 and W.S. 180. The highest growth rate occurred at W.S. 120, left and right, and the growth histories are charted on Figures 72 and 73, respectively.

TABLE VI - CRACK LENGTHS IN FATIGUE TEST ARTICLE SURFACE PANELS

CONDITION	WING LOWER SURFACE										WING UPPER SURFACE							
	WS 120L	WS 120R	WS 180L		WS 180R		WS 214L		WS 214R		WS 214L				WS 214R			
			FWD	AFT	FWD	AFT	FWD	AFT	FWD	AFT	UPPER HOLE		LOWER HOLE		UPPER HOLE		LOWER HOLE	
											FWD	AFT	FWD	AFT	FWD	AFT	FWD	AFT
Artificial Induced Damage	1.91 (.75)	1.88 (.74)	1.52 (.60)	1.73 (.68)	1.68 (.66)	1.37 (.54)	.74 (.29)	.74 (.29)	.61 (.24)	.61 (.24)	.43 (.17)	.51 (.20)	.46 (.18)	.46 (.18)	.36 (.14)	.43 (.17)	.38 (.15)	.41 (.16)
End of Forty-First Pass	6.68 (2.63)	2.95 (1.16)	1.65 (.65)	1.85 (.73)	1.70 (.67)	1.45 (.57)	.74 (.29)	.74 (.29)	.61 (.24)	.61 (.24)	.43 (.17)	.51 (.20)	.46 (.18)	.46 (.18)	.36 (.14)	.43 (.17)	.38 (.15)	.41 (.16)
56% Complete Forty-Second Pass	8.81 (3.47)	8.26 (3.25)	1.78 (.70)	1.98 (.78)	1.70 (.67)	1.45 (.57)	.74 (.29)	.74 (.29)	.61 (.24)	.61 (.24)	.43 (.17)	.51 (.20)	.46 (.18)	.46 (.18)	.36 (.14)	.43 (.17)	.38 (.15)	.41 (.16)
End of Forty-Second Pass	9.78 (3.85)	10.90 (4.29)	1.80 (.71)	2.06 (.81)	1.73 (.68)	1.45 (.57)	.74 (.29)	.74 (.29)	.61 (.24)	.61 (.24)	.43 (.17)	.51 (.20)	.46 (.18)	.46 (.18)	.36 (.14)	.43 (.17)	.38 (.15)	.41 (.16)
30% Complete Forty-Third Pass *	11.61 (4.57)	12.12 (4.77)	1.85 (.73)	2.16 (.85)	1.93 (.76)	1.63 (.64)	.74 (.29)	.74 (.29)	.61 (.24)	.61 (.24)	.43 (.17)	.51 (.20)	.46 (.18)	.46 (.18)	.36 (.14)	.43 (.17)	.38 (.15)	.41 (.16)
90% Complete Forty-Third Pass	14.61 (5.75)	14.45 (5.69)	2.03 (.80)	2.24 (.88)	2.01 (.79)	1.73 (.68)	.74 (.29)	.74 (.29)	.61 (.24)	.61 (.24)	.43 (.17)	.51 (.20)	.46 (.18)	.46 (.18)	.36 (.14)	.43 (.17)	.38 (.15)	.41 (.16)

* Cracks were detected in hat-section Stringer 20 at Wing Station 120, Left and Right.

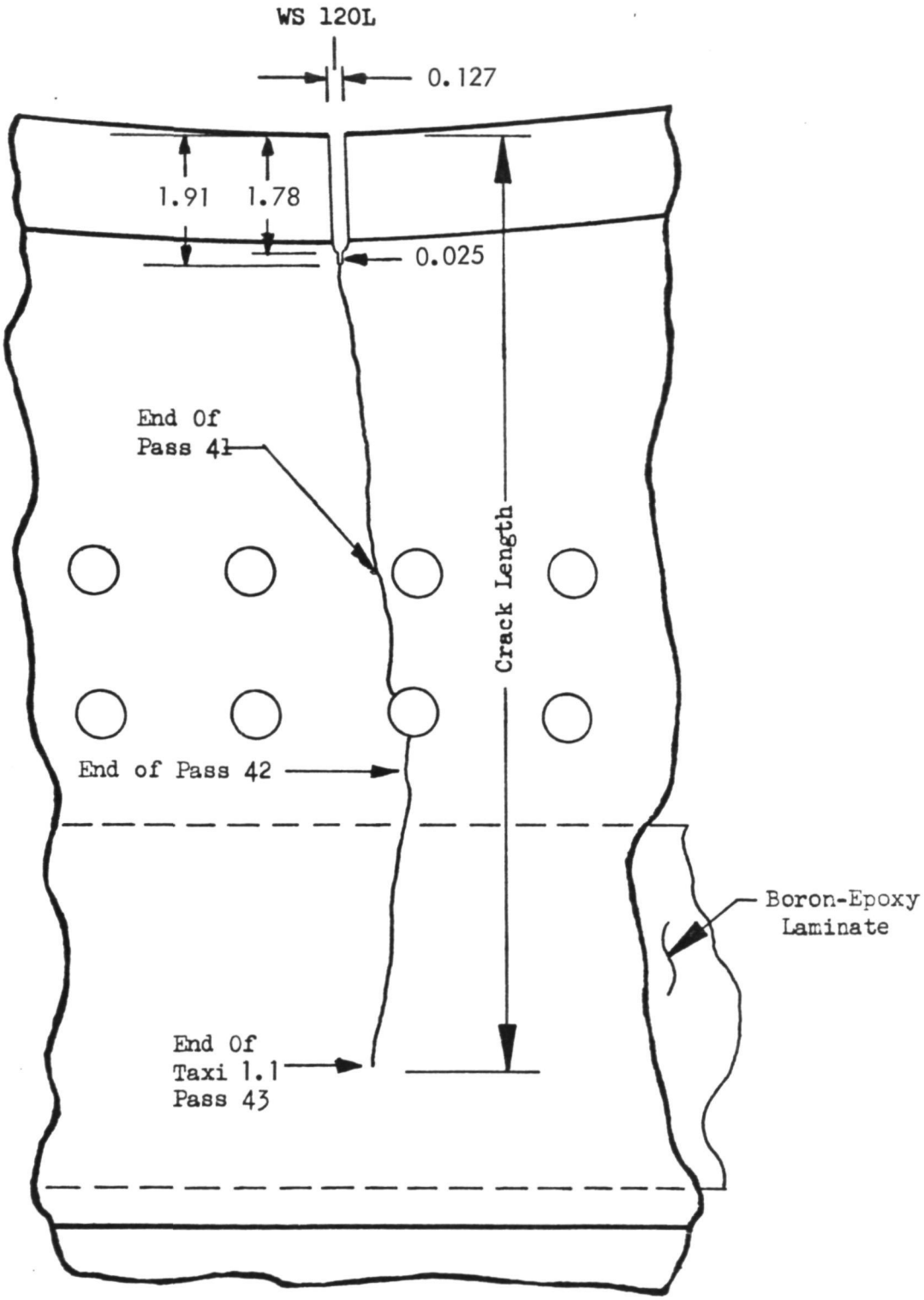

NOTE: All dimensions are in centimeters.

FIGURE 72 - CRACK GROWTH HISTORY IN LOWER WING SURFACE PLANK AT W.S. 120 LEFT

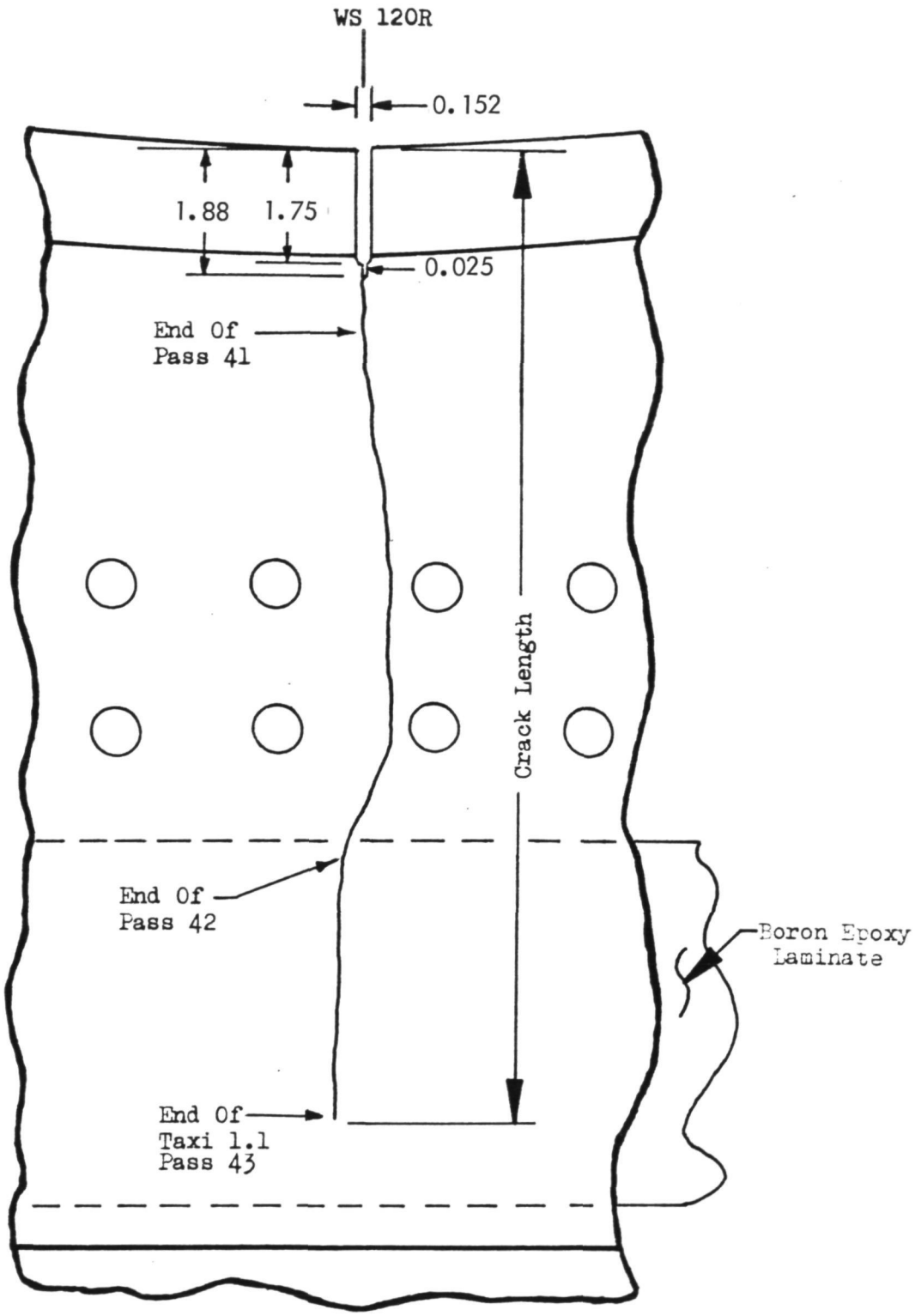

NOTE: All dimensions are in centimeters.

FIGURE 73 - CRACK GROWTH HISTORY IN LOWER WING SURFACE PLANK AT W.S. 120 RIGHT

3.11 RESIDUAL STRENGTH TESTS

Upon suspension of the crack growth test, a limit load upbending test was conducted on the fatigue test article. This test was conducted in a similar manner to previous upbending proof load tests. Prior to conducting the limit load upbending test, the cracked hat-section stringer at Wing Station 120, left and right, was repaired by adding a portion of a hat-section stringer to the damaged area. Each repair member was 28.96 cm (11.4 inches) in length and was attached to the cracked stiffener as shown in Figure 74. A filler shim was required to be located between the oblique leg of the repair member and the oblique leg of the cracked stringer. Necessary tapered interference fasteners in the stringer flange-to-wing skin plank were removed and replaced by tapered interference fasteners installed in the original members plus the repair member flange. Also, two rows of blind Jo-bolts were installed in the vertical and oblique legs of the repair member and the cracked hat-section stringer.

Five axial strain gages and three crack wire installations were added to the existing instrumentation for adequately monitoring the strain conditions in the artificially-damaged areas at Wing Station 120 and 214 of the fatigue test article. The purpose of the crack wires was to monitor crack tip extension. Upon the crack extending beneath the wire, the opening of the crack would cause the wire to break and a signal (light) is transmitted to the control panel signifying that the crack tip has reached that location.

One of the five additional axial strain gages was located on the crown of the cracked hat-section Stringer 20 at Wing Station 120.5. A second axial strain gage was located on the crown of the cracked hat-section Stringer at Wing Station 115.0. These strain gage locations were selected for assessment of strains in the near vicinity of the Stringer 20 cracks. The third axial strain gage was located on the exterior surface of the wing skin plank adjacent to the cracked wing skin plank at Wing Station 120. This strain gage was located forward of the thickness taper of the wing skin plank and at the centerline of Stringer 21. The remaining two axial strain gages were located on the exterior surface of the wing skin plank at Wing Station 214. One of those two strain gages was located on the centerline of Stringer 20 and the other strain gage was located on the centerline of Stringer 19.

Two of the three crack wire installations were located on the exterior surface of the wing in the region of Wing Station 120, and the third crack wire installation was located on the exterior surface of the wing in the region of Wing Station 214. At Wing Station 120, one of the crack wire installations was bonded to the wing skin plank for a length of 5.08 cm (2.0 in.) in the spanwise direction and located directly in front of the crack tip halfway between the crack tip and the nearest edge of the spanwise splice. The second crack wire installation at Wing Station 120 was bonded at the same spanwise location as the first installation but on the adjacent wing skin plank between the visible edge of the spanwise splice and the nearest row of fasteners attaching Stringer 21 to the wing skin plank. The crack wire installation at Wing Station 214 was located in the spanwise direction and the bonded area extended from the end of the fatigue test article at Wing Station 220 to a distance 2.54 cm (1.0 in.) inboard of the most inboard fastener in the boron-epoxy laminate runout area of Stringer 19.

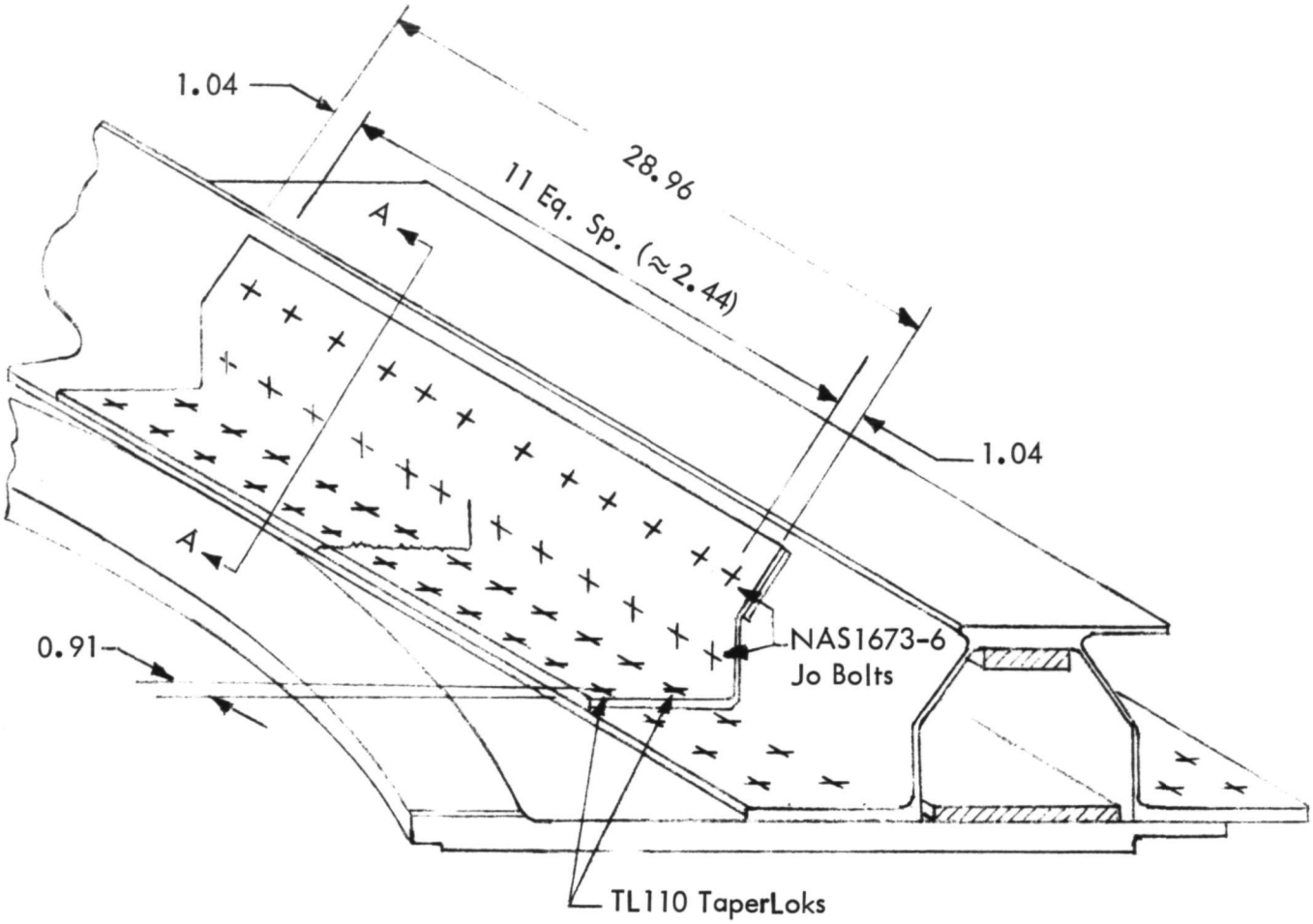

Note: All dimensions are in centimeters.

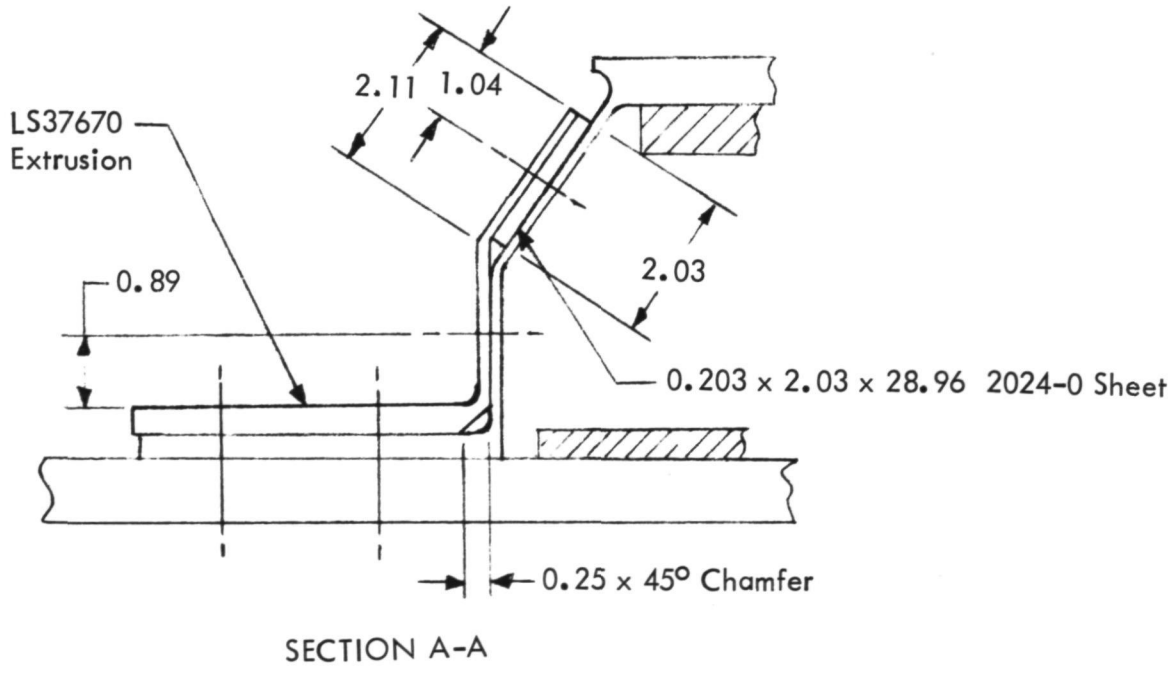

SECTION A-A

FIGURE 74 - REPAIR FOR HAT-SECTION STRINGER AT W.S. 120 IN FATIGUE TEST ARTICLE

During the test, strain data were recorded with existing and the five additional strain gages. Differentials in strain readings taken in this test like those in previous upbending tests were within the normal scatter for the measurements. Also, the damaged areas in the Wing Station 120 region were continuously scanned by closed circuit video. Upon completion of the limit load upbending test, the fatigue test article was visually inspected and no additional damage was detected.

An additional upbending test was conducted on the fatigue test article after removal of the repair members from the Wing Station 120 areas, left and right. After removing the repair members, the double row of tapered interference fasteners joining the flange of the cracked hat-section stringer and wing skin plank were replaced. Prior to conducting this test, two 16-mm movie cameras were installed at the two Wing Station 120 locations to cover those areas during the latter portion of the test. During this test, strain data were recorded as in the previous tests. Differentials in strain readings taken in this test were within the normal scatter for measurements up to 100 percent design limit load. In the range of 100 to 120 percent design limit load, two clearly distinguishable audible sounds were heard. The two strain gages located on the crown of hat-section Stringer 20 above the crack in the stringer showed nonlinearities (strain versus applied load) at 110 percent design limit load indicating load redistribution in that area. The test continued until 133 percent of design limit load was attained at which time one of the hydraulic jack actuators in the shear loading system reached its total stroke and the test was suspended. During the test, the cracks in the wing skin plank at Wing Station 120, left and right, propagated to the edge of the closest spanwise skin splice and extended beneath the external splice strap. Also, the local exterior surface areas around several fasteners in the spanwise wing skin plank splice located near the crack tips showed discolorations in the surface finish. These discolorations indicated the occurrence of large strains which may have further indicated plastic deformations around the fasteners.

Upon suspension of this test, the fatigue test article was visually and ultrasonically inspected. During the visual inspection, it was discovered that the heads of two 2.54-cm (1.0-in.) steel bolts in the shear loading fixture had failed. Thus, it was concluded that the source of the two audible noise reports that occurred during the test was the failure of the bolts. The ultrasonic inspection of the bondlines in the fatigue test article did not reveal any additional disbonds nor any propagation in any of the previously known disbonds.

3.12 VERIFICATION OF DISBONDS IN THE FATIGUE TEST ARTICLE

After the first proof load test, disbonds were detected in the boron-epoxy laminate-to-upper wing surface plank bondline in the vicinity of W.S. 20 location. It is noted that a repair was accomplished on this bondline in the same general area during subassembly. The repair consisted of installing mechanical fasteners in the boron-epoxy laminate-to-wing surface plank bonded joint. Several ultrasonic inspections of the area in which the disbonds were detected performed after subsequent tests did not reveal any propagations in the disbonds.

Upon completion of the last static test on the fatigue test article, verification of the disbonds was accomplished after removal of the section of the wing upper surface containing the disbonds. Both contact and immersion ultrasonic inspections were conducted on the section of the wing upper surface that was removed. These inspections confirmed the disbonds that were detected previously. Then, the wing surface plank-to-laminate bondline containing the disbonds was physically separated. The separation revealed a section of polyethylene protective liner for the adhesive approximately twenty-four inches in length. The polyethylene liner had been inadvertently left in the bondline during assembly. Figure 75 shows the bondline after separation including the extremities of the polyethylene liner. It is noted that the liner extended into the repaired area of the bondline which is identified by the fastener hole locations on Figure 75. Separation of the bondline over the area containing the polyehtylene liner showed a total disbond of the adhesive to the boron-epoxy laminate. Contact ultrasonics did not reveal the disbonded area during the inspection conducted immediately after the bondline was cured because the laminate was pressed sufficiently tight against the polyethylene liner to allow transmission of the ultrasonic wave through the bondline. (Note: The ultrasonic inspection technique does not discriminate a weak bond from a strong bond. It only establishes that a bond does or does not exist.) After the application of the first proof load to the center wing test article, the condition between the boron-epoxy laminate and the polyethylene liner changed sufficiently to prevent ultrasonic transmission during subsequent inspections which indicated the presence of disbonds.

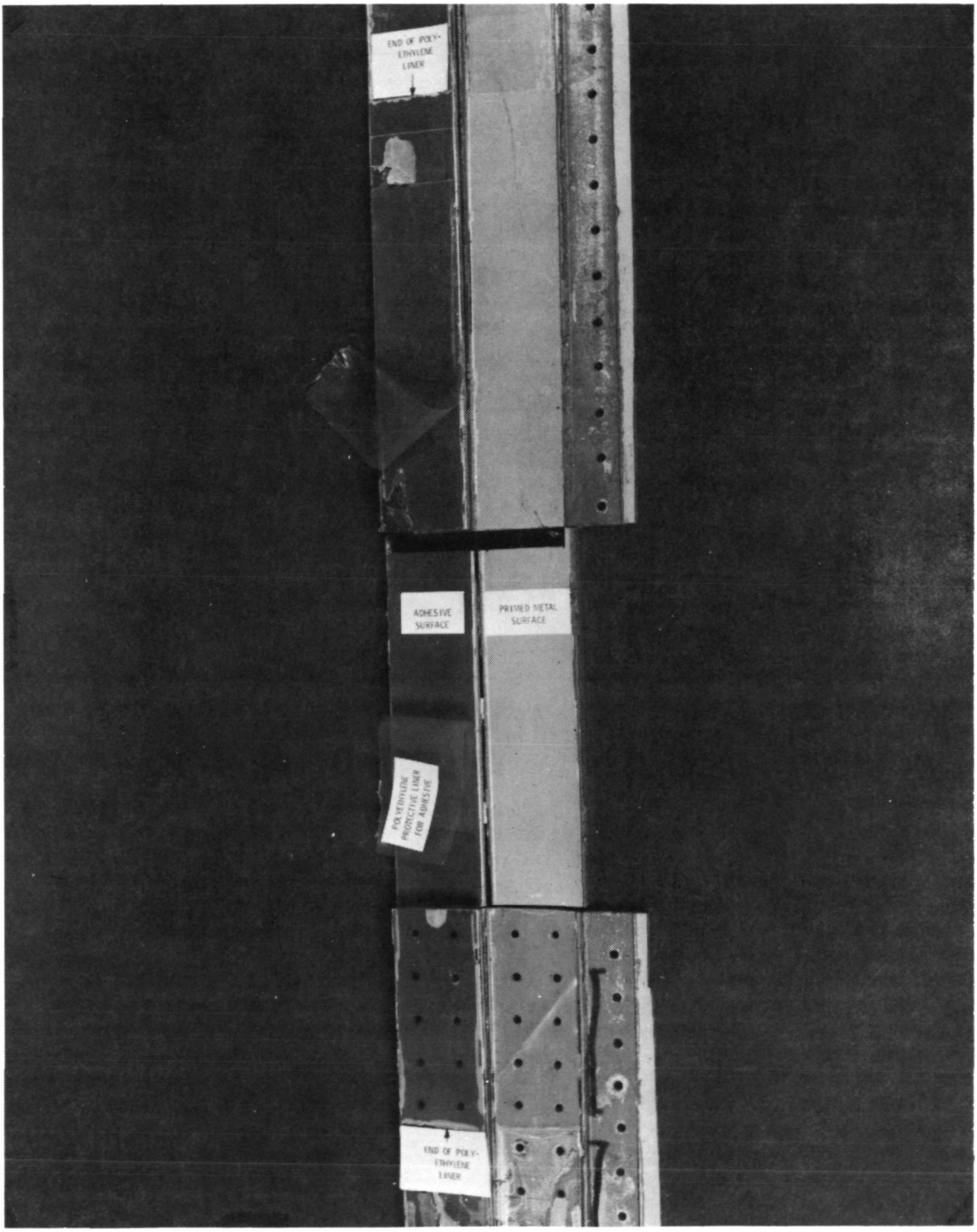

FIGURE 75 - BONDLINE AREA CONTAINING POLYETHYLENE PROTECTIVE LINER FOR ADHESIVE

4.0 PROGRAM SUPPORT ACTIVITIES

4.1 FIRST ARTICLE CONFIGURATION INSPECTION

The First Article Configuration Inspection (FACI) was conducted on the two composite-reinforced center wings that are being evaluated on Air Force C-130 operational aircraft at the Lockheed-Georgia Company. Attendees included representation from NASA-Langley, United States Air Force, and Lockheed. Although this program was not conducted under overall AFSCM-375 requirements, the FACI served as a convenient vehicle for verying the acceptability of the two wing units. The following areas that were verified with summary remarks and disposition at the time of FACI are listed in Table VII.

TABLE VII - FIRST ARTICLE CONFIGURATION INSPECTION RECORD

Area Being Verified	Summary Remarks (Constraints)	Disposition
1. End Item Specification vs. Hardware	Acceptable	Closed
2. Engineering Drawings vs. Hardware	Acceptable	Closed
3. Test Procedures vs. Test Results	Proof Load Tests & Ground Vibration Tests have not been completed	Satisfactory Completion of the tests will constitute closure of FACI
4. Engineering Release System and Change Control Procedures	Acceptable	Closed
5. Review of DD Form 250	N/A per contract schedule, Part VII	Closed
6. Deviations	None	Closed

Subsequent to the FACI, Item 3 in the above table was satisfactorily completed with submittal of proof load test and ground vibration test data that had been approved by the cognizant representive of Air Force Plant Representative's Office (AFPRO).

4.2 SPARE C-130 PRODUCTION CENTER WINGS

Although no flight service problems are expected to occur with the composite-reinforced wing boxes, two all-metal production center wings were fabricated and are stored at Lockheed for replacement of the composite-reinforced wing boxes if required. One of the completed spare center wing boxes is shown in Figure 76. At the direction of the Air Force, trailing edges were omitted from the spare wing box assemblies to facilitate storage and shipment, if required. Also, fuselage attachment and shear panels were not drilled to minimize fit-up difficulties should the spares be required.

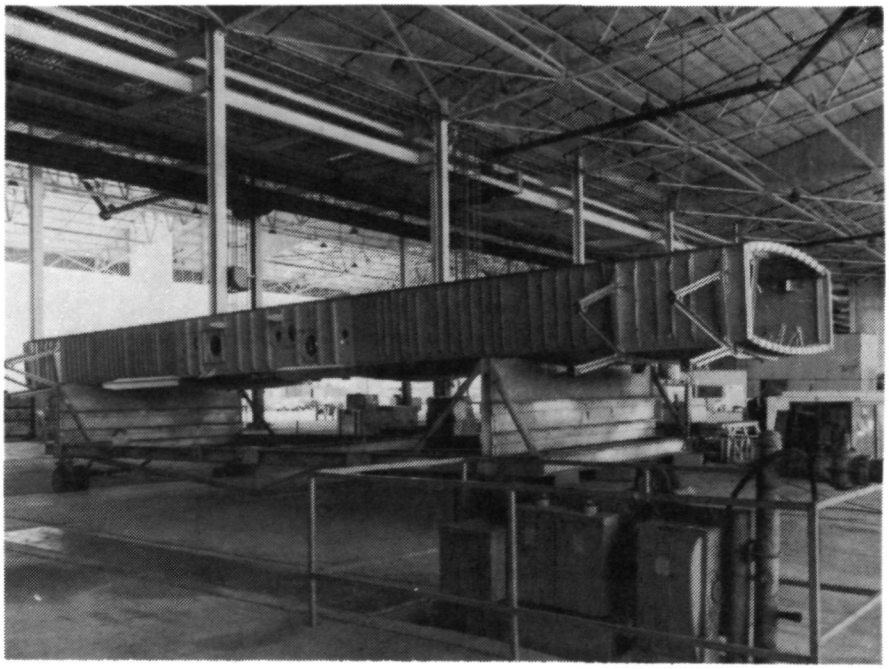

FIGURE 76 - SPARE CENTER WING BOX FOR C-130
AF73-01592 (LAC 4557)

4.3 DOCUMENTARY FILM ON PROGRAM

A documentary film covering all phases of the program was produced. During the course of the program, significant developments were photographed. The film script was prepared, reviewed by NASA-Langley personnel, and then finalized with incorporation of requested changes. After cutting the film to correspond to the script and producing the sound track, it was reviewed at the interlock stage of production with NASA-Langley personnel. Several changes were incorporated and final film prints were produced and forwarded to NASA-Langley.

4.4 MANUFACTURING RELIABILITY OF THE COMPOSITE-REINFORCED CENTER WING

The objective of this analysis is to determine a lower bound manufacturing reliability of the boron-epoxy laminate-to-metal structure adhesive bondlines in the C-130 center wing box assembly. Reliability analyses were accomplished at two points in the development/life cycle of the center wing box assembly. They occur at the completion of fabrication of the center wing box and at delivery of a C-130 aircraft possessing a composite-reinforced center wing. The derivation of the mathematical relationships used in the analysis is presented in Appendix B. The development of the mathematical relationships included in Appendix B is based on the approach presented in Reference 19.

It is noted that the metallic components in the composite-reinforced center wing structure were manufactured in accordance with the same procedures and material alloys used in the production of all-metal center wing boxes. The Phase II analyses reported in Reference 2 showed that the metallic components in the composite-reinforced center wing box are not subjected to environments or stresses that are more severe than the comparable metallic components in the all-metal center wings. Thus, the reliability of the metallic components in the composite-reinforced center wing boxes is at least that of the all-metal center wing. The principal elements of composite-reinforced center wing box from the aspect of structural reliability are the adhesive bonds that join the boron-epoxy laminates to the metallic structure. Therefore, the adhesive bonds received the major emphasis in determination of the reliability of the composite-reinforced center wing.

In this analysis, reliability of the bondline is defined as the probability that no individual void or disbond larger than 0.323 cm^2 (0.050 $in.^2$) in area is present and undetected in the bondlines of the center wing box. This disbonded area represents a threshold type of size because disbonds equal to or greater in area are likely to be detected as discussed in the following paragraph on Inspection Reliability. Furthermore, voids or disbonds of this size or less are not expected to degrade structural integrity. Also, prediction of structural reliability on voids or disbonds this small is conservative as shown by the residual strength and disbond analysis presented in Section 3.9 and the center wing test results contained in Sections 3.10 and 3.11. In that analysis, the disbond is assumed to completely span the laminate-to-skin panel bondline width of 5.08 cm (2.00 in.). The disbond length would have to be 0.0636 cm (0.0250 in.) for an area of 0.323 cm^2 (0.050 $in.^2$). The tendency to propagate the disbond is measured by the strain energy release rate which is independent of the disbond length. One disbond much longer than 0.0636 cm (0.250 in.) did not propagate during the fatigue and static tests of the wing test article. If by some mechanism the disbond were to become very lengthy, the load sustaining capacity of the center wing box could be reduced if the disbond was in the compression loaded surface of the center wing. The reduction could result from the tendency of the boron-epoxy laminate to buckle away from the metallic component. However, a design criterion adhered to during the design phase of the program (Phase II) was that all boron-epoxy laminates could become disbonded and the remaining metallic structure would satisfy failsafe requirements. Therefore, disbonding and buckling of one boron-epoxy laminate would have negligible effects on structural integrity of the composite-reinforced center wing box. This conclusion was demonstrated in the upbending proof tests described in Sections 3.5 and 3.11. Consequently, the

selection of a disbond area of 0.323 cm^2 (0.050 $in.^2$) provides a confident base for use in determining the fabrication and inspection reliabilities without compromising the structural integrity of the composite-reinforced center wing.

Major parameters that affect bondline reliability during fabrication are disbond occurrence rate and inspection reliability. Extreme lower and upper bounds of these major parameters are used in the analysis to gain a practical degree of confidence that the actual reliability would lie within the resulting intervals. The analysis assumes that the disbonds that occur during fabrication and installation are random in nature. For analysis purposes, it is assumed that the distribution of the disbonds occurs in accordance with a Poisson density process and/or the exponential density function as appropriate. The effects of aging and other in-service environmental conditions on bondline integrity are not conclusively known at this time, and results from the three-year in-service evaluation program should provide better insight into bondline reliability.

The following sub-sections describe the data input, analysis considerations, and determination of bondline reliability during manufacture of the composite-reinforced center wing box. It is noted that the terms "voids" and "disbonds" are used interchangeably throughout the analysis.

4.4.1 Data Input and Analysis Considerations

Fabrication Disbond Occurrence Rate - The following data on the adhesive bondlines in the composite-reinforced center wings were generated during fabrication of the three C-130 center wings:

Production Data	Voids Detected	Bonded Area	Void Rate Per m^2 ($ft.^2$)
Static/Fatigue Test Article	64	15.61 m^2 (168.00 $ft.^2$)	4.1000 (0.3810)
Flight Article #1 (C-130 AF73-01592)	57	15.61 m^2 (168.00 $ft.^2$)	3.6515 (0.3393)
Flight Article #2 (C-130 AF73-01594)	17	15.61 m^2 (168.00 $ft.^2$)	1.0890 (0.1012)

The above data shows a downward trend in the occurrence of number of voids and/or disbonds per center wing assembly as a function of the production sequence. These data suggest that the number of voids and/or disbonds occurring during fabrication of each succeeding center wing box assembly will decrease in accordance with an exponential function of the following form:

$$\text{Voids/Assembly} = Be^{M(\text{Production Sequence Number})}$$

where B and M are empirical constants and e = 2.71828, the Naperian logarithmic base. Applying the above data in determination of B and M using the least squares curve fitting technique, the following relationship results:

$$\text{Voids/Assembly} = 149\, e^{-.6628(\text{Production Sequence Number})}$$

In accordance with the above relationship, the fabrication void occurrence rate is less than one void per assembly by the time that the eighth production unit is assembled. Therefore, it is conservative to assume that the void rate occurring in a C-130 composite-reinforced center wing production program would not exceed an average of five voids per assembly. In fact, the void rate could be as low as 0.01 over a large production contract. Thus, a steady state fabrication void occurrence rate in the center wing box assembly, LS, is reasonably certain to fall within the interval, (0.01, 5.0).

In-Service Disbond Occurrence Rate - The in-service disbond occurrence rate for the composite-reinforced center wing assembly is relatively small number based on available data. An equivalent of four lifetimes of fatigue loadings, representing 40,000 flight hours, were applied to the center wing fatigue test article and no additional disbonds exceeding specification limits were detected. Also, approximately 2600 flight hours had been accumulated at the end of July, 1976, on the two composite-reinforced center wing boxes installed on operational C-130 aircraft. Inspections on these wing boxes have not revealed any disbonds that exceeded specification limits. For analysis purposes, it is conservatively assumed that one disbond which exceeded specification limits occurred immediately after completing the fatigue test and flight evaluation period ending July, 1976. The application of these statistics and assumptions with associated Chi Square, χ^2, confidence interval techniques provide a 90 percent probability that the in-service disbond rate, L_sS, per center wing box assembly is bounded by the following inequality:

$$.0012/10^3 \text{ hrs} \leqq L_sS \leqq .0703/10^3 \text{ hrs}$$

Fabrication Reliability - The probability of fabricating an adhesive bonded structure without having any voids that exceed the specification limits is a function of the average void rate, LS. As previously concluded, LS will probably be in the interval, (0.01, 5.0). Adapting Equation (24) of Appendix B for this LS interval, the probability (reliability) is determined to fall in the range (0.006738, 0.990050). This is a wide range of probabilities and the interpretation of the higher extreme of this range is simply that, if the fabrication void occurrence rate is as low as 0.01 per center wing box assembly, there is approximately 99 percent probability that a randomly selected center wing assembly will not contain any voids upon completion of fabrication. For the lower extreme, the average void occurrence rate is taken as high as 5 which results in a very low probability that a randomly selected center wing box assembly will not contain voids in the bondlines.

After ultrasonic inspection of the bondlines, the reliability is increased significantly as there is the probability that no disbonds remain undetected that exceed specification limits. If, during an inspection, disbonds were detected that exceeded specification limits, it was assumed that they were adequately repaired. The post-fabrication bondline reliability after an inspection of the bondlines is given by Equation (24) of Appendix B. Reliabilities after inspection are presented below for the assumed extremes of fabrication void occurrence rates and ultrasonic inspection reliabilities of 90 and 95 percent.

Fabrication Void Rate, LS	Ultrasonic Inspection Reliability, R	Bondline Reliability After Fabrication Inspection, Percent
0.01	0.95	99.9500
0.01	0.90	99.9000
5.0	0.95	77.8801
5.0	0.90	60.6531

As shown above, the worst condition results in a 61 percent probability that the bonded center wing box assembly contains no voids and/or disbonds that exceed the specification limit of 0.323 cm^2 (0.050 $in.^2$) in area.

Inspection Reliability - The reliability of the inspection process is defined as the probability of detecting a void or disbond in the laminate-to-metal structure bondlines that is equal to or greater than 0.323 cm^2 (0.05 $in.^2$) in area. This void area is the greatest area allowed by specification requirements that does not require repair. Ultrasonic inspection equipment is calibrated using a quality standard containing the maximum allowed defects by the specification prior to each inspection. Use of the calibrated ultrasonic inspection equipment by experienced operators will result in estimated reliabilities ranging from 90 to 99 percent. Confirmation of these estimated reliabilities can be established only by a reliability inspection program on the composite-reinforced center wing box. However, the computation of the inspection reliability will depend on the required confidence limits placed on the probability of detection of voids in the bondlines. For example, assuming a confidence interval of 95 percent, the reliability may be 90 percent and for a 50 percent confidence interval, the reliability may approach 99 percent. For this analysis, it is assumed that the inspection reliability will lie in the (0.90, 0.95) interval.

4.4.2 Determination of Wing Box Reliabilities

Bondline reliabilities in the composite-reinforced center wing box were determined using the approach presented in Appendix B, and the data input and analysis considerations in the preceding paragraphs. Reliability is determined at point of aircraft delivery.

Reliability at the Point of Delivery - There was no evidence that there were additional disbonds introduced into bondlines of the center wing box assemblies during installation in the two C-130 aircraft. However, it is conservatively assumed that in production the installation operation will introduce disbonds at a maximum rate equivalent to 100 hours of aircraft in-service flight time. Applying this assumption, the reliability of the structure after the inspection at the point of delivery is given by the following adaptation of Equation (24) of Appendix B:

$$R_d = e^{-(LS\,(1 - R) + L_s ST)\,(1 - R)}$$

The additional terms in the exponent of the above equation result from the foregoing assumptions including the assumption that each composite-reinforced center wing box has been inspected twice. Bondline reliabilities are computed at the point of delivery of the aircraft for the best and worst conditions assuming a fabrication void occurrence rate

range of 0.01 to 5.0 and an inspection reliability interval of 0.90 to 0.95. A list of the calculated bondline reliabilities at the point of delivery for the best and worst conditions is given below.

Fabrication Void Rate, LS	In-Service Disbond Rate, $L_S S$ Per 1000 Hrs.	Inspection Reliability, R	Bondline Reliability After Delivery Inspection, Percent
0.01	0.0012	0.95 (best)	99.9969
0.01	0.0012	0.90	99.9888
0.01	0.0703	0.95	99.9624
0.01	0.0703	0.90	99.9197
5.0	0.0012	0.95	98.7572
5.0	0.0012	0.90	95.1218
5.0	0.0703	0.95	98.7572
5.0	0.0703	0.90 (worst)	95.1218

The above data shows that even for the worst condition considered, the composite-reinforced center wing box at the point of delivery has at least a 95 percent probability of being free of bondline voids.

4.4.3 Conclusions Drawn from the Reliability Analysis

The following conclusions are drawn from the foregoing analysis.

1. The technology used in the program produces a bonded structure that has reliability (probability of no undetected disbonds) of at least 95 percent at the point of delivery as an installed unit in a C-130 aircraft.

2. Random introduction of disbonds in the bondlines of the center wing box is likely to be very small. This conclusion is based on exceedingly low rate of disbonds (none detected) developed from four lifetimes of fatigue testing and limited flight history on two center wings. The rate of disbonds per 1000 flight hours has a high probability of lying in the interval (0.0012, 0.0703).

3. The ultrasonic inspection procedure is an effective method for increasing and maintaining the reliability of the bonded structure (assuming adequate repair of identical disbonds). The ultrasonic inspection equipment will not necessarily detect tight disbonds in bondlines. A quality bond may be indicated if the disbond is sufficiently tight to allow transmission of the ultrasonic wave through the bondline. One such case occurred in a bondline in the fatigue test article.

4. The learning curve extrapolated from the fabrication of three composite-reinforced center wing boxes is given in paragraph 4.4.1. Using that relationship, it is concluded that the occurrence of disbonds during fabrication would average less than one per center wing box assembly very early in a production program.

5.0 NASA-LANGLEY STRAIN LEVELS EXCEEDANCE COUNTERS

Strain level exceedance counters that were developed by the Langley Research Center of NASA were installed on the composite-reinforced center wing box that was fatigue tested and the two composite-reinforced center wings that are being flight-service evaluated. The strain level exceedance data collected from the instruments are being used for comparing the cyclic strain spectra encountered during the flight-service program to the cyclic spectrum applied in the fatigue test. Documenting the flight service loading and the test loading will aid in drawing conclusions related to the performance of the boron-reinforced wing structure during the flight-service program.

5.1 DESCRIPTION AND PURPOSE OF STRAIN LEVEL EXCEEDANCE COUNTERS

The strain level exceedance counter is a rectangular-shaped instrument (15.2 cm x 20.3 cm x 5.1 cm) and weighs 1.36 kilograms. These electronic instruments use strain gages in conjunction with a 28-volt direct current power source to continuously monitor the strain history on the structure where the strain gage is located. The number of times the measured strain exceeds the pre-selected strain levels is recorded in the counter electromechanically. A photograph of a strain exceedance counter is shown in Figure 77. In operation, once the strain exceeds the preset value for a particular counter, the counter will increment. Also, the strain must then decrease below a reset value and then increase to at least the preset value before the counter will increment again. This feature prevents small oscillations around the preset strain value from incrementing the counter. A more detailed description of the strain counting system is contained in NASA TN D-5944.

5.2 STRAIN COUNTERS ON THE FATIGUE TEST ARTICLE

Two strain level exceedance counting systems were installed on the fatigue test article during the inspection period following one lifetime of fatigue testing. The systems were functionally identical with each using an electrical resistance-type strain gage sensor, microelectronic and discrete solid-state circuits for signal processing, and electromechanical counters for data storage. Each system had four electromechanical counters, one for each of the four different preset strain levels.

Strain gages were installed at three different locations inside of the test article. Installations were accomplished on each of the crowns of the lower surface hat-section stringers designated 21, 22 and 23 at W.S. 0. The strain gage installations are shown on Figure 78. For each active strain gage, three additional gages were installed on a separate 7075-T6 aluminum alloy plate to complete the bridge. This aluminum plate was attached to the lower surface stringers so as to experience the same temperature environment as the stringer crowns but not develop any strain. The four gages at each location were then wired into a full bridge arrangement as illustrated in Figure 79.

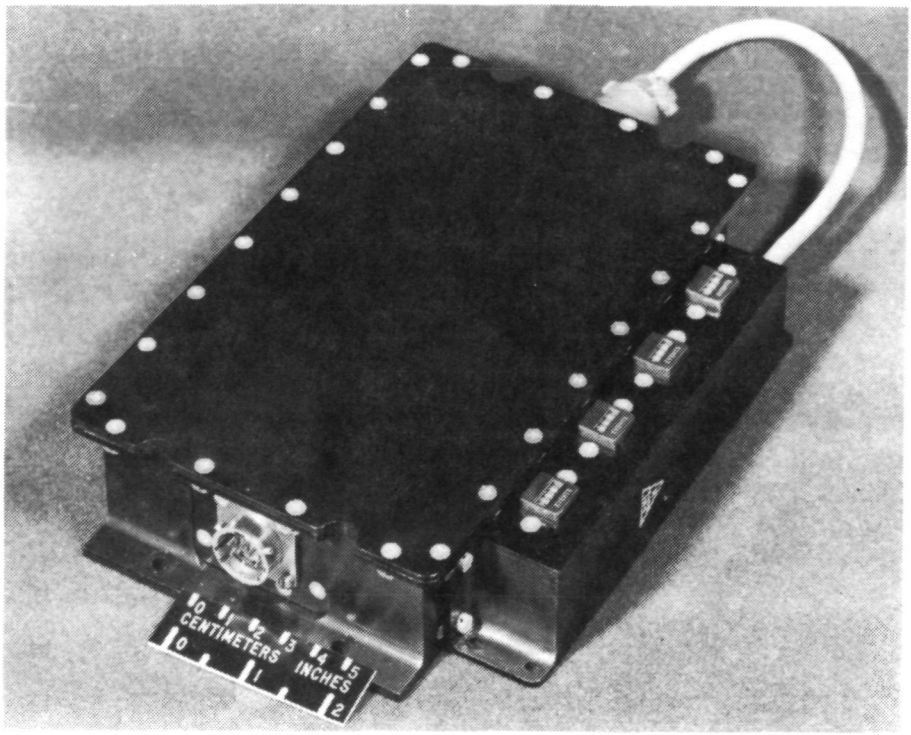

FIGURE 77 - NASA-LANGLEY STRAIN LEVEL EXCEEDANCE COUNTER

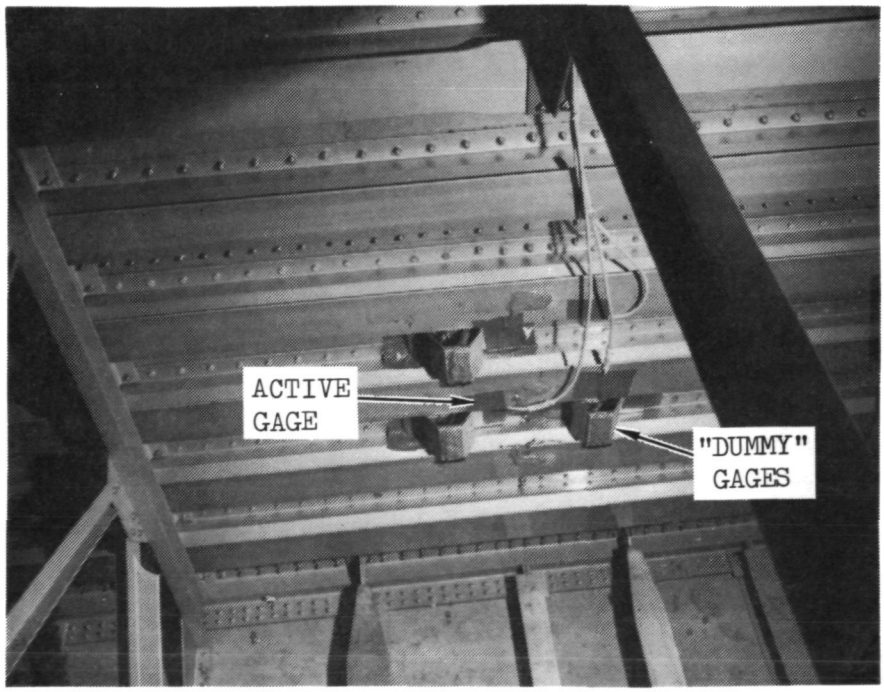

FIGURE 78 - GAGE INSTALLATIONS FOR TEST ARTICLE STRAIN COUNTERS

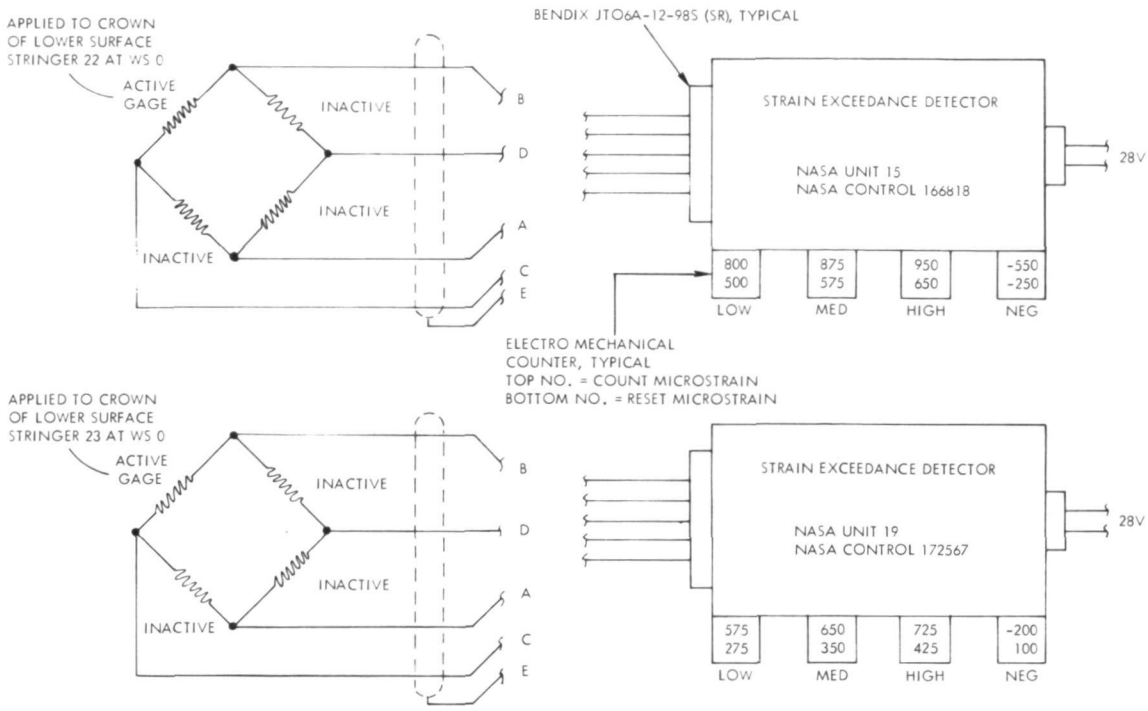

FIGURE 79 - SCHEMATIC OF STRAIN COUNTER SYSTEM

Two of the bridges were connected to strain counters furnished by NASA-Langley. The third bridge served as a spare for the other two bridges in the event that either became inoperative. The spare bridge with the active gage was on stringer 21 at W.S. 0. The strain counter units were mounted on the side of a console in the control room and are shown in Figure 80.

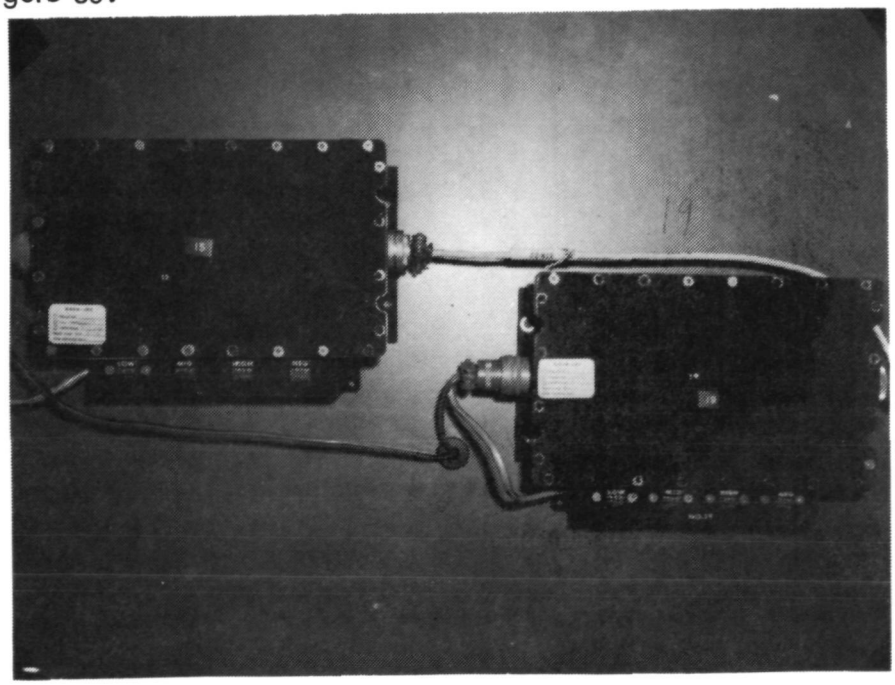

FIGURE 80 - STRAIN COUNTERS FOR TEST ARTICLE

After installation, NASA-Langley personnel made final adjustments to set each counter to the desired count and reset microstrain levels. When final adjustments had been completed, 14 cycles of the GUST 1.1 loading in Pass 11 had been applied. Basic counter readings were taken at that time in the fatigue test. Strain counter readings were taken at frequent intervals and recorded for the duration of the fatigue test. All of these counter readings were transmitted to NASA-Langley for use in comparison with similar measurements taken in the flight-service program.

5.3 STRAIN COUNTERS ON THE C-130 CENTER WINGS BEING FLIGHT EVALUATED

Similar strain level exceedance counter systems were installed on the two C-130 aircraft which had the composite-reinforced center wings as that installed on the test article. The counter systems were installed on C-130 AF73-01592 (LAC 4557) and C-130 AF73-01594 (LAC 4563). Production drawings for the strain counter systems were prepared, serialized, and released for providing the proper installation and aircraft configuration control. The installation in the composite-reinforced center wing of C-130 AF73-01592 is shown in Figure 81. The strain counter installation is shown in Figure 82 which is inside of the aircraft fuselage on the right side of the cabin immediately forward of the main landing gear pod.

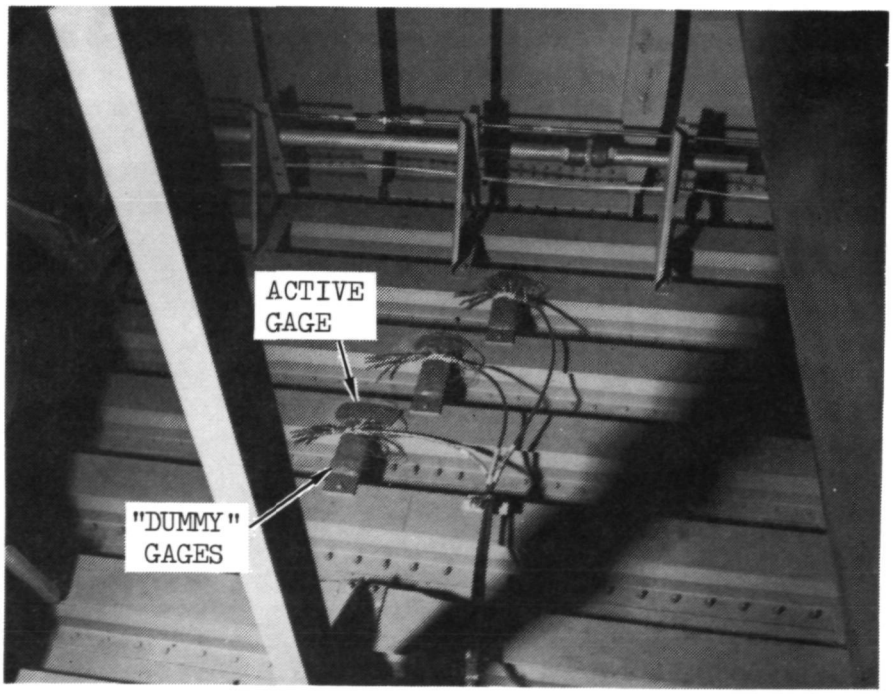

FIGURE 81 - STRAIN GAGE INSTALLATIONS ON C-130 AF73-01592 (LAC 4557)

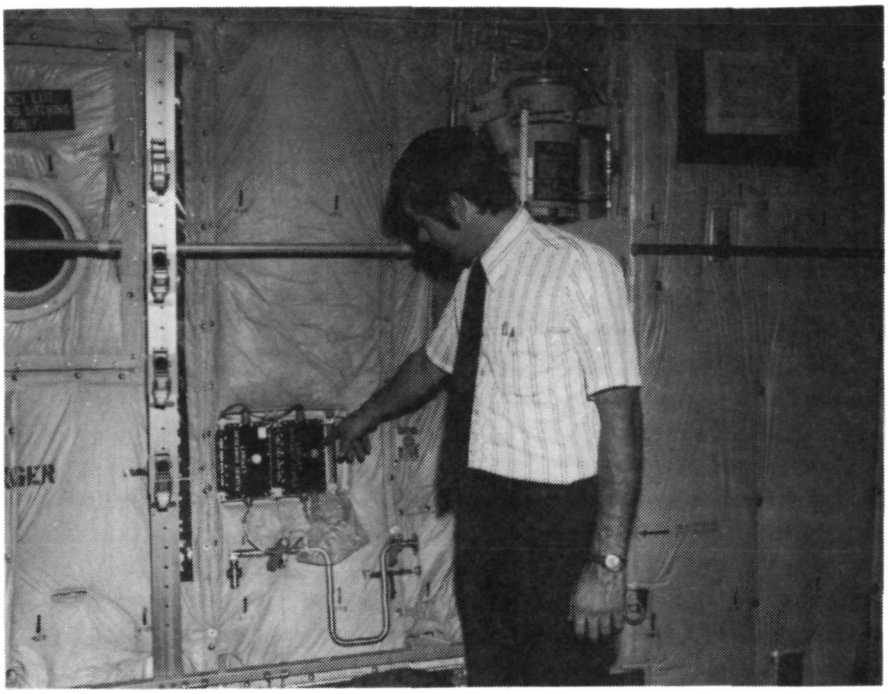

FIGURE 82 - STRAIN COUNTER INSTALLATION ON C-130
AF73-01592 (LAC 4557)

6.0 SERVICE EVALUATION OF THE COMPOSITE - REINFORCED CENTER WINGS

Upon completion of the flight acceptance tests, both of the C-130 aircraft, AF73-01592 and AF73-01594, with the composite-reinforced center wing boxes were delivered to the Air Force. Both aircraft were flown to the Little Rock Air Force Base, Jacksonville, Arkansas, where they are currently being used in basic and proficiency training including cargo airlift missions. This is the regular assignment for the operational command which includes rotation of aircraft to other widely dispersed bases.

During Phase V, inspections of the composite-reinforced center wing boxes will be conducted at the aircraft's home station over the flight service monitoring period of approximately three years by highly-qualified Lockheed personnel. A comprehensive ultrasonic inspection procedure has been assembled for field inspection of the boron-epoxy laminates and the laminate-to-metal adhesive bondlines in the center wing boxes. This written procedure includes the ultrasonic calibration procedure, illustrations of the wing areas to be inspected, part or assembly preparation, and equipment. The book form procedure is carried by the Lockheed inspectors in the field. The portable ultrasonic inspection equipment that is being used is illustrated in Figure 83.

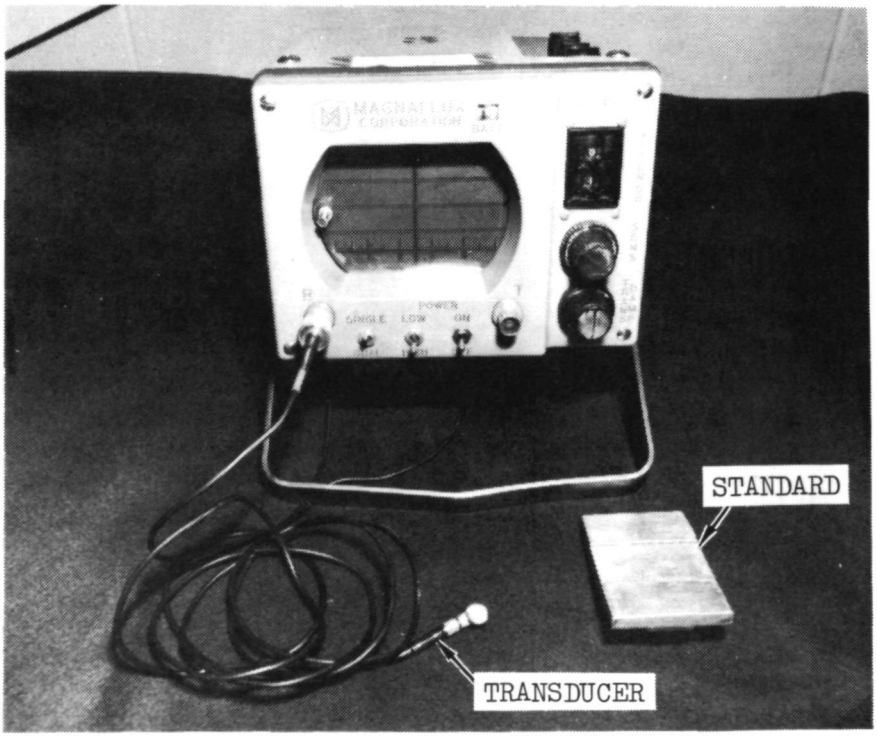

FIGURE 83 - PORTABLE ULTRASONIC INSPECTION EQUIPMENT

Initial plans were for the center wing box inspections to coincide with Air Force regularly-scheduled aircraft phased inspections. The plans were subsequently changed after the first inspection as the result of the C-130 aircraft transfer from the Tactical Air Command to the Military Airlift Command. Currently, the inspections are being conducted on an isochronal schedule. Seven inspections are planned for each center

wing box and the current inspection schedules for the two C-130 aircraft are given in Tables VIII and IX. These tables show that two of the seven planned inspections have been accomplished. In each of the first six inspections, all accessible composite-reinforced bonded joints in the center wing box are inspected. The bondlines include those inside of the wing dry bay areas, upper outer wing surface, lower outer wing surface inside the interior of the aircraft fuselage, and the lower outer wing surfaces between the inboard engines and fuselage fairings. The seventh inspection is planned to be a depot maintenance (PDM) inspection which will include the aforementioned areas plus the areas where the fuel tank blatters will be removed, the lower outer wing surface areas from which the fuselage-to-wing fairings will be removed, and the upper and lower wing surface areas from which the inboard nacelle fairings will be removed.

During Phase V, the Air Force involvement includes notification of Lockheed of the inspection schedule for each center wing box, provision for inspection accessibility, and replacement of furnishings, equipment and access doors upon completion of inspections. In the past four inspections, the Air Force has made the aircraft available to Lockheed for conducting the inspections two days prior to the regular inspection. This procedure has proven to be most satisfactory and continuation of this procedure for the remaining inspections would be highly beneficial for completion of the program.

TABLE VIII - C-130 COMPOSITE-REINFORCED CENTER WING INSPECTIONS - AF73-01592

INSPECT. NO.	DATE		AT INSPECTION		INSPECT. REPORTED VIA LGD/	RESULTS/COMMENTS
	PLANNED	ACTUAL	LOCATION	FLT. HRS.		
1	Jan., 1975	1/9-10/75	L.R. A.F.B.*	162	714237	No disbonds detected that exceeded specification limits and no surface finish breaks.
2	June, 1975	6/17-18/75	L.R. A.F.B.	551	718968	" " " " "
3	Oct., 1975	10/16-17/75	L.R. A.F.B.	826	722564	" " " " "
4	Mar., 1976	3/24-25/76	L.R. A.F.B.	1120	727111	" " " " "
5	Sept., 1976	9/23-24/76	L.R. A.F.B.	1581	731909	" " " " "
6	Apr., 1977					
7	Oct., 1977					

* Little Rock Air Force Base

TABLE IX - C-130 COMPOSITE-REINFORCED CENTER WING INSPECTIONS - AF73-01594

INSPECT. NO.	DATE		AT INSPECTION		INSPECT. REPORTED VIA LGD/	RESULTS/COMMENTS
	PLANNED	ACTUAL	LOCATION	FLT. HRS.		
1	Feb., 1975	2/18-19/75	L.R. A.F.B.*	187	715635	No disbonds detected that exceeded specification limits and no surface finish breaks.
2	July, 1975	7/29-30/75	L.R. A.F.B.	499	720329	" " " " "
3	Dec., 1975	12/4-5/75	L.R. A.F.B.	727	723693	" " " " "
4	May, 1976	5/19-20/76	L.R.A.F.B.	1064	728790	" " " " "
5	Nov., 1976					
6	May, 1977					
7	Nov., 1977					

* Little Rock Air Force Base

REFERENCES

1. Harvill, W. E., et al., "Program for Establishing Long-Time Flight Service Performance of Composite Materials in the Center Wing Structure of C-130 Aircraft: Phase I - Advanced Development," NASA CR-112126, Lockheed-Georgia Company, November 1972.

2. Harvill, W. E., et al., "Program for Establishing Long-Time Flight Service Performance of Composite Materials in the Center Wing Structure of C-130 Aircraft: Phase II - Detailed Design," NASA CR-112272, Lockheed-Georgia Company, April 1973.

3. Harvill, W. E., and Kays, A. O., "Program for Establishing Long-Time Flight Service Performance of Composite Materials in the Center Wing Structure of C-130 Aircraft: Phase III - Fabrication," NASA CR-132495, Lockheed-Georgia Company, September 1974.

4. Petit, P. H., "An Application Study of Advanced Composite Materials to the C-130 Center Wing Box," NASA CR 66979, Lockheed-Georgia Company, June 1970.

5. Staff, Quarterly Progress Reports for NAS 1-11100 Contract, "Advanced Composite Reinforcement of C-130 Center Wing Box," Lockheed-Georgia Company:

   - Seventh QPR: Phase III - Fabrication & Phase IV - Ground/Flight Acceptance Tests, August 1973
   - Eighth QPR: Phase III - Fabrication & Phase IV - Ground/Flight Acceptance Tests, November 1973
   - Ninth QPR: Phase III - Fabrication & Phase IV - Ground/Flight Acceptance Test, February 1974
   - Tenth QPR: Phase III - Fabrication & Phase IV - Ground/Flight Acceptance Tests, May 1974
   - Eleventh QPR: Phase III - Fabrication & Phase IV - Ground/Flight Acceptance Tests, August 1974
   - Twelfth QPR: Phase III - Fabrication, Phase IV - Ground/Flight Acceptance Tests, and Phase V - Service Evaluation, November 1974

6. NAS1-9485 Contract reported in NASA Contractor Report NASA CR-2075 entitled, "Residual Strength and Crack Propagation Tests on C-130 Airplane Center Wings with Service-Imposed Fatigue Damage," Lockheed-Georgia Company, July 1972.

7. McGee, W. M., "Static and Fatigue Tests on the C-130 Composite-Reinforced Center Wing Box," LG76ER0099, Lockheed-Georgia Company.

8. Toor, P. M., "Fracture Mechanics Methodology and Analytical Procedures," SMN 366A, Lockheed-Georgia Company, September 1972.

9. Roderick, G. L., et al, "Debond Propagation in Composite-Reinforced Metals," NASA TM-X-71948, December 1973.

10. Poe, C. C., Jr., "Stress-Intensity Factor for a Cracked Sheet with Riveted and Uniformly Spaced Stringers," NASA TR-R-358, May 1971.

11. Bloom, J. M., and Sanders, J. L., Jr., "The Effect of a Riveted Stringer on the Stress in a Cracked Sheet," ASME Trans., Ser. E, Journal of Applied Mechanics, Vol. 33, No. 3, September 1966.

12. Wilhem, D. P., "Fracture Mechanics Guidelines for Aircraft Structural Applications," AD 702528, Northrop Corporation, Aircraft Division, February 1970.

13. Stronge, W. J., "Modeling Damaged Wings--Element Selection and Constraint Specification," NASA TMX-3278, September 1975, page 105.

14. Wilkinson, R. F., and Kelley, J. W., "A Failsafe Analysis Using NASTRAN's Piecewise Linear Analysis and a Nine Node Linear Cracked Element," NASA TMX-3278, September 1975, page 181.

15. Sih, G. C., "Handbook of Stress Intensity Factors for Researchers and Engineers," Lehigh University Press, November 1973.

16. Sanga, R. V., "The 747 Failsafe Structural Verification Program," technical paper presented at the 7th ICAF Symposium, London, England, July 18-20, 1973, Boeing Commercial Airplane Company.

17. Dickson, J. N., et al, "Development of an Understanding of the Fatigue Phenomena of Bonded and Bolted Joints in Advanced Filamentary Composite Materials," AFFDL-TR-72-64, June 1972.

18. Cremens, W. S., et al, "Advanced Structural Materials Handbook," SMN 356, Vol. II, Lockheed-Georgia Company, February 1972.

19. Davidson, J. R., "Reliability After Inspection," NASA TMX-71969, December 1973.

APPENDIX A

RELATIONSHIP BETWEEN SI UNITS AND U.S. CUSTOMARY UNITS

BASIC SI UNITS		
Physical Concept	Measurement	Abbreviation
Length	meter	m
Mass	kilogram	kg
Time	second	s
Force	Newton	N
Thermodynamic Temperature	degree Kelvin	°K
Density	kilograms/meter^3	kg/m^3

PREFIXES		
Factor By Which Unit Is Multiplied	Prefix	Symbol
10^9	giga	G
10^6	mega	M
10^3	kilo	k
10^2	hecto	h
10	deca	da
10^{-1}	deci	d
10^{-2}	centi	c
10^{-3}	milli	m
10^{-6}	micro	μ

CONVERSION FACTORS		
To Convert From	To	Multiply By
Celsius (temps.)	kelvin	$t_K = t_c + 273.15$
Fahrenheit (temp.)	kelvin	$t_K = (5/9)(t_F + 459.67)$
foot	meter	3.048×10^{-1}
inch	meter	2.54×10^{-2}
pound mass (lbm avoirdupois)	kilogram	4.536×10^{-1}
pound mass force (lbf)	newton	4.44822
$lbm/inch^3$	$kilogram/meter^3$	2.768×10^4
psi	$newton/meter^2$	6.895×10^3
ksi $\sqrt{in.}$	$(MN/m^2)\sqrt{m}$	1.100

APPENDIX B

MATHEMATICAL RELATIONSHIPS FOR THE RELIABILITY ANALYSIS OF THE C-130 COMPOSITE-REINFORCED CENTER WING

In this appendix the necessary mathematical relationships are developed for preparing a reliability analysis of adhesive bonds between the composite reinforcements and the metallic components of the C-130 center wing assembly. The approach used in the following developments is based on the analysis presented in Reference 19. In the referenced analysis, derivations are made for relationships among the probability of having manufacturing defects, the probability of detecting a disbond, and the final reliability. Application of statistical distribution functions are necessary in development of the mathematical relationships to be used in reliability analysis. Specific data such as the actual history of disbonds detected during manufacture, frequency of interim inspections, disbonds detected during each inspection, and aircraft flight hours accumulated were input data for accomplishing the reliability analysis. In addition, other physical data must be known or assumed in the mathematical developments.

Upon initiating the development of the mathematical relationships, the following definitions are made:

L = Disbond rate per square meter of bonded area

(LS) = Average number of disbonds in a structural assembly having a bonded area of S square meters

A_n = n disbonds exist in assembly

B_k = k disbonds detected during the inspection

$P(A_n \cdot B_k)$ = Probability that n disbonds exist and k are detected during the inspection
$= P(B_k \mid A_n)P(A_n)$

$P(A_n)$ = Probability of n disbonds and is represented by the Poisson density function as follows:
$$= \left[(LS)^n \cdot e^{-(LS)}\right] / n ! \qquad (1)$$

$P(B_k \mid A_n)$ = Probability that k disbonds are detected during the inspection given that n disbonds exist

In an inspection covering 100 percent of the bonded area of the structural assembly, the probability of exactly k disbond detections out of a possible n number of disbonds applying the binomial density function is $C_k^n (R)^k (Q)^{n-k}$. Thus, the equation for $P(B_k \mid A_n)$ may therefore be the general term of the binomial density function, and is written as,

$$P(B_k \mid A_n) = C_k^n (R)^k (Q)^{n-k} \qquad (2)$$

where, $C_k^n = (n!)/[k!\ (n-k)!]$

R = Inspection reliability per unit of bonded area, i.e., detection probability

Q = Inspection failure probability per unit of bonded area

It is noted that the detection process is independent from assembly to assembly, so the fact that some bonded areas have no disbonds does not degrade the probability of detection of disbonds that exist in other bonded areas.

Furthermore, the probability that n disbonds exist in the structural assembly and k disbonds are detected during the inspection, $P(A_n \cdot B_k)$ can be obtained by combining equations (1) and (2) above. Thus,

$$P(A_n \cdot B_k) = \left[C_k^n (R)^k (Q)^{n-k} (LS)^n \cdot e^{-(LS)}\right]/n! \qquad (3)$$

The average number of disbonds remaining after the first inspection is given by

$$E_{a1} = \sum_{r=0}^{\infty} r\, P(r) \qquad (4)$$

where, P(r) is the probability that n-k = r disbonds are not detected during the inspection. P(r) is determined by the summation of mutually exclusive events. For example,

$$P(1) = P(A_1 \cdot B_0) + P(A_2 \cdot B_1) + \ldots + P(A_n \cdot B_{n-1}) + \ldots$$

$$P(2) = P(A_2 \cdot B_0) + P(A_3 \cdot B_1) + \ldots + P(A_n \cdot B_{n-2}) + \ldots \text{ etc.}$$

Therefore,

$$P(r) = \sum_{n=r}^{\infty} \left[C_r^n (R)^{n-r} \cdot (Q)^r (LS)^n \cdot e^{-(LS)}\right]/n! \qquad (5)$$

$$E_{a1} = \sum_{r=o}^{\infty} \sum_{n=r}^{\infty} r\left[C_r^n (R)^{n-r} \cdot (Q)^r (LS)^n \cdot e^{-(LS)}\right]/n! \qquad (6)$$

After a bonded structural assembly is fabricated, inspected, and tested or entered into operational service, additional disbonds may develop in a random manner at some given rate, L_s. Thus, L_s is defined as an in-service disbond rate per unit of bondline area per unit of time. Furthermore, the expected number of disbonds in a structural assembly just prior to the second inspection is the sum of those existent after the first inspection, E_{a1}, plus those accruing between the first and second inspections. In equation form, the total number of disbonds in a structural assembly immediately prior to the second inspection is

$$E_{b2} = E_{a1} + L_s (S)(T) \qquad (7)$$

where, S = number of units of bonded area in the structural assembly

T = number of units of operating time between the first and second inspections

The average number of disbonds existent in the structural assembly after the second inspection is denoted E_{a2} and defined in equation form is

$$E_{a2} = \sum_{r=o}^{\infty} \sum_{n=r}^{\infty} r \left[C_r^n (R)^{n-r} \cdot (Q)^r \cdot (E_{b2})^n \cdot e^{-(E_{b2})} \right] / n! \qquad (8)$$

In general, the number of disbonds existent in the structural assembly after the ith inspection is

$$E_{bi} = E_{a(i-1)} + L_S (S)(T) \qquad (9)$$

$$E_{ai} = \sum_{r=o}^{\infty} \sum_{n=r}^{\infty} r \left[C_r^n (R)^{n-r} \cdot (Q)^r \cdot (E_{bi})^n \cdot e^{-(E_{bi})} \right] / n! \qquad (10)$$

The double series equations above have the disadvantage of being tedious to apply. However, referring to equation (6), it is observed that the expected value of E_{a1} can be rewritten as

$$E_{a1} = \sum_{n=o}^{\infty} \frac{(LS)^n \cdot e^{-(LS)}}{n!} \left[\sum_{r=o}^{n} r C_r^n (R)^{n-r} \cdot (Q)^r \right] \qquad (11)$$

The bracketed portion of equation (11) is the binomial distribution expected value and is equal to n(Q). Thus, the equation for E_{a1} simplifies to

$$E_{a1} = Q \sum_{n=o}^{\infty} \left[n (LS)^n \cdot e^{-(LS)} \right] / n! \qquad (12)$$

However, equation (12) is simply Q times the expected value of the Poisson distribution and is equal to Q(LS). Rewriting the equation for E_{a1}, the average number of disbonds in the structural assembly after the first inspection,

$$E_{a1} = (LS)(Q) = (LS)(1-R) \qquad (13)$$

Upon introducing an in-service disbond rate L_s, in disbonds per unit area, S, per unit time, T, the average number of disbonds existent just prior to the second inspection may be defined as

$$E_{b2} = E_{a1} + L_s (ST) = (LS)(1-R) + L_s (ST) \qquad (14)$$

Likewise, the average number of disbonds in the structural assembly after the second inspection may be defined by the following relationship.

$$E_{a2} = E_{b2}(1-R)$$
$$= \left[(LS)(1-R) + L_s\ (ST)\right](1-R) \qquad (15)$$
$$= (LS)(1-R)^2 + L_s\ (ST)(1-R)$$

Furthermore,

$$E_{b3} = E_{a2} + L_s\ (ST) = (LS)(1-R)^2 + L_s\ (ST)(1-R) + L_s(ST)$$
$$E_{a3} = (LS)(1-R)^3 + L_s\ (ST)(1-R)^2 + L_s\ (ST)(1-R)$$

From the relationships immediately above, it can be shown that after the *ith inspection the average number of disbonds in the structural assembly is*

$$E_{ai} = (LS)(1-R)^i + L_s\ (ST)\left[(1-R) + (1-R)^2 + \ldots + (1-R)^{i-1}\right] \qquad (16)$$

Also, immediately before the ith inspection the average number of disbonds existent in the structural assembly is

$$E_{bi} = (LS)(1-R)^{i-1} + L_s\ (ST)\left[1 + (1-R) + \ldots + (1-R)^{i-2}\right] \qquad (17)$$

The reliabilities (i.e., probability of no disbonds) just prior to and subsequent to the ith inspection are respectively

$$R_{bi} = e^{-(E_{bi})} \text{ and } R_{ai} = e^{-(E_{ai})} \qquad (18)$$

It is observed from the above equation for E_{bi} that the number of existent disbonds after repeated inspections will be stabilized. The limit of E_{ai} in equation (16) as $i \to \infty$ is as follows.

$$\lim_{i\to\infty} E_{ai} = \lim_{i\to\infty} (LS)(1-R)^i + \lim_{i\to\infty} (L_s)(ST)\left[(1-R) + (1-R)^2 + \ldots + (1-R)^{i-1}\right]$$
$$= L_s\ (ST)\left[\frac{1-R}{R}\right] \qquad (19)$$

Therefore, a steady in-service residual after inspection disbond level of $L_s(ST)\left[\frac{1-R}{R}\right]$ is approached. Also, the E_{q1} quality level degrades after inspection to a maximum of $E_{bi} = L_s(ST)/R$ just prior to the next inspection. It is noted that as a practical consideration these steady state limit values are approached after only a few inspections even when the inspection, production, and in-service operational reliabilities are not very high. For example, if

$L = 0.05$, the production disbond rate per unit bonded area

$L_s = 0.01$, the in-service random disbond rate per unit bonded area per 1000 operational service hours

S = 500 units of bonded area inspected

T = 3200 flight hours, the frequency of inspection

R = 0.99, inspection reliability per unit area

The steady state disbond condition denoted by E_a is

$$E_a = (0.01)\,(500)\,\left(\frac{3200}{1000}\right)\left(\frac{1-0.99}{0.99}\right) = 0.1616161$$

and similarly for E_b,

$$E_b = (0.01)\,(500)\,(3.2)/0.99 = 16.16161$$

After the original plus three in-service inspections,

$$E_{a4} = (0.05)(500)(0.01)^4 + (0.01)(500)(3.2)\left[0.01 + (0.01)^2 + (0.01)^3\right] = 0.1616162$$

$$E_{b4} = (0.05)(500)(0.01)^3 + (0.01)(500)(3.2)\left[1 + 0.01 + (0.01)^2\right] = 16.16162$$

The differences between E_{a4} and $E_a = 0.0000001$, and E_{b4} and $E_b = 0.00001$. Thus, the steady state reliability levels are realized after a rather few inspections.

The in-service operational reliability of the bonded area of the structural assembly after inspection is

$$R_a = e^{-L_s(ST)(1-R)/R} \tag{20}$$

and just before the inspection is

$$R_b = e^{-(L_s)(ST)/R} \tag{21}$$

It is of further interest to note that equation (8) of Reference 19 provides results that are nearly equivalent to those provided by equation (20) above. Equation (8) from Reference 19 is

$$R_2 = \frac{1}{1 + \dfrac{\exp\left(\lambda S P(B' \mid A)\right) - 1}{P(B' \mid A')}} \tag{22}$$

The difference in equations (20) and (22) is in the inclusion of T, the time between inspections in equation (20), the (1/R) factor in equation (20) to account for existing disbonds from prior inspections, and the $P(B' \mid A')$ factor of equation (22).

Noting that λS in equation (22) has the same definition as LS in equation (20) and $P(B' \mid A)$ has the same definition as (1-R) in equation (20). Then,

$$R_2 = \frac{1}{1 + \dfrac{\exp\left(LS(1-R)\right) - 1}{P(B' \mid A')}} \tag{23}$$

If no disbonds are detected and none exists, the $P(B' \mid A') = 1.0$. Making this assumption, equation (23) becomes

$$R_2 = \frac{1}{\exp\left(LS\,(1-R)\right)} = e^{-(LS)(1-R)} \qquad (24)$$

The interpretation of equation (8) in Reference 19 (also, equation (22) above) is unlike equation (20) above because of the difference in reliability definition. Equation (8) in Reference 19 is defined to be the probability that no flaws (disbonds) exist after inspection given that none is indicated by the inspection. Equation 20 above is simply the probability that no flaws (disbonds) exist after the inspection (assuming those disbonds detected were repaired). There is no conditional requirement that no disbonds be detected during an inspection. In both cases defined by equation (8) of Reference 19 and equation (20), the reliability of the inspection procedure applied in detecting existing disbonds is used in an identical manner. However, as reflected in Equation (20), the probability of no false indications of disbonds is not pertinent to the probability that the disbonds exist. The existence of a disbond after an inspection is independent of false indications. Therefore, the factor, $P(B' \mid A')$, that is correctly included in equation (8) of Reference 19 is appropriately missing from equation (20) above.

APPENDIX C

FATIGUE DAMAGE REPORTS ON COMPOSITE-REINFORCED CENTER WING TEST ARTICLE

Fatigue damage reports on the fastener failures and beam web cracks are included in this appendix. All of the failures occurred during the fatigue test of the composite-reinforced center wing test article. Each report describes the damage and each is accompanied by a photograph of the damaged area. Also, the repair for each failure is described in the damage report.

FATIGUE DAMAGE REPORT - COMPOSITE REINFORCED

C-130 CENTER WING BOX FATIGUE TEST

TEST PROGRAM: CONTRACT NAS1-11100, PHASE IV
DAMAGE ITEM NUMBER 1

	YES	NO
DAMAGED PART CONSIDERED TO BE TEST SPECIMEN	X	
DAMAGE CONSIDERED TO BE MAJOR		X
REPAIR NECESSARY	X	
DISCREPANCY REPORT NUMBER	060066	

PROGRAM COMPLETED WHEN DAMAGE WAS DETECTED: Pass Number 20, Condition GUST 1.1, Cycle 87, Approximate Number of Flight Hours and/or landings Simulated 20,000 Hours and 14,434 Landings.

PART NUMBER AND DESCRIPTION:	LOCATION:
Huk-bolt ($\frac{1}{4}$-inch dia.) in 390619-5 Fitting	WS 220L (Front Beam, Lower Surface)

DATE FOUND: 1/10/75 FOUND BY: R.I. Prescott VERIFIED BY: H.F. Ortwein

METHOD OF DETERMINATION: Visual

SKETCH OR PHOTO:

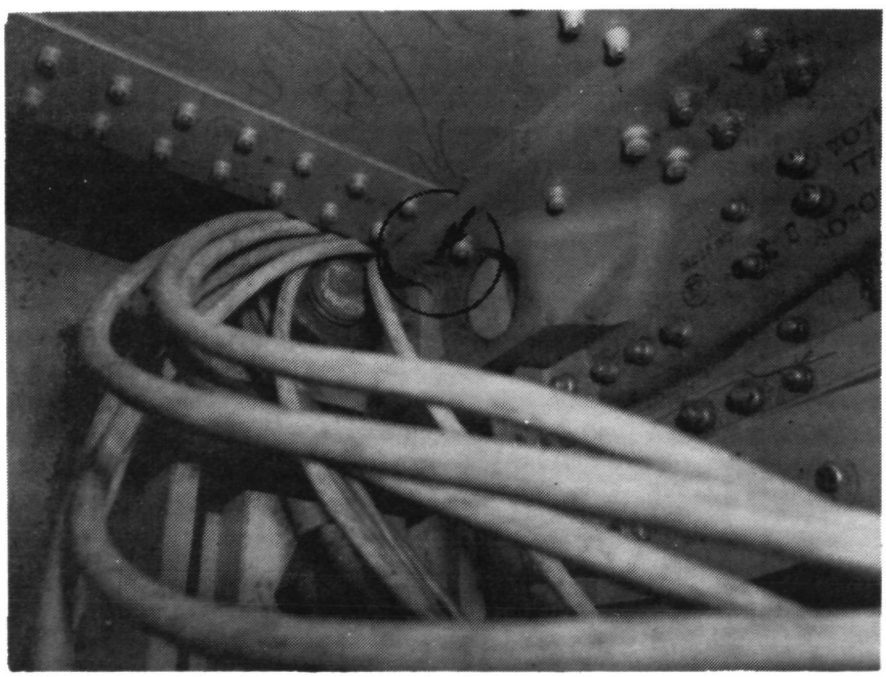

REMARKS:
A $\frac{1}{4}$-inch diameter Huk-bolt in the 390619-5 Fitting had broken head. Fracture surface had fatigue markings. Eddy current inspection of fastener hole wall revealed no cracks. Hole was reamed to accept HL-56 fastener which was installed wet with STM 40-111 sealant.

FATIGUE DAMAGE REPORT - COMPOSITE REINFORCED

C-130 CENTER WING BOX FATIGUE TEST

TEST PROGRAM: CONTRACT NAS1-11100, PHASE IV
DAMAGE ITEM NUMBER 2

	YES	NO
DAMAGED PART CONSIDERED TO BE TEST SPECIMEN	X	
DAMAGE CONSIDERED TO BE MAJOR		X
REPAIR NECESSARY	X	
DISCREPANCY REPORT NUMBER	060066	

PROGRAM COMPLETED WHEN DAMAGE WAS DETECTED: Pass Number 20, Condition GUST 1.1, Cycle 87, Approximate Number of Flight Hours and/or landings Simulated 20,000 Hours and 14,434 Landings.

PART NUMBER AND DESCRIPTION:
Huk-bolt (3/16-in. dia.) in the 371231-1L, Rib Installation

LOCATION:
WS 140.2L (Rear Beam, Upper Surface)

DATE FOUND: 1/10/75 FOUND BY: R.I. Prescott VERIFIED BY: H.F. Ortwein

METHOD OF DETERMINATION: Visual

SKETCH OR PHOTO:

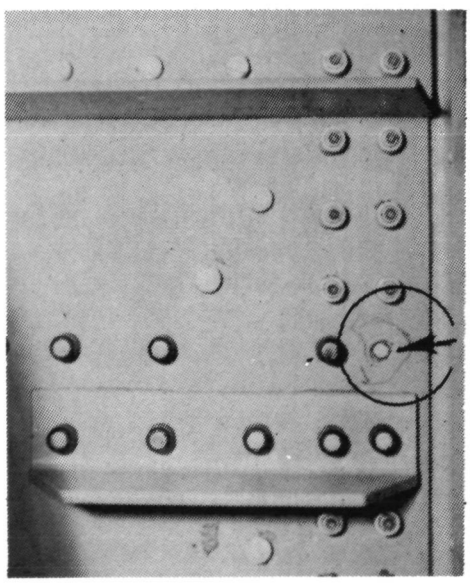

REMARKS:
A 3/16-inch diameter Huk-bolt in the 371231-1L, Rib Installation, had failed at the collar. Fracture surface had fatigue markings. Eddy current inspection of fastener hole wall revealed no cracks. Failed fastener was replaced with an HL-18 fastener installed wet with STM 40-111 Sealant.

FATIGUE DAMAGE REPORT - COMPOSITE REINFORCED

C-130 CENTER WING BOX FATIGUE TEST

TEST PROGRAM: CONTRACT NAS1-11100, PHASE IV
DAMAGE ITEM NUMBER 3

	YES	NO
DAMAGED PART CONSIDERED TO BE TEST SPECIMEN	X	
DAMAGE CONSIDERED TO BE MAJOR		X
REPAIR NECESSARY	X	
DISCREPANCY REPORT NUMBER	060066	

PROGRAM COMPLETED WHEN DAMAGE WAS DETECTED: Pass Number 20, Condition GUST 1.1, Cycle 87, Approximate Number of Flight Hours and/or landings Simulated 20,000 Hours and 14,434 Landings.

PART NUMBER AND DESCRIPTION	LOCATION:
Two Huk-bolts (3/16-inch dia.) in 388196-48, Strap	WS 220R (Front Beam, Upper Surface)

DATE FOUND: 1/10/75 FOUND BY: R.I. Prescott VERIFIED BY: H.F. Ortwein

METHOD OF DETERMINATION: Visual

Sketch or Photo:

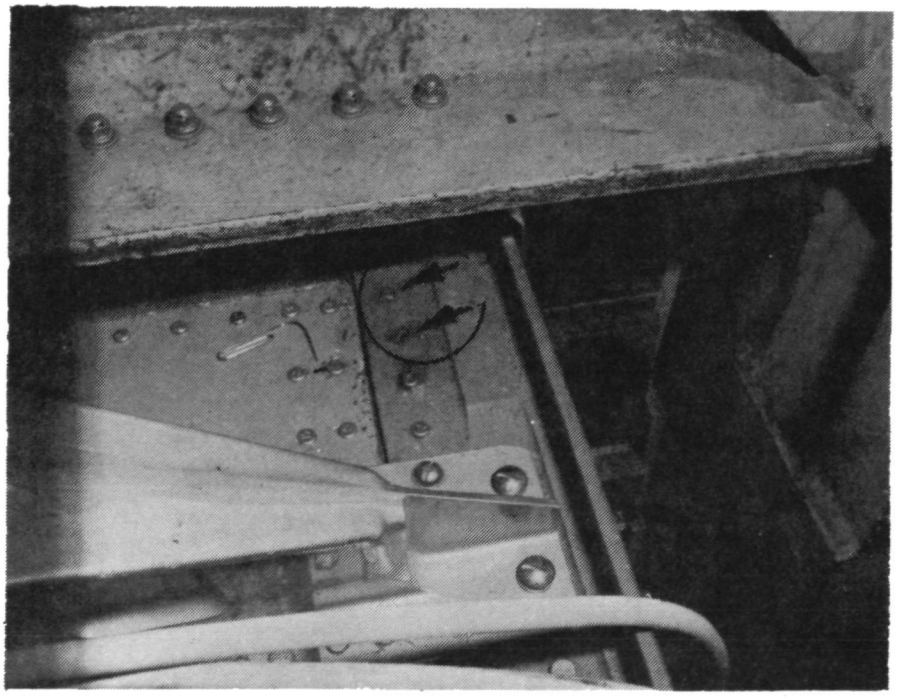

REMARKS:
Two Huk-bolts in 388196-48 Strap had broken heads. Fracture surfaces had fatigue markings. Eddy current inspection of hole walls revealed no cracks. Holes were reamed to accept HL-56 fasteners which were installed wet with STM 40-111 Sealant.

FATIGUE DAMAGE REPORT - COMPOSITE REINFORCED
C-130 CENTER WING BOX FATIGUE TEST

TEST PROGRAM: CONTRACT NAS1-11100, PHASE IV
DAMAGE ITEM NUMBER 4

	YES	NO
DAMAGED PART CONSIDERED TO BE TEST SPECIMEN	X	
DAMAGE CONSIDERED TO BE MAJOR		X
REPAIR NECESSARY	X	
DISCREPANCY REPORT NUMBER	060066	

PROGRAM COMPLETED WHEN DAMAGE WAS DETECTED: Pass Number 20, Condition GUST 1.1, Cycle 87, Approximate Number of Flight Hours and/or landings Simulated 20,000 Hours and 14,434 Landings.

PART NUMBER AND DESCRIPTION:	LOCATION:
Three Huk-bolts (3/16-inch dia.) in 388196-47 Strap	WS 220L (Front Beam, Upper Surface)

DATE FOUND: 1/10/75 FOUND BY: R.I. Prescott VERIFIED BY: H.F. Ortwein

METHOD OF DETERMINATION: Visual

SKETCH OR PHOTO:

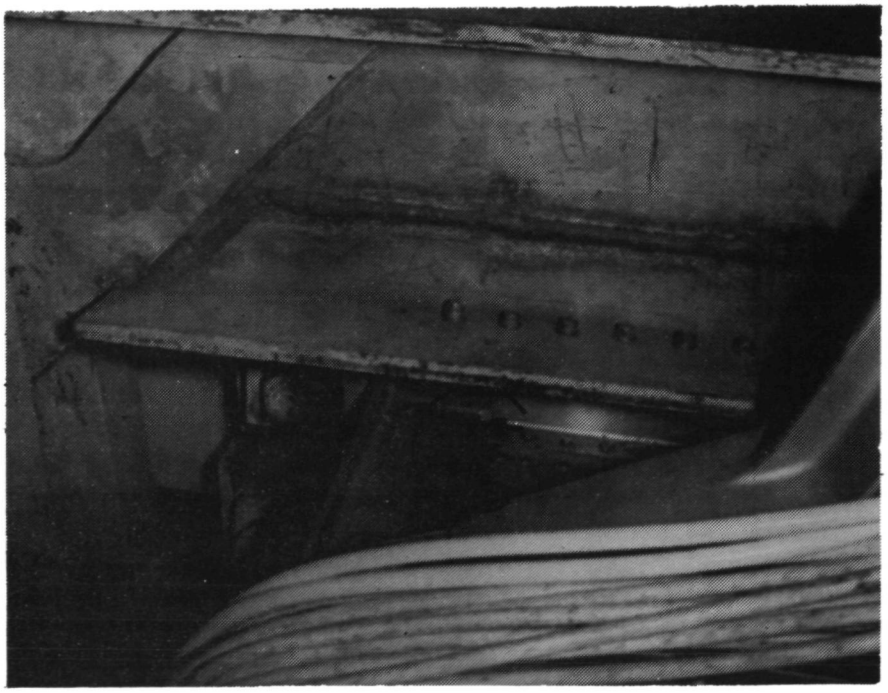

REMARKS:
Three Huk-bolts in 388196-47 strap had broken heads. Fracture surfaces had fatigue markings. Eddy current inspection of hole walls revealed no cracks. Holes were reamed to accept HL-56 fasteners which were installed wet with STM 40-111 sealant.

FATIGUE DAMAGE REPORT - COMPOSITE REINFORCED
C-130 CENTER WING BOX FATIGUE TEST

TEST PROGRAM: CONTRACT NAS1-11100, PHASE IV
DAMAGE ITEM NUMBER 5

	YES	NO
DAMAGED PART CONSIDERED TO BE TEST SPECIMEN.	X	
DAMAGE CONSIDERED TO BE MAJOR.		X
REPAIR NECESSARY.	X	
DISCREPANCY REPORT NUMBER.	060256	

PROGRAM COMPLETED WHEN DAMAGE WAS DETECTED: Pass Number 23, Condition GUST 2.2, Cycle 250, Approximate Number of Flight Hours and/or landings Simulated 23,000 Flight Hours and 16,600 Landings

PART NUMBER AND DESCRIPTION:	LOCATION:
Two Hi-Loks (3/16-inch dia.) in Part 388196-47 Strap	WS 220L (Front Beam, Upper Surface

DATE FOUND: 2/4/75 FOUND BY: H.F. Ortwein VERIFIED BY: R.I. Prescott

METHOD OF DETERMINATION: Visual

SKETCH OR PHOTO:

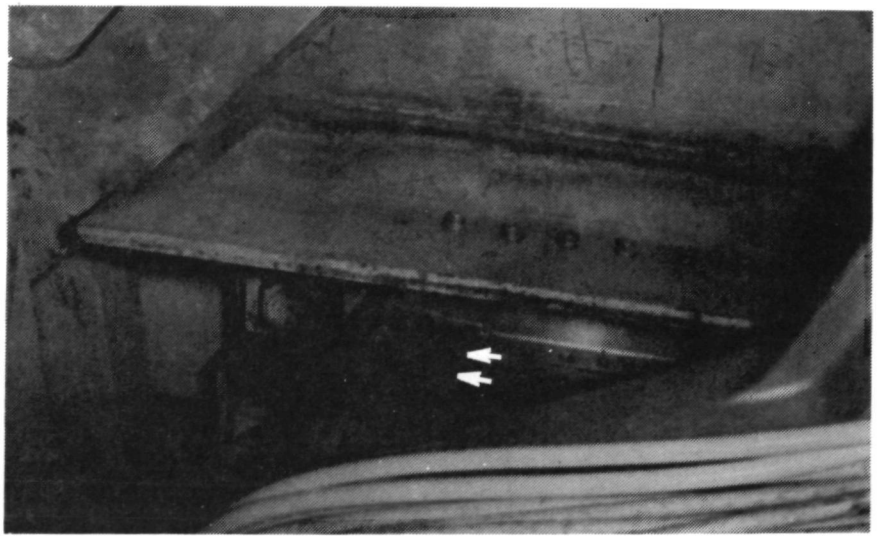

REMARKS:
Two 3/16-inch diameter Hi-Loks, which replaced broken Huk-bolts per Discrepancy Report Number 060066, in the 388196-47 strap had broken at collars. All fixture bolts shearing P_z load into the front and rear beam webs at CWS 220 left and right were checked for looseness and were retorqued as required. Several bolts required some retorquing. Failed fasteners were replaced with HL-36 fasteners with TLN 1000 nuts installed wet with STM 40-111 sealant. Also, one previously installed Hi-Lok was found to be loose and was replaced with fastener equivalent to HL-36.

FATIGUE DAMAGE REPORT - COMPOSITE REINFORCED
C-130 CENTER WING BOX FATIGUE TEST

TEST PROGRAM: CONTRACT NAS1-11100, PHASE IV
DAMAGE ITEM NUMBER 6

	YES	NO
DAMAGED PART CONSIDERED TO BE TEST SPECIMEN.	X	
DAMAGE CONSIDERED TO BE MAJOR.		X
REPAIR NECESSARY.	X	
DISCREPANCY REPORT NUMBER.	054084	

PROGRAM COMPLETED WHEN DAMAGE WAS DETECTED: Pass Number 24, Condition GUST 2.4, Cycle 4100, Approximate Number of Flight Hours and/or landings Simulated 24,000 Flight Hours and 17,300 Landings

PART NUMBER AND DESCRIPTION:
Two Huk-Bolts (3/16-inch dia.); one each in 370521-3 & -4 Fittings

LOCATION:
WS 220 L&R (Ream Beam, Upper Surface)

DATE FOUND: 2/11/75 FOUND BY: R.I. Prescott VERIFIED BY: H.F. Ortwein

METHOD OF DETERMINATION: Visual

SKETCH OR PHOTO:

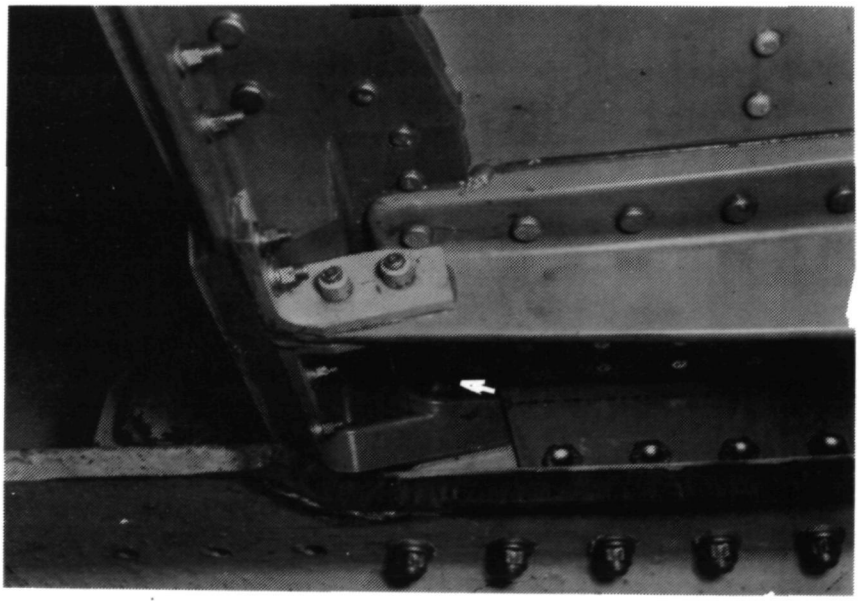

REMARKS:
One 3/16-inch diameter Huk-bolt in the 370521-3 Fitting and one 3/16-inch diameter Huk-bolt in the 370521-4 Fitting had broken heads. Fracture surfaces had fatigue markings. In conjunction with Discrepancy Report No. 060256 all fixture bolts shearing P_z load into the front and rear beam webs at CWS 220 left and right were checked for looseness and were retorqued as required. Several bolts required a small amount of retorquing. Fastener holes were reamed to accept HL-56 fasteners which were installed wet with STM 40-111 sealant.

FATIGUE DAMAGE REPORT - COMPOSITE REINFORCED
C-130 CENTER WING BOX FATIGUE TEST

TEST PROGRAM: CONTRACT NAS1-11100, PHASE IV
DAMAGE ITEM NUMBER 7

	YES	NO
DAMAGED PART CONSIDERED TO BE TEST SPECIMEN.	X	
DAMAGE CONSIDERED TO BE MAJOR.		X
REPAIR NECESSARY.	X	
DISCREPANCY REPORT NUMBER.	054040	

PROGRAM COMPLETED WHEN DAMAGE WAS DETECTED: Pass Number 26, Condition GUST 3.1, Cycle 130, Approximate Number of Flight Hours and/or landings Simulated 25,597 Flight Hours and 18,473 Landings

PART NUMBER AND DESCRIPTION:	LOCATION:
Two Hi-Loks (3/16-inch dia.) in Part 388196-47 Strap	WS 220L (Front Beam, Upper Surface

DATE FOUND: 2/25/75 FOUND BY: R.I. Prescott VERIFIED BY: H.F. Ortwein

METHOD OF DETERMINATION: Visual
SKETCH OR PHOTO:

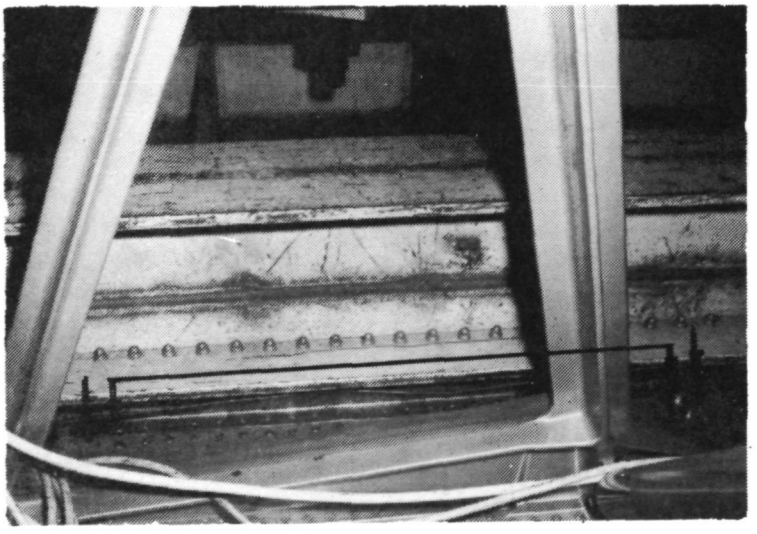

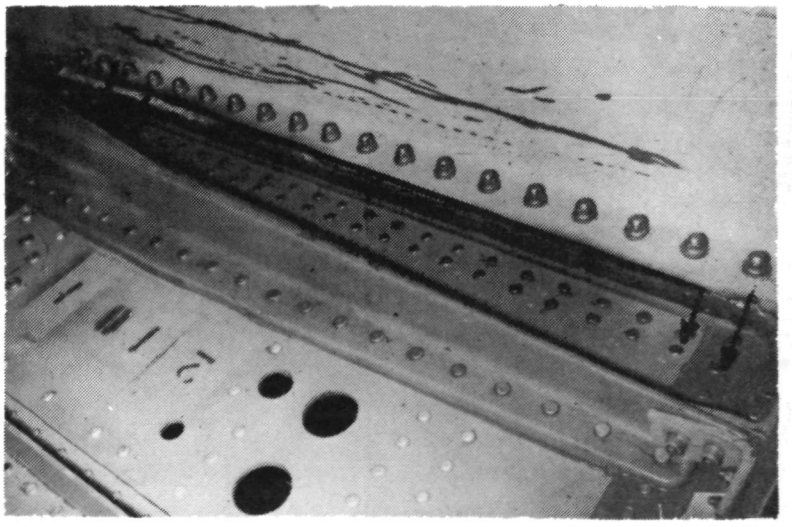

REMARKS:
One 3/16-inch diameter Hi-Lok in the 388196-47 strap had broken at the collar and one 3/16-inch Hi-Lok in the 388196-47 strap had broken at the nut. (Reference Damage Item Number 5).

Also, all existing fasteners common to the wing splice angles and beam webs at WS 220 L&R, front and rear beam, and fasteners common to the corner fittings, were replaced with standard oversize Hi-Lok fasteners installed wet with STM 40-111 sealant.

FATIGUE DAMAGE REPORT - COMPOSITE REINFORCED
C-130 CENTER WING BOX FATIGUE TEST

TEST PROGRAM: CONTRACT NAS1-11100, PHASE IV
DAMAGE ITEM NUMBER 8

	YES	NO
DAMAGED PART CONSIDERED TO BE TEST SPECIMEN.	X	
DAMAGE CONSIDERED TO BE MAJOR.		X
REPAIR NECESSARY	X	
DISCREPANCY REPORT NUMBER.	054028	

PROGRAM COMPLETED WHEN DAMAGE WAS DETECTED: Pass Number 30, Condition GUST T 1.1, Cycle All, Approximate Number of Flight Hours and/or Landings Simulated 30,000 Flight Hours and 21,651 Landings

PART NUMBER AND DESCRIPTION: 3/16" diameter Huk-Bolt in P/N 370539-1 Web

LOCATION: W.S. 100L at Rear Beam

DATE FOUND: 4/10/75 FOUND BY: R.I. Prescott VERIFIED BY: H.F. Ortwein

METHOD OF DETERMINATION: Visual

SKETCH OR PHOTO:

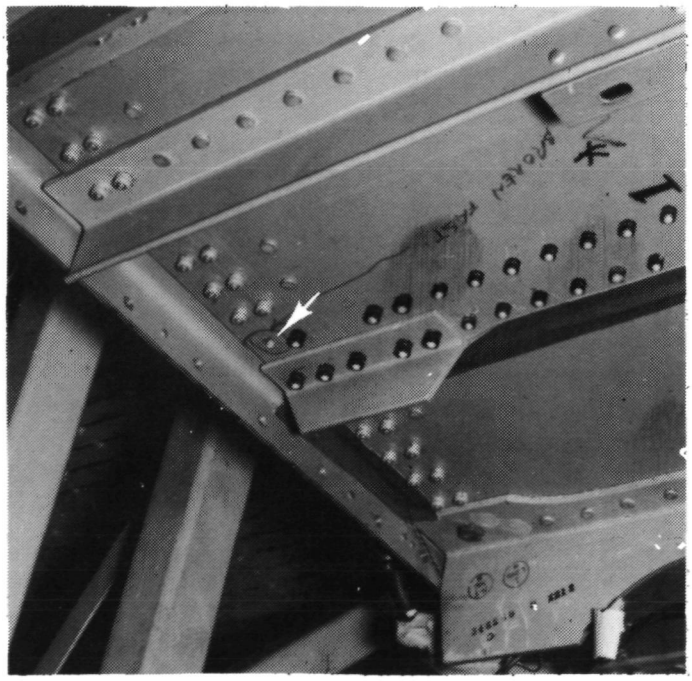

REMARKS:
No cracks were detected upon inspection of hole with eddy current meter. Fastener was replaced with HL-18 Hi-Lok installed wet with STM 40-111 sealant.

FATIGUE DAMAGE REPORT - COMPOSITE REINFORCED
C-130 CENTER WING BOX FATIGUE TEST

TEST PROGRAM: Contract NAS1-11100, Phase IV
DAMAGE ITEM NUMBER 9

	YES	NO
DAMAGED PART CONSIDERED TO BE TEST SPECIMEN.	X	
DAMAGE CONSIDERED TO BE MAJOR.		X
REPAIR NECESSARY.	X	
DISCREPANCY REPORT NUMBER.	054246	

PROGRAM COMPLETED WHEN DAMAGE WAS DETECTED: Pass Number 40, Condition Gust 1.5, Cycle 560, Approximate Number of Flight Hours and/or Landings Simulated 39,900 Hours and 28,795 Landings

PART NUMBER AND DESCRIPTION:
370532-5 Web

LOCATION:
WS 73L and 74L
(Front Beam, Lower Surface)

DATE FOUND: 7/23/75 FOUND BY: R.E. Sykes VERIFIED BY: R.I. Prescott

METHOD OF DETERMINATION: Visual

SKETCH OR PHOTO:

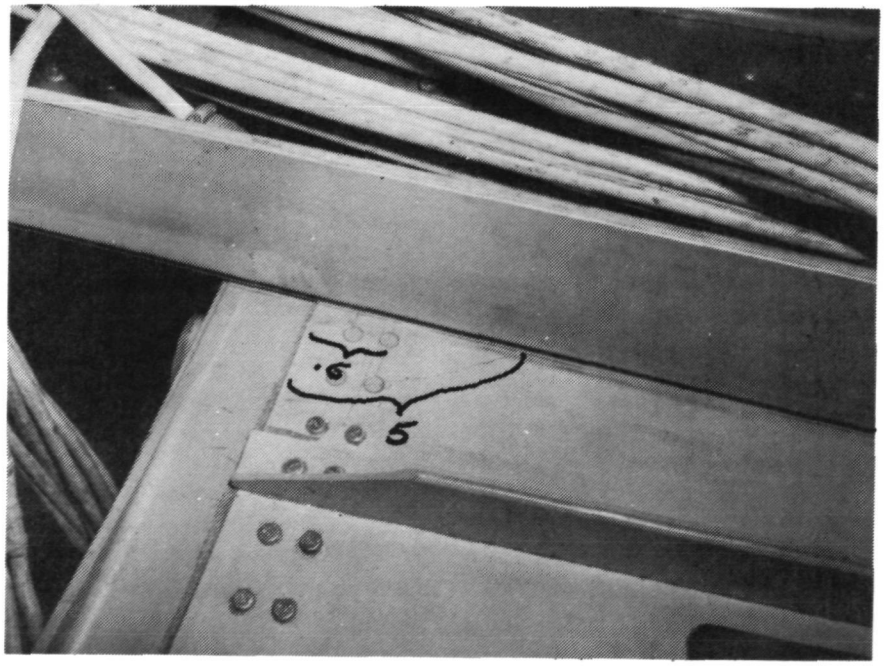

REMARKS:
The 370532-5 Web had two cracks. One 0.6-inch long at WS 73L running through two fasteners to the edge of the web. The other was 5.0-inches long at WS 74L running through two fasteners to edge of the web. Cycling was continued until completion of fourth lifetime with periodic inspections revealing no crack growth. The area was repaired per S-5420 which specified web reinforcement with steel doublers.

FATIGUE DAMAGE REPORT - COMPOSITE REINFORCED
C-130 CENTER WING BOX FATIGUE TEST

TEST PROGRAM: Contract NAS1-11100, Phase IV
DAMAGE ITEM NUMBER: 10

	YES	NO
DAMAGED PART CONSIDERED TO BE TEST SPECIMEN.	X	
DAMAGE CONSIDERED TO BE MAJOR.		X
REPAIR NECESSARY.	X	
DISCREPANCY REPORT NUMBER	054240	

PROGRAM COMPLETED WHEN DAMAGE WAS DETECTED: Pass Number 40, Condition All, Cycle All, Approximate Number of Flight Hours and/or Landings Simulated 40,000 Hours and 28,868 Landings

PART NUMBER AND DESCRIPTION
Huk-bolt (3/16-in. dia.) in the 370532-5 Web

LOCATION:
WS 100L
(Front Beam, Upper Surface)

DATE FOUND: 8/1/75 FOUND BY: H.F. Ortwein VERIFIED BY: R.I. Prescott

METHOD OF DETERMINATION: Visual

SKETCH OR PHOTO:

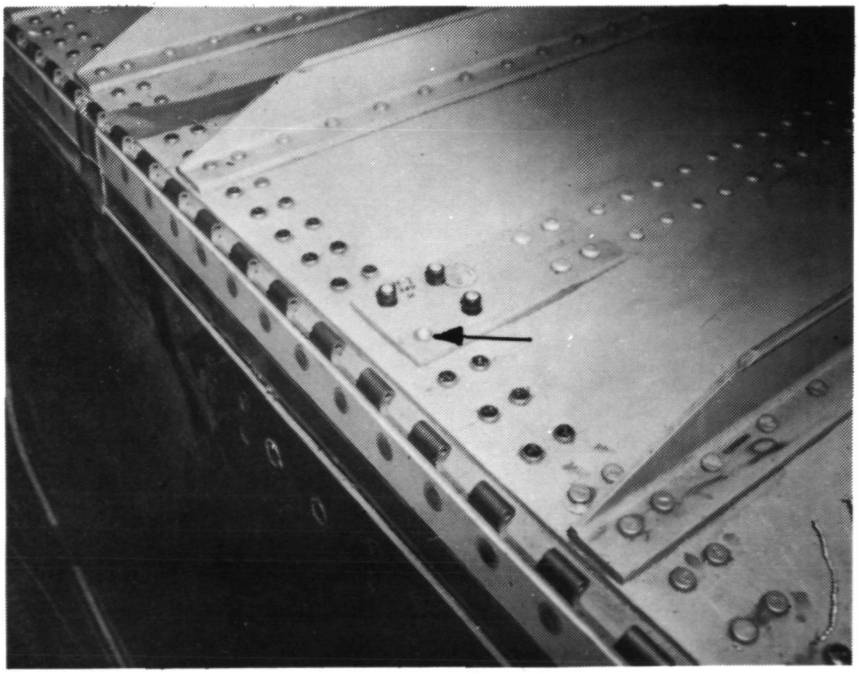

REMARKS:

A 3/16-inch diameter Huk-bolt common to the 370532-5 web and the 341929-6 Plate had failed at the collar. Fracture surface had fatigue markings. Failed fastener was replaced with an HL-18 fastener installed wet with STM 40-111 Sealant.

FATIGUE DAMAGE REPORT - COMPOSITE REINFORCED
C-130 CENTER WING BOX FATIGUE TEST

TEST PROGRAM: Contract NAS1-11100, Phase IV
DAMAGE ITEM NUMBER: 11

	YES	NO
DAMAGED PART CONSIDERED TO BE TEST SPECIMEN.	X	
DAMAGE CONSIDERED TO BE MAJOR.		X
REPAIR NECESSARY.	X	
DISCREPANCY REPORT NUMBER.	054240	

PROGRAM COMPLETED WHEN DAMAGE WAS DETECTED: Pass Number 40, Condition All, Cycle All, Approximate Number of Flight Hours and/or Landings Simulated 40,000 Hours and 28,868 Landings

PART NUMBER AND DESCRIPTION
Huk-bolt (3/16-in. dia.) in the 370539-1 Web

LOCATION:
WS 100L
(Rear Beam, Upper Surface)

DATE FOUND: 8/1/75 FOUND BY: H.F. Ortwein VERIFIED BY: R.I. Prescott

METHOD OF DETERMINATION: Visual

SKETCH OR PHOTO:

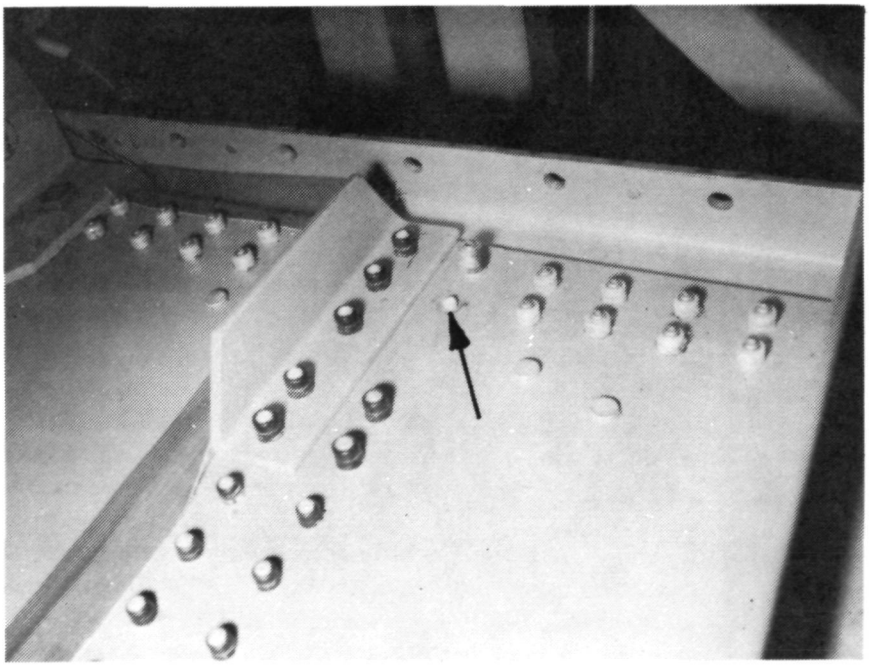

REMARKS:
A 3/16-inch diameter Huk-bolt in the 370539-1 web had failed at the collar. Fracture surface had fatigue markings. Failed fastener was replaced with an HL-18 fastener installed wet with STM 40-111 Sealant.

FATIGUE DAMAGE REPORT - COMPOSITE REINFORCED
C-130 CENTER WING BOX FATIGUE TEST

TEST PROGRAM: Contract NAS1-11100, Phase IV
DAMAGE ITEM NUMBER: 12

	YES	NO
DAMAGED PART CONSIDERED TO BE TEST SPECIMEN.	X	
DAMAGE CONSIDERED TO BE MAJOR.		X
REPAIR NECESSARY.	X	
DISCREPANCY REPORT NUMBER.	054215	

PROGRAM COMPLETED WHEN DAMAGE WAS DETECTED: Pass Number 40, Condition All, Cycle All, Approximate Number of Flight Hours and/or Landings Simulated 40,000 Hours and 28,868 Landings plus upbending limit load

PART NUMBER AND DESCRIPTION
370539-3 Web

LOCATION:
WS 145.5L (Rear Beam, Lower Surface)

DATE FOUND: 8/18/75 FOUND BY: R.E. Sykes VERIFIED BY: H.R. Michael

METHOD OF DETERMINATION: Visual

SKETCH OR PHOTO:

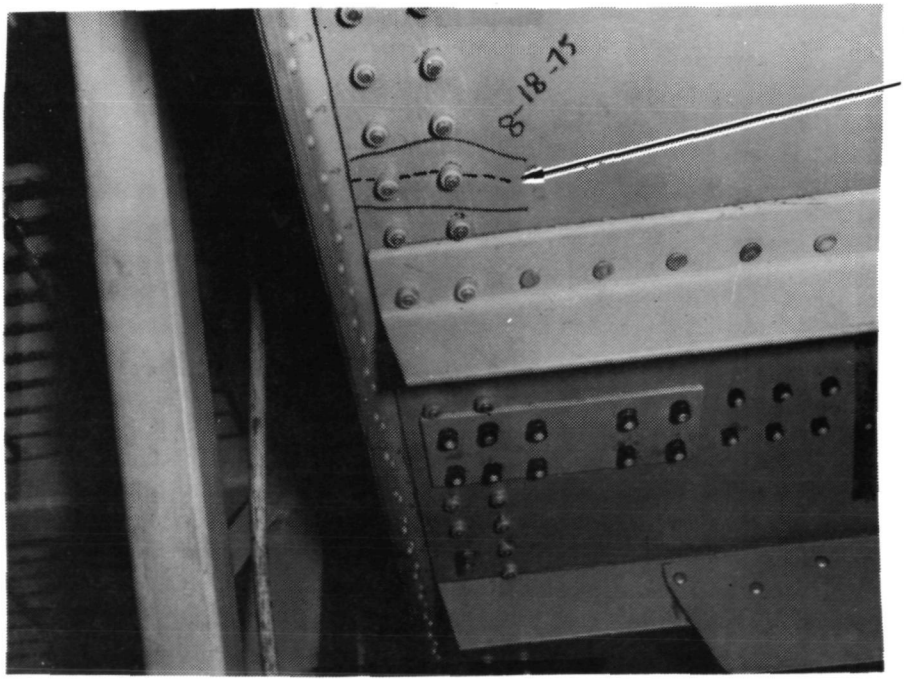

REMARKS:

The 370539-3 Web, Rear Beam had a 2.0-inch long crack starting at a fastener hole common to the Rear Beam Cap at WS 145.5L. The crack was stop drilled and a TL 200-3 fastener was installed in the stop drill hole. A 7075-T6 aluminum alloy doubler, 0.126 inch thick, was installed with HL 18-6 fasteners to reinforce the cracked area.

FATIGUE DAMAGE REPORT - COMPOSITE REINFORCED
C-130 CENTER WING BOX FATIGUE TEST

TEST PROGRAM: Contract NAS1-11100, Phase IV
DAMAGE ITEM NUMBER: 13

	YES	NO
DAMAGED PART CONSIDERED TO BE TEST SPECIMEN.	X	
DAMAGE CONSIDERED TO BE MAJOR.		X
REPAIR NECESSARY.	X	
DISCREPANCY REPORT NUMBER.	054214	

PROGRAM COMPLETED WHEN DAMAGE WAS DETECTED: Pass Number 40, Condition All, Cycle All, Approximate Number of Flight Hours and/or Landings Simulated 40,000 Hours and 28,868 Landings plus upbending limit load

PART NUMBER AND DESCRIPTION	LOCATION
S-5420 (Repair - NASA C-130 Wing Box for DR 054246)	WS 73L (Front Beam, Lower Surface)

DATE FOUND: 8/18/75 FOUND BY: W.M. McGee VERIFIED BY: H.R. Michael

METHOD OF DETERMINATION: Visual

SKETCH OR PHOTO:

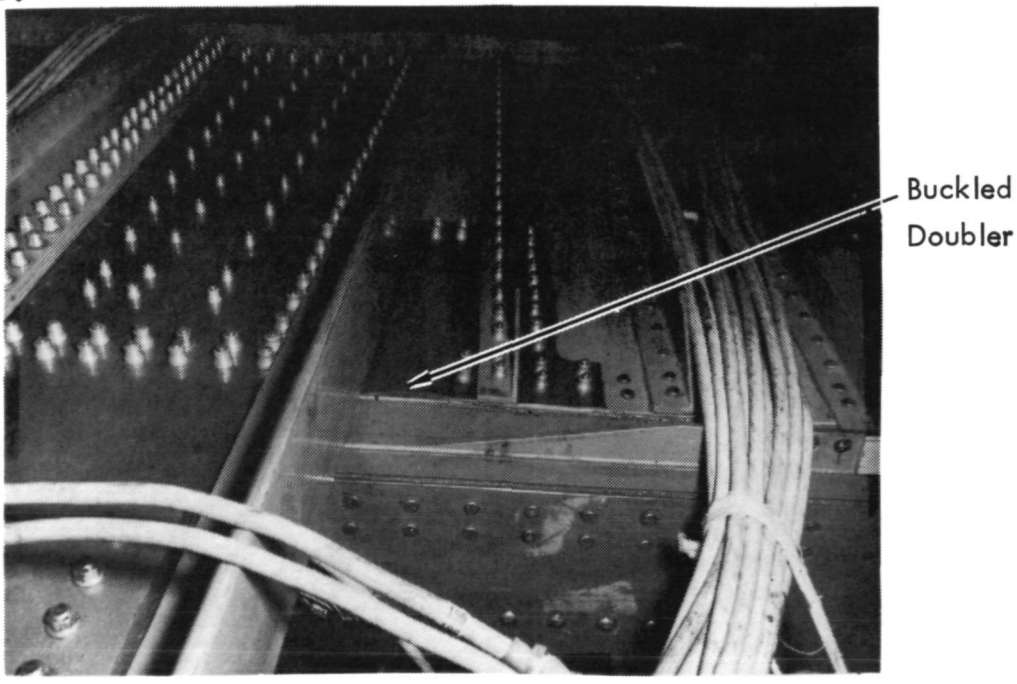

REMARKS:
The S-5420 Repair doublers buckled at WS 73L during Limit Load Test (Upbending Strain Survey, Case 1102, Limit Load). The double row of fasteners in the top edge of the repair was extended parallel to the buckle. The fasteners common to the web and the beam cap in this double row were omitted.